THE MECHANICS OF SUBMERGED MULTIPORT DIFFUSERS FOR BUOYANT DISCHARGES IN SHALLOW WATER

by

GERHARD HERMANN JIRKA

Dipl. Ing., Hochschule für Bodenkultur,
Vienna, Austria
(1969)
S.M., Massachusetts Institute of Technology
(1971)

Submitted in partial fulfillment

of the requirements for the degree of

Doctor of Philosophy

at the

Massachusetts Institute of Technology

March 1973

Signature of Author . . . . . .
Department of Civil Engineering, March 9, 1973

Certified by . . . . . .
Thesis Supervisor

Accepted by . . . . . .
Chairman, Departmental Committee on Graduate Students of the Department of Civil Engineering

ABSTRACT

THE MECHANICS OF SUBMERGED MULTIPORT DIFFUSERS
FOR BUOYANT DISCHARGES IN SHALLOW WATER

by

GERHARD HERMANN JIRKA

Submitted to the Department of Civil Engineering on March 9, 1973 in partial fulfillment of the requirements for the degree of Doctor of Philosophy

A submerged multiport diffuser is an effective device for disposal of water containing heat or other degradable wastes into a natural body of water. A high degree of dilution can be obtained and the environmental impact of concentrated waste can be constrained to a small area.

An analytical and experimental investigation is conducted for the purpose of developing predictive methods for buoyant discharges from submerged multiport diffusers. The following physical situation is considered: A multiport diffuser with given length, nozzle spacing and vertical angle of nozzles is located on the bottom of a large body of water of uniform depth. The ambient water is unstratified and may be stagnant or have a uniform current which runs at an arbitrary angle to the axis of the diffuser. The general case of a diffuser in arbitrary depth of water and arbitrary buoyancy is treated. However, emphasis is put on the diffuser in shallow receiving water with low buoyancy, the type used for discharge of condenser cooling water from thermal power plants.

A multiport diffuser will produce a general three-dimensional flow field. Yet the predominantly two-dimensional flow which is postulated to exist in the center portion of the three-dimensional diffuser can be analysed as a two-dimensional "channel model", that is a diffuser section bounded by walls of finite length and openings at both ends into a large reservoir. Matching of the solutions for the four distinct flow regions which can be discerned in the channel model, namely, a buoyant jet region, a surface impingement region, an internal hydraulic jump region and a stratified counterflow region, yields these results: The near-field zone is stable only for a limited range of jet densimetric Froude numbers and relative depths. The stability is also dependent on the jet discharge angle. It is only in this limited range that previous buoyant jet models assuming an unbounded receiving water are applicable to predict dilutions. Outside of the parameter range which yields stable near-field conditions, the diffuser-induced dilutions are essentially determined by the interplay of two factors:

frictional effects in the far-field and the horizontal momentum input of the jet discharge. Three far-field flow configurations are possible, a counter flow system, a stagnant wedge system and a vertically fully mixed flow, which is the extreme case of surface and bottom interaction.

A three-dimensional model for the diffuser-induced flow field is developed. Based on equivalency of far-field effects, the predictions of the two-dimensional channel model can be linked to the three-dimensional diffuser characteristics. Diffusers with an unstable near-field produce three-dimensional circulations which lead to recirculation at the diffuser line: effective control of these circulations is possible through horizontal nozzle orientation.

The diffuser in an ambient cross-current is studied experimentally. Different extreme regimes of diffuser behaviour can be described. Performance is dependent on the arrangement of the diffuser axis with respect to the crossflow direction.

Experiments are performed in two set-ups, investigating both two-dimensional slots and three-dimensional diffusers. Good agreement between theoretical predictions and experimental results is found.

The results of this study are presented in form of dilution graphs which can be used for three-dimensional diffuser design or preliminary design if proper schematization of the ambient geometry is possible. Design considerations are discussed and examples are given. For more complicated ambient conditions, hydraulic scale models are necessary. The results of this study indicate that only undistorted scale models simulate the correct areal extent of the temperature field and the interaction with currents, but are always somewhat conservative in dilution prediction. The degree of conservatism can be estimated. Distorted models are less conservative in predicting near-field dilutions, but exaggerate the extent of the near-field mixing zone.

Thesis Supervisor: Donald R. F. Harleman

Title: Professor of Civil Engineering

ACKNOWLEDGEMENTS

I wish to acknowledge the financial support received from Stone and Webster Engineering Corporation, Boston, during the major portion of my studies at M.I.T. In addition, a significant share of the basic experiments reported in this work was sponsored by Stone and Webster as part of applied diffuser design studies. This foresightedness and generosity in supporting basic research beyond the immediate needs of a specific project is gratefully acknowledged.

I express my deep appreciation to my thesis advisor, Professor Donald R. F. Harleman, for his guidance and encouragement throughout this work.

I greatly benefited from lively discussions with Eric Adams and Masa Watanabe with whom it was also fun to share an office. Many thanks, too, to Masa Watanabe and Don Evans for their assistance in constructing and operating the experiments. I also want to make particular mention of Ed McCaffrey, Roy Milley and Steve Ellis for their help in the experimental program. Bob Shillman helped with the illustrations. Finally, many thanks to Kathy Emperor, Sandy Williams and Stephanie Demeris who all did a charming job in typing this thesis.

für Sonia

FOREWORD

The research contained in this report is part of a continuing research effort by the Ralph M. Parsons Laboratory for Water Resources and Hydrodynamics on the engineering aspects of waste heat disposal from electric power generation by means of submerged multiport diffusers. Future research activities will be coordinated with the Waste Heat Management Group in the Energy Laboratory of the Massachusetts Institute of Technology. The guiding objective of the research program is the development of predictive models for diffuser discharge which form the basis of sound engineering design compatible with environmental requirements. In addition, site-related studies concerned with optimized diffuser design under specific ambient conditions are conducted.

Previous reports related to submerged diffuser studies are:

"Thermal Diffusion of Condenser Water in a River During Steady and Unsteady Flows" by Harleman, D. R. F., Hall, L. C. and Curtis, T. G., M.I.T. Hydrodynamics Laboratory Technical Report No. 111, September 1968.

"A Study of Submerged Multi-Port Diffusers for Condenser Water Discharge with Application to the Shoreham Nuclear Power Station" by Harleman, D. R. F., Jirka, G. and Stolzenbach, K. D., M.I.T. Parsons Laboratory for Water Resources and Hydrodynamics Technical Report No. 139, August 1971.

"Investigation of a Submerged, Slotted Pipe Diffuser for Condenser Water Discharge from the Canal Plant, Cape Cod Canal" by Harleman, D. R. F., Jirka, G., Adams, E. E. and Watanabe, M., M.I.T. Parsons Laboratory for Water Resources and Hydrodynamics Technical Report No. 141, October 1971.

"Experimental Investigation of Submerged Multiport Diffusers for Condenser Water Discharge with Application to the Northport Electric Generation Station" by Harleman, D. R. F., Jirka, G. and Evans, D. H., M.I.T. Parsons Laboratory for Water Resources and Hydrodynamics, Technical Report No. 165, February 1973.

TABLE OF CONTENTS

I. INTRODUCTION

In managing the waste water which accrues as a result of man's domestic and industrial activities different methods of treatment, recycling and disposal are used. The choice of a specific scheme of waste water management is determined by economic and engineering considerations, such as costs and available technology, and by considerations of environmental quality, each scheme having a certain impact on the natural environment.

In many instances the discharge of water containing heat or other degradable wastes into a natural body of water is a viable economic and engineering solution. "Water quality standards" have been established to regulate the adverse effects of such discharges on the receiving water. These standards are based on existing scientific knowledge of the biological, chemical and physical processes which occur in response to the waste water discharge. The standards have the objective of preserving or enhancing the use of the natural water body for a variety of human needs.

A common feature of all water quality standards, as set forth by various legal authorities, is a high dilution requirement: Within a limited mixing zone the waste water has to be thoroughly mixed with the receiving water. The purpose of this requirement is to constrain the impact of concentrated waste water to a small area.

It is against this background that the increasing application of submerged multiport diffusers as an effective device for disposal of waste water must be understood. A submerged multiport diffuser is essentially a pipeline laid on the bottom of the receiving water. The

waste water is discharged in the form of round turbulent jets through ports or nozzles which are spaced along the pipeline. The resulting distribution of concentration of the discharged waste materials within the receiving water depends on a variety of physical processes. A clear understanding of these processes is needed so that predictive models can be developed which form the basis of a sound engineering design.

1.1 Historical Perspective

For several decades many coastal cities have utilized submerged multiport diffusers for the discharge of municipal sewage water. Noteworthy aspects of these "sewage diffusers" are: 1) Water quality standards dictate dilution requirements in the order of 100 and higher when sewage water is discharged. As a consequence these diffusers are limited to fairly deep water (more than 100 feet deep). 2) The buoyancy of the discharged water is significant. The relative density difference between sewage water and ocean water is about 2.5%.

Only in very recent years have multiport diffusers found application for the discharge of heated condenser cooling water from thermal power plants. The main impetus has come from the implementation of stringent temperature standards. Depending on the water quality classification of the receiving water and on the cooling water temperature rise dilutions between about 5 and 20 are required within a specified mixing area. This dilution requirement frequently rules out relatively simple disposal schemes, such as discharge by means of a surface canal or a single submerged pipe. On the other hand, multiport diffusers can be placed in relatively shallow water (considerably less than 100 ft. deep) and still attain the required dilutions. The economic advantage in

keeping the conveyance distance from the shoreline short might be substantial, in particular in lakes, estuaries or coastal waters with extended shallow nearshore zones. "Thermal diffusers" have these characteristics: 1) They may be located in relatively shallow water. 2) The buoyancy of the discharged water is low. Relative density differences are in the order of 0.3% corresponding to a temperature differential of about 20°F, an average value for thermal power plants.

Due to these essential differences, regarding depth of the receiving water and buoyancy of the discharge, there is a pronounced difference in the mechanics of "sewage diffusers" and "thermal diffusers". Consequently, predictive models which have been established and verified for the class of "sewage diffusers" fail to give correct predictions when applied for the class of "thermal diffusers".

1.2 Basic Features of Multiport Diffusers for Buoyant Discharges

The performance characteristics of a multiport diffuser, that is the distributions of velocities, densities and concentrations which result when the diffuser is operating, are influenced by many physical processes. These processes may be conveniently -- yet somewhat loosely -- divided into two groups.

"Near-field" processes are directly governed by the geometric, dynamic and buoyant characteristics of the diffuser itself and of the ambient water in the immediate diffuser vicinity. Significant features are: Turbulent jet diffusion produces a gradual increase in jet thickness ("jet spreading") and a simultaneous reduction of velocities and concentrations within the jets through entrainment of ambient water. The trajectory of the jets is determined by the initial angle and by influence

of buoyancy causing a rise towards the surface. Before surfacing the jet spreading becomes so large that lateral interference between adjacent jets forms a two-dimensional jet along the diffuser line. Upon impingement on the surface of the receiving water the jet is transformed into a horizontally moving buoyant layer. Stability of this layer is of crucial importance. Instabilities result in re-entrainment of already mixed water into the jet diffusion process. In addition to these basic processes, ambient conditions such as cross-currents and existing natural density stratification can have a strong effect on the near-field.

"Far-field" processes influence the motion and distribution of mixed water away from the near-field zone. The mixed water is driven by its buoyancy against interfacial frictional resistance as density currents, thus a flow away from the diffuser is generated. Conversely, a flow toward the diffuser against interfacial and bottom friction is set up as the turbulent entrainment into the jets acts like a sink for ambient water. Furthermore the convection of the mixed water by ambient currents and the diffusion by ambient turbulence and the concentration reduction through time-dependent decay processes may be important processes.

The efficiency of the near-field processes (notably jet mixing) in reducing the concentrations of the discharged water is dominant over far-field processes which usually act over a longer time scale. However, there is a coupling between near and far-field processes, near-field processes affecting the far-field and vice versa. Thus in general, a total prediction of the performance characteristics of a multiport diffuser must include this coupling.

Yet in special cases the coupling effect may be so weak that the near-field processes may be assumed not to be influenced by the far-field. Diffusers in deep water with high buoyancy of the discharge ("sewage diffusers") fall into this category. These diffusers produce a stable surface layer which moves away from the diffuser as a density current. Near-field dilutions are then primarily caused by jet entrainment and the diffuser can be analyzed as a series of round interacting jets in infinite water. This analysis is the basis of most existing predictive models for diffuser discharges.

On the other hand, diffusers in shallow water with low buoyancy ("thermal diffusers") may not create a stable surface layer. Subsequently, already mixed water gets re-entrained into the jets to such a degree that the increased buoyancy force of the surface layer is sufficient to overcome the frictional effects in the far-field. Hence in this case a composite analysis of near-field and far-field must be undertaken in developing predictive models.

This contrasting difference between these two types of diffusers is qualitatively illustrated in Figure 1-1. Examples are shown for vertical and non-vertical discharges without ambient currents. As an extreme case of the non-vertical discharge in shallow water a uni-directional flow of ambient water toward the diffuser and of mixed water away from the diffuser is established (see Figure 1-1d).

1.3 Objectives of this Study

This investigation is concerned with the development of predictive methods for buoyant discharges from submerged multiport diffusers. The following physical situation is considered: A multiport diffuser with

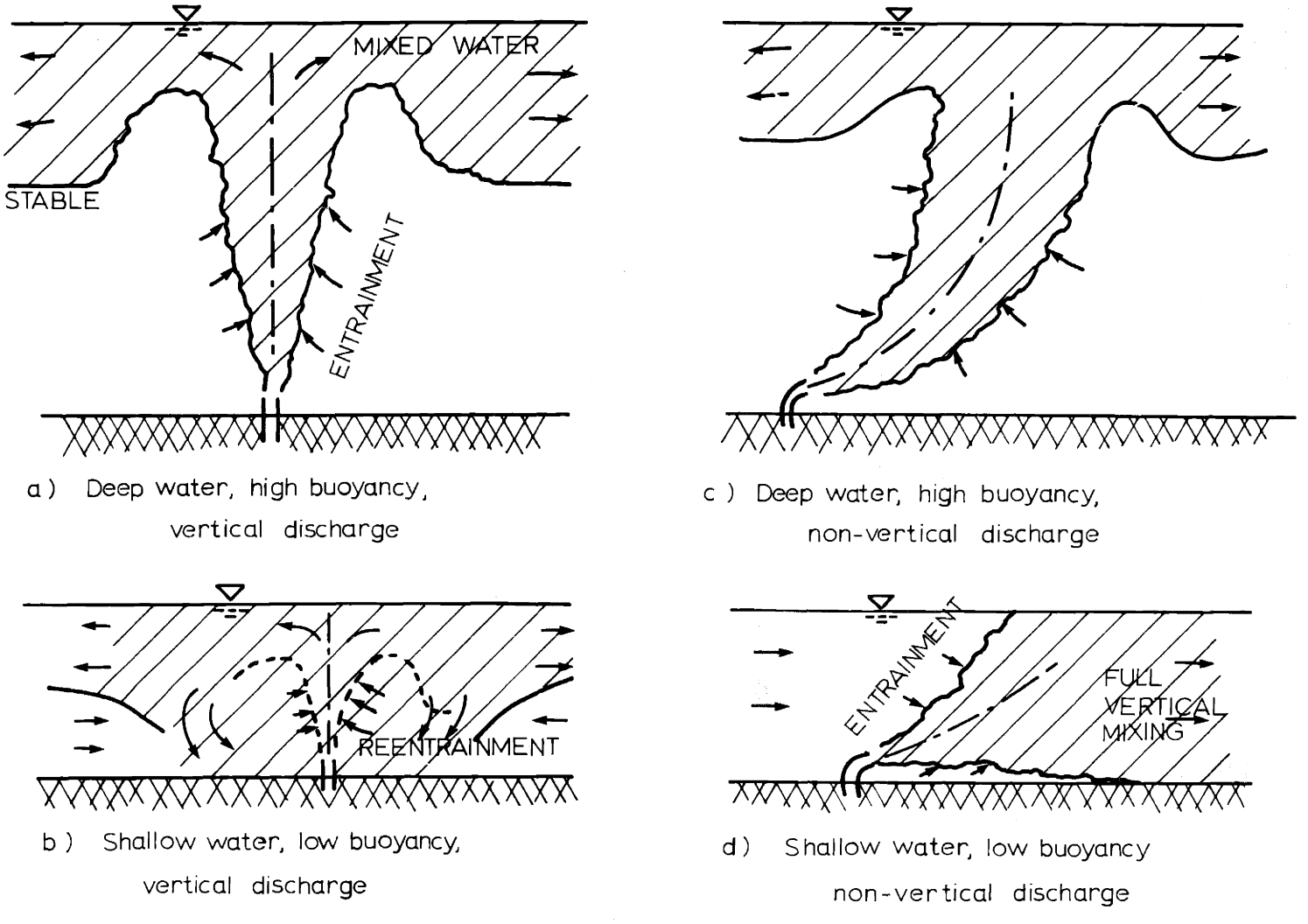

a) Deep water, high buoyancy, vertical discharge

c) Deep water, high buoyancy, non-vertical discharge

b) Shallow water, low buoyancy, vertical discharge

d) Shallow water, low buoyancy non-vertical discharge

Fig. 1-1: Qualitative Illustrations of Resulting Distributions of Mixed Water (no ambient currents)

given length, nozzle spacing and vertical angle of nozzles is located on the bottom of a large body of water of uniform depth. The ambient water is unstratified and may be stagnant or have a uniform current which runs at an arbitrary angle to the axis of the diffuser.

All of the near-field processes but only part of the far-field processes (excluding effects of ambient turbulence and decay processes) are taken into account.

This study addresses the general case of a diffuser in arbitrary depth of water and arbitrary buoyancy. However, special emphasis is put on the diffuser in shallow receiving water with low buoyancy, the type frequently used for discharge of condenser cooling water from thermal power plants. The study is not concerned with the internal hydraulics of the diffuser pipe (manifold design problem).

Application of the results of this investigation is anticipated for various aspects:

-- Economical design of the diffuser structure.

-- Design to meet specific water quality requirements.

-- Evaluation of the impact in regions away from the diffuser, such as the possibility of recirculation into the cooling water intake of thermal power plants.

-- Design and operation of hydraulic scale models.

1.4 Summary of the Present Work

An analytical and experimental investigation is conducted.

In Chapter 2 a critical review of existing prediction techniques for multiport diffusers is given.

Chapter 3 presents the theoretical framework for the study of

diffusers without ambient crossflow: Recognizing the predominantly two-dimensional flow pattern which prevails in the centerportion of a diffuser, predictive models are developed for a two-dimensional "channel model", i.e. a diffuser section is bounded laterally by walls of finite length. This conceptualization allows the analysis of vertical and longitudinal variations of the diffuser-induced flow field.

Chapter 4 discusses three-dimensional aspects of diffuser discharge. Through a quantitative analysis regarding far-field effects (frictional resistance in the flow away zone) the length of the two-dimensional channel model is linked to the three-dimensional diffuser length. Thus the theoretical predictions developed for the two-dimensional channel model become applicable to the general three-dimensional case. Chapter 4 also discusses the control of horizontal circulations induced by the diffuser action.

The experimental facilities and procedures are described in Chapter 5. Experiments were performed both on two-dimensional models ("channel models") and three-dimensional models.

In Chapter 6 experimental results for diffusers without ambient crossflow are reported and compared to theoretical predictions.

The effect of a uniform ambient crossflow on diffuser performance is studied in Chapter 7. This part is mainly experimental; however, limiting cases of crossflow influence are discussed theoretically. Diffuser arrangements with the diffuser axis either perpendicular or parallel to the crossflow direction were tested.

The application of the results to practical problems of diffuser design and operation of hydraulic scale models is discussed in Chapter 8.

II. CRITICAL REVIEW OF PREVIOUS PREDICTIVE MODELS FOR SUBMERGED MULTIPORT DIFFUSERS

Existing predictive techniques for the analysis of submerged multiport diffusers fall into two restricted groups: First, buoyant jet models describe the physical processes governing buoyant jets in an infinite body of water. In applying these models it is usually tacitly (without proof) assumed that the effect of the finite water depth can be neglected and a stable flow away from the line of surface impingement exists. There is a large amount of literature on buoyant jets. Only the most significant contributions are reviewed. Secondly, one-dimensional average models for horizontal diffuser discharge assume full vertical mixing downstream of the diffuser and are valid only for shallow receiving water.

2.1 Investigations of Buoyant Jets

2.1.1 General Characteristics

Turbulent buoyant jets (also called forced plumes) are examples of fluid motion with shear-generated free turbulence. Special cases of the turbulent buoyant jet are the simple non-buoyant jet, driven by the momentum of fluid discharged into a homogeneous medium, and the simple plume, emanating from a concentrated source of density deficiency and driven by buoyancy forces.

Dominating transport processes governing the distribution of flow quantities are convection by the mean velocities, acceleration in the direction of the buoyancy force and turbulent diffusion by the irregular eddy motion within the jet.

Main properties of the jet flow field and their important implications on possible methods of analysis are (Abramovich (1963), Schlichting (1968)):

1) Gradual spreading of the jet width. The jet width is small compared to the distance from the source along the axis of the jet. This allows to make the typical boundary layer assumptions: Convection by mean transverse velocities can be neglected compared to convection by mean axial velocities. Diffusion in the axial direction is small compared to diffusion in the transverse direction.
2) Self-similarity of the flow. The transverse profiles of velocity, mass and heat at different axial distances along the jet are similar to each other. Local jet quantities can be expressed as a function of centerline quantities and jet width.
3) Fluctuating turbulent quantities are small compared to mean centerline quantities.
4) For jets issuing into unconfined regions pressure gradients are negligible.

If semi-empirical relationships relating the turbulent structure of the jet to its mean properties (such as the mixing length hypothesis) are invoked, a similarity solution to the simplified governing equations with specified boundary conditions is possible. This is shown by Schlichting (1968) for simple jets. The solution requires the specification of one experimentally determined constant and yields the function

of the similarity profile and gross jet characteristics as a function of longitudinal distance.

An alternate approach, somewhat more convenient to use, is the a priori specification of similarity functions. The governing equations can then be integrated in the transverse direction. The resulting set of equations shows only dependence on the axial coordinate. Again, full solution requires an experimentally determined coefficient. The coefficient either refers to the rate of spreading (method first described by Albertson et.al. (1950)) or to the rate of entrainment (first described by Morton et.al. (1956)), both coefficients being related to each other. In general, these coefficients are not constants, being different for single jet and plumes. Usage of the integral technique for buoyant jet prediction is common to models described in the following sections.

2.1.2 Round Buoyant Jets

The schematics of a round buoyant jet are shown in Figure 2-1. After an initial zone of flow establishment the jet motion becomes self-similar. Experimental data show that a Gaussian profile can usually be well fitted to the observed distribution of velocity, density deficiency and mass:

$$\tilde{u}(s,r) = \tilde{u}_c(s)\, e^{-\left(\frac{r}{b}\right)^2} \qquad (2\text{-}1)$$

$$\rho_a - \rho(s,r) = (\rho_a - \rho_c(s))\, e^{-\left(\frac{r}{\lambda b}\right)^2} \qquad (2\text{-}2)$$

$$c(s,r) = c_c(s)\, e^{-\left(\frac{r}{\lambda b}\right)^2} \qquad (2\text{-}3)$$

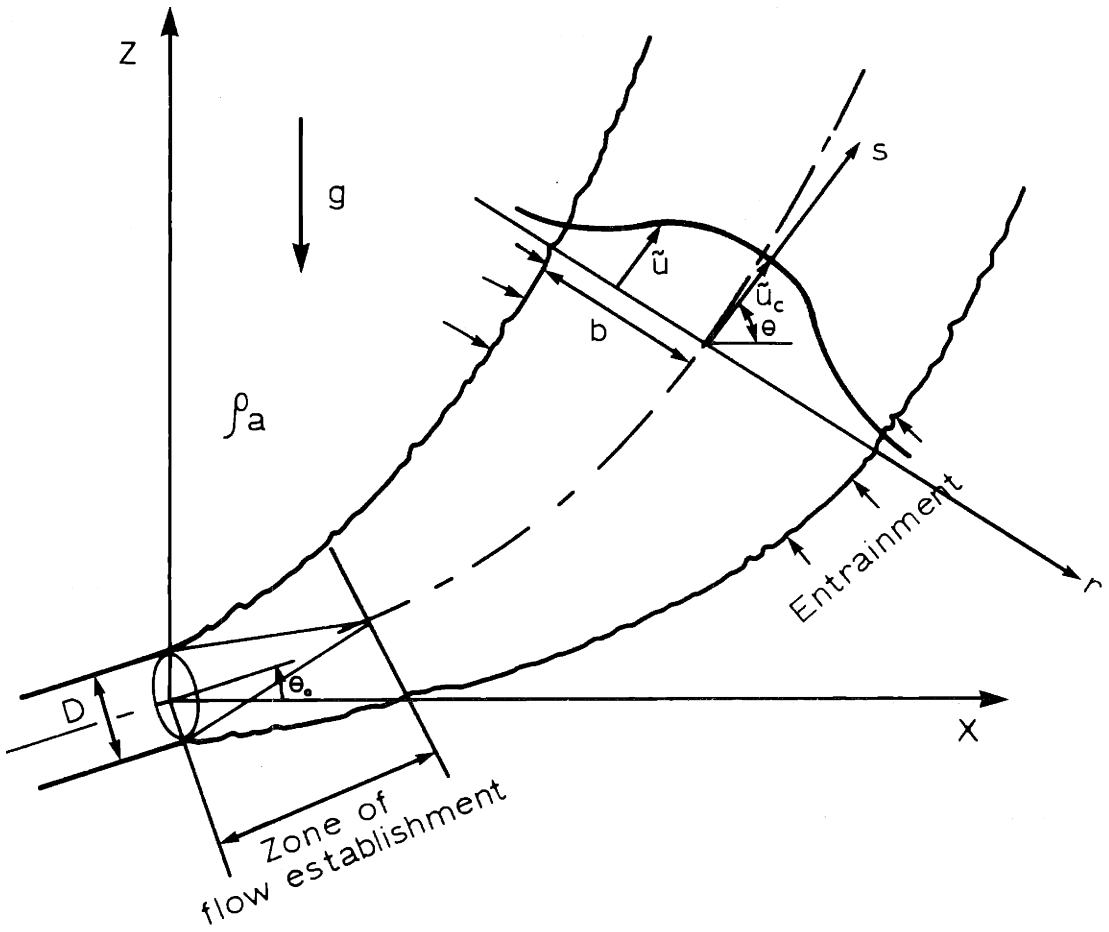

Fig. 2-1: Schematics of a Round Buoyant Jet

where

s, r = axial and transverse coordinates

$\tilde{u}$ = axial velocity

$\tilde{u}_c$ = centerline axial velocity

b = nominal jet width

ρ_a = ambient density

ρ = density in the jet

ρ_c = density in jet centerline

λ = spreading ratio between velocity and mass

c = concentration of some discharged material

c_c = centerline concentration

The spreading ratio λ accounts for the fact that experimental observations show in general stronger lateral diffusion ($\lambda > 1$) for scalar quantities such as mass or heat than for velocities. With the specification of the velocity profile a volume flux is determined as

$$Q(s) = 2\pi \int_0^\infty \tilde{u}(s,r)\, dr = \pi\, \tilde{u}_c b^2 \qquad (2\text{-}4)$$

The entrainment concept as formulated by Morton et.al. assumes a transverse entrainment velocity v_e at the nominal jet boundary b to be related to the centerline velocity as

$$v_e = -\alpha\, \tilde{u}_c \qquad (2\text{-}5)$$

where α is a coefficient of proportionality (entrainment coefficient). With this assumption the change in volume flux follows as

$$\frac{dQ}{ds} = 2\pi b \cdot \alpha \tilde{u}_c \qquad (2\text{-}6)$$

Using the profile assumptions (2-1), (2-2) and (2-3), integrated conservation equations for the vertical and horizontal momentum and for mass can be written.

Solution to the system of ordinary differential equations with initial discharge conditions yields the shape of the jet trajectory and values of $\tilde{u}_c$, ρ_c, c_c and b along the trajectory.

This approach forms the basis of many buoyant jet theories since Morton et. al. (1956). The theories, however, differ on specific assumptions regarding the entrainment coefficient α . Examination of experimental data shows that α is clearly a function of the local buoyant characteristics of the jet which can be expressed in an average fashion by a local Froude number F_L

$$F_L = \frac{\tilde{u}_c}{\left(\frac{\rho_a - \rho_c}{\rho} gb\right)^{1/2}} \qquad (2\text{-}7)$$

The value of α is dependent on the form of the similarity profile. For Gaussian profiles as specified above, data by Albertson et.al. (1950) suggest for the simple jet ($F_L \to \infty$)

$$\alpha = 0.057 \qquad (2\text{-}8)$$

and data by Rouse et.al. (1952) for the plume (F_L small)

$$\alpha = 0.082 \qquad (2\text{-}9)$$

Buoyant jets tend to the condition of a simple plume far away from the source when the initial momentum becomes small in comparison to the buoyancy induced momentum. Accordingly, Morton (1959) and Fan and Brooks (1966) assumed $\alpha = 0.082$ constant throughout the jet. For jets with substantial initial momentum a certain error is inherent.

Using the integrated energy conservation equation Fox (1970) showed that the dependence of the entrainment coefficient on F_L as

$$\alpha = \alpha_1 + \frac{\alpha_2(\lambda)}{F_L^2} \tag{2-10}$$

for the case of vertical discharge ($\theta_o = 90°$). For non-vertical discharge Hirst (1971) extended Fox's argument to show

$$\alpha = \alpha_1 + \frac{\alpha_2(\lambda)}{F_L^2} \sin\theta \tag{2-11}$$

where θ is the local angle of the jet trajectory. In both Equations (2-10) and (2-11) α_1 can be determined from the simple jet ($F_L \to \infty$) from Equation (2-8) and α_2 is found as a unique function of the spreading ratio λ.

Buoyant jet models based on the integral technique but with specification of a coefficient of the spreading rate were developed by Abraham (1963). Similar to the entrainment coefficient the spreading rate is found to be variable in buoyant jets, approaching a constant value for the limiting cases of simple jet and plume. In the analysis of the vertically discharged buoyant jet Abraham assumed a constant rate of spreading. For the case of a horizontally discharged jet the spreading rate was postulated to be related to the local jet angle, and not to

the local buoyant characteristics as is physically more reasonable.

Solution graphs for round buoyant jets discharged at various angles θ_o have been published by Fan and Brooks (1969), Abraham (1963) and others. In all these models some adjustment is made for the initial zone of flow establishment. From the practical standpoint there is little variation between the predictions of various models, typical variations in centerline dilutions for example being less than 20%, well below the scatter of usual experimental data (see Fan (1967)). The choice of a particular model is thus determined by the correctness of the presentation of the physical processes and by the applicability to varying design problems, such as discharge into stratified ambients. In this respect an integral model with entrainment coefficients as given by Fox seems to be most satisfying.

2.1.3 Slot Buoyant Jets

Figure 2-2 shows the two-dimensional flow pattern for a buoyant jet issuing from a slot with width B and vertical angle θ_o. After the initial zone of flow establishment the following similarity profiles fit well to experimental data:

$$\tilde{u}(s,n) = \tilde{u}_c(s) \; e^{-\left(\frac{n}{b}\right)^2} \tag{2-12}$$

$$\rho_a - \rho(s,n) = (\rho_a - \rho_c(s)) \; e^{-\left(\frac{n}{\lambda b}\right)^2} \tag{2-13}$$

$$c(s,n) = c_c(s) \; e^{-\left(\frac{n}{\lambda b}\right)^2} \tag{2-14}$$

where s,n = axial and transverse coordinates.

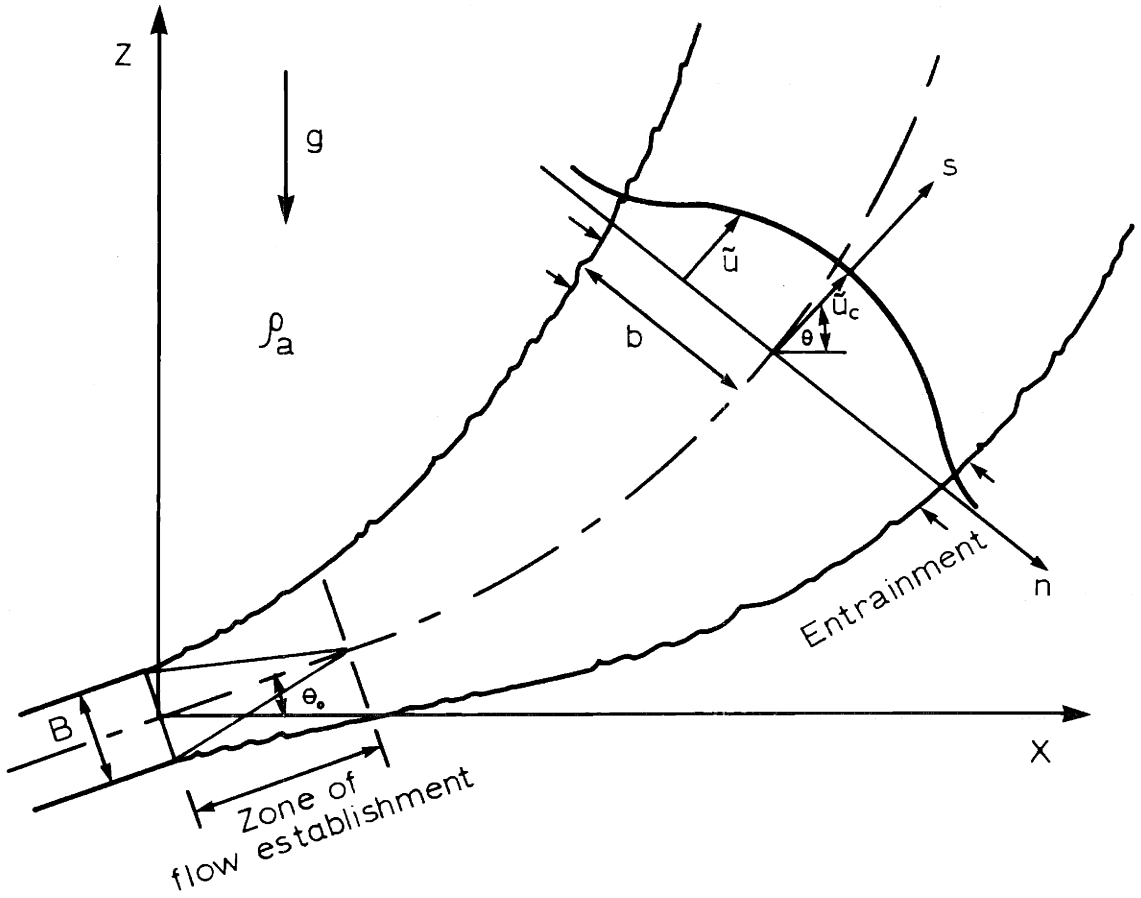

Fig. 2-2: Schematics of a Slot Buoyant Jet

The volume flux in the axial direction is then

$$q(s) = \int_{-\infty}^{\infty} \tilde{u}(s,n)\, dn = \sqrt{\pi}\ \tilde{u}_c b \qquad (2\text{-}15)$$

The entrainment velocity at the jet boundaries is assumed as

$$v_e = \pm\ \alpha \tilde{u}_c \qquad (2\text{-}16)$$

similar to the round jet. Thus the continuity equation is

$$\frac{dq}{ds} = 2\alpha \tilde{u}_c \qquad (2\text{-}17)$$

After formulation of the other conservation equation solutions proceed analogously to the round buoyant jet. The dependence of the entrainment coefficient on the buoyant characteristics of the jet is indicated by experimental data. For the simple jet α is found as

$$\alpha = 0.069 \qquad (2\text{-}18)$$

(Albertson et. al. (1950)) and for the plume

$$\alpha = 0.16 \qquad (2\text{-}19)$$

(Rouse et.al. (1952)).

An analysis with a constant α was first carried out by Lee and Emmons (1962) and later by Fan and Brooks (1969).

An an improvement, dependence on the local Froude number was proposed for the vertical buoyant jet by Fox (1970) in a relationship analogous to Equation (2-10) but with different values for α_1 and α_2.

Abraham (1963) treated the slot buoyant jet (vertical and hori-

zontal discharge) in a fashion similar to the round buoyant jet as described above.

Less experimental data is available on slot buoyant jets. Cederwall (1971) gives a comparison of experimental values with the theories by Abraham and Fan and Brooks. Reasonable agreement is found.

2.1.4 Lateral Interference of Round Buoyant Jets

In a submerged multiport diffuser the round buoyant jets issuing with velocity U_o from nozzles with diameter D and spaced at a distance ℓ gradually begin to interact with each other a certain distance away from the discharge. In a transition zone the typical similarity profiles of the series of round jets are modified to two-dimensional jet profiles. From then on the discharge behaves like a slot buoyant jet. This process is indicated in Figure 2-3. Mathematical analysis along the above outlined procedures is impossible as the assumption of self-similarity is not valid in the transition zone. Hence some approximate assumptions are usually made in the analytical treatment.

The flow field of the multiport diffuser can be compared to that of an "equivalent slot diffuser". By requiring the same discharge per unit diffuser length and the same momentum flux per unit length a width B of the equivalent slot diffuser can be related to the dimensions of the multiport diffuser by

$$B = \frac{D^2 \pi}{4\ell} \tag{2-20}$$

A common criterion regarding the merging between round jets to two-dimensional jets is to assume transition when

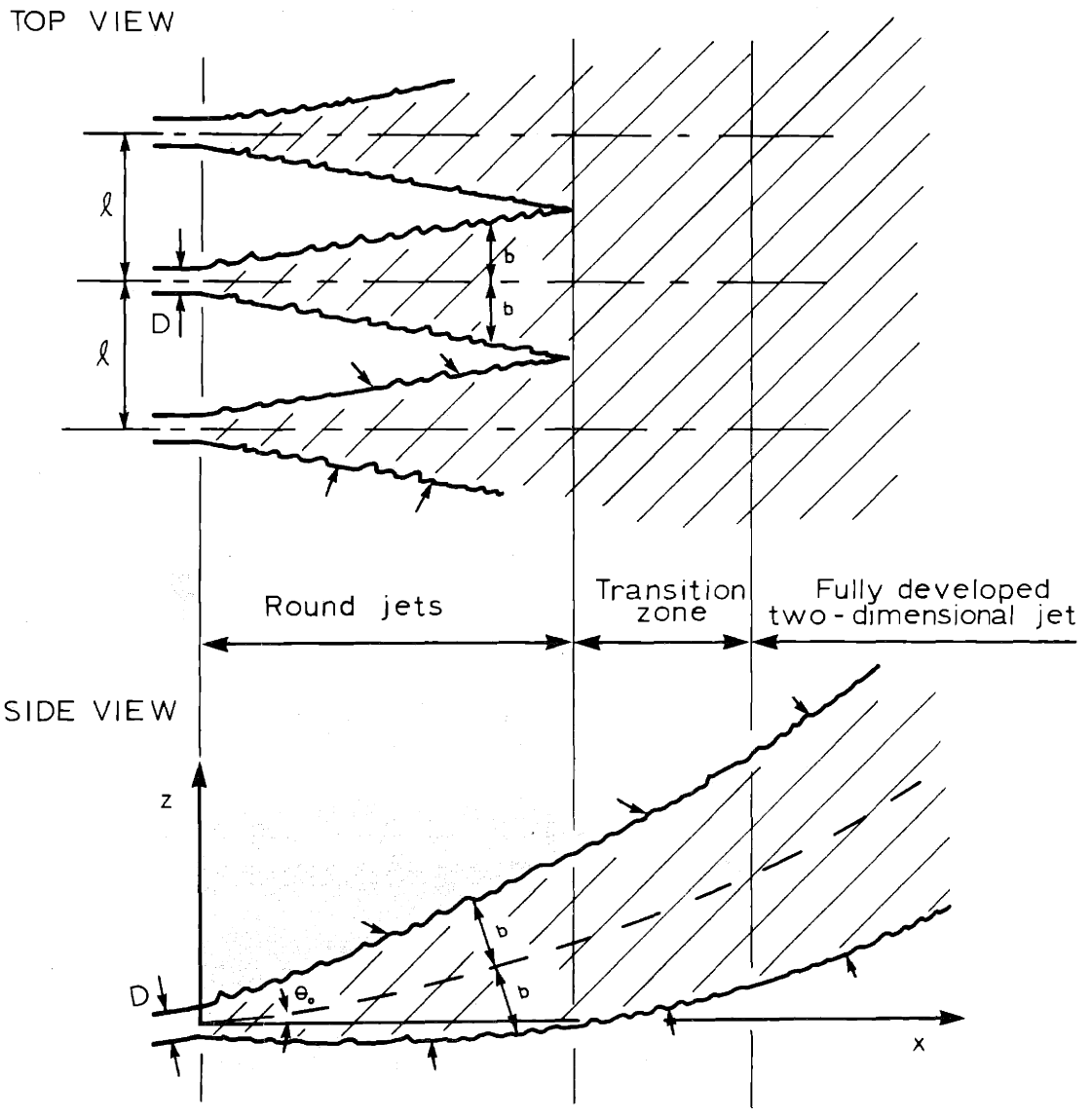

Fig. 2-3: Jet Interference for a Submerged Multiport Diffuser

$$b = \ell/2 \tag{2-21}$$

The nominal jet width b (as defined by Eq. 2-1) is only a characteristic measure of the transverse jet dimension, namely the distance where the jet velocity becomes 1/e of the centerline velocity. Thus the assumption of Equation (2-21) cannot be supported by physical arguments, but only on intuitive grounds, reasoning that when the velocity profiles overlap to such a degree the lateral entrainment is largely inhibited. Using the assumptions of Equation 2-19 Cederwall (1971) carried out a comparison between the average dilutions produced by a multiport diffuser and by its equivalent slot diffuser at the distance of interference of the multiport diffuser. He used experimentally determined relationships for the volume flux and rate of spreading published by Albertson et.al. on the simple jet and by Rouse et.al. on the plume. Cederwall found for the simple non-buoyant jet:

$$R = \frac{\text{dilution of the multiport diffuser}}{\text{dilution of the equivalent slot diffuser}} = 0.95 \tag{2-22}$$

and for the buoyant plume:

$$R = 0.78 \tag{2-23}$$

In view of the uncertainty involved these values of R should only be interpreted on an order of magnitude basis, indicating practically similar dilution characteristics for slot jets and interfering round jets.

Another comparison can be made as follows. Koh and Fan (1970) proposed a transition criterion as when the entrainment rate into the

round jets becomes equal to that the equivalent slot jet. They remarked that this assumption yielded essentially the same result as the assumption of Equation (2-21). Their criterion was applied by Shirazi and Davis (1972) to compute multiport diffuser characteristics for a variety of conditions regarding jet angle θ_o, relative spacing ℓ/D and the dynamics of the discharge given by the Froude number

$$F_n = \frac{U_o}{\left(\frac{\rho_a - \rho_o}{\rho_a} gD\right)^{1/2}} \tag{2-24}$$

as a function of the dimensionless vertical distance z/D. The dilutions of a slot jet with discharge Froude number

$$F_s = \frac{U_o}{\left(\frac{\rho_a - \rho_o}{\rho_a} gB\right)^{1/2}} \tag{2-25}$$

are calculated by the same numerical method as used by Shirazi and Davis using their values for the coefficients α and λ. Centerline dilutions S_c are plotted as a function of the dimensionless vertical distance z/B and F_s in Figure 2-4 for the case of horizontal discharge. This can be compared to Shirazi and Davis' results by using the definition of the equivalent slot width (Eq. 2-40) namely

$$\frac{z}{B} = \frac{z}{D} \frac{4\ell}{\pi D} \tag{2-26}$$

and

$$F_s = F_n \left(\frac{4\ell}{\pi D}\right)^{1/2} \tag{2-27}$$

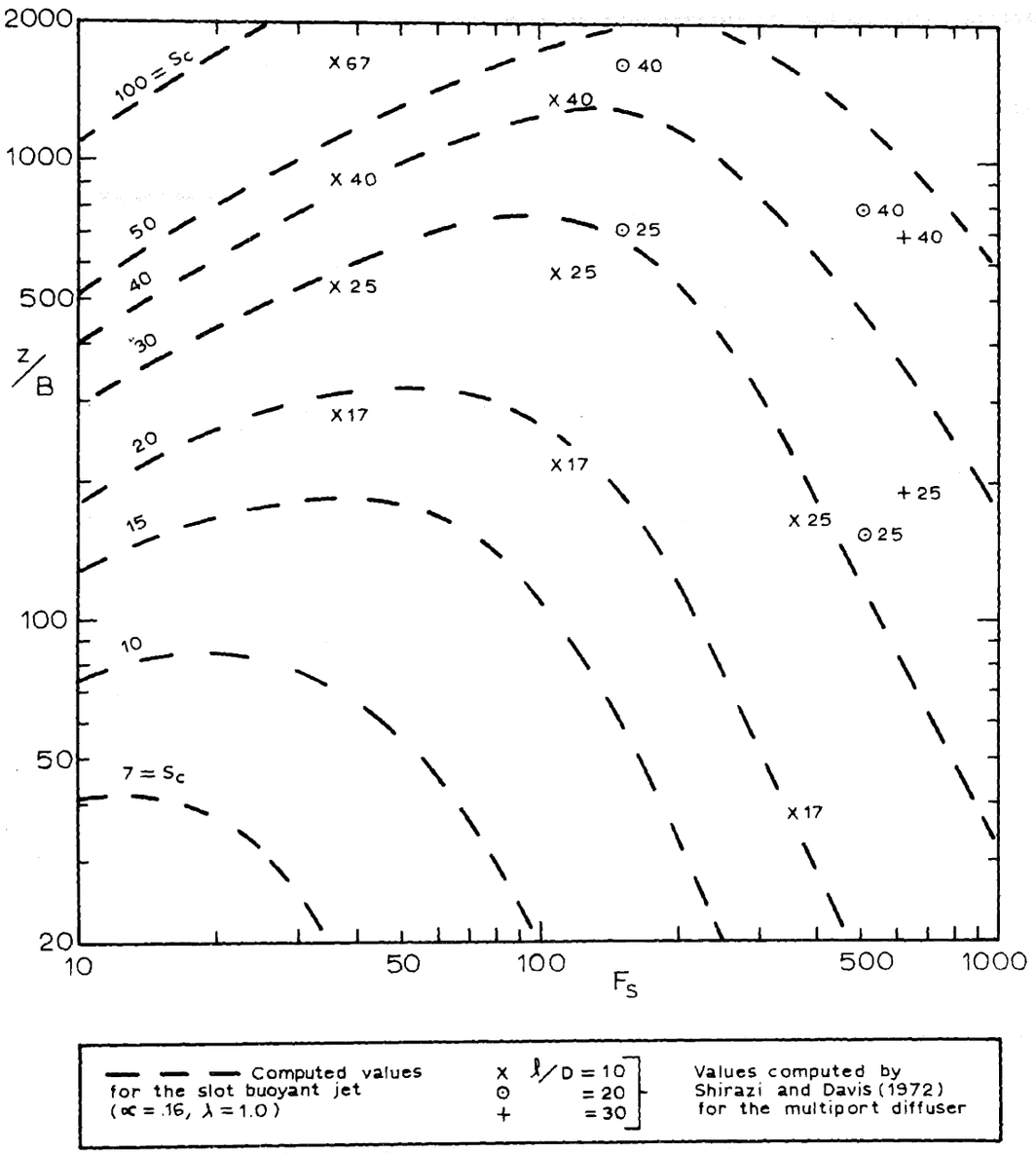

Fig. 2-4: Centerline Dilutions S_c for a Slot Buoyant Jet With Horizontal Discharge

Values converted in this fashion for points after the transition zone and for the range of ℓ/D = 10, 20 and 30 and of F_n = 10, 30 and 100 are shown in Figure 2-4. In general, Shirazi and Davis' results show no variability with ℓ/D and have the same functional dependence on z/B and F_s as the results for the slot jet. However, there is a systematic underestimation of dilution, this of course being a specific consequence of the adopted criterion for transition.

Thus, until experimental evidence to the contrary becomes available -- and this question can only be settled experimentally -- it suffices for all practical purposes to assume that the flow field characteristics of a multiport diffuser are equally presented by its equivalent slot diffuser.

A frequently used diffuser geometry is discharge through ports or nozzles issuing into alternating directions from the common manifold pipe (see Figure 2-5). With this arrangement a complicated flow pattern

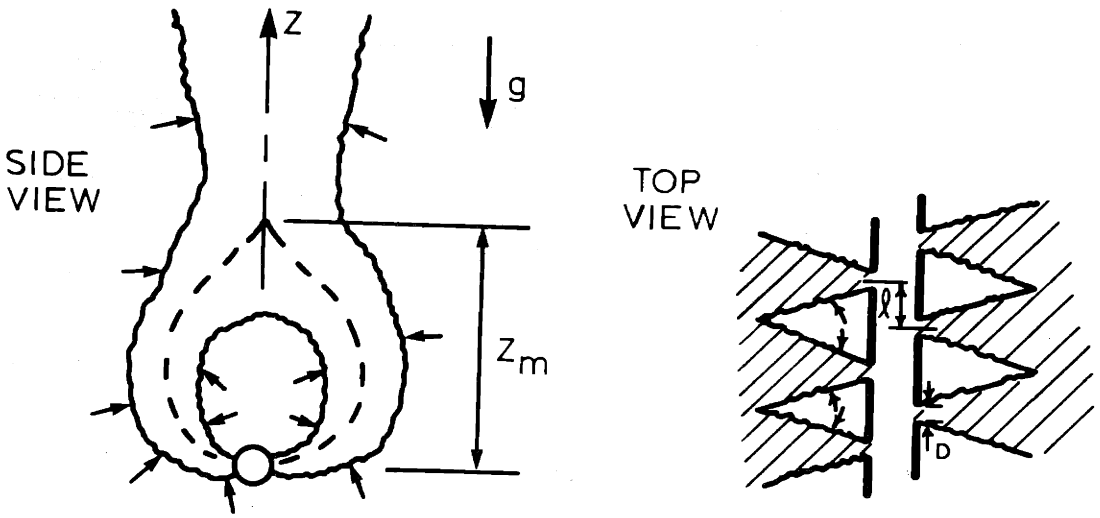

Fig. 2-5: Multiport Diffuser with Alternating Ports in Deep Water

evolves. The jets at both sides interfere laterally and rise upward under the influence of buoyancy. Only a limited amount of ambient water can penetrate into the region between the rising two-dimensional jets as the area between the jets before lateral interference is restricted. As the turbulent entrainment at the inner jet boundaries acts like a suction mechanism, a low pressure area is created between the jets. Consequently, the jets are gradually bent over until merging over the diffuser line. This case was extensively studied in a series of experiments by Liseth (1971). Averaged values of centerline dilutions measured at different levels z/ℓ were presented in graphical form. Liseth's study also yielded an approximate expression for the location z_m of merging above the diffuser

$$z_m/\ell \approx F_n \tag{2-28}$$

As the discharge by means of alternating horizontal buoyant jets does not introduce any initial momentum in the vertical direction, the flow above the line of merging can be compared to the flow in the buoyant plume. The relationship for the centerline density deficiency $\Delta\rho_c$ in the buoyant plume is given by Rouse et.al. (1952) as

$$\Delta\rho_c = \rho_a - \rho_c = \frac{2.6}{g}\left[\frac{\rho_a w^2}{z^3}\right]^{1/3} \tag{2-29}$$

in which w is the flux of weight deficiency emanating from the line source. For the discharge from the slot w can be expressed as

$$w = \Delta\rho_o \, g \, U_o B \tag{2-30}$$

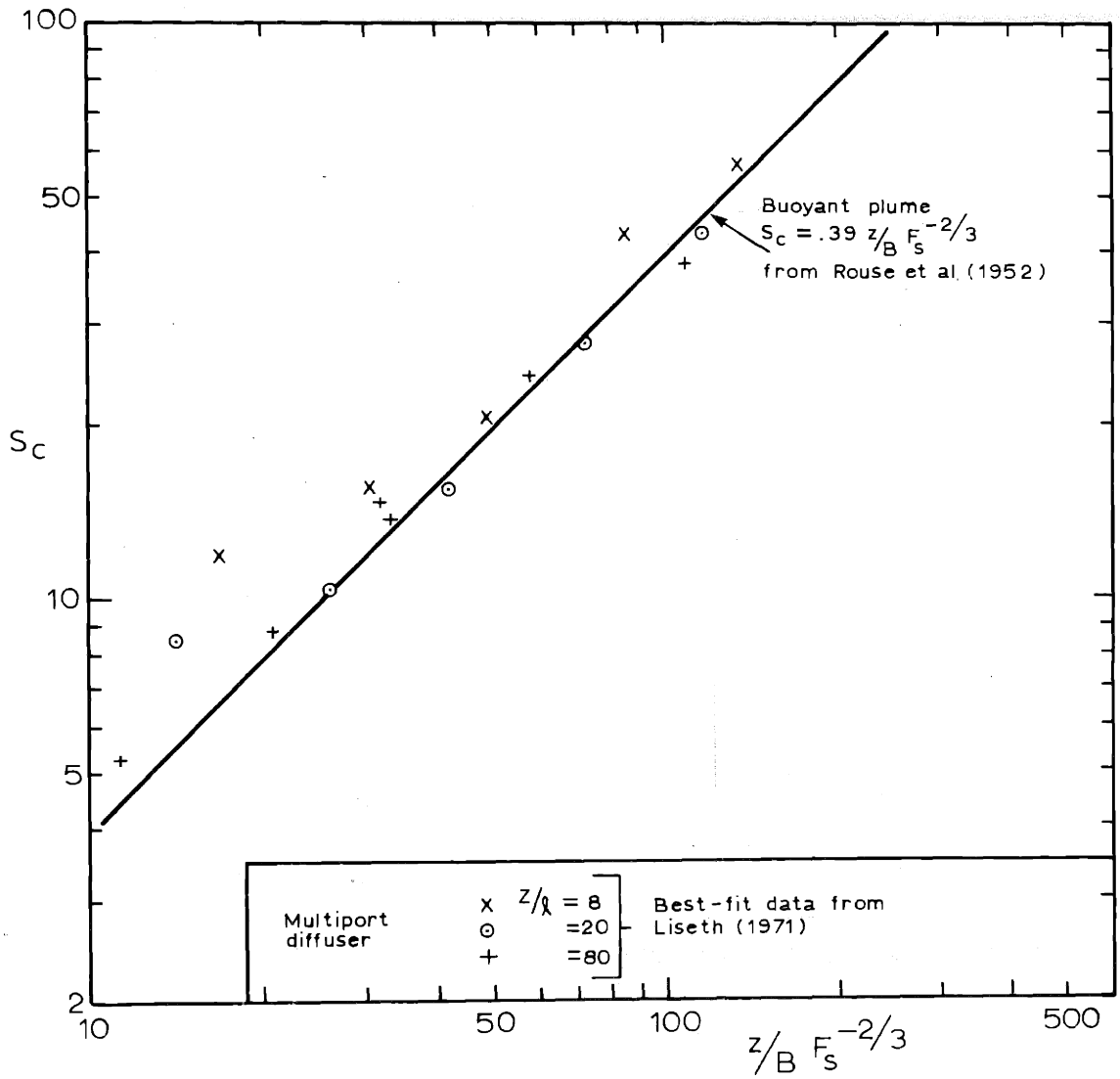

Fig. 2-6: Comparison Between the Centerline Dilutions Above the Point of Merging for a Buoyant Plume and a Multiport Diffuser with Alternating Nozzles

where $\Delta\rho_o = \rho_a - \rho_o$ is the initial density deficiency. Using the definition of the slot Froude number F_s (Eq. (2-25)) Eq. (2-29) can be transformed to give the centerline dilution S_c

$$S_c = \frac{\Delta\rho_o}{\Delta\rho_c} = .39\ z/B\ F_s^{-2/3} \qquad (2\text{-}31)$$

In Figure 2-6 this relationship is compared to a series of data points for z/ℓ = 8, 20 and 80 taken from Liseth's best-fit curves. The data points were converted using the relationships between multiport diffusers and equivalent slot diffusers. Data points for which $z_m/\ell \leq F_n$ were excluded. There is good agreement, again indicating that local details of the discharge geometry, such as nozzle spacing, have indeed a negligible influence on the overall characteristics of multiport diffusers.

2.1.5 Effect of the Free Surface

The density discontinuity at the air-water interface acts as an effective barrier to the upward motion of the buoyant jet. Depending on the kinetic energy of the jet only a small surface rise will occur. As a consequence the jet will spread laterally along the surface in a layer of a certain thickness.

As all the buoyant jet theories discussed in the preceding presume discharge into an unconfined environment, the presence of the free surface is usually accounted for by assuming effective entrainment into the jets up to the lower edge of the surface layer. In the absence of an analytical model for the estimation of the surface layer thickness, experimental values reported by Abraham (1963) are often used. For the slot buoyant jet (after lateral interaction) Abraham gives the layer thickness

to be equal to about 1/4 of the length of the jet trajectory.

2.1.6 Effect of Ambient Density Stratification

Stable density stratification -- that is decreasing density with elevation due to variations in temperature and salinity -- is a common occurrence, in particular for deep water outfalls in oceans and lakes. Under such conditions the jet can reach an equilibrium level and spreads laterally in the form of an internal current when its density becomes equal to the ambient density. Prediction of this phenomenon is important. Jet theories for discharge into linearly stratified ambients are all based on the entrainment concept (Morton et.al. (1956), Fan (1967), Fox (1970)). These methods have also been adapted for arbitrarily stratified stable environments (Ditmars (1969), Shirazi and Davis (1972)).

2.1.7 Effect of Crossflow

A single round buoyant jet discharged into a crossflow u_a gets deflected into the direction of the crossflow. The deflection is affected by two force mechanisms acting on the jet, a pressure drag force

$$F_D = C_D \frac{\rho_a u_a^2}{2} 2b \qquad (2\text{-}32)$$

where C_D is a drag coefficient and a force F_e resulting from the rate of loss of ambient momentum due to entrainment of ambient fluid into the jet

$$F_e = \rho_a u_a (2\pi b v_e) \qquad (2\text{-}33)$$

Characteristic features of jets in cross flow is a significant distortion of the usually symmetric jet profiles to horse-shoe like shapes with a strong wake region. The entrainment concept was modified by Fan (1967)

to

$$v_e = \alpha \left| \bar{u}_a - \bar{u}_c \right| \qquad (2\text{-}34)$$

where the term $\left| \bar{u}_a - \bar{u}_c \right|$ denotes the magnitude of the vector difference between ambient velocity and jet velocity to account for the effect of crossflow velocity on the entrainment mechanism (shearing action). Values for α when still retaining the assumption of Gaussian profiles are considerably larger than in the stagnant case, indicating the increased dilution efficiency in the presence of a crossflow.

No analytical models have yet been advanced for the deflection of a series of interacting round jets as in the multiport diffuser or for a slot diffuser. The deflecting mechanism is highly complicated in these cases with eddying and re-entrainment in the wake zone behind the jet as has been observed experimentally by Cederwall (1971). The assumption of self-similarity is not valid any longer.

2.2 One-Dimensional Average Models for Horizontal Diffuser Discharge into Shallow Water

A severe example of the inadequacy of buoyant jet models developed on the assumption of an unbounded receiving water is given by the horizontal (or near horizontal) diffuser discharge into shallow water. In this case strong surface and bottom interaction causes a vertically fully mixed concentration field downstream of the discharge as illustrated in Figure 1-1d. Making use of this fully mixed condition the problem can be analyzed in a gross fashion.

2.2.1 The Two-Dimensional Channel Case

With the rationale to examine the approximately two-dimensional

flow field which persists in the center portion of a diffuser line Harleman et.al. (1971) studied the following configuration; An array of diffuser nozzles is put between vertical walls of finite length 2L. The channel thus formed is placed in a large basin as shown in Figure 2-7.

The jet discharge sets up a current of magnitude u_m through the entrainment process. Ambient water is accelerated from zero velocity outside in the basin (far field) to velocity u_m in the channel. Inside the channel the current experiences a head loss expressed as usual as $\Sigma k \frac{u_m^2}{2g}$ against frictional resistance, where Σk is the sum of head loss coefficients describing the channel geometry. Upon leaving the channel at the downstream end the velocity head $u_m^2/2g$ is dissipated. Hence the total head loss is

$$\Delta H = (1 + \Sigma k) \frac{u_m^2}{2g} \tag{2-35}$$

In steady state the pressure force caused by this head loss is balanced by the momentum flux of the jet discharge. Thus a one-dimensional momentum equation (per unit channel width) can be written between sections 1 and 2 of Figure 2-7 as

$$\rho_o U_o^2 \frac{D^2\pi}{4} \frac{1}{\ell} = \rho_m g \Delta H H \tag{2-36}$$

The dilution S in the fully mixed flow away is simply given by the volume flux ratio

$$S = \frac{u_m H \ell}{U_o \frac{D^2\pi}{4}} \tag{2-37}$$

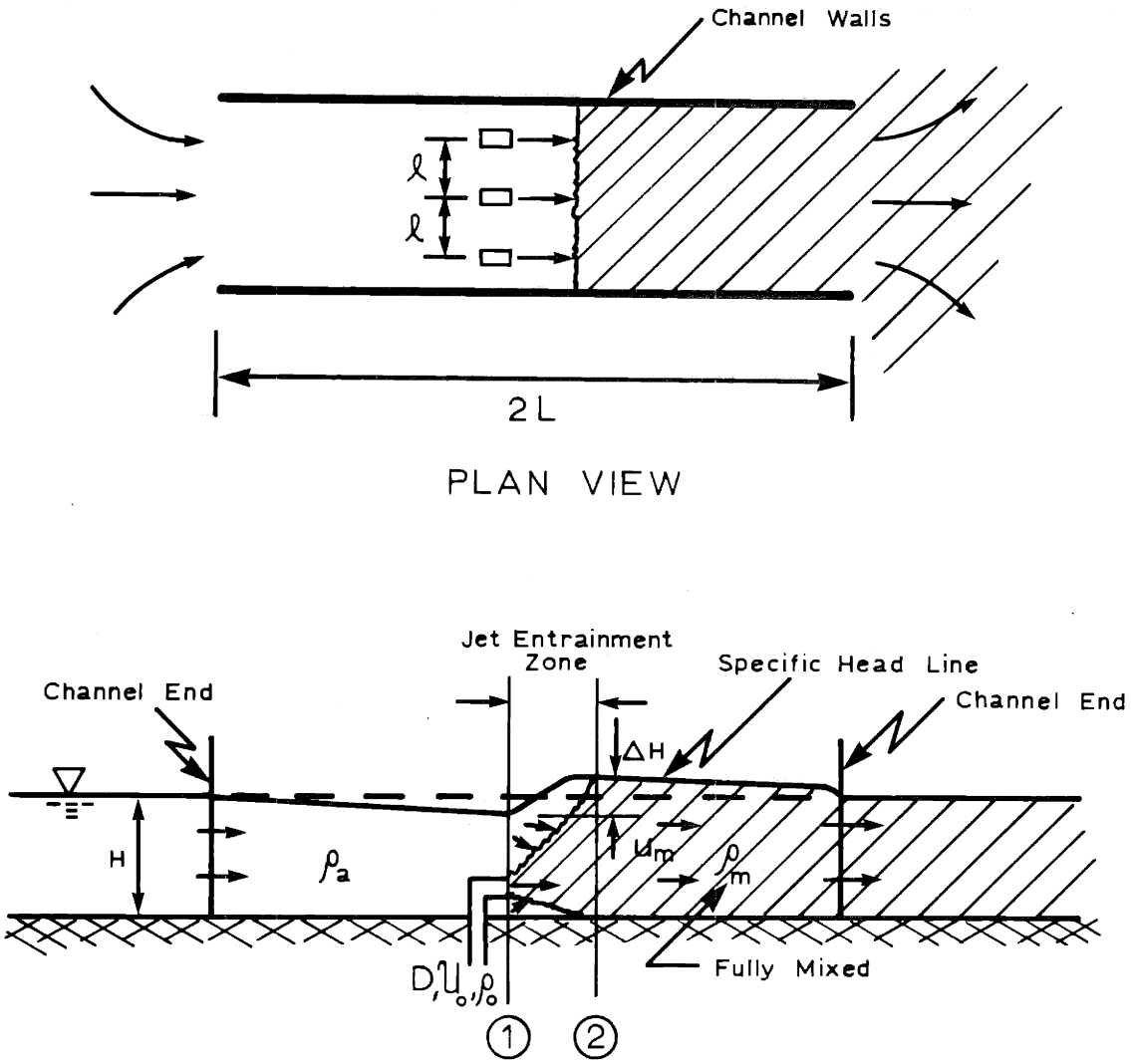

Fig. 2-7: Schematics of Channel Model for a Multiport Diffuser with Horizontal Discharge in Shallow Water

If the approximations $\rho_o/\rho_m \approx 1$, $S/S-1 \approx 1$ (large dilutions) and the definition for the equivalent slot diffuser, Eq. (2-20) are introduced, the dilution can be expressed as

$$S = \frac{1}{(1+\Sigma k)^{1/2}} \left(2 \frac{H}{B}\right)^{1/2} \qquad (2\text{-}38)$$

The striking features of this equation are the independence on the Froude number of the discharge and on the local diffuser geometry, i.e. nozzle spacing. The validity is of course restricted to the fully mixed condition.

Satisfactory agreement with experimental results was found.

2.2.2 The Three-Dimensional Case

The three-dimensional aspects of horizontal diffuser discharge in shallow water with or without the presence of an ambient current u_a were studied by Adams (1972). He observed in the absence of confining walls (as in the previous case) a contraction of the flow downstream of the diffuser line as indicated in Figure 2-8. Using a scaling argument Adams neglected local frictional dissipation and made a one-dimensional inviscid analysis similar to that used for ideal propeller theory (Prandtl (1952)) to arrive at an estimation of the induced average dilution S downstream of the diffuser. Referring to Figure 2-8 the flow is accelerated from a section 1 far behind the diffuser to $u_2 \approx u_3$ at the diffuser line.

After passing over the diffuser line and being mixed with the jet discharge the flow field continues to contract due to its inertia until section 4 where the specific head returns to its original value H.

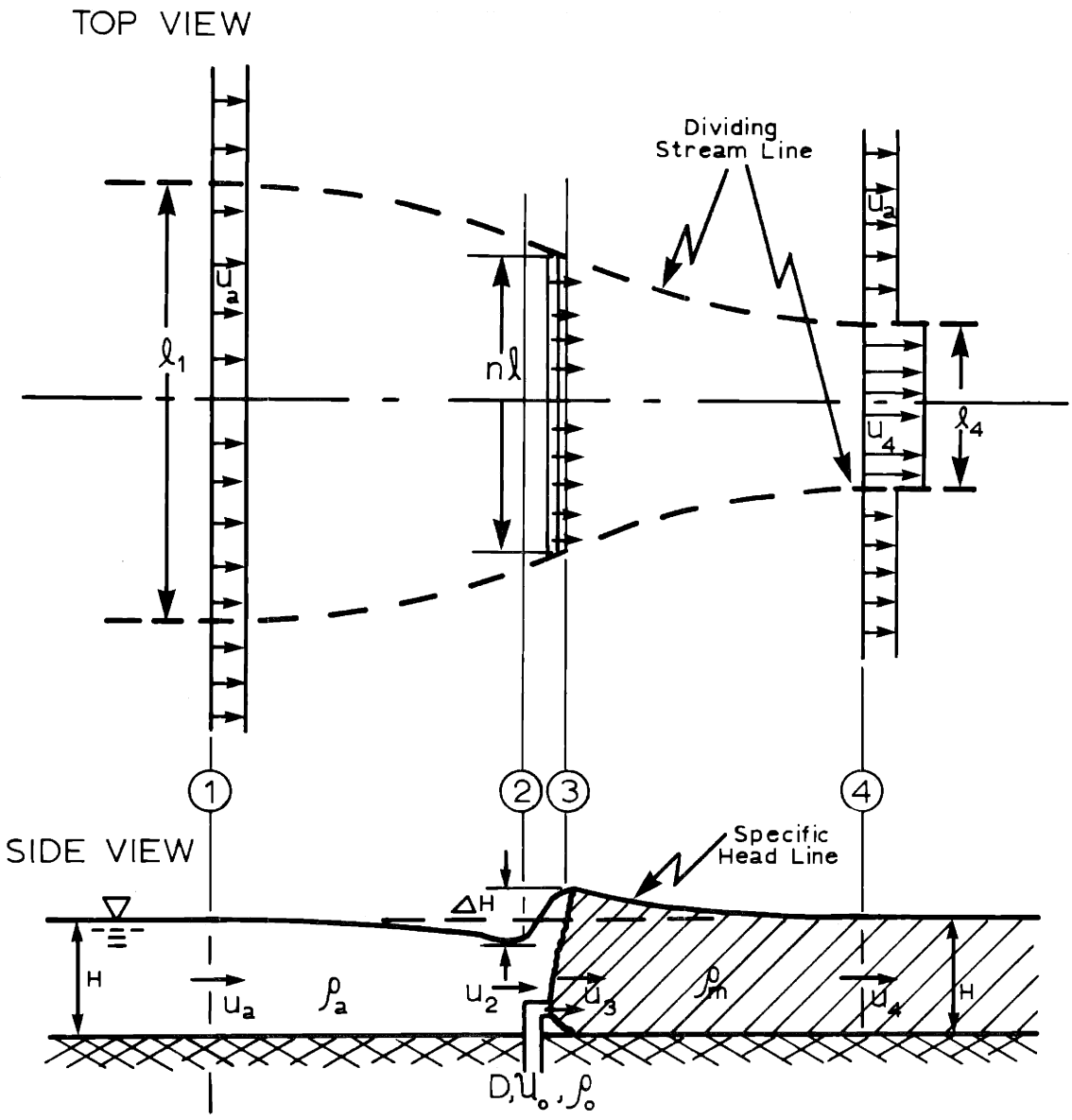

Fig. 2-8: Schematics for One-Dimensional Analysis of a Multiport Diffuser with Horizontal Discharge in Shallow Water

The theory does not treat the region beyond section 4 in which the flow gradually will return to its original velocity u_a through viscous dissipation of the excess velocity head $(u_4^2 - u_a^2)/2g$.

Applying Bernoulli's theorem between sections 1 and 2 and sections 3 and 4 yields the head change across the diffuser

$$\Delta H = \frac{1}{2g} (u_4^2 - u_a^2) \tag{2-39}$$

The pressure force thus produced is balanced by the momentum flux of the diffuser which consists of n nozzles with spacing ℓ, so that, using $\rho_a \approx \rho_o \approx \rho_m$,

$$\rho_a U_o^2 \frac{D^2\pi}{4} \frac{1}{\ell} = \rho_a g \Delta H H \tag{2-40}$$

as in the two-dimensional channel case. Another momentum equation can be written for the control volume between sections 1 and 4

$$\rho_a u_a^2 \ell_1 H + \rho_a U_o^2 \frac{D^2\pi}{4} n = \rho_a u_4^2 \ell_4 H \tag{2-41}$$

For large dilutions

$$u_a \ell_1 H \approx u_4 \ell_2 H \tag{2-42}$$

so that

$$S \approx \frac{u_a \ell_1 H}{U_o \frac{D^2\pi}{4} n} \tag{2-43}$$

Solving the equations and using the equivalent slot jet concept the

dilution is

$$S = \frac{1}{2} \frac{u_a}{U_o} \frac{H}{B} + \frac{1}{2} \left[\left(\frac{u_a}{U_o} \frac{H}{B} \right)^2 + 2 \frac{H}{B} \right]^{1/2} \tag{2-44}$$

For stagnant receiving water, $u_a = 0$, Eq. (2-44) reduces to

$$S = \frac{1}{2} \left(2 \frac{H}{B}\right)^{1/2} \tag{2-45}$$

For the case when the crossflow is very large Eq. (2-44) becomes

$$S = \frac{u_a}{U_o} \frac{H}{B} \tag{2-46}$$

indicating proportional mixing with the oncoming flow. The contraction coefficient c_c of the flow between the diffuser and section 4 is found to be

$$c_c = \frac{\ell_4}{n\ell} = \frac{1}{2} + \frac{1}{2} \frac{u_a}{u_4} \tag{2-47}$$

which reduces to

$$c_c = \frac{1}{2} \tag{2-48}$$

in the case of zero ambient flow.

It is illuminating to compare Eq. (2-42) with Eq. (2-38) for the two-dimensional channel case making the similar assumption of neglecting friction inside the channel ($\Sigma k = 0$), namely

$$S = \left(2 \frac{H}{B}\right)^{1/2} \tag{2-49}$$

Thus the predicted dilution capacity of the three-dimensional case is one half of the two-dimensional channel. The difference is attributable

to the contraction which occurs in the former case which causes more velocity head to be dissipated in the region beyond.

Despite the approximations involved -- no bottom friction, no diffusion at the boundary of the current -- Adams found satisfactory agreement with experimentally determined average dilutions in a section downstream from the discharge (see Chapter 7).

2.3 Appraisal of Previous Knowledge About the Characteristics of a Multiport Diffuser

The objective of predictive models for multiport diffusers is the determination of velocities and concentration distributions induced by the diffuser discharge. The review of existing prediction techniques has shown two constrasting limiting cases of diffuser discharge: discharge in practically unconfined deep water in form of buoyant jets and discharge into fairly shallow water with extreme boundary interaction resulting in a uniformly mixed current. This striking difference in the resultant behavior immediately suggests questions regarding the diffuser performance in the intermediate range (confined receiving water) and the applicability of such "simple" models as discussed in the review -- simple in the sense that they consider only one dominating physical process.

Detailed observations regarding the degree of established physical understanding can be summarized;

A. Areas of Adequate Understanding

In these problem areas understanding has been achieved to such a point that fairly reliable predictions can be made.

1) Buoyant Jets in Deep Water

The different theories for round and slot buoyant jets have been largely verified in laboratory experiments. Predictions between models do not vary appreciably although various assumptions regarding the jet characteristics have been made. Choice of a particular model should be based on the physical "correctness" of these assumptions and on the applicability to different situations. In this respect an integral analysis with variable entrainment coefficients depending on the local buoyant characteristics seems to be preferable.

2) Interference of Round Buoyant Jets

The lateral interference of the round buoyant jets issuing from a multiport diffuser to form a two-dimensional jet has not yet been studied experimentally. However, reasonable assumptions regarding a transition criterion in the analytical treatment can be made. Comparisons show that the flow field produced by a multiport diffuser is similar to that one produced by an "equivalent slot diffuser". Hence for mathematical convenience this concept should be retained. The same argument pertains to the merging of jets above the diffuser line in the case of alternatingly discharging nozzles as studied by Liseth.

3) Horizontal Diffusers in Shallow Water

Horizontal diffusers discharging into fairly shallow water produce full vertical mixing due to strong boundary inter-

actions. Predictions of average dilutions downstream of the discharge line can be made using Adams' experimentally validated relationship.

B. Areas of Insufficient Knowledge

1) Effect of a Vertically Confined Flow Region

This is the general case of a diffuser discharge. Solution of this problem requires the assessment of:

a) The effect of the free surface. Prediction of the thickness of the surface impingement layer as a function of jet parameters. This defines the upper level up to which effective entrainment takes place into the jet.

b) The stability of the surface layer. The flow spreading from the line of impingement can be unstable. Hence water can be re-entrained into the jet region.

c) The flow away from the diffuser line in the form of a density current.

d) The effect of bottom interaction. Jets discharged horizontally and close to the bottom can become attached to the bottom.

Solution of this general problem will encompass the limiting cases of discharge in fairly deep and fairly shallow water. Hence, criteria of applicability of the "simple" models reported above can be presented.

2) Three-Dimensional Behavior

As exemplified by the case of horizontal diffuser discharge

into shallow receiving water which produces a flow away with significant contraction thus reducing dilution, three-dimensional aspects of the diffuser flow field are extremely important.

3) Effect of Crossflow

The effect of crossflow has only been investigated for the single round jet. No quantitative information on interacting diffuser jets or slot jets is available. In general the three-dimensional diffuser induced flow field is superposed on, but also modified by, the ambient flow field. The overall layout of the diffuser axis with respect to the ambient current direction is an important factor, as shown by experimental investigations reported by Harleman, et.al. (1971).

All these problem areas are addressed in the following chapters of this study.

III. THEORETICAL FRAMEWORK: TWO-DIMENSIONAL CHANNEL MODEL

3.1 Basic Approach

The review of the preceding chapter showed the limitations of existing theories for the prediction of multiport diffuser behavior. Analytical models are available only for the extreme cases of (1) buoyant jets in deep water, neglecting the dynamic effects caused by the free surface, and (2) discharge into shallow water with strong boundary interaction resulting in a vertically mixed current. No mathematical models have been developed for the intermediate range in which boundary effects are important and no criteria of applicability for the existing models have been derived. The present study attempts to fulfill this need.

The complexity of the general three-dimensional problem of multiport diffuser discharge is such that no single analytical description (a single set of governing equations with the appropriate boundary conditions) of the fluid flow can be solved by available methods. Hence, the following approach is undertaken in the development of a predictive model:

1) The theoretical treatment is limited to the diffuser-induced steady-state flow field without the presence of an ambient cross flow.
2) A two-dimensional "channel model" simulates the predominantly two-dimensional flow field which is postulated to exist in the center portion of a three-dimensional diffuser. This is illustrated in Figure 3-1 for the case of a stable flow away zone. The two-dimensional

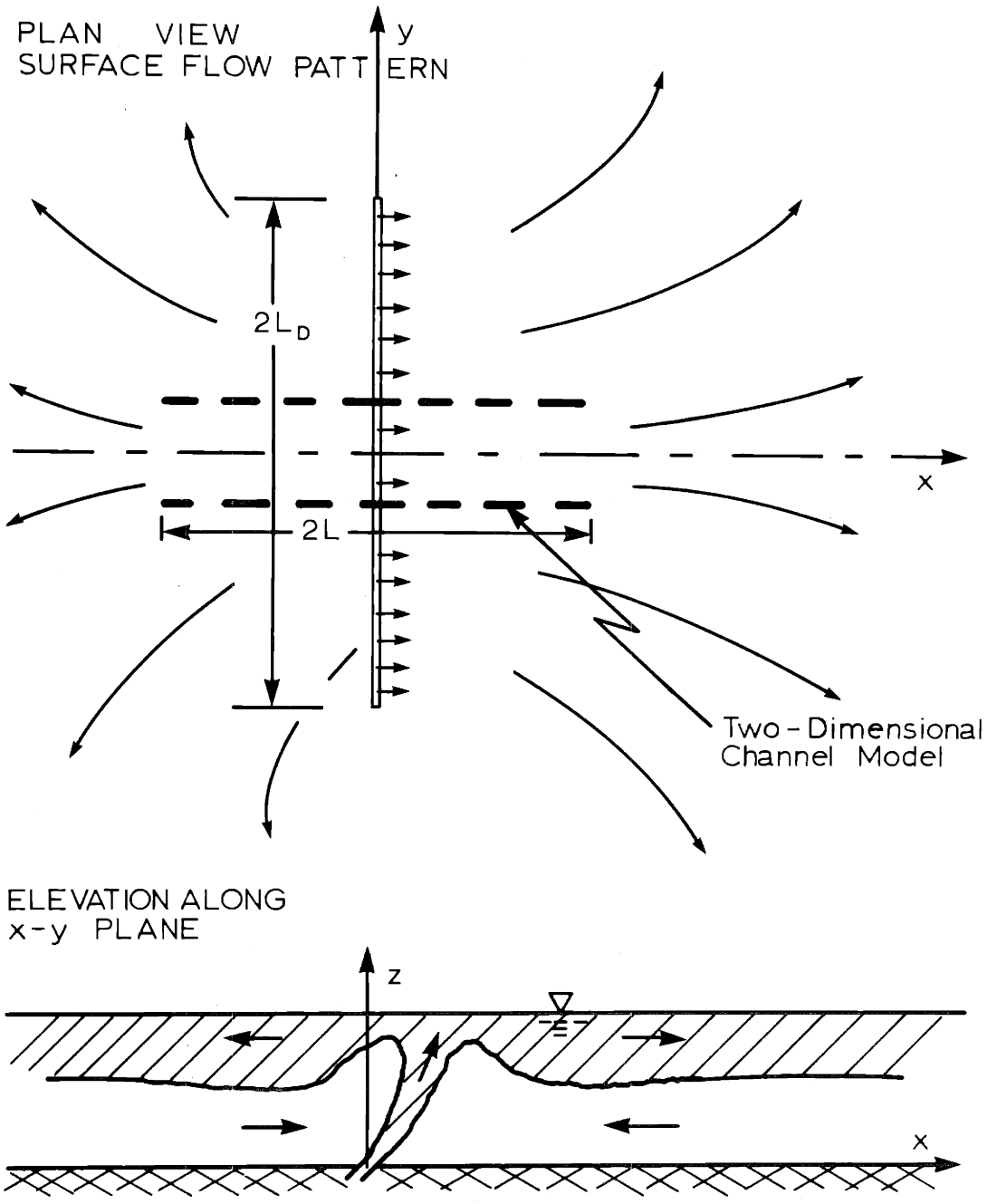

Fig. 3-1: Three-Dimensional Flow Field for a Submerged Diffuser

Two-Dimensional Behavior in Center Portion

(Stable Flow Away Zone)

channel model assumes a diffuser section bounded laterally by walls of finite length, 2L. This conceptualization allows the analysis of the vertical and longitudinal variation of the diffuser-induced flow field.

3) Through a quantitative analysis regarding far-field effects (frictional resistance of the flow away zone) the length, 2L, of the two-dimensional channel model is linked to the length of the three-dimensional diffuser, $2L_D$. In this manner theoretical predictions of the two-dimensional channel model become applicable to the general three-dimensional case.

4) The interaction of the diffuser induced flow with a cross flow in the receiving water body is studied experimentally.

In this chapter the theoretical framework for the treatment of the flow distribution in the two-dimensional "channel model" is developed. The diffuser discharge exhibits several distinct flow regions. Analytical treatment of each of these regimes becomes possible by introducing approximations to the governing equations of fluid motion.

Matching of the solutions at the boundaries of the various regions results in an overall prediction of the two-dimensional channel flow field. In Chapter 4 the quantitative comparison between the flow fields in the two-dimensional "channel model" and the general three-dimensional case is made.

In Chapter 6, the theoretical model predictions are compared with experimental results. Experiments were performed both for the two-dimen-

sional channel model and the three-dimensional case.

In Chapter 7, the modification of the diffuser-induced flow field through the effects of ambient cross flow is studied experimentally. For the purpose of establishing scaling relationships the analytical treatment is directed toward the discharge of heated water. This is motivated by the fact that thermal diffusers located in shallow water, with low buoyancy of the discharge, typically are strongly influenced by the finite depth of the receiving water body.

3.2 Problem Definition: Two-Dimensional Channel Model

Referring to Figure 3-2 the following problem is considered: The steady-state discharge of heated water with temperature T_o and velocity U_o through a slot with width B and vertical orientation θ_o into a channel of uniform depth H, unit width and length 2L. The height h_s of the slot opening above the bottom is small compared to the total depth,

$$h_s/H << 1 \qquad (3\text{-}1)$$

The channel opens at both ends into a large reservoir.

The rationale for studying this model is provided by:

a) In the mathematical treatment a multiport diffuser can be represented by an equivalent slot diffuser as discussed in the previous chapter (Eq. (2-20)).

b) The channel model approximates the predominantly two-dimensional flow field which is postulated to exist in the center portion of a three-dimensional diffuser as shown in Figure 3-1. It will be shown later that

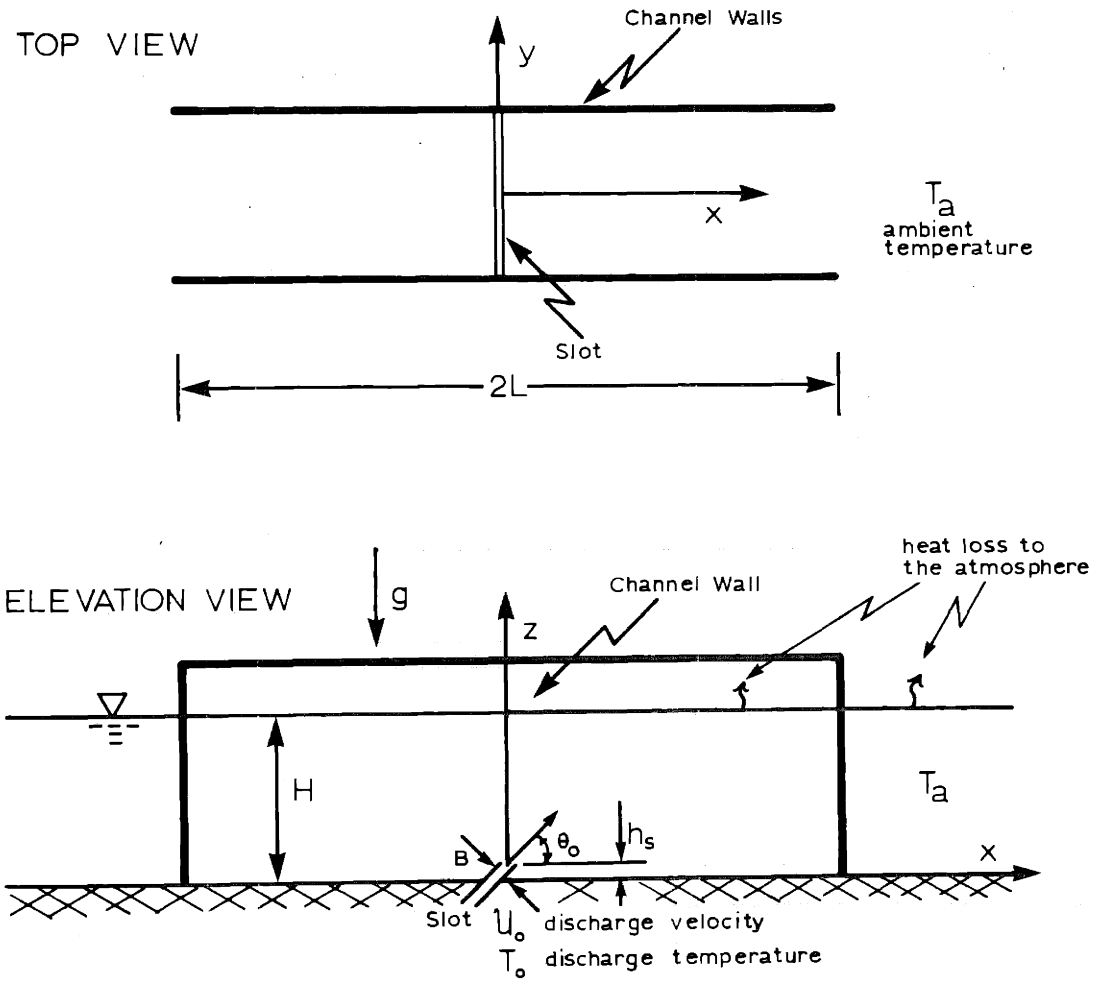

Fig. 3-2: Problem Definition: Two-Dimensional Channel Model

under certain conditions, namely instability of the flow away, the diffuser discharge does not exhibit this predominantly two-dimensional region. However, through variation of the horizontal nozzle orientation it is possible to control the three-dimensional flow so as to approximate the two-dimensional behavior. In the interest of achieving high dilutions this control is desirable. These three-dimensional aspects of diffuser discharge are treated in more detail in Chapters 4 and 6.

3.3 Solution Method

For the problem defined, the governing equations of fluid motion and heat conservation are written under the following assumptions:

1) The flow field is two-dimensional in the vertical or xz-plane. No lateral variations with y occur.
2) The flow is turbulent, but steady in the mean. Local flow quantities are composed of a mean and a fluctuating component.
3) Molecular transport processes for momentum, mass and heat are neglected in comparison to transport by the fluctuating eddy velocities.
4) The Boussinesq approximation is applied. Density deviations $\Delta\rho$ from the ambient density ρ_a introduced by the diffuser discharge are small compared to the local density $\rho(x,z)$

$$\frac{\Delta\rho}{\rho} << 1 \qquad (3\text{-}2)$$

Hence ρ is approximated by ρ_a in all terms except the gravitational (buoyant) terms. Furthermore the mass conservation equation is replaced by the equation of incompressibility.

5) In the heat conservation equation, the heat production due to viscous dissipation is neglected in comparison with the heat added by the heated discharge.

With these approximations, the time-averaged equations of motion and heat conservation are

$$\frac{\partial u}{\partial x} + \frac{\partial w}{\partial z} = 0 \tag{3-3}$$

$$\rho_a u \frac{\partial u}{\partial x} + \rho_a w \frac{\partial u}{\partial z} = - \frac{\partial p}{\partial x} - \rho_a \frac{\partial \overline{w'^2}}{\partial x} - \rho_a \frac{\partial \overline{u'w'}}{\partial z} \tag{3-4}$$

$$\rho_a u \frac{\partial w}{\partial x} + \rho_a w \frac{\partial w}{\partial z} = - \frac{\partial p}{\partial z} + \rho g - \rho_a \frac{\partial \overline{u'w'}}{\partial x} - \rho_a \frac{\partial \overline{w'^2}}{\partial z} \tag{3-5}$$

$$u \frac{\partial T}{\partial x} + w \frac{\partial T}{\partial z} = - \frac{\partial \overline{u'T'}}{\partial x} - \frac{\partial \overline{w'T'}}{\partial z} \tag{3-6}$$

in which

x,z = Cartesian coordinates, with z upwards against the gravity force

u,w = mean velocities in x,z directions

u',w' = velocity fluctuations

ρ = mean local density

ρ_a = constant ambient density

p = mean pressure

T = mean temperature

T' = temperature fluctuation

and the bar denotes the time-averaged turbulent transfer terms. A linearized equation of state relates density and temperature

$$\rho = \rho_a [1 - \beta(T - T_a)] \tag{3-7}$$

where β is the coefficient of thermal expansion. The simultaneous solution of Equations (3-3) to (3-7) with given boundary conditions determines the flow and temperature field. No such general solution is possible by present analytical techniques.

However, inspection of actual diffuser performance -- as can be made in a laboratory experiment -- indicates that the flow field is actually made up of several regions with distinct hydrodynamic properties. By making use of these properties, additional approximations to the governing equations can be introduced. This enables solutions to be obtained by analytical or simple numerical methods within these regions. By matching these solutions, an overall description of the flow-field can be given.

The observed vertical structure of the flow field for a diffuser discharge within the two-dimensional channel is indicated in Figure 3-3 for the case of a stable near-field zone without re-entrainment. Four flow regions can be discerned in this general case:

1) Buoyant Jet Region: Forced by its initial momentum and under the action of gravity, the two-dimensional slot

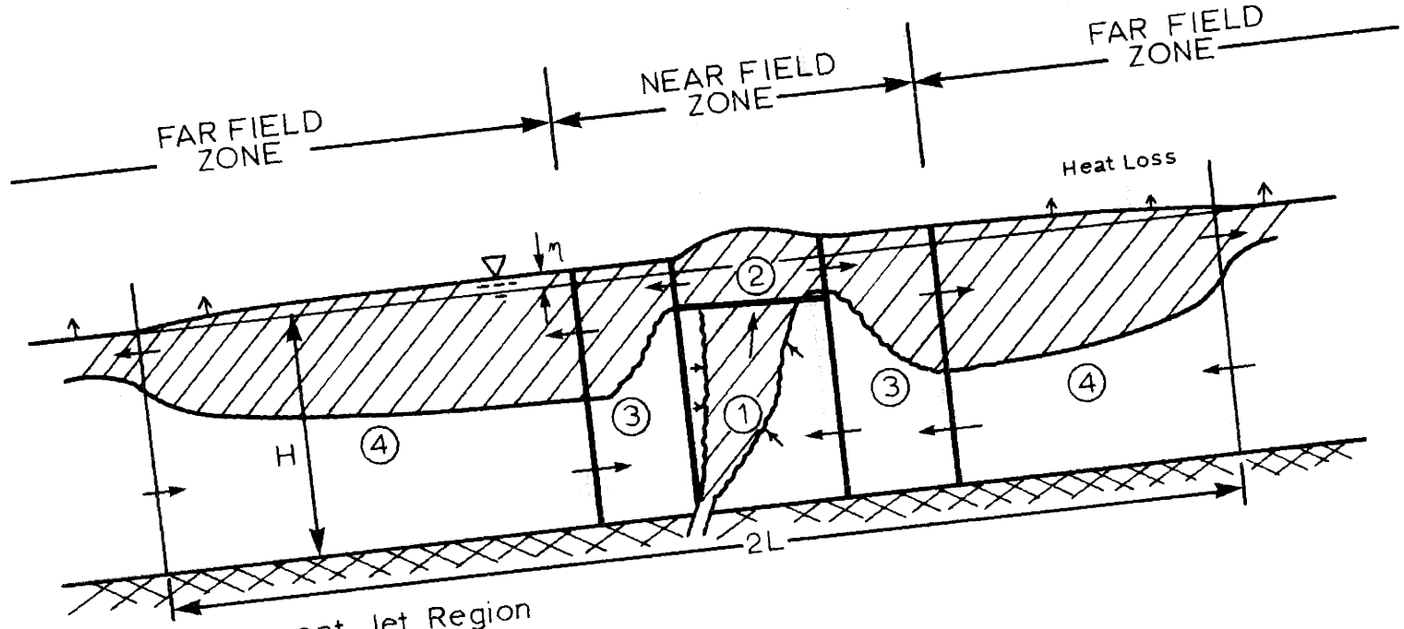

① Buoyant Jet Region
② Surface Impingement Region
③ Hydraulic Jump Region
④ Stratified Counterflow Region

Fig. 3-3: Vertical Structure of Diffuser Induced Flow Field

jet rises towards the surface entraining ambient water.

2) Surface Impingement Region: The presence of the free surface, with its density discontinuity, diverts the impinging jet in the horizontal directions.

3) Hydraulic Jump Region: An abrupt transition between the high velocity flow in the surface impingement region to lower velocities in the flow away zone is provided by an internal hydraulic jump.

4) Stratified Counterflow Region: A counterflow system is set up as a buoyancy-driven current in the upper layer and an entrainment-induced current in the lower layer.

Region 1, 2 and 3 constitute the near-field zone; region 4 and the water body outside the channel, the far-field zone. Surface heat loss to the atmosphere is only important in the far-field zone due to the areal restriction of the near-field.

The analytical treatments for these four dominant flow regions are given in the following sections.

3.4 Dominant Flow Regions

3.4.1 Buoyant Jet Region

3.4.1.1 Approximations and Governing Equations

The definition of a local coordinate system s, n with velocity components $\tilde{u}$, $\tilde{v}$ is convenient for the upward curved jet trajectory, as shown in Figure 3-4.

In terms of this coordinate system the governing Equations (3-3)

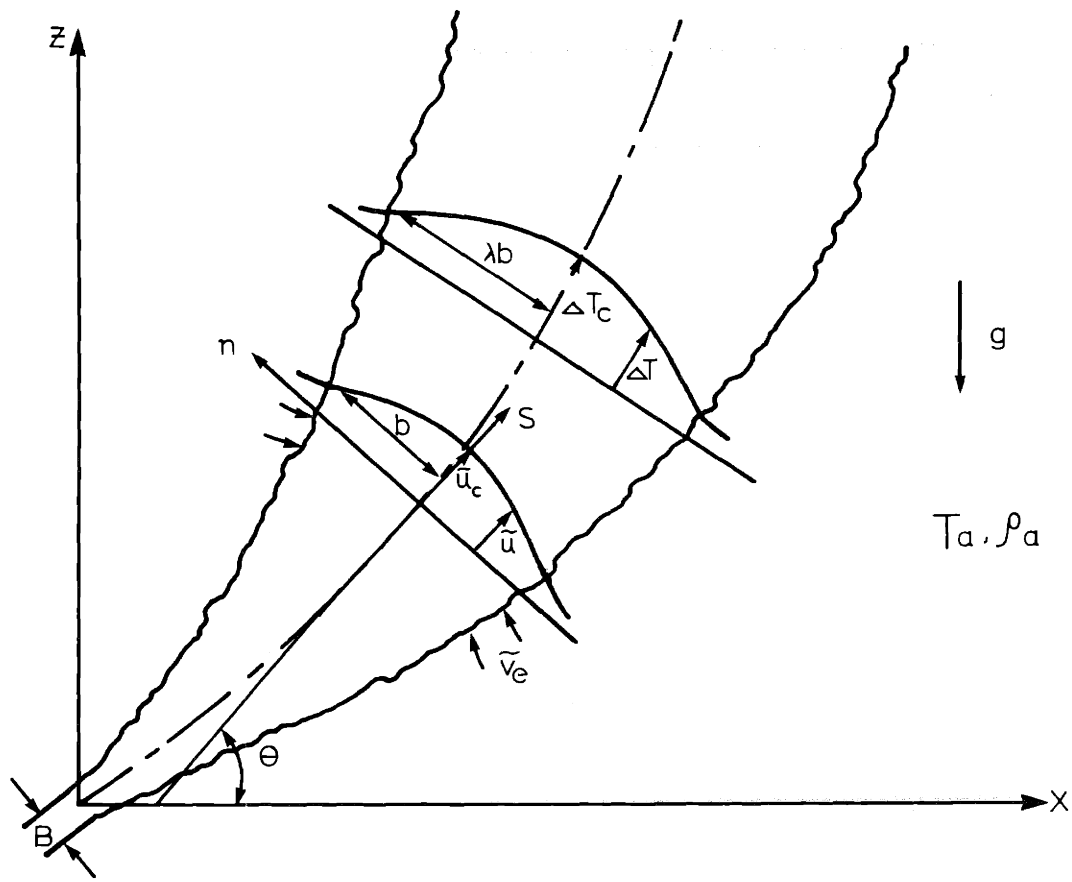

Fig. 3-4: Definition Diagram for Buoyant Jet Region

to (3-6) can be transformed

$$\frac{\partial \tilde{u}}{\partial s} + \frac{\partial \tilde{v}}{\partial n} = 0 \tag{3-8}$$

$$\rho_a \tilde{u} \frac{\partial \tilde{u}}{\partial s} + \rho_a \tilde{v} \frac{\partial \tilde{u}}{\partial n} = -\frac{\partial p}{\partial s} + \rho g \sin\theta - \rho_a \frac{\partial \overline{\tilde{u}'^2}}{\partial s} - \rho_a \frac{\partial \overline{\tilde{u}'\tilde{v}'}}{\partial n} \tag{3-9}$$

$$\rho_a \tilde{u} \frac{\partial \tilde{v}}{\partial s} + \rho_a \tilde{v} \frac{\partial \tilde{v}}{\partial n} = -\frac{\partial p}{\partial n} + \rho g \cos\theta - \rho_a \frac{\partial \overline{\tilde{u}'\tilde{v}'}}{\partial s} - \rho_a \frac{\partial \overline{\tilde{v}'^2}}{\partial n} \tag{3-10}$$

$$\tilde{u} \frac{\partial T}{\partial s} + \tilde{v} \frac{\partial T}{\partial n} = -\frac{\partial \overline{\tilde{u}'T'}}{\partial s} - \frac{\partial \overline{\tilde{v}'T'}}{\partial n} \tag{3-11}$$

with θ = angle between s and x axes.

From jet observations the following approximations are inferred:

1) The flow phenomenon is predominantly in the longitudinal direction,

$$\frac{b}{s} << 1 \tag{3-12}$$

By continuity it follows that induced velocities in the lateral direction are small

$$\frac{\tilde{v}}{\tilde{u}} << 1 \tag{3-13}$$

This boundary-layer approximation allows the neglect of certain terms in the governing equations which are found to be of secondary importance by a straightforward scaling procedure using Equations (3-12) and (3-13).

2) The pressure outside the jet proper is hydrostatic, p_h, and satisfies

$$\frac{\partial p_h}{\partial z} - \rho_a g = 0 \tag{3-14}$$

Consequently, the pressure in the jet itself can be written as

$$p = p_h + p_r \tag{3-15}$$

where p_r is a reduced pressure, namely the pressure disturbance due to jet motion.

The two components of Eq. (3-14) in s, r are

$$\begin{aligned} \frac{\partial p_h}{\partial s} - \rho_a g \sin\theta &= 0 \\ \frac{\partial p_h}{\partial n} - \rho_a g \cos\theta &= 0 \end{aligned} \tag{3-16}$$

Noting that

$$\rho = \rho_a + \Delta\rho \tag{3-17}$$

where $\Delta\rho$ is the density deficiency due to the temperature anomaly $\Delta T = T - T_a$, pressure and gravitational terms in the momentum equations (3-9) and (3-10) can be simplified as

$$-\frac{\partial p}{\partial s} + \rho g \sin\theta = -\frac{\partial p_r}{\partial s} + \Delta\rho g \sin\theta \tag{3-18}$$

and

$$-\frac{\partial p}{\partial n} + \rho g \cos\theta = -\frac{\partial p_r}{\partial n} + \Delta\rho g \cos\theta \tag{3-19}$$

respectively.

Experimental observations have shown that the pressure deviation p_r is practically negligible in the absence of boundaries. In the diffuser problem boundaries are given by the bottom and the free surface. Thus in making the approximation

$$p_r = 0 \tag{3-20}$$

it is implied that the jet stays clear of the bottom (as jet attachment) and that the effect of the free surface where the pressure deviation is documented by the surface hump (see Fig. 3-3) is limited to the jet impingement region. This is discussed in more detail in the consideration of the jet impingement region.

The simplified governing equations for the buoyant slot jet are, using the continuity equation in the transformation of the convective terms,

$$\frac{\partial \tilde{u}}{\partial s} + \frac{\partial \tilde{v}}{\partial n} = 0 \tag{3-21}$$

$$\frac{\partial \tilde{u}^2}{\partial s} + \frac{\partial \tilde{u}\tilde{v}}{\partial n} = + \frac{\Delta\rho}{\rho_a} g \sin\theta - \frac{\partial \overline{\tilde{u}'\tilde{v}'}}{\partial n} \tag{3-22}$$

$$0 = + \frac{\Delta\rho}{\rho_a} g \cos\theta - \frac{\partial \overline{\tilde{v}'\tilde{v}'}}{\partial n} \tag{3-23}$$

$$\frac{\partial \tilde{u}\Delta T}{\partial s} + \frac{\partial \tilde{v}\Delta T}{\partial n} = - \frac{\partial \overline{\tilde{v}'T'}}{\partial n} \tag{3-24}$$

The lateral momentum equation (3-23) is replaced by the horizontal momentum equation, a linear combination of (3-22) and (3-23),

$$\left(\frac{\partial \tilde{u}^2}{\partial s} + \frac{\partial \tilde{u}\tilde{v}}{\partial n} \right) \cos\theta = - \frac{\partial \overline{\tilde{u}'\tilde{v}'}}{\partial n} \cos\theta + \frac{\partial \overline{\tilde{v}'\tilde{v}'}}{\partial n} \sin\theta \qquad (3\text{-}25)$$

which relates directly to the boundary condition of horizontal momentum flux at the slot opening as is shown below. The further solution procedure uses the entrainment concept proposed by Morton et al. (1956). A variable entrainment coefficient dependent on the local buoyant characteristics of the jet is assumed of the form Eq. (2-11). The method of obtaining this dependence follows the procedure used by Fox (1970) for vertical round and slot jets and by Hirst (1971) for non-vertical round jets. For this purpose a simplified energy equation describing the flux of mechanical energy in the longitudinal direction with velocity $\tilde{u}$ is found from Eq. (3-22) as

$$\tilde{u} \frac{\partial \tilde{u}^2}{\partial s} + \tilde{u} \frac{\partial \tilde{u}\tilde{v}}{\partial n} = + \frac{\Delta\rho}{\rho_a} g \tilde{u} \sin\theta - \tilde{u} \frac{\partial \overline{\tilde{u}'\tilde{v}'}}{\partial n} \qquad (3\text{-}26)$$

or by virtue of the continuity equation

$$\frac{\partial \tilde{u}^3}{\partial s} + \frac{\partial \tilde{u}^2\tilde{v}}{\partial n} = + 2 \frac{\Delta\rho}{\rho_a} g \tilde{u} \sin\theta - 2\tilde{u} \frac{\partial \overline{\tilde{u}'\tilde{v}'}}{\partial n} \qquad (3\text{-}27)$$

Based on experimental evidence the following similarity functions are specified for $\tilde{u}$ and T

$$\tilde{u}(s,n) = \tilde{u}_c(s) e^{-\left(\frac{n}{b}\right)^2} \qquad (3\text{-}28)$$

$$\Delta T(s,n) = \Delta T_c(s) e^{-\left(\frac{n}{\lambda b}\right)^2} \qquad (3\text{-}29)$$

in which λ is a dispersion ratio between momentum and heat or mass. The profile for $\Delta\rho$ is related to (3-29) by the equation of state, thus

$$\Delta\rho(s,n) = \Delta\rho_c(s)e^{-\left(\frac{n}{\lambda b}\right)^2} \tag{3-30}$$

$\tilde{u}_c$, T_c , $\Delta\rho_c$ are centerline values.

These functions are introduced into Eqs. (3-21), (3-22), (3-24) and (3-25) and the equations are integrated in the normal direction n . If the boundary conditions

$$\begin{aligned} \overline{\tilde{u}'\tilde{v}'} &\to 0 \\ \overline{\tilde{v}'\tilde{v}'} &\to 0 \qquad \text{as} \qquad n \to \pm\infty \\ \overline{\tilde{v}'T'} &\to 0 \\ \tilde{v} &\to \mp\, \tilde{v}_e \\ \Delta T &\to 0 \end{aligned} \tag{3-31}$$

are noted, the resulting ordinary differential equations are,

$$\frac{d}{ds}\left[\int_{-\infty}^{\infty} \tilde{u}_c\, e^{-\left(\frac{n}{b}\right)^2} dn\right] - 2\,\tilde{v}_e = 0 \tag{3-32}$$

$$\frac{d}{ds}\left[\int_{-\infty}^{\infty} \tilde{u}_c^2\, e^{-2\left(\frac{n}{b}\right)^2} dn\right] = + \int_{-\infty}^{\infty} \frac{\Delta\rho_e}{\rho_a}\, g \sin\theta\; e^{-\left(\frac{n}{\lambda b}\right)^2} dn \tag{3-33}$$

$$\frac{d}{ds}\left[\int_{-\infty}^{\infty} \tilde{u}_c^2 \cos\theta\, e^{-2\left(\frac{n}{b}\right)^2} dn\right] = 0 \qquad (3\text{-}34)$$

$$\frac{d}{ds}\left[\int_{-\infty}^{\infty} \tilde{u}_c\, \Delta T_c\, e^{-\left(1+\frac{1}{\lambda^2}\right)\left(\frac{n}{b}\right)^2} dn\right] = 0 \qquad (3\text{-}35)$$

The normal velocities at the jet boundary, $\tilde{v}_e$, i.e. the "entrainment velocity" is assumed to be related to the characteristic jet velocity $\tilde{u}_c$

$$|\tilde{v}_e| = \alpha\, \tilde{u}_c \qquad (3\text{-}36)$$

This constitutes the entrainment concept by Morton et al. After evaluation of the integrals the equations become

continuity:

$$\frac{d}{ds}(\tilde{u}_c\, b) = \frac{2}{\sqrt{\pi}}\, \alpha\, \tilde{u}_c \qquad (3\text{-}37)$$

axial momentum:

$$\frac{d}{ds}(\tilde{u}_c^2\, b) = \sqrt{2}\, \frac{\Delta\rho_c}{\rho_a}\, g\, \lambda b \sin\theta \qquad (3\text{-}38)$$

horizontal momentum:

$$\frac{d}{ds}(\tilde{u}_c^2\, b \cos\theta) = 0 \qquad (3\text{-}39)$$

heat conservation:

$$\frac{d}{ds}(\tilde{u}_c\, \Delta T_c\, b) = 0 \qquad (3\text{-}40)$$

or alternatively instead of (3-40)

conservation of density deficiency:

$$\frac{d}{ds}\,(\tilde{u}_c\,\Delta\rho_c\,b) \;=\; 0 \qquad (3\text{-}41)$$

3.4.1.2 Dependence of the Entrainment on Local Jet Characteristics

Experimentally deduced values for α as reported in the previous chapters, Eqs. (2-18) and (2-19) show the dependence of α with the buoyant jet characteristics. This dependence can be examined using the energy equation (3-27) following Fox's approach for the vertical jet. To integrate this equation it is assumed that the stress $\overline{\tilde{u}'\tilde{v}'}$ is distributed in a similarity profile $f(n/b)$ and related to the center-line velocity $\tilde{u}_c$

$$\overline{\tilde{u}'\tilde{v}'} \;=\; \tilde{u}_c^2 f\left(\frac{n}{b}\right) \qquad (3\text{-}42)$$

There is experimental support to this assumption (Mih and Hoopes (1972)) but the accuracy of the data does not allow specification of f. With (3-42) and the other similarity profiles the energy equation (3-27) is integrated to

$$\frac{d}{ds}\left[\int_{-\infty}^{\infty} \tilde{u}_c^3\, e^{-3(n/b)^2}\, dn\right] \;=\; 2\int_{-\infty}^{\infty} \frac{\Delta\rho_c}{\rho_a}\, g\, \tilde{u}_c \sin\theta\, e^{-(1+\frac{1}{\lambda^2})(\frac{n}{b})^2}\, dn \qquad (3\text{-}43)$$

$$- 2\int_{-\infty}^{\infty} \tilde{u}_c^3\, e^{-(n/b)^2}\, \frac{d}{dn} f\,(n/b)\, dn$$

and after evaluation

$$\frac{d}{ds}\,(u_c^3\, b\, \sqrt{\pi/3}\,) \;=\; 2\sqrt{\pi}\sqrt{\frac{\lambda^2}{1+\lambda^2}}\,\frac{\Delta\rho_c}{\rho_a}\, g\, \tilde{u}_c\, b \sin\theta \;-\; 2\,\tilde{u}_c^3\, I \qquad (3\text{-}44)$$

where

$$I = \int_{-\infty}^{\infty} e^{-(n/b)^2} \frac{d}{dn} f(n/b)\, dn \tag{3-45}$$

Noting the identity

$$\frac{d}{ds}(\tilde{u}_c^3 b) = 2\tilde{u}_c \frac{d}{ds}(\tilde{u}_c^2 b) - \tilde{u}_c^2 \frac{d}{ds}(\tilde{u}_c b) \tag{3-46}$$

Equation (3-44) can be transformed using the axial momentum Eq. (3-38) to

$$\frac{d}{ds}(\tilde{u}_c b) = 2\frac{\Delta\rho_c}{\rho_a} g b \frac{1}{\tilde{u}_c}\left[\sqrt{2}\lambda - \sqrt{3}\sqrt{\frac{\lambda^2}{1+\lambda^2}}\sin\theta\right] + 2\sqrt{\frac{3}{\pi}}\tilde{u}_c I \tag{3-47}$$

When this equation is compared with the continuity Eq. (3.37) the entrainment coefficient α is expressed as

$$\alpha = \sqrt{3} I + \left[\sqrt{2} - \sqrt{\frac{3}{1+\lambda^2}}\sin\theta\right]\frac{\sqrt{\pi}\lambda}{F_L^2} \tag{3-48}$$

if a local densimetric Froude number is defined

$$F_L = \frac{\tilde{u}_c}{\left(\frac{\Delta\rho_c}{\rho_a} g b\right)^{1/2}} \tag{3-49}$$

Equation (3-48) is similar to Fox's equation except for the factor $\sin\theta$. The expression (3-48) consists of two parts

$$\alpha = \alpha_1 + \alpha_2(\lambda, \sin\theta)\frac{1}{F_L^2} \tag{3-50}$$

showing a constant α_1 , as first postulated by Morton et al (1956), modified by a function which depends on the buoyant jet characteristics, F_L , λ , and the jet geometry, $\sin\theta$. This dependence is further explored.

For the simple non-buoyant momentum jet α reduces to

$$\alpha = \alpha_1 = \sqrt{3}\, I \quad \text{as} \quad F_L \to \infty \tag{3-51}$$

As the lack of specification of a similarity profile for $\overline{\tilde{u}'\tilde{v}'}$ does not allow evaluation of the integral I , α_1 is determined from experimental data for the momentum jet

$$\alpha_1 = 0.069 \tag{3-52}$$

by Albertson et al (1950) which value has been well substantiated by other investigations.

For distances far from the discharge point all buoyant jets tend to the condition of a pure vertically rising plume. This asymptotic case is characterized by a constant densimetric Froude $\hat{F}_L$ number as is shown below.

The change in the local densimetric Froude number F_L along the jet trajectory s is from Eq. (3-49)

$$\frac{dF_L}{ds} = F_L \frac{1}{2} \frac{1}{\tilde{u}_c b} \left[\frac{1}{\tilde{u}_c} \frac{d}{ds} (\tilde{u}_c^2\, b) - \frac{d}{ds} (\tilde{u}_c b) - \frac{1}{\Delta\rho_c} \frac{d}{ds} (\tilde{u}_c\, \Delta\rho_c b) \right] \tag{3-53}$$

after some manipulation. Using Eqs. (3-37), (3-38) and (3-40) this becomes

$$\frac{dF_L}{ds} = F_L \frac{1}{2} \frac{1}{\tilde{u}_c b} \left[\frac{1}{\tilde{u}_c} \sqrt{2} \frac{\Delta\rho_c}{\rho_a} g \lambda b \sin\theta - \frac{2}{\sqrt{\pi}} \alpha \tilde{u}_c \right] \qquad (3\text{-}54)$$

or in a simpler, implicit form

$$\frac{dF_L}{ds} = F_L \frac{1}{\sqrt{2}} \frac{\lambda}{b} \left[\frac{1}{F_L^2} - \sqrt{\frac{2}{\pi}} \frac{\alpha}{\lambda} \frac{1}{\sin\theta} \right] \qquad (3\text{-}55)$$

For the vertically rising plume $\sin\theta = 1$.

The necessary conditions for an asymptotic value $\hat{F}_L$ are

$$\frac{dF_L}{ds} = 0 \qquad \text{as} \qquad F_L = \hat{F}_L$$

and

$$\frac{dF_L}{ds} > 0 \qquad \text{if} \qquad F_L < \hat{F}_L \qquad (3\text{-}56)$$

$$\frac{dF_L}{ds} < 0 \qquad \text{if} \qquad F_L > \hat{F}_L$$

These conditions are satisfied for

$$\hat{F}_L = \left(\frac{\pi}{2} \right)^{1/4} \left(\frac{\hat{\lambda}}{\hat{\alpha}} \right)^{1/2} \qquad (3\text{-}57)$$

where $\hat{\alpha}$ is the entrainment coefficient and $\hat{\lambda}$ the spreading ratio of the simple plume. If the Froude number of the discharge is less than $\hat{F}_L$, then the jet will be accelerated and will monotonically approach the plume condition. Convection phenomena over line fires belong in this group. Of direct interest in the submerged diffuser case is discharge with large Froude numbers $F_L > \hat{F}_L$ where the flow

becomes gradually decelerated until the balance between buoyancy and shear forces which is typical of the plume is reached. This behavior and the existence of the asymptotic value was first described by Lee and Emmons (1962), referring to the two cases as restrained and impelled sources, respectively.

In the vertically rising buoyant plume condition the equation for the entrainment (3-50) should be satisfied by $\hat{\alpha}$, $\hat{\lambda}$, and $\hat{F}_L$ from Eq. (3-57) with $\sin \theta = 1$, thus

$$\hat{\alpha} = 0.069 + [\sqrt{2} - \sqrt{\frac{3}{1 + \lambda^2}}]\sqrt{2}\ \hat{\alpha} \qquad (3\text{-}58)$$

The only extensive experimental investigation regarding plume behavior was made by Rouse et al (1952) on buoyancy sources from line fires. Measurements of velocity and temperature were taken at distances above the source such that the influence of an initial deviation $F_L \neq \hat{F}_L$ can be neglected and true plume values are approached. However, their data fitting procedure which yielded the frequently used values

$$\hat{\alpha} = 0.160 \quad \text{and} \quad \hat{\lambda} = 0.89 \qquad (3\text{-}59)$$

implied linear spreading from the source, a condition which is violated when the initial $F_L \neq \hat{F}_L$. The values (3-59) do not satisfy Eq. (3-58). Abraham (1963) re-examined Rouse et al.'s data and found that in the region above the source where there is effective plume behavior the values

$$\hat{\alpha} = 0.130 \quad \text{and} \quad \hat{\lambda} = 1.24 \qquad (3\text{-}60)$$

describe the distributions much better. A spreading ratio $\hat{\lambda} > 1$ is

also consistent with observations on other free turbulent phenomena. Introducing $\hat{\lambda} = 1.24$ into Eq. (3-58) yields $\hat{\alpha} = 0.128$. This good agreement for $\hat{\alpha}$ must be judged somewhat fortuitous since it is based only on a single set of experiments, but seems to support the validity of the functional dependence of α on the buoyant jet characteristics expressed by Eq. (3-48). With these values the magnitude of local Froude number for a simple plume is $\hat{F}_L = 3.48$.

The spreading ratio λ also shows some variation with jet buoyancy as indicated by experiments. A variation between $\lambda = 1.41$ for the simple momentum jet (Reichardt (1942)) and $\hat{\lambda} = 1.24$ for the plume (3-60) is observed. However, as the second term in the entrainment relationship is important only for plume-like behavior a constant $\lambda = \hat{\lambda} = 1.24$ is assumed throughout the jet domain.

With these data, the following quantitative form is proposed for the entrainment relationship (3-50) in a slot buoyant jet

$$\alpha = 0.069 + [3.11 - 2.39 \sin\theta] \frac{1}{F_L^2} \qquad (3\text{-}61a)$$

and a constant spreading ratio

$$\lambda = 1.24 \qquad (3\text{-}61b)$$

3.4.1.3 Initial Conditions: Zone of Flow Establishment

The governing equations (3-37) to (3-41) do not adequately describe the zone of flow establishment in which a transition between the uniform slot exit velocity U_o and the velocity distribution in the general flow region takes place as seen in Fig. 3-5. Therefore for the specification of initial conditions some approximate steps are taken:

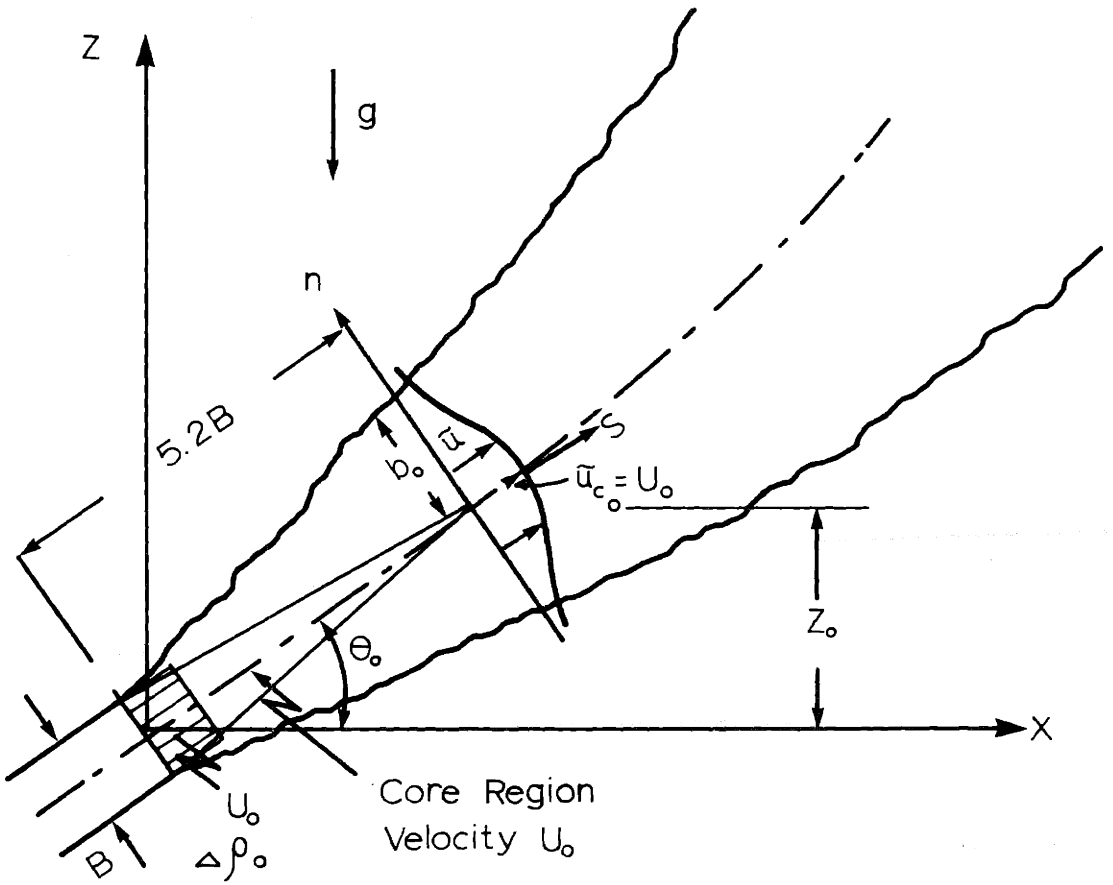

Fig. 3-5: Zone of Flow Establishment

1) The initial conditions are specified at the end of the zone of flow establishment and are related to the slot discharge conditions by conservation equations.

2) The effect of buoyancy in the zone of establishment is neglected.

Requiring constant momentum flux in the axial direction one obtains

$$U_o^2 B = \int_{-\infty}^{\infty} \tilde{u}_{o_c}^2 e^{-2(n/b)^2} dn = \sqrt{\frac{\pi}{2}} U_o^2 b_o \qquad (3\text{-}62)$$

thus

$$b_o = \sqrt{\frac{2}{\pi}} B \qquad (3\text{-}63)$$

The volume flux at the end of the zone follows then

$$\int_{-\infty}^{\infty} \tilde{u}_{c_o} e^{(-n/b)^2} dn = \sqrt{\pi} U_o b_o = \sqrt{2} U_o B \qquad (3\text{-}64)$$

which is in close agreement on experimentally derived relationships for the zone of establishment by Albertson et al (1950)

$$\frac{q_e}{U_o B} = 1 + 0.080 \frac{s}{B} \qquad (3\text{-}65)$$

evaluated for the length of the zone $s = 5.2\ B$ as

$$q_e = 1.42\ U_o B \qquad (3\text{-}66)$$

in which q_e = volume flux.

Finally, conservation of density deficiency requires

$$U_o B\ \Delta\rho_o = \int_{-\infty}^{\infty} \tilde{u}_{o_c}\ \Delta\rho_{c_o}\ e^{-(1 + 1/\lambda^2)(n/b)^2} dn \qquad (3\text{-}67)$$

and with (3-62)

$$\Delta\rho_{c_o} = \sqrt{\frac{1 + \lambda^2}{\lambda^2}}\ \Delta\rho_o \tag{3-68}$$

as the initial condition at the end of the zone.

In the further treatment, the extent $s/B = 5.2$ of the zone of establishment will be neglected as the region of interest s/B is considerably larger.

3.4.1.4 Solution of the Equations

The complete statement of the heated buoyant jet problem is summarized as follows:

$$\frac{d}{ds}(\tilde{u}_c b) = \frac{2}{\sqrt{\pi}}\ \alpha\ \tilde{u}_c \tag{3-69}$$

$$\frac{d}{ds}(\tilde{u}_c^2\, b) = \sqrt{2}\ \frac{\Delta\rho_c}{\rho_a}\ g\ \lambda\ b \sin\theta \tag{3-70}$$

$$\frac{d}{ds}(\tilde{u}_c^2\, b \cos\theta) = 0 \tag{3-71}$$

$$\frac{d}{ds}(\tilde{u}_c\ \Delta\rho_c\ b) = 0 \tag{3-72}$$

including geometric relations describing the jet trajectory

$$\frac{dx}{ds} = \cos\theta \tag{3-73}$$

$$\frac{dz}{ds} = \sin\theta \tag{3-74}$$

with

$$\alpha = 0.069 + [3.11 - 2.39 \sin\theta]\ \frac{1}{F_L^2} \tag{3-75}$$

and

$$\lambda = 1.24 \tag{3-76}$$

The centerline temperature rise ΔT_c above the ambient temperature is related to $\Delta\rho_c$ by the equation of state

$$\Delta T_c = \frac{1}{\beta} \Delta\rho_c \tag{3-77}$$

The initial conditions are

$$\left.\begin{aligned} \tilde{u}_c &= U_o \\ b &= 0 \\ \Delta\rho_c &= \Delta\rho_{c_o} \\ \theta &= \theta_o \end{aligned}\right\} \text{ at } \quad s = 0 \tag{3-78}$$

$$x = 0$$

$$y = 0$$

which are given at the end of the zone of flow establishment and are related to the slot exit conditions by Eqs. (3-63) and (3-68).

Solution of the equations is not possible in closed analytical form. However, the initial value problem is readily integrated by numerical methods. A fourth order Runge-Kutta integration technique is used. The buoyant jet discharge is governed by the following dimensionless parameters determined from the slot exit conditions:

densimetric Froude number $$F_s = \frac{U_o}{\sqrt{\frac{\Delta\rho_o}{\rho_a} g B}} \tag{3-79}$$

angle of discharge $$\theta_o \tag{3-80}$$

If in addition the distance s is scaled by B

$$\text{dimensionless distance} \quad \frac{s}{B} \tag{3-81}$$

the buoyant jet properties, namely velocity, density deficiency, width and trajectory, are functionally dependent as

$$\left[\frac{\tilde{u}_c}{u_o} , \frac{\Delta\rho_c}{\Delta\rho_o} , \frac{b}{B} , \frac{x}{B} , \frac{z}{B} , \theta \right] = f\left[\frac{s}{B} , F_s , \theta_o \right] \tag{3-82}$$

An important resulting parameter is the jet centerline dilution S_c which determines the decrease in density deficiency (or temperature) with respect to the discharge

$$S_c = \frac{\Delta\rho_o}{\Delta\rho_c} = \frac{\Delta T_o}{\Delta T_c} \tag{3-83}$$

and with respect to the end of zone of flow establishment

$$S_c = \frac{\Delta\rho_{co}}{\Delta\rho_c} \sqrt{\frac{2\lambda^2}{1 + \lambda^2}} \tag{3-84}$$

by virtue of Eq. (3-68).

An average dilution $\overline{S}$ is defined as the ratio of flow at any distance s to the discharge at the slot.

$$\overline{S} = \frac{\int_{-\infty}^{\infty} \tilde{u}\, dn}{U_o B} = \frac{\tilde{u}_c\, b\, \sqrt{\pi}}{U_o B} \tag{3-85}$$

Mass conservation gives the relation

$$\overline{S} = S_c \sqrt{\frac{1 + \lambda^2}{\lambda^2}} \tag{3-86}$$

A comparison between theoretical predictions for centerline dilution S_c without surface effects using a variable entrainment coefficient as proposed in Eq. (3-75) versus using a constant entrainment coefficient (Fan and Brooks (1969), $\alpha = 0.16$) is given in Fig. 3-6 for a vertical and in Fig. 3-7 for a horizontal jet discharge. Limited experimental data are also included.

For the vertical discharge both predictions are about equal in the low Froude number range. Fan and Brooks' prediction is, however, too high for large F_s (due to the chosen value of α), while the predictions of this study approach Albertsen et al.'s (1950) experimentally verified result for the average dilution $\overline{S}$ in non-buoyant jets

$$\overline{S} = 0.62 \sqrt{s/B} \tag{3-87}$$

which can be converted to

$$S_c = 0.62 \sqrt{\frac{\lambda^2}{1 + \lambda^2}} \sqrt{\frac{z}{B} + 5.2} \tag{3-88}$$

by virtue of Eq. (3-86) and taking account of the proper initial condition at the end of the zone of flow establishment. Some measurements of S_c were made in the experimental part of this study (see Chapter 5) and the agreement is better with the theoretical prediction of this study.

For the horizontal discharge this study predicts somewhat higher dilutions for low F_s. The strong slope of Fan and Brook's solution for high F_s is again due to the constant value of α. Experimental data are reported by Cederwell (1971) and are limited to the very low

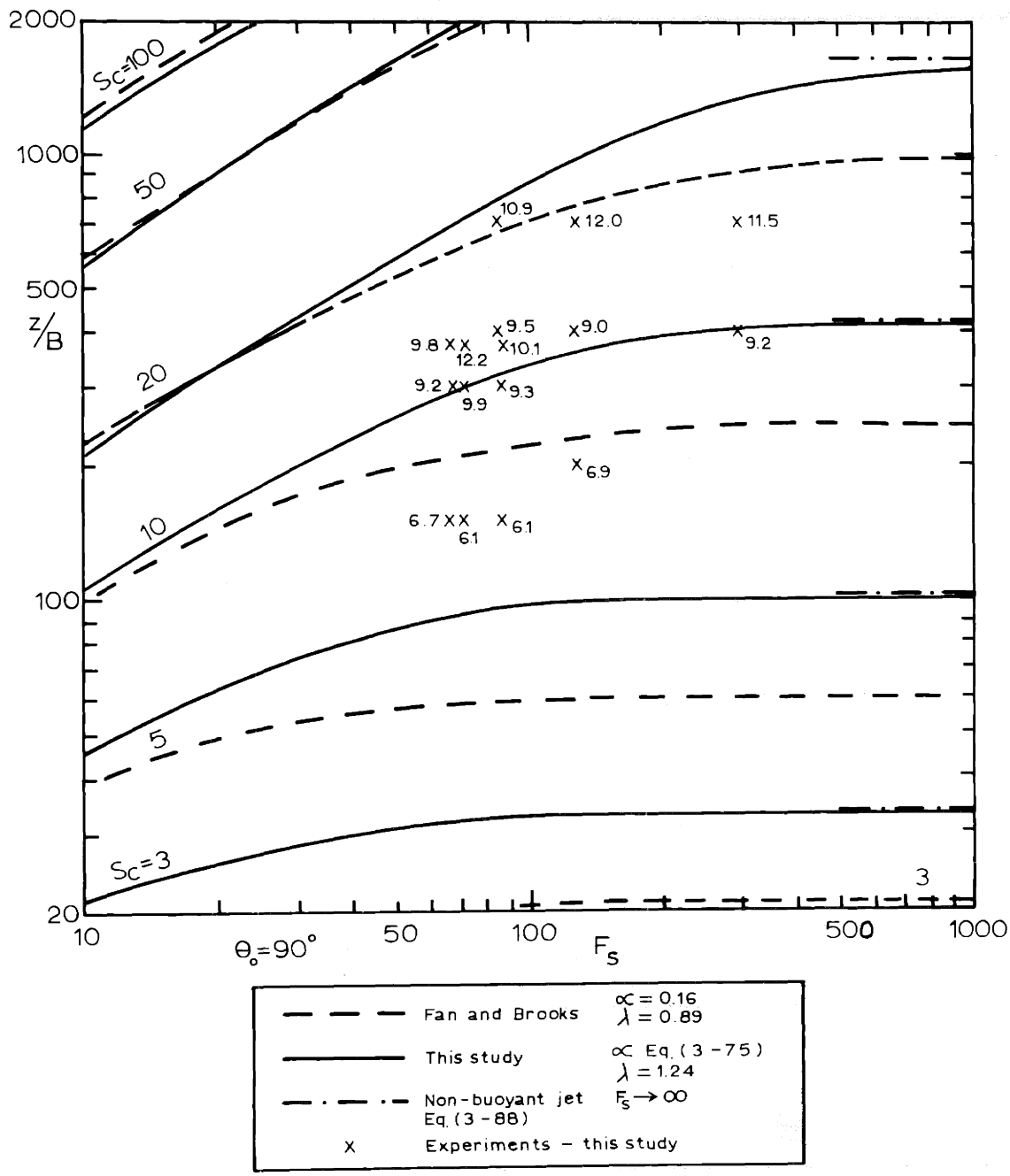

Fig. 3-6: Centerline Dilutions S_c for Buoyant Slot Jets Without Surface Interaction. Vertical Discharge. Comparison of theory and experiments.

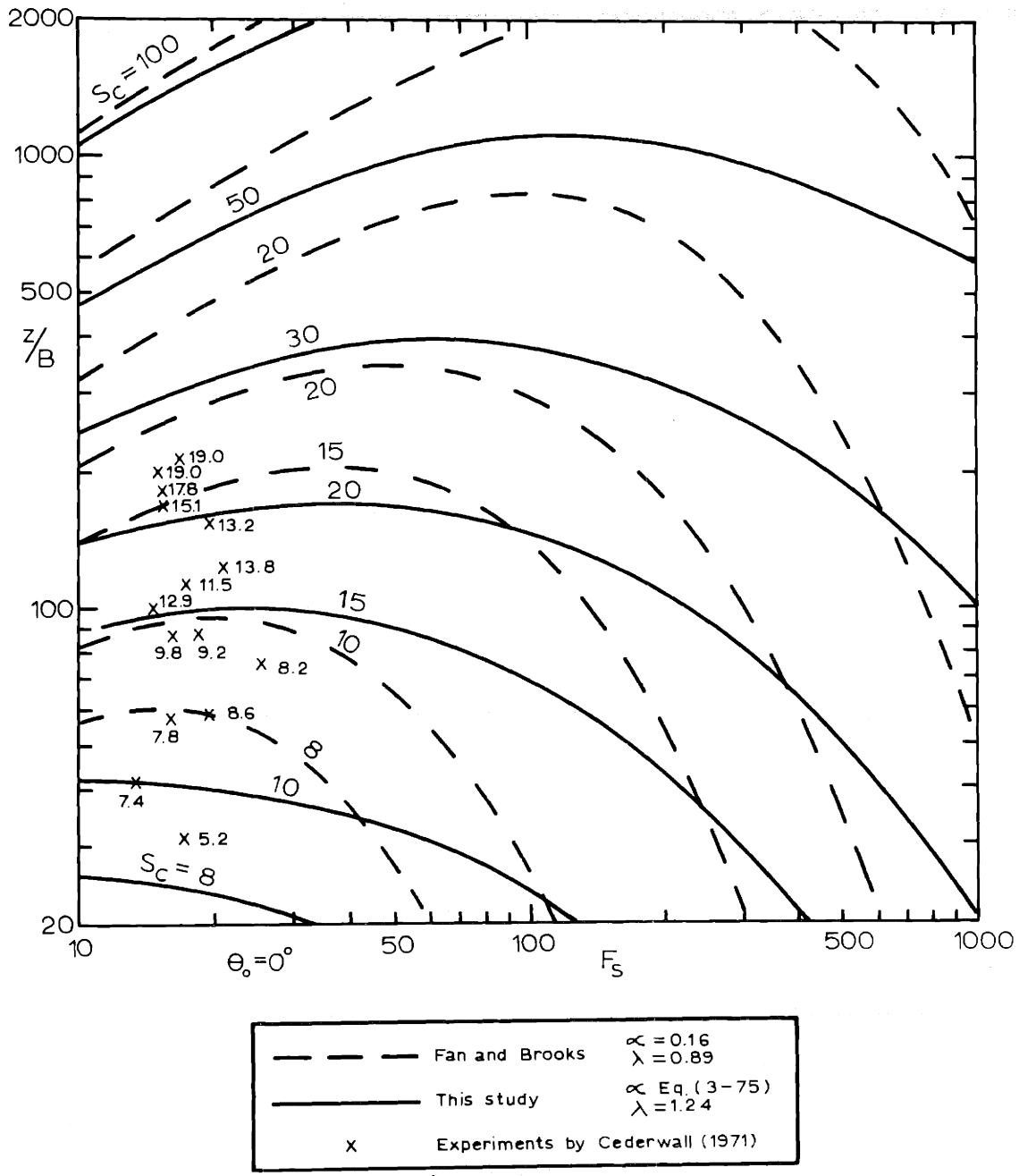

Fig. 3-7: Centerline Dilutions S_c for Buoyant Slot Jets Without Surface Interaction. Horizontal Discharge. Comparison of Theory and Experiments.

F_s range. All data lie between the predictions of both investigations, the agreement being somewhat closer with Fan and Brooks' solution.

3.4.2 Surface Impingement Region

3.4.2.1) General Solution

The buoyant jet region is bounded by the surface impingement region in which an abrupt transition between the jet flow, with a strong vertical component, to a horizontal spreading motion occurs. Discussion of the jet impingement at the surface also has some relevance to the buoyant jet region in particular with regard to the previous assumption of negligible reduced pressure p_r.

The main features of the impingement are indicated in Fig. 3-8. The momentum of the jet sets up a surface hump η in conjunction with a pressure deviation P_r decreasing in the vertical direction. This pressure gradient causes a stagnation of the vertical flow accompanied by a horizontal spreading in both directions.

The buoyant jet impingement is a complex flow phenomenon. Thus no attempt is made to solve for flow properties inside the region. Rather, a control volume approach is taken which yields a description of the horizontal spreading layers after impingement. The thickness of the spreading layers determines the elevation ($H = h_i$) to which effective jet entrainment occurs and the dynamic characteristics are decisive for the stability of the flow away zone.

Referring to Fig. 3-8, a control volume is defined by section i with the incoming jet flow, by sections a, b with the horizontal spreading motion and by the free surface. The flow is described by a set of simplified spatially averaged equations:

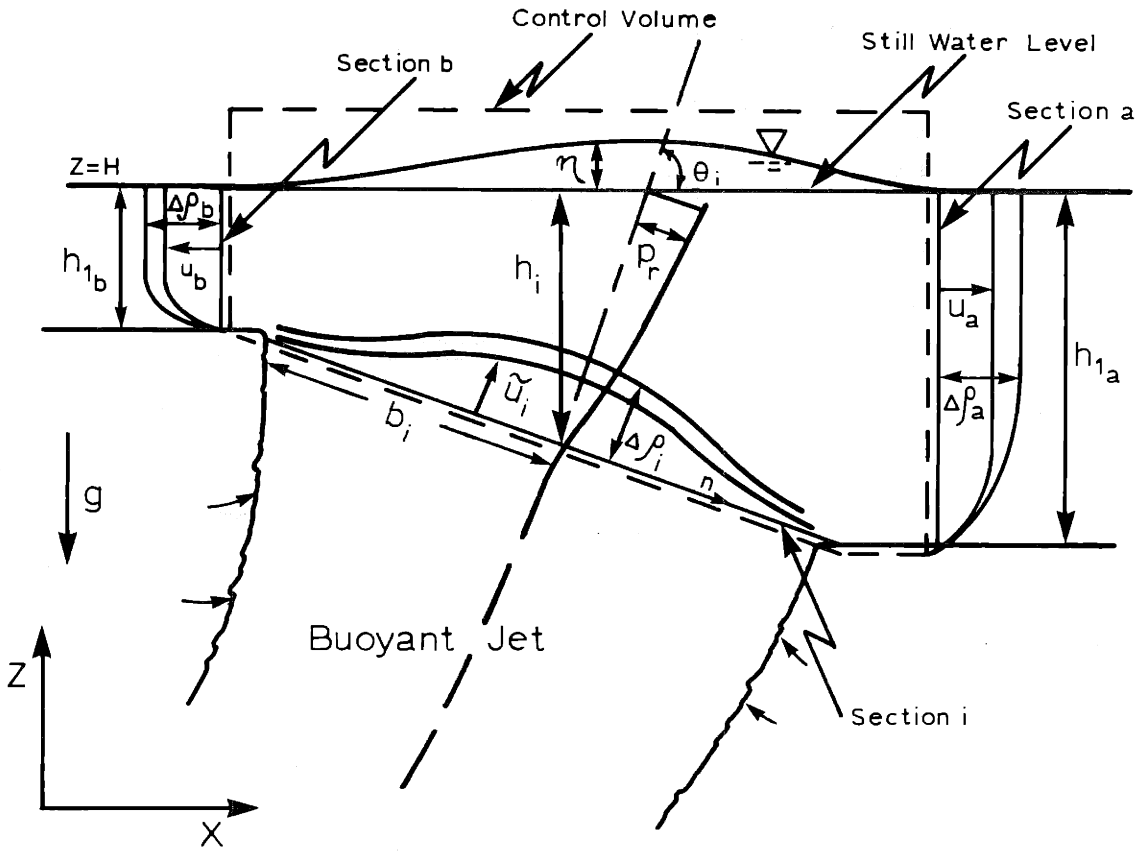

Fig. 3-8: Schematics of Surface Impingement Region

Energy equations:

$$\rho_a \frac{\overline{\tilde{u}_i^2}}{2g} - \overline{\Delta\rho_i z} = \rho_a \frac{\overline{u_{l_a}^2}}{2g} - \overline{\Delta\rho_a z} + \rho_a h_{L_a} \qquad (3\text{-}89)$$

$$\rho_a \frac{\overline{\tilde{u}_i^2}}{2g} - \overline{\Delta\rho_i z} = \rho_a \frac{\overline{u_{l_b}^2}}{2g} - \overline{\Delta\rho_b z} + \rho_a h_{L_b} \qquad (3\text{-}90)$$

Horizontal momentum equation:

$$\int_{-\infty}^{\infty} \rho_a \tilde{u}_i^2 \cos\theta_i \, dn + \int_{H-h_{l_b}}^{H} \rho_a u_{l_b}^2 \, dz = \int_{H-h_{l_a}}^{H} \rho_a u_{l_a}^2 \, dz \qquad (3\text{-}91)$$

Continuity:

$$\int_{-\infty}^{\infty} \tilde{u}_i \, dn = \int_{H-h_{l_b}}^{H} u_{l_b} \, dz + \int_{H-h_{l_a}}^{H} u_{l_a} \, dz \qquad (3\text{-}92)$$

where h_{L_a} , h_{L_b} = energy losses in the impingement process. This formulation includes some of the assumptions made in the treatment of the buoyant jet region, notably the Boussinesq approximation. Furthermore, these assumptions are inherent:

a) The distribution of the pressure deviation p_r : The vertical extent of the pressure influence is limited. Experiments by Cola (1966) and Murota and Muraoka (1967) on vertical non-buoyant jets show that the pressure influence is negligible below $z/H < 0.75$. Thus the pressure p_r is neglected at section i as a first approximation. The horizontal extent

of the pressure influence is related to the jet width b_i. Sections a and b are assumed to be located outside this zone.

b) Entrainment in the spreading process is negligible.

Solution of these equations requires the specification of velocity and density profiles for all sections as well as expressions for the energy losses. Hence the following additional assumptions are introduced:

c) Velocity and density distributions at section i are represented by the Gaussian profiles Eqs. (3-28) and (3-30) typical of the buoyant jet region. Distributions at sections a and b are dependent on the buoyant characteristics of the impinging jet. Cola and Murota and Muraoka found the velocity distribution for non-buoyant jets to be essentially jet-like. For buoyant jets, however, the buoyancy in the spreading layer exerts a stabilizing effect on the flow which suppresses the jet diffusion in the vertical direction. Velocity and density profiles can be reasonably approximated by a rectangular profile. This can be seen in Fig. 3-9. Photograph (Fig. 3-9a) shows the dye traces obtained from an instantaneous dye injection by means of a probe which had holes spaced at 1" intervals. Due to the diffusion of the injected dye, the probe cannot be used for quantitative determination of velocities. However, the photograph shows the qualitative velocity distribution, namely a strong approximately uniform flow in the upper 5 in. of the depth and a weak counterflow to the left in the lower

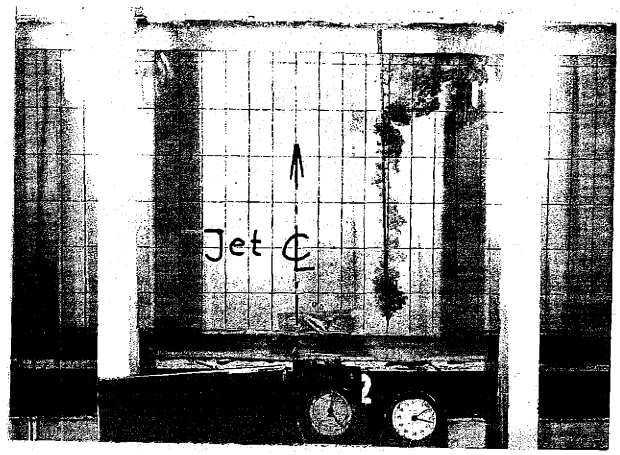

Grid Size
2 in. x 4 in.

a) Dye Traces From Instantaneous Injection Showing Velocity Distribution

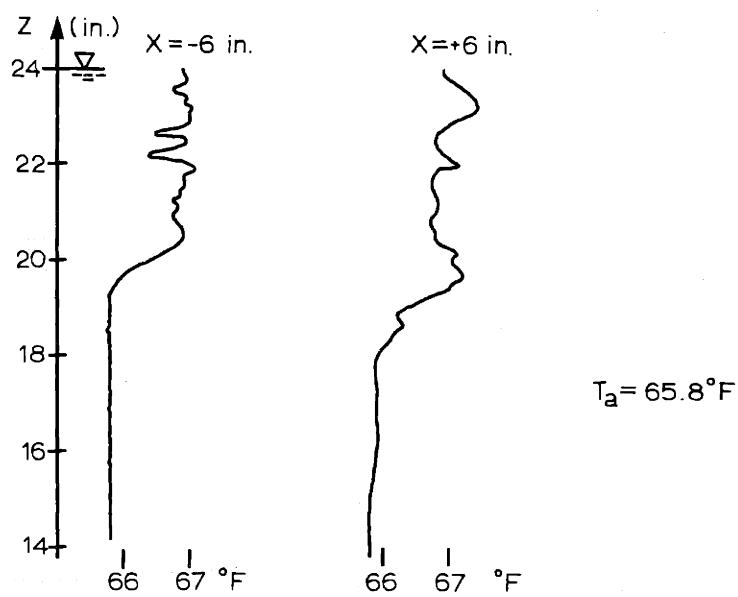

b) Temperature Profiles at Sections a and b

Fig. 3-9: Observed Velocity and Temperature (Density) Distributions for Vertical Buoyant Jet (F_s = 31, H/B = 416)

portion caused by the jet entrainment. Similarly, the observed temperature distributions after impingement are approximately uniform except for typical turbulent fluctuations. (The experimental set-up is described in detail in Chapter 5.) Thus the velocity and density distributions are in section a

$$u_{l_a}(z) = u_{l_a} \qquad H - h_{l_a} < z < H \tag{3-93}$$

$$\Delta\rho_a(z) = \Delta\rho_a$$

and in section b

$$u_{l_b}(z) = u_{l_a} \qquad H - h_{l_b} < z < H \tag{3-94}$$

$$\Delta\rho_b(z) = \Delta\rho_b$$

A consequence of the uniformly mixed distributions in the spreading layers is

$$\Delta\rho_a = \Delta\rho_b = \overline{\Delta\rho_i} \tag{3-95}$$

d) The energy losses due to secondary circulations in the impingement process are related to the velocity head at section i as

$$h_{L_a} = k_{L_a} \frac{\overline{\tilde{u}_i^2}}{2g}$$

$$h_{L_b} = k_{L_b} \frac{\overline{\tilde{u}_i^2}}{2g} \tag{3-96}$$

where k_{L_a} , k_{L_b} are head loss coefficients which are dependent on the angle and curvature of the flow bending and can be approximated by experimentally determined head loss coefficients for flows in smooth pipe bends (for example, Ito (1960)).

With the assumed similarity profiles the sectionally averaged quantities in the energy equation can be defined as:

$$\frac{\overline{\tilde{u}_i^2}}{2g} = \frac{1}{2g} \frac{\int_{-\infty}^{\infty} \tilde{u}_i^3 \, dn}{\int_{-\infty}^{\infty} \tilde{u}_i \, dn} = \frac{1}{2g} \frac{\tilde{u}_{c_i}^2}{\sqrt{3}} \qquad (3\text{-}97)$$

$$\overline{\Delta\rho_i z} = \frac{\int_{-\infty}^{\infty} \Delta\rho_i \, \tilde{u}_i \, dn}{\int_{-\infty}^{\infty} \tilde{u}^i \, dn} (H - h_i) = \Delta\rho_{c_i} \sqrt{\frac{\lambda^2}{1 + \lambda^2}} (H - h_i) \qquad (3\text{-}98)$$

$$\frac{\overline{u_{1_a}^2}}{2g} = \frac{u_{1_a}^2}{2g} \quad ; \quad \frac{\overline{u_{1_b}^2}}{2g} = \frac{u_{1_b}^2}{2g} \qquad (3\text{-}99)$$

$$\overline{\Delta\rho_a z} = \Delta\rho_a (H - \frac{h_{1_a}}{2}) \quad ; \quad \overline{\Delta\rho_b z} = \Delta\rho_a (H - \frac{h_{1_b}}{2}) \qquad (3\text{-}100)$$

and

$$h_i = \frac{h_{1_a} + h_{1_b}}{2} \qquad (3\text{-}101)$$

The Eqs. (3-89) to (3-92) become, after consideration of Eq. (3-95)

$$(1 - k_{L_a}) \frac{\tilde{u}_{c_i}^2}{2g} \frac{1}{\sqrt{3}} = \frac{u_{1_a}^2}{2g} - \frac{\Delta\rho_{c_i}}{\rho_a} \sqrt{\frac{\lambda^2}{1+\lambda^2}} \frac{h_{1_b}}{2} \qquad (3\text{-}102)$$

$$(1 - k_{L_b}) \frac{\tilde{u}_{c_i}^2}{2g} \frac{1}{\sqrt{3}} = \frac{u_{1_b}^2}{2g} - \frac{\Delta\rho_{c_i}}{\rho_a} \sqrt{\frac{\lambda^2}{1+\lambda^2}} \frac{h_{1_a}}{2} \qquad (3\text{-}103)$$

$$\tilde{u}_{c_i}^2 \, b_i \sqrt{\frac{\pi}{2}} \cos\theta_i + u_{1_b}^2 \, h_{1_b} = u_{1_a}^2 \, h_{1_a} \qquad (3\text{-}104)$$

$$\tilde{u}_{c_i} \, b_i \sqrt{\pi} = u_{1_a} \, h_{1_a} + u_{1_b} \, h_{1_b} \qquad (3\text{-}105)$$

These 4 equations determine the 4 unknowns u_{1_a}, h_{1_a} and u_{1_b}, h_{1_b} as a function of jet conditions at section i, that is

$$\tilde{u}_{c_i}, \Delta\rho_{c_i}, b_i = f(z = H - h_i) \qquad (3\text{-}106)$$

as obtained from the solution of the buoyant jet equations (3-69) to (3-76). As no closed form solutions to the buoyant jet equations are possible, the algebraic equations (3-102) to (3-105) of the surface impingement can be simplified by substituting a linear approximation of Eqs. (3-106) in the range of z where the layer depth is expected. The algebra equations are then easily solvable by simple numerical techniques, such as the Newton-Raphson method.

3.4.2.2 Special Cases

Valuable insight on the relative importance of the terms in Eqs. (3-102) to (3-104) is gained by considering the vertical discharge case for both the simple momentum jet and the simple plume. The flow pattern is then symmetric $u_{l_a} = u_{l_b} = u_l$, $h_{l_a} = h_{l_b} = h_i$, $k_{L_a} = k_{L_b} = k_L$ and the equations reduce to

$$(1 - k_L) \frac{\tilde{u}_{c_i}^2}{2g} \frac{1}{\sqrt{3}} = \frac{u_l^2}{2g} - \frac{\Delta\rho_{c_i}}{\rho_a} \sqrt{\frac{\lambda^2}{1 + \lambda^2}} \frac{h_i}{2} \tag{3-107}$$

$$\tilde{u}_{c_i} b_i \sqrt{\pi} = 2 u_l h_i \tag{3-108}$$

and by substitution

$$(1 - k_L) \frac{\tilde{u}_{c_i}^2}{2g} \frac{1}{\sqrt{3}} = \frac{\tilde{u}_{c_i}^2}{2g} \frac{\pi b_i^2}{4 z_i^2} - \frac{\Delta\rho_{c_i}}{\rho_a} \sqrt{\frac{\lambda^2}{1 + \lambda^2}} \frac{h_i}{2} \tag{3-109}$$

a) Vertical Momentum Jet ($\Delta\rho_{c_i} = 0$): Eq. (3-109) becomes

$$h_i = \frac{b_i \sqrt{\pi}}{2} \sqrt{\frac{\sqrt{3}}{1 - k_L}} \tag{3-110}$$

The jet width b_i is obtained from the solution of the buoyant jet equations. From Eq. (3-70) one obtains

$$\tilde{u}_c^2 b = U_o^2 B \sqrt{\frac{2}{\pi}} \tag{3-111}$$

by considering the initial condition (3-63). Substitution into Eq. (3-69) yields (s = z)

$$\frac{db}{dz} = \frac{4}{\sqrt{\pi}} \alpha \tag{3-112}$$

and integrated

$$b = \frac{4}{\sqrt{\pi}} \alpha z \tag{3-113}$$

if the initial width b_o is neglected for large z, $b >> b_o$. Hence at $z = H - h_i$

$$b_i = \frac{4}{\sqrt{\pi}} \alpha (H - h_i) \tag{3-114}$$

and after substituting into Eq. (3-110)

$$\frac{h_i}{H} = \frac{1}{1 + \frac{1}{2\alpha}\sqrt{\frac{1 - k_L}{\sqrt{3}}}} \tag{3-115}$$

For the momentum jet $\alpha = 0.069$, and k_L is estimated from Ito's (1960) data as $k_L \sim 0.2$ for a 90° bend and a wide range of curvatures. The variation of h_i/H with k_L is seen in the following table:

k_L =	0	0.2	0.4
$\frac{h_i}{H}$ =	0.152	0.167	0.188

b) Plume: The constancy of the local densimetric Froude number $F_L = \hat{F}_L$ has been shown in Section 3.4.1.2. This fact, in combination with the constant buoyancy flux Eq. (3-72), implies that the jet centerline velocity $\tilde{u}_c$ is also constant in the convective plane plume. Thus Eq. (3-69) can be simplified to

$$\frac{db}{ds} = \frac{2}{\sqrt{\pi}} \hat{\alpha} \tag{3-116}$$

and integrated for $z = H - h_i$

$$b_i = \frac{2}{\sqrt{\pi}} \hat{\alpha}(H - h_i) \tag{3-117}$$

again neglecting the initial width. After substitution and rearranging using the value of $\hat{F}_L$ (Eq. (3-57)) Eq. (3-109) becomes

$$\frac{1 - k_L}{\sqrt{3}} = \hat{\alpha}^2 \left(\frac{1 - \frac{h_i}{H}}{\frac{h_i}{H}} \right)^2 - \frac{1}{2} \sqrt{\frac{2}{1 + \hat{\lambda}^2}} \frac{\frac{h_i}{H}}{1 - \frac{h_i}{H}} \tag{3-118}$$

With $k_L = 0.2$, $\hat{\alpha} = 0.128$ and $\hat{\lambda} = 1.24$ the equation is evaluated as

$$\frac{h_i}{H} = 0.149 \tag{3-119}$$

The second term on the right side of Eq. (3-118) expresses the effect of buoyancy on the thickness. If this term is neglected

$$\frac{h_i}{H} = 0.159 \tag{3-120}$$

exhibiting only weak sensitivity.

Thus calculations for both the vertical momentum jet and the plume show that the thickness of the spreading layer is about 1/6 of the total depth H and the jet entrainment region can be assumed to extend to this elevation. Preliminary evidence of this result can be seen in Fig. 3.9. The result somewhat violates the assumption of neglecting the pressure deviation p_r at section i made in the preceding sections. However, the error introduced appears to be small.

3.4.2.3 Vertical Flow Distribution Prior to the Hydraulic Jump

After the combined evaluation of the buoyant jet and the impingement regions, the vertical flow distribution can be determined. With reference to Fig. 3-10, at both Sections a and b, a counterflow system is present with flow in the upper layer away from the line of impingement and flow in the lower layer towards jet entrainment

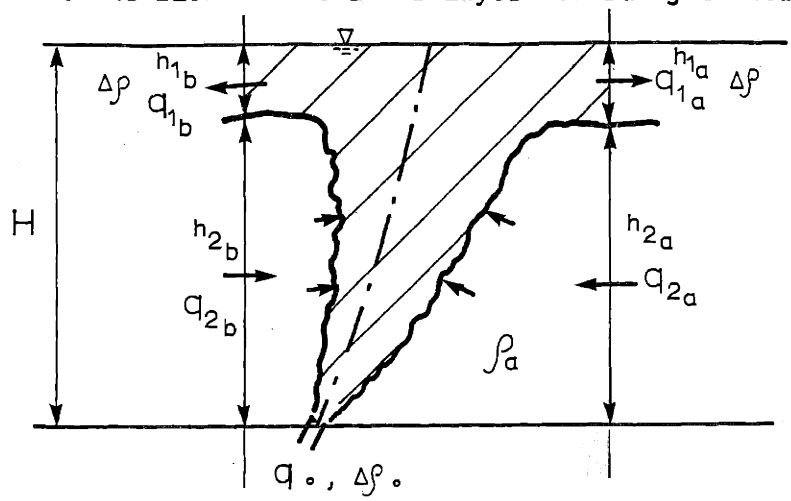

Fig. 3-10: Schematic of Vertical Flow Distribution Prior to Internal Hydraulic Jump.

Initial and surface layer volume fluxes per unit channel width are

$$q_o = U_o B \tag{3-121}$$

$$q_{1_a} = u_{1_a} h_{1_a} \tag{3-122}$$

$$q_{1_b} = u_{1_b} h_{1_b}$$

respectively. The average dilution is by definition

$$\overline{S} = \frac{q_{1_a} + q_{1_b}}{q_o}$$

and the total entrainment flow q_e follows as

$$q_e = (\bar{S} - 1)q_o = q_{2_a} + q_{2_b} \tag{3-123}$$

The magnitude of q_{2_a} and q_{2_b} is obtained by considering a horizontal momentum equation between a and b . Writing this equation notice can be made of the fact that the horizontal jet discharge momentum is actually conserved within the buoyant jet region and the impingement region (Eq. (3-104)). Thus a momentum equation can be written for the lower layer alone excluding these regions. With the assumptions of hydrostatic pressure and uniform velocity distribution this is simply

$$\frac{q_{2_a}^2}{h_{2_a}} = \frac{q_{2_b}^2}{h_{2_b}} \tag{3-124}$$

Substitution of Eq. (3-123) gives

$$q_{2_a} = \frac{(\bar{S} - 1)\, q_o}{1 + \sqrt{h_{2_b}/h_{2_a}}}$$

$$q_{2_b} = \frac{(\bar{S} - 1)\, q_o}{1 + \sqrt{h_{2_a}/h_{2_b}}} \tag{3-125}$$

Gross densimetric Froude numbers for upper and lower layers are important variables affecting the stability in the subsequent internal hydraulic jump region and are defined as (omitting the second subscript)

$$F_1 = \frac{q_1}{\left(\frac{\Delta\rho}{\rho_a} g h_1\right)^{3/2}} \tag{3-126}$$

$$F_2 = \frac{q_2}{\left(\frac{\Delta\rho}{\rho_a} g h_1\right)^{3/2}} \tag{3-127}$$

in which $\Delta\rho = \overline{\Delta\rho_i}$ the uniform density deficiency in the upper layer.

Indications of the magnitude of these Froude numbers are drawn from the special cases considered earlier. For the vertical momentum jet,

$$F_1 \, , \, F_2 \to \infty \tag{3-128}$$

For the plume,

$$\begin{aligned} F_1 &= [2(1 + \hat{\lambda}^2)]^{1/4} \hat{\alpha} \left(\frac{H}{h_1} - 1\right)^{3/2} \\ F_2 &= F_1 \left(\frac{h_1}{h_2}\right)^{3/2} \end{aligned} \tag{3-129}$$

following a similar procedure to that used in the derivation of Eq. (3-118), with $\hat{\lambda} = 1.24$, $\hat{\alpha} = 0.128$ and $h_i/H = 0.149$ (Eq. (3-119)), one gets

$$\begin{aligned} F_1 &= 2.63 \\ F_2 &= 0.19 \end{aligned} \tag{3-130}$$

For vertical buoyant jets Eq. (3-130) gives the lower bounds on the Froude numbers.

3.4.3 Internal Hydraulic Jump Region

3.4.3.1) General Solution

The internal hydraulic jump region provides the transition between the flow conditions at the end of the surface impingement region and the flow away into the far field. The region is analyzed as an internal hydraulic jump in a two-layered counterflow.

The definition diagram, Fig. 3-11, shows the upstream and down-

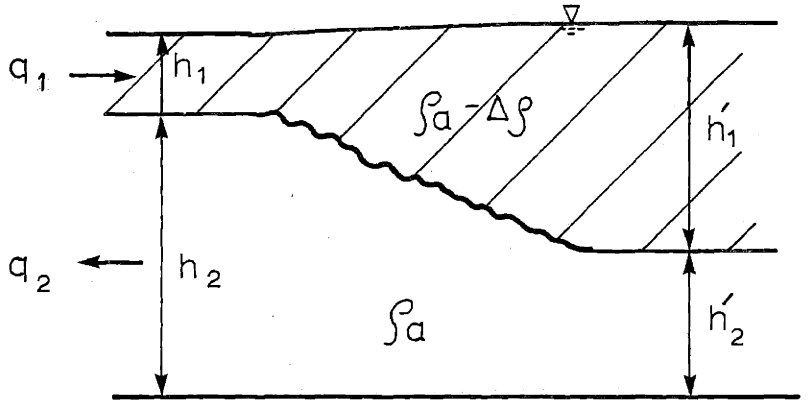

Fig. 3-11: Definition Diagram: Internal Hydraulic Jump.

stream conditions of the internal hydraulic jump. These conditions are referred to as conjugate to each other, that is they represent two flow states which are dynamically possible with regard to the governing momentum equation. The abrupt change of flow states in the jump is associated with considerable energy losses and possible entrainment at the interface.

An approximate analysis of the jump can be made by applying the momentum conservation principle to both flow layers between the up- and downstream sections. The analysis assumes hydrostatic pressure

distribution and uniform velocities at both sections. Furthermore the entrainment in the jump is neglected as are the interfacial and bottom shear. All these assumptions are consistent with those made in the analysis of simple one-layered jumps.

The momentum equation is first given for the control volume comprising the lower layer as

$$\rho_a\, q_2^2\left(\frac{1}{h_2'} - \frac{1}{h_1}\right) = h_2 h_1(\rho_a - \Delta\rho)g + \frac{1}{2}\, h_2^2\, \rho_a\, g$$

$$+ \frac{1}{2}\,(h_1 + h_1')(h_2' - h_2)(\rho_a - \Delta\rho)g \qquad (3\text{-}131)$$

$$- h_2' h_1(\rho_a - \Delta\rho)g - \frac{1}{2}\, h_1'^2 \rho_a\, g$$

in which the mean head acting over the jump section is approximated by $\frac{1}{2}(h_1 + h_1')$. For the upper layer it follows

$$(\rho_a - \Delta\rho)\, q_1^2\left(\frac{1}{h_1'} - \frac{1}{h_1}\right) = \frac{1}{2}\, h_1^2\,(\rho_o - \Delta\rho)g - \frac{1}{2}\,(h_1 + h_1')$$

$$(h_2' - h_2)(\rho_a - \Delta\rho)g \qquad (3\text{-}132)$$

$$- \frac{1}{2}\, h_1'^2(\rho_a - \Delta\rho)g$$

If free surface Froude numbers are defined in the usual form

$$F_1^{*2} = \frac{q_1^2}{g\, h_1^3}$$

$$F_2^{*2} = \frac{q_2^2}{g\, h_2^3} \qquad (3\text{-}133)$$

Equations (3-131) and (3-132) can be rewritten as

$$\frac{h_2'}{h_2} = \frac{2F_1^{*2} h_1^2(h_1' - h_1)}{h_2 h_1'(h_1 + h_1')} + 1 - \frac{h_1' - h_1}{h_2} \qquad (3\text{-}134)$$

$$\frac{h_1'}{h_1} = \frac{2 F_2^{*2} h_2^2(h_2' - h_2)}{\frac{\rho_a - \Delta\rho}{\rho_a} h_1 h_2'(h_2 + h_2')} + 1 - \frac{h_2' - h_2}{\frac{\rho_a - \Delta\rho}{\rho_a} h_1} \qquad (3\text{-}135)$$

This derivation was first given by Yih and Guha (1955). These authors also discussed the possible solutions for h_1'/h_1 and h_2'/h_2. In general, there are 9 roots to the above equations, out of which only 4 are positive and thus physically meaningful. These 4 roots are given by the intersection of two parabolic branches of the equations as illustrated in Fig. 3-12a. The energy content (specific head) for each of the 4 conjugate states can be evaluated. It is found (Yih (1965)) that the 4 solutions have different specific heads as indicated in Fig. 3-12a with 1 for the condition with highest energy. A jump can only occur from a state of higher energy to one of lower energy. For the internal jump state 3 is the given upstream state and state 4 is the conjugate state with lower energy. This follows from the fact that in the internal jump the lower layer decreases, and the upper layer increases its thickness. Only states 3 and 4 satisfy this requirement.

Under certain conditions there is no conjugate state to the given state (3) as shown in Fig. 3-12b. The physical implication of this fact is discussed in the sequel.

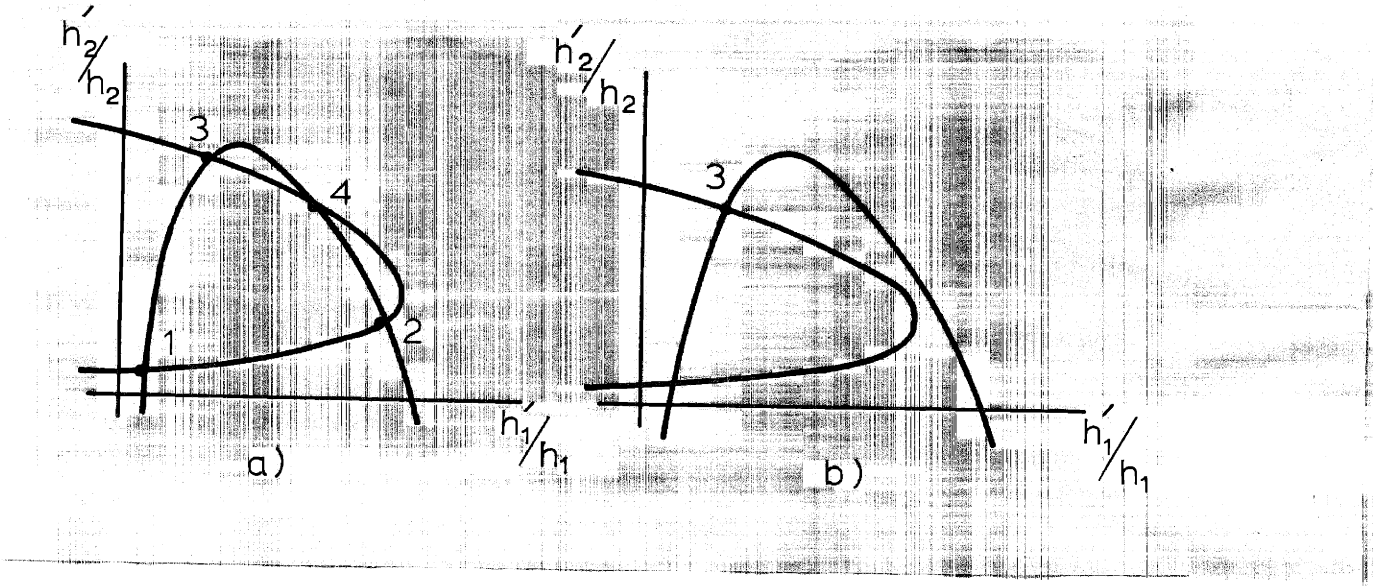

Fig. 3-12: Solution graph for the momentum equations
a) General case with 4 conjugate states,
b) Case with only 2 conjugate states, no internal jump possible.

3.4.3.2 Solution for Jumps with Low Velocities and Low Buoyancy

Yih's solution, Eqs. (3-134) and (3-135), give the jump conditions as a function of 4 parameters

$$\frac{h_1'}{h_1}, \frac{h_2'}{h_2} = f\left[\frac{h_1}{h_2}, F_1^*, F_2^*, \frac{\rho_a - \Delta\rho}{\rho_a}\right] \qquad (3\text{-}136)$$

In the problem of interest, namely, diffuser discharge, both free surface Froude numbers and relative density differences are small. Hence an asymptotic solution is attempted of the form

$$\left.\begin{array}{l} F_1^*,\ F_2^* \rightarrow 0 \\ \\ \dfrac{\Delta\rho}{\rho_a} \rightarrow 0 \end{array}\right\} \text{ while } \begin{array}{l} F_1 = F_1^*/\left(\dfrac{\Delta\rho}{\rho_a}\right)^{1/2} \\ \\ F_2 = F_2^*/\left(\dfrac{\Delta\rho}{\rho_a}\right)^{1/2} \end{array} \text{ finite} \qquad (3\text{-}137)$$

so that the jump conditions are a function of 3 parameters only

$$\frac{h_1'}{h_1}\ ,\ \frac{h_2'}{h_2} = f\left[\frac{h_1}{h_2}\ ,\ F_1, F_2\right] \qquad (3\text{-}138)$$

Equations (3-134) and (3-135) are transformed into linearly dependent equations in which this limiting process can be made validly. For this purpose

$$\Delta h_1 = h_1' - h_1\ ,\ \Delta h_2 = h_2' - h_1 \qquad (3\text{-}139)$$

are defined and the expressions for $\Delta h_2/\Delta h_1$ obtained from Eq. (3-134) and (3-135) are equated to give

$$\left[\frac{h_1'}{h_1}\left(\frac{h_1'}{h_1}+1\right) - 2F_1^2\right]\left[\frac{h_2'}{h_2}\left(\frac{h_2'}{h_2}+1\right) - 2F_2^2\right] = 4\left(\frac{\rho_a - \Delta\rho}{\rho_a}\right)F_1^2 F_2^2 \qquad (3\text{-}140)$$

A second equation is obtained by taking the inverse of Eq. (3-134) and again forming the expression for $\Delta h_2/\Delta h_1$ which is then equated with the $\Delta h_2/\Delta h_1$ from Eq. (3-135), thus

$$\left[\frac{h_1'}{h_1}\left(\frac{h_1'}{h_1}+1\right) - 2F_1^2\right] = -2F_1^2\ \frac{\dfrac{h_1'}{h_1}\left(\dfrac{h_1'}{h_1}+1\right)}{\dfrac{h_2'}{h_2}\left(\dfrac{h_2'}{h_2}+1\right)}\ \frac{\left(\dfrac{h_2'}{h_2}-1\right)}{\left(\dfrac{h_1'}{h_1}-1\right)}\ \frac{h_2}{h_1} \qquad (3\text{-}141)$$

The expression $(\rho_a - \Delta\rho)/\rho_a$ in Eq. (3-140) can be approximated to unity. A simple equation for h_1'/h_1 can then be formed by substituting the value of h'_2/h_2 from Eq. (3-140) into (3-141), namely

$$\left[\left(\frac{h_1'}{h_1} - 1\right)\frac{h_1}{h_2} - \frac{3}{2}\right]^2 = \frac{1}{4} + \frac{2F_2^2}{1 - \frac{2F_1^2}{\frac{h_1'}{h_1}\left(\frac{h_1'}{h_1} + 1\right)}} \qquad (3\text{-}142)$$

The deviation introduced by substituting the asymptotic solution for h_1'/h_1 Eq. (3-142) to the true solution Eqs. (3-134) and (3-135) is negligible. For $\Delta\rho/\rho_a = 0.05$ which is considerably higher than density differences in practical diffuser applications (e.g., see Section 1.1) the error is about 1%. Thus Eq. (3-142) describes the dynamics of an internal hydraulic jump with low velocities and low density differences.

Important information regarding the existence of a hydraulic jump can be derived from Eq. (3-142). A critical state is defined as one which is conjugate to itself, that is $h_1'/h_1 = 1$. With this value the equation gives the critical condition

$$F_1^2 + F_2^2 = 1 \qquad (3\text{-}143)$$

In analogy to free surface flow supercritical flow is characterized by

$$F_1^2 + F_2^2 > 1 \qquad (3\text{-}144)$$

and subcritical flow by

$$F_1^2 + F_2^2 < 1 \qquad (3\text{-}145)$$

A hydraulic jump can only occur from supercritical to subcritical flow as the energy content is lower for the latter and energy is dissipated in the jump. That the upstream condition in the problem considered is indeed supercritical is demonstrated by substituting the values of densimetric Froude numbers Eqs. (3-130), which as plume conditions represent lower bounds for buoyant jets: Condition (3-144) is satisfied. A jump will occur which changes this supercritical state to the subcritical state prevailing in the stratified counterflow region.

For certain combinations of F_1 , F_2 and h_1/h_2 , however, Eq. (3-142) does not give a conjugate subcritical downstream section with lower energy (see Fig. 3-12b).

The physical implication of the non-existence of a solution is a hydrodynamically unstable condition. The excess energy is dissipated by turbulent diffusion over the whole region, leading to re-entrainment of already mixed water, into the jet region, as depicted in Fig. 3-13. A vertical region is thus formed in the near field zone. In steady state this diffusion and re-entrainment process will act to such a degree that outside the mixing region the critical relation (3-143) is obtained. In other words, through decrease in kinetic energy and increase in buoyancy the supercritical state, after jet impingement, is transformed into the limiting case of a subcritical state, a critical state. The critical state is then a starting condition for the subsequent stratified counterflow region which is characterized by subcritical flow as the next section will show.

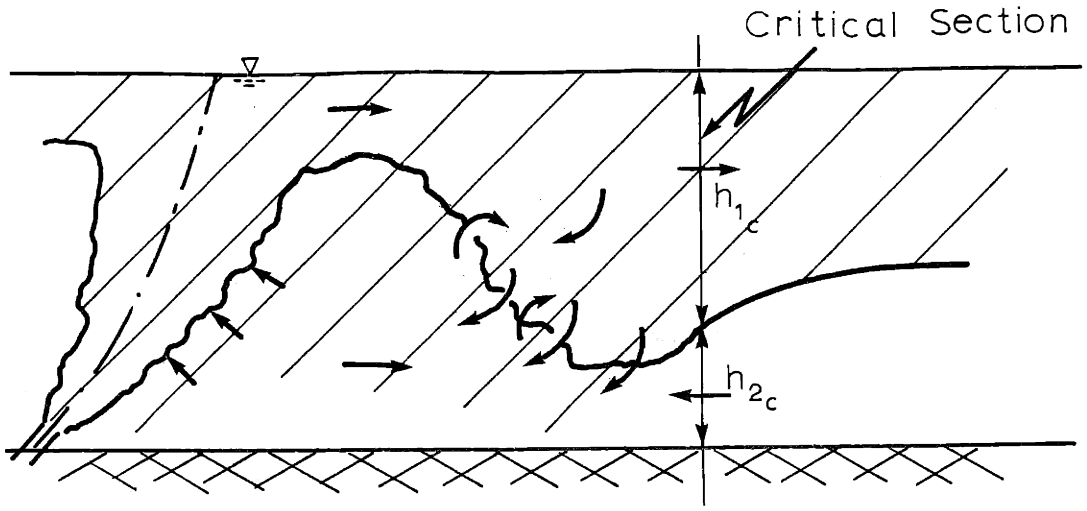

Fig. 3-13: Non-existence of an internal hydraulic jump: Turbulent diffusion and re-entrainment.

3.4.4 Stratified Counterflow Region

3.4.4.1 Approximations and Governing Equations

The governing equations for slowly varying stratified counterflow in the far-field, with heat dissipation to the atmosphere, are developed. Figure 3-14 defines the problem of a two-layered fluid flow with a fairly distinct density change $\Delta\rho = \beta\,\Delta T$ across the interface defined as the elevation of the zero horizontal velocity point. The flow is predominantly horizontal, the thickness of the upper and lower layer is h_1 and h_2, respectively.

Under these circumstances the governing equations (3-3) to (3-6) can be simplified, neglecting vertical accelerations and longitudinal turbulent transport terms, to

$$\partial u/\partial x + \partial w/\partial z = 0 \qquad (3\text{-}146)$$

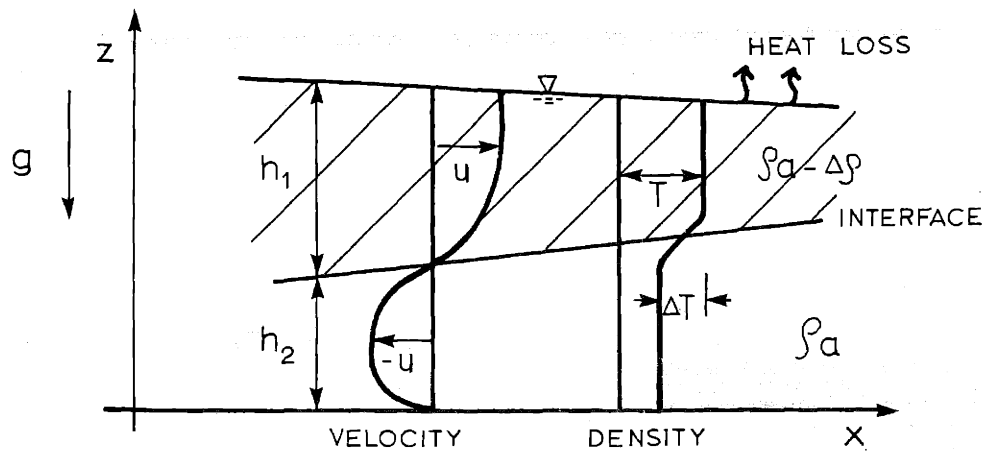

Fig. 3-14: Stratified flow definitions.

$$\rho_a u \frac{\partial u}{\partial x} + \rho_a w \frac{\partial u}{\partial z} = - \frac{\partial p}{\partial x} + \rho_a \frac{\partial}{\partial z} (\varepsilon_z \frac{\partial u}{\partial z}) \qquad (3\text{-}147)$$

$$0 = - \frac{\partial p}{\partial z} + \rho g \qquad (3\text{-}148)$$

$$u \frac{\partial T}{\partial x} + w \frac{\partial T}{\partial z} = \frac{\partial}{\partial z} (K_z \frac{\partial T}{\partial z}) \qquad (3\text{-}149)$$

where

ε_z = Vertical eddy diffusion coefficient for momentum

K_z = Vertical eddy diffusion coefficient for mass or heat

and the turbulent transfer terms have been written in diffusion analogy as

$$\begin{aligned} - \overline{u'w'} &= \varepsilon_z \frac{\partial u}{\partial z} \\ - \overline{w'T'} &= K_z \frac{\partial T}{\partial z} \end{aligned} \qquad (3\text{-}150)$$

The further analysis makes use of the distinctly layered flow structure: The flow-field is divided into two layers which are coupled through kinematic , dynamic and heat flux conditions at the interface. Similarity profiles for horizontal velocity and temperature are defined for each layer so that the equations can be integrated vertically.

a) Kinematic boundary conditions are specified as:

$$\begin{aligned} &\text{surface} && u_s \frac{\partial (h_1 + h_2)}{\partial x} = w_s && \text{at} \quad z = h_1 + h_2 \\ &\text{interface} && u_i \frac{\partial h_2}{\partial x} = w_i && \text{at} \quad z = h_1 \\ &\text{bottom} && w_b = 0 && \text{at} \quad z = 0 \end{aligned} \qquad (3\text{-}151)$$

The interface condition (3-151b) assumes that there is no mean flow across the interface, hence the volume flux in each layer is constant. This assumption does not allow for entrainment. The salient features of the entrainment process as discussed earlier are the existence of a zone of fluid flow with high turbulent intensity as compared to the surrounding fluid. Turbulence at the zone boundary leads to incorporation of ambient fluid into the active zone. No such active zone exists in the case of stratified counterflow: both layers move as density currents and have approximately equal turbulent characteristics. Furthermore, even if such an active layer would prevail, the existence of a stable density stratification greatly reduces the entrainment at the boundary. Experimental studies by Ellison and Turner (1959) show that for bulk Richardson numbers

$$R_i \gtrsim 0.85 \qquad (3\text{-}152)$$

vertical entrainment practically ceases, where R_i is defined and related to a Froude number F by

$$R_i = \frac{\frac{\Delta\rho}{\rho} g h}{V^2} = \frac{1}{F^2} \tag{3-153}$$

with h = depth of turbulent layer

V = layer velocity

The stratified counterflow regime of interest in this study is subcritical as will be shown below, hence condition (3-145) is applicable and simultaneously condition (3-152) is satisfied.

Zero entrainment, however, does not rule out transport of mass by fluctuating velocities across the interface, that is, interfacial mixing.

b) Dynamic boundary conditions are given as:

$$\left.\begin{array}{lll} \text{surface:} & \tau_s = \rho_a \varepsilon_z \frac{\partial u}{\partial z} = 0 & \\ & p = 0 & \end{array}\right\} z = h_1 + h_2 \qquad (3\text{-}154)$$

$$\begin{array}{lll} \text{interface:} & \tau_i = \rho_a \varepsilon_z \frac{\partial u}{\partial z} & z = h_2 \\ \text{bottom:} & \tau_b = \rho_a \varepsilon_z \frac{\partial u}{\partial z} & z = 0 \end{array}$$

where τ_s, τ_i and τ_b are shear stresses which are later related to the mean flow quantities.

c) Heat flux conditions: The flux of heat, q_{H_s}, from the free surface to the atmosphere, which is induced by the elevated water temperature, can be considered in a simple concept by (Edinger and Geyer (1965)):

$$q_{H_s} = -\rho\, c_p\, \kappa (T_s - T_e) \qquad (3\text{-}155)$$

in which

c_p = specific heat

κ = heat exchange coefficient

T_s = water surface temperature = $T(z = h_1 + h_2)$

T_e = equilibrium temperature

Both factors T_e and κ are dependent on meteorological parameters, which determine the transfer processes across the water surface. T_e is defined as the water temperature at which there would be no net heat flux across the surface. In general, T_e is not equal to the ambient temperature T_a (without heat input), only on a long term average.

The remaining heat flux conditions are:

$$\text{interface:} \quad q_{H_i} = \rho\, c_p\, K_z \frac{\partial T}{\partial z} \qquad z = h_2$$

$$\text{bottom:} \quad q_{H_b} = \rho\, c_p\, K_z \frac{\partial T}{\partial z} \qquad z = 0 \qquad (3\text{-}156)$$

d) Both velocity and temperature are approximated to be uniform in each layer and are averaged by

$$\text{upper layer:} \quad u_1 = \frac{q_1}{h_1} = \frac{1}{h_1} \int_{h_2}^{h_1+h_2} u\, dz$$

$$\rho_1 = \frac{1}{h_1} \int_{h_2}^{h_1+h_2} \rho\, dz \qquad (3\text{-}157)$$

CONT'D.

lower layer: $$u_2 = \frac{q_2}{h_2} = \frac{1}{h_2} \int_0^{h_2} u \, dz$$

(3-157)

$$\rho_2 = \frac{1}{h_2} \int_0^{h_2} \rho \, dz$$

Using these profile assumptions and boundary conditions, Eqs. (3-146) to (3-149) can be transformed into ordinary differential equations for each layer. The hydrostatic equation (3-148) is integrated to

$$p = \rho_1 g(h_1 + h_2 - z) \tag{3-158}$$

which can be substituted into the momentum equation (3-147) to give

$$\frac{\partial u^2}{\partial x} + \frac{\partial uw}{\partial z} = -\frac{g}{\rho_a}\left[(h_1 + h_2 - z)\frac{\partial \rho_1}{\partial x} + \rho_1\left(\frac{\partial h_1}{\partial x} + \frac{\partial h_2}{\partial x}\right)\right] + \frac{\partial}{\partial z}\left(\varepsilon_z \frac{\partial u}{\partial z}\right) \tag{3-159}$$

also making use of the continuity equation (3-146). Equation (3-159) is integrated in the z direction over the upper layer.

$$\int_{h_2}^{h_1+h_2} \frac{\partial u^2}{\partial x} dz + \int_{h_2}^{h_1+h_2} \frac{\partial uw}{\partial z} dz = -\frac{g}{\rho_a}\frac{\partial \rho_1}{\partial x}\frac{h_1^2}{2} - \frac{g}{\rho_a}\rho_1\left(\frac{\partial h_1}{\partial x} + \frac{\partial h_2}{\partial x}\right)h_1 + \left(\varepsilon_z \frac{\partial u}{\partial z}\right)_{h_2}^{h_1+h_2} \tag{3-160}$$

The left hand side is integrated, using Leibniz's rule on the first integral, to

$$\frac{\partial}{\partial x}\int_{h_2}^{h_1+h_2} u^2 dz - u_s^2 \frac{\partial (h_1 + h_2)}{\partial x} + u_i^2 \frac{\partial h_2}{\partial x} + u_s w_s - u_i w_i$$

and after use of the kinematic conditions (3-151) only the first term, $\frac{\partial}{\partial x}\ (u_1^2\ h_1)$, remains. Finally, Eq. (3-160) becomes, using $q_1 = u_1 h_1$

$$-\frac{q_1^2}{g\ h_1^3}\ \frac{dh_1}{dx} = -\frac{1}{\rho_a}\ \frac{d\rho_1}{dx} - \frac{\rho_1}{\rho_a}\left(\frac{dh_1}{dx} + \frac{dh_2}{dx}\right) - \frac{\tau_i}{\rho_a\ g\ h_1} \qquad (3\text{-}161)$$

The heat conservation equation for the upper layer is integrated, after substitution of the continuity equation, to

$$\int_{h_2}^{h_1+h_2} \frac{\partial uT}{\partial x}\, dz + \int_{h_2}^{h_1+h_2} \frac{\partial wT}{\partial z}\, dz = \left(K_z \frac{\partial T}{\partial z}\right)_{h_2}^{h_1+h_2} = \frac{q_{H_s} - q_{H_i}}{\rho_a\ c_p} \qquad (3\text{-}162)$$

Again making use of the Leibniz rule and the kinematic conditions leads to

$$\frac{q_1}{h_1}\ \frac{dT_1}{dx} = -\frac{\kappa}{\rho_a\ c_p\ h_1}\ (T_1 - T_e) - \frac{q_{H_i}}{\rho_a\ c_p\ h_1} \qquad (3\text{-}163)$$

In an analogous manner equations for the lower layer are found as

$$-\frac{q_2^2}{g\ h_2}\ \frac{dh_1}{dx} = -\frac{1}{\rho_a}\left(\frac{d\rho_1}{dx}\ h_1 + \rho_1\ \frac{dh_1}{dx} + \frac{d\rho_2}{dx}\ \frac{h_2}{2} + \rho_2\ \frac{dh_2}{dx}\right) + \frac{(\tau_i - \tau_b)}{\rho_a\ g\ h_2} \qquad (3\text{-}164)$$

and

$$\frac{q_2}{h_2}\ \frac{dT_2}{dx} = \frac{q_{H_i}}{\rho_a\ c_p\ h_2} \qquad (3\text{-}165)$$

Equations (3-161), (3-163), (3-164) and (3-165) are the general equations describing the motion and temperature distribution of non-entraining stratified flow with heat dissipation to the atmosphere. Dependent variables are the mean flow properties h_1, h_2 and T_1, T_2, which require statement of boundary conditions at some position x. τ_i, τ_b and q_{H_i} can be related to the mean flow properties by empirical relations.

The solution of this set of equations is not readily achieved. Thus in the following section the equations are simplified by appropriate scaling procedures for the flow area in the diffuser vicinity.

3.4.4.2) Simplified Equations, Neglecting Surface Heat Loss and Interfacial Mixing

It can be shown that under typical diffuser design conditions surface heat loss and interfacial mixing can be neglected for the stratified flow region in the diffuser vicinity, as the time scale for these processes is considerably larger than that for the convective transport. For this purpose, Equation (3-163) will be scaled and typical prototype magnitudes for the scaling parameters are inserted to compare the relative importance of the terms.

Dimensionless variables (with asterisks) are defined by

$$\begin{aligned} x^* &= x/L \\ h^* &= h_1/H \\ u^* &= u_1/U \\ \Delta T^* &= \Delta T/\Delta T_o \end{aligned} \qquad (3\text{-}166)$$

in which

L = channel length

H = water depth

U = typical induced velocity

ΔT_o = typical surface temperature difference

The interfacial heat flux term is substituted from Eq. (3-156a) and approximated as

$$q_{H_i} \simeq \rho c_p K_z \frac{T_1 - T_2}{H} \tag{3-167}$$

Substituting the variables (3-166) into the heat transport equation one obtains, dividing by $U\Delta T_o/L$

$$u^* \frac{d\Delta T^*}{dx^*} \simeq -\left(\frac{\kappa}{\rho_a c_p H} \frac{L}{U} \right)\Delta T^* - \left(\frac{K_z}{H} \frac{L}{U} \right)\Delta T^* \tag{3-168}$$

Characteristic magnitudes for the scaling parameters in prototype conditions for a thermal diffuser are:

L = 1000 ft. (In Chapter 4 the channel length L is shown to be related to the characteristic horizontal diffuser dimension, its half length L_D as $L \simeq L_D$).

H = 30 ft

U = 0.1 ft

ΔT_s = 5°F

κ = 150 BTU/°F, ft^2, day

K_z = 10^{-4} ft^2/sec. The vertical eddy diffusion is strongly inhibited by the density stratification. Koh and Fan (1970) compiled available data and fitted an empirical

relation which is an inverse function of the density gradient. The density gradient at the interface was approximated as in Eq. (3-167), but is in fact much higher.

Further:

$$\rho_a \, c_p = 62 \text{ BTU/ft}^3$$

With these values the expressions in parentheses are calculated to be of the magnitude ~0.01 for the surface heat loss and ~0.03 for interfacial mixing. Consequently, these transfer processes become only important for larger distances L and can be neglected in the channel problem considered. Thus, the heat equation is simplified to

$$\frac{dT_1}{dx} = 0 \tag{3-169}$$

and by similar arguments it is found

$$\frac{dT_2}{dx} = 0 \tag{3-170}$$

Hence the problem reduces to the well-known equations for the stratified flow with constant densities, first derived by Schijf and Schönfeld (1953):

$$\frac{q_1^2}{g\, h_1^3} \frac{dh_1}{dx} = \frac{\rho_1}{\rho_a} \left(\frac{dh_1}{dx} + \frac{dh_2}{dx} \right) + \frac{\tau_i}{\rho_a\, g\, h_1} \tag{3-171}$$

$$\frac{q_2^2}{g\, h_2^3} \frac{dh_2}{dx} = \frac{\rho_1}{\rho_a} \frac{dh_1}{dx} + \frac{dh_2}{dx} - \frac{(\tau_i - \tau_b)}{\rho_a\, g\, h_2} \tag{3-172}$$

with

$$\rho_2 = \rho_a \quad .$$

With the definition of free surface Froude numbers (3-133) these equations can be transformed to

$$\frac{dh_1}{dx} = \frac{\frac{\tau_b}{\rho_a g h_2} - \frac{\tau_i}{\rho_a g}\left(\frac{1 - F_2^{*2}}{h_1} + \frac{1}{h_2}\right)}{\frac{\Delta\rho}{\rho_a} - F_1^{*2} - F_2^{*2} + F_1^{*2}F_2^{*2}} \tag{3-173}$$

$$\frac{dh_2}{dx} = \frac{\frac{-\tau_b}{\rho_a g h_2}(1 - F_1^{*2}) + \frac{\tau_i}{\rho_a g}\left(\frac{1}{h_1} + \frac{1 + F_1^{*2}}{h_2}\right)}{\frac{\Delta\rho}{\rho_a} - F_1^{*2} - F_2^{*2} + F_1^{*2}F_2^{*2}} \tag{3-174}$$

Adding up these equations gives the change in total depth

$$\frac{d}{dx}(h_1 + h_2) = \frac{\frac{\tau_b}{\rho_a g h_2} F^{*2} + \frac{\tau_i}{\rho_a g}\left(\frac{F_2^{*2}}{h_1} + \frac{F_1^{*2}}{h_2}\right)}{\frac{\Delta\rho}{\rho_a} - F_1^{*2} - F_2^{*2} + F_1^{*2}F_2^{*2}} \tag{3-175}$$

Considering Fig. 3-15 the total depth is written as

$$h_1 + h_2 = H + \eta$$

where H is the still water depth and η the disturbance. From hydrostatic considerations and also by inspection of Eqs. (3-175) and (3-174)

$$\frac{d\eta}{dx} \approx \frac{\Delta\rho}{\rho_a}\frac{dh_2}{dx} \approx F^{*2}\frac{dh_2}{dx} \tag{3-176}$$

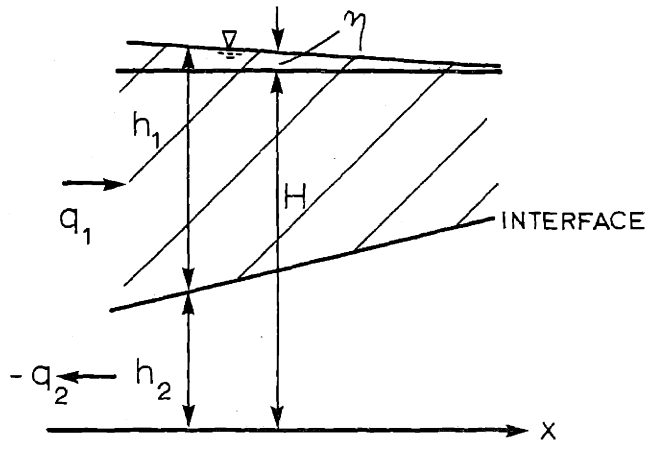

Fig. 3-15: Depth relationships in stratified flow

Thus for $\Delta\rho/\rho_a \ll 1$, $F^{*2} \ll 1$ the change in surface elevation is small compared to the interfacial depth change dh_2/dx. Consequently, as a first approximation dh_2/dx can be calculated by assuming

$$h_1 + h_2 = \text{const.} = H \tag{3-177}$$

The solution for $h_1(x)$, $h_2(x)$ thus obtained can then be used to evaluate the surface disturbance $\eta(x)$. Knowledge of η which is caused by frictional forces is important in the analysis of diffuser discharges which introduce horizontal momentum which is balanced by frictional forces.

Then substituting Eq. (3-177) into Eq. (3-173) which is subtracted from Eq. (3-174) one obtains

$$\frac{dh_2}{dx} = \frac{\frac{1}{\Delta\rho/\rho_a}\left[-\frac{\tau_b}{\rho_a\, g\, h_2} + \frac{\tau_i}{\rho_a\, g}\left(\frac{1}{H-h_2} + \frac{1}{h_2}\right)\right]}{1 - F_1^2 - F_2^2} \tag{3-178}$$

where F_1, F_2 are densimetric Froude numbers and $\Delta\rho/\rho$, F^{*2} have been neglected with respect to unity. At this point bottom and interfacial stresses are expressed in terms of mean flow parameters as

$$\tau_b = \frac{f_o}{8} \rho_a u_2 |u_2|$$

$$\tau_i = \frac{f_i}{8} \rho_a (u_1 - u_2) |u_1 - u_2| \qquad (3\text{-}179)$$

or

$$\tau_b = \frac{f_o}{8} \rho_a \left(\frac{q_2}{h_2} \right)^2 \text{sign } (q_2)$$

$$\tau_i = \frac{f_i}{8} \rho_a \left(\frac{q_1}{h_1} - \frac{q_2}{h_2} \right)^2 \text{sign } (q_1 - q_2) \qquad (3\text{-}180)$$

Substitution into Eq. (3-178) gives

$$\frac{dh_2}{dx} = \frac{-\frac{f_o}{8} F_2^2 \text{ sign}(q_2) + \frac{f_i}{8} F_1^2 \frac{H}{h_2} \left(1 - \frac{q_2}{q_1} \left(\frac{H}{h_2} - 1 \right)\right)^2 \text{sign}(q_1 - q_2)}{1 - F_1^2 - F_2^2} \qquad (3\text{-}181)$$

This equation is put into non-dimensional form by

$$X, H_1, H_2 = (x, h_1, h_2)/H \qquad (3\text{-}182)$$

Constant densimetric Froude numbers based on the total depth are defined as

$$F_{1H}^2 = F_1^2 H_1^3$$

$$F_{2H}^2 = F_2^2 H_2^3 \qquad (3\text{-}183)$$

A flow ratio is given by

$$Q = \frac{q_1}{q_2} \tag{3-184}$$

Hence

$$F_{1H}^2 = F_{2H}^2 \, Q^2/(1 - H_2)^3 \tag{3-185}$$

For counterflow, always

$$\frac{\text{sign}(q_1 - q_2)}{\text{sign}(q_2)} = -1 \tag{3-186}$$

Using these definitions the counterflow equation is written

$$\frac{dH_2}{dX} = \frac{F_{2H}^2}{8} \frac{f_o(1 - H_2)^3 + f_i[Q\,H_2 - (1 - H_2)]^2}{F_{2H}^2[Q^2\,H_2^3 + (1-H_2)^3] - H_2^3(1-H_2)^3} \text{sign}\,(q_2) \tag{3-187}$$

and can be integrated in inverted form

$$X_2 - X_1 = \int_{H_2(X_1)}^{H_2(X_2)} \frac{8}{F_{2H}^2} \frac{F_{2H}^2[Q^2\,H_2^3 + (1-H_2)^3] - H_2^3(1-H_2)^3}{f_o(1-H_2)^3 + f_i[Q\,H_2 - (1-H_2)]^2} \text{sign}(q_2)\, d\,H_2 \tag{3-188}$$

Equation (3-188) has been given in a slightly different form by Rigter (1970). The general form of the solution is given in Fig. 3-16 for sign $(q_2) = -1$ and consists of 3 branches which are divided by critical sections, where the slope of the interface goes to infinity. The critical relation is obtained by setting the denominator in Eq. (3-187) equal to 0,

$$F_{2H}^2[Q^2\,H_2^3 + (1 - H_2)^3] - H_2^3\,(1-H_2)^3 = 0 \tag{3-189}$$

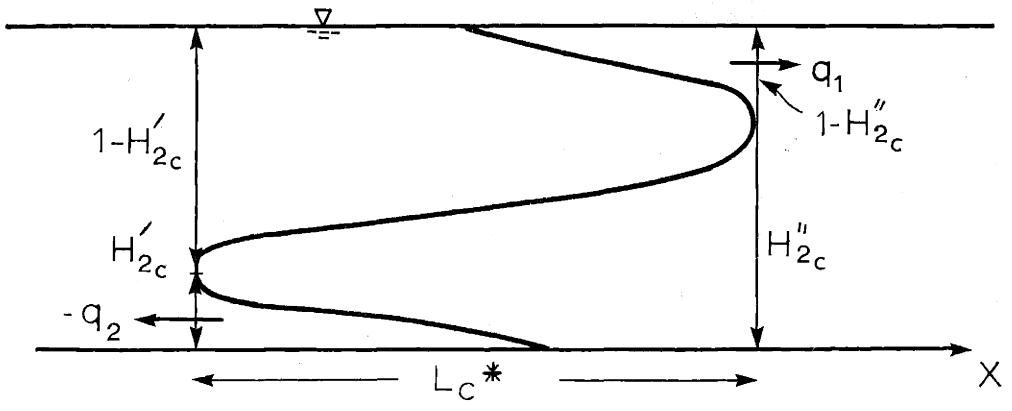

Fig. 3-16: Interfacial Height in Counterflow from Eq. (3-188)

The solution to this critical equation is plotted in Fig. 3-17 as a function of F_{2H} and $|Q|$. Subcritical flow is only possible if

$$\sqrt{F_{2H}} < \frac{1}{1 + \sqrt{|Q|}} \tag{3-190}$$

In this case there exist two critical section H'_{2_c} and H''_{2_c}. A critical section delineates the transition between subcritical and supercritical flow states and can be explained by energy considerations. In general, a critical section is given by abrupt changes in flow geometry. The channel ending in a large reservoir (see Fig. 3-2) is such a situation. In addition, a critical section can form the end of a local mixing region in case of an unstable internal hydraulic jump force, as discussed in Section 3.4.3.2. The length of the subcritical flow zone L^*_c between two critical sections is found by evaluating the integral (3-188) with limits H'_{2_c} and H''_{2_c}. This integration was carried out by Rigter (1970) numerically for the parameter range. Analytical solutions for special cases of Q are given in Section 3.4.4.4.

3.4.4.3 Head Loss in Stratified Flow

The change in total depth $H+\eta$ relates to the head loss incurred by the motion against shear forces at the bottom and interface. As commented in the preceding section the depth change is calculated by solving Eq. (3-175) with the flow field obtained through the constant depth approximation (3-177). One can write

$$\frac{d(\eta+H)}{dh_2} = \frac{d\eta}{dh_2} = \frac{d(h_1 + h_2)}{dx} \frac{dx}{dh_2} \tag{3-191}$$

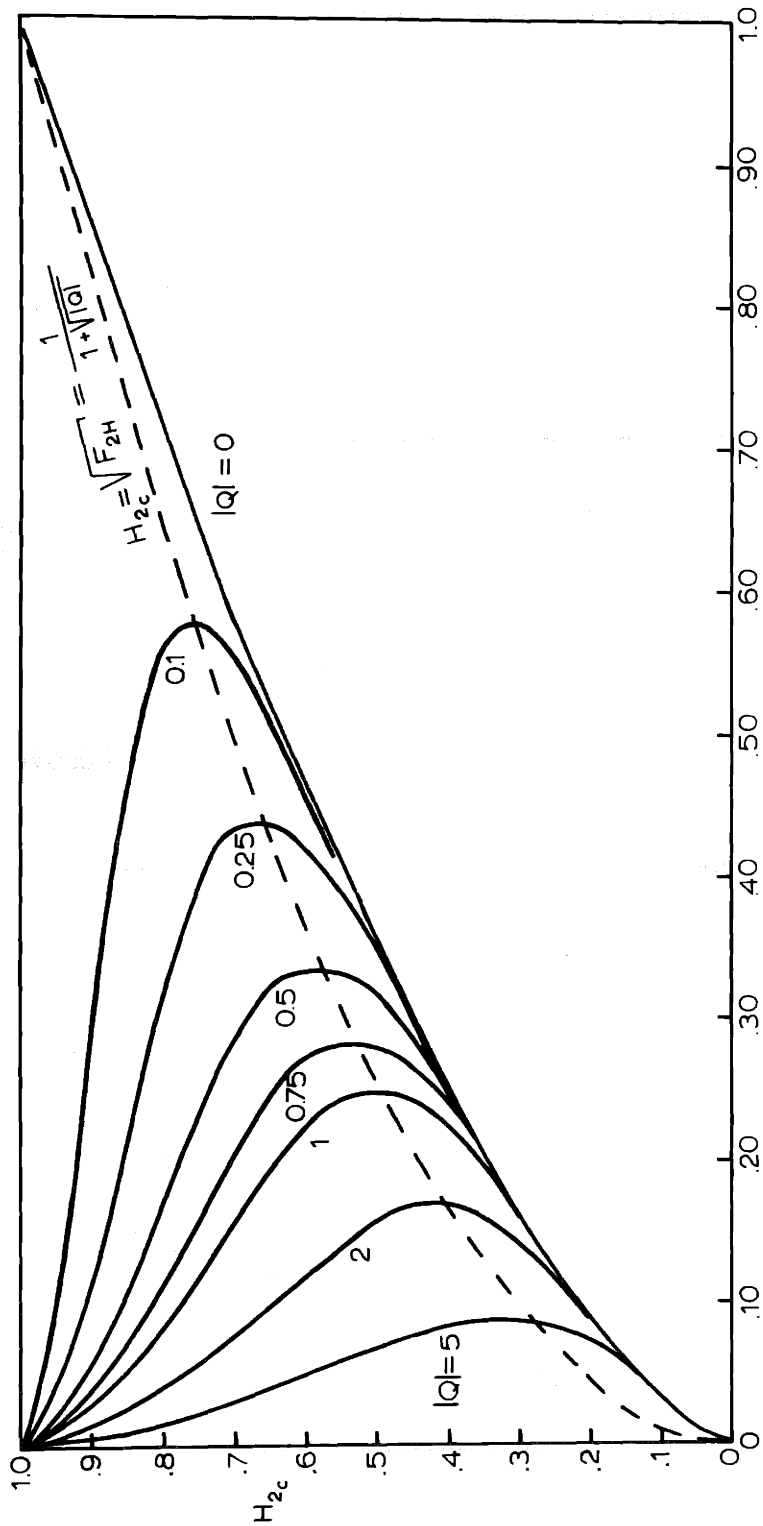

Fig. 3-17: Critical Depth H_{2_c} as a Function of F_{2_H}, $|Q|$

and substituting Eq. (3-175) and the inverted Eq. (3-174)

$$\frac{d\eta}{dh_2} = \frac{\tau_b \frac{F_1^{*2}}{h_2} + \tau_i \left(\frac{F_2^{*2}}{h_1} + \frac{F_1^{*2}}{h_2} \right)}{-\tau_b \frac{1-F_1^{*2}}{h_2} + \tau_i \left(\frac{1}{h_1} + \frac{1 + F_1^{*2}}{h_2} \right)} \tag{3-192}$$

Dividing both sides by $\Delta\rho/\rho_a$ and neglecting F_1^{*2}, $F_2^{*2} << 1$ in the denominator yields the equation for the normalized depth change

$$\frac{d}{dh_2} \left(\frac{\eta}{\Delta\rho/\rho_a} \right) = \frac{\tau_b \frac{F_1^2}{h_2} + \tau_i \left(\frac{F_2^2}{h_1} + \frac{F_1^2}{h_2} \right)}{-\tau_b \frac{1}{h_2} + \tau_i \left(\frac{1}{h_1} + \frac{1}{h_2} \right)} \tag{3-193}$$

Using the shear stress definitions and non-dimensionalizing as before, with

$$\eta^* = \eta/H \tag{3-194}$$

in addition, one obtains

$$\frac{d}{dH_2} \left(\frac{\eta^*}{\Delta\rho/\rho_a} \right) = - F_{2H}^2 Q^2 \left(\frac{1}{1 - H_2} \right) + F_{2H}^2 \frac{Q^2 \left(\frac{1}{1 - H_2} \right)^3 - \left(\frac{1}{H_2} \right)^3}{\left[\frac{f_o}{f_i} \frac{1}{\frac{H_2}{[Q \left(\frac{H_2}{1-H_2} \right) - 1]^2}} + 1 \right] \left(\frac{1-H_2}{H_2} \right) + 1} \tag{3-195}$$

This equation can be integrated between the same limits as Eq. (3-188) to give the head change $\frac{\eta^*}{\Delta\rho/\rho_a}\Big|_{X_1}^{X_2}$ and in particular the head change over the critical length L_c^*, $\frac{\Delta H^*}{\Delta\rho/\rho_a}$, can be found. Integration has to be numerical, except in special cases, as discussed in the following section.

3.4.4.4 Special Cases

Direct integrations of the interface Eq. (3-188) and the head loss Eq. (3-195) can be given for special values of Q. All these cases have strong significance in buoyant discharge problems.

a) $Q=0$: stagnant surface wedge

Equation (3-188) reduces to

$$X_2 - X_1 = \int_{H_2(X_1)}^{H_2(X_2)} \frac{8}{F_{2H}^2} \frac{F_{2H}^2(1-H_2) - H_2^3(1-H_2)}{f_o(1-H_2) + f_i} \operatorname{sign}(q_2)\, dh_2 \tag{3-196}$$

Integration gives (Bata (1957))

$$X_2 - X_1 = \frac{8}{f_o F_{2H}^2}\left[\frac{H_2^4}{4} + \frac{A}{3} H_2^3 + \frac{A(1+A)}{2} H_2^2 \right.$$

$$+ [A(1+A)^2 - F_{2H}^2]H_2 + A[(1+A)^3 \tag{3-197}$$

$$\left. - F_{2H}^2] \ln(1 + A - H_2) \right]_{H_1(x)}^{H_2(X)} \operatorname{sign}(q_2)$$

in which $$A = \frac{f_i}{f_o}$$

The intrusion length of the wedge, L^*_{ss}, upstream from a critical section is found by taking the limits

$$H_2(0) = 0 \tag{3-198}$$

$$H_2(L^*_{ss}) = F^{2/3}_{2_H}$$

There is zero depth change over the length of the intrusion as is evident from Eq. (3-195)

$$\frac{\Delta H^*}{\Delta\rho/\rho_a} = 0 \tag{3-199}$$

b) $Q \to \infty$: <u>stagnant bottom wedge</u>

In this case $F_{2_H} = 0$ as well, so that it is advantageous to rewrite Eq. (3-188) in terms of F_{1_H} :

(3-200)

$$X_2 - X_1 = -\int_{H_2(X_1)}^{H_2(X_2)} \frac{8}{F^2_{1_H}} \frac{F^2_{1_H}\left[H_2^3 + \frac{1}{Q^2}(1-H_2)^3\right] - H_2^3(1-H_2)^3}{f_o \frac{1}{Q^2}(1-H_2)^3 + f_i\left[H_2 - \frac{1}{Q}(1-H_2)\right]^2} \text{sign}\,(q_1)\,dH_2$$

with $Q \to \infty$

(3-201)

$$X_2 - X_1 = -\int_{H_2(X_1)}^{H_2(X_2)} \frac{8}{F^2_{1_H}} \frac{F^2_{1_H} H_2 - H_2(1-H_2)^3}{f_i} \text{sign}\,(q_1)\,dH_2$$

or integrated

(3-202)

$$X_2 - X_1 = -\frac{8}{F^2_{1_H} f_i}\left[(F^2_{1_H} - 1)\frac{H_2^2}{2} + H_2^3 - \frac{3}{4}H_2^4 + \frac{H_2^5}{5}\right]_{H_2(X_1)}^{H_2(X_2)} \text{sign}(q_1)$$

The length of the wedge intrusion, $L^*_{s_b}$, upstream from critical section is found by taking the limits

$$H_2(0) = 0$$

$$H_2(L^*_{s_b}) = 1 - F_{1_H}^{2/3} \tag{3-203}$$

This expression for the intrusion length was given by Schijf and Schönfeld (1953). The total head change over the intrusion length is after similar modification of Eq. (3-195)

$$\frac{\Delta H^*}{\Delta\rho/\rho_a} = \int_0^{1-F_{1_H}^{2/3}} \left(- F_{1_H}^2 \frac{1}{(1-H_2)^3} + F_{1_H}^2 \frac{h}{(1-H_2)^3}\right) dH_2 \tag{3-204}$$

and

$$\frac{\Delta H^*}{\Delta\rho/\rho_a} = + F_{1_H}^2 \left(\frac{1}{F_{1_H}^{2/3}} - 1\right) \tag{3-205}$$

c) $Q = -1$: <u>equal counterflow</u>

In this case Eq. (3-188) is given by ($F_{1_H} = F_{2_H} = F_H$)

$$X_2 - X_1 = \int_{H_2(X_1)}^{H_2(X_2)} \frac{8}{F_H^2} \frac{F_H^2(H_2^3 - (1-H_2)^3) - H_2^3(1-H_2)^3}{f_o(1-H_2)^3 + f_i} \operatorname{sign}(q_2)\, dH_2 \tag{3-206}$$

which can be integrated to

$$X_2 - X_1 = \frac{8}{f_o F_H^2}\Bigg[-\frac{1}{4}(1-H_2)^4 + (1-H_2)^3 - \frac{3}{2}(1+H_2)^2$$

$$+ (1+a^3)(1-H_2) + (-a + a^2 - a^4 \qquad (3\text{-}207)$$

$$+ \left(\frac{1}{2a} - \frac{1}{6a^2}\right)F_H^2)\ln\frac{(a+(1-H_2)^2}{(a+1-H_2)^2 - 3a(1-H_2)}$$

$$- (a^3 - F_H^2)\ln[a^3 + (1-H_2)^3] +$$

$$+ \left(\frac{-a + 3a^2 + a^4}{\sqrt{3}} - \frac{1}{a^3\sqrt{3}}F_H^2 + \frac{\sqrt{3}}{a}F_H^2\right)$$

$$\tan^{-1}\left(\frac{2(1-H_2) - a}{a\sqrt{3}}\right)\Bigg]_{H_2(X_1)}^{H_2(X_2)}$$

in which $$a = (A)^{1/3} = \left(\frac{f_i}{f_o}\right)^{1/3}$$

The length of the subcritical flow section, L_c, is found by substituting the solutions of the critical equation

$$H_{2_c}^3(1 - H_{2_c})^3 - F_H^2(H_{2_c}^3 + (1 - H_{2_c})^3) = 0 \qquad (3\text{-}208)$$

as limits into Eq. (3-207). Closed form integration of the depth change is also possible, but is omitted here, as it is not needed in the further analysis. Inspection of Eq. (3-208) which is plotted as the curve $|Q| = 1$ in Fig. 3-16 shows that equal counterflow can only

exist if

$$F_H \leq 0.25 \tag{3-209}$$

For the limiting value $F_H = 0.25$ it is found that $H_{1_c} = H_{2_c}$ and $L_c = 0$.

3.5 Matching of Solutions

In the preceding section the four flow regions which can be discerned in the flow field induced by a multiport diffuser discharge were analyzed. Governing equations were developed which took account of the distinct hydrodynamic properties of each region and solutions were given or outlined. The solutions for each region can be matched to provide an overall prediction of the diffuser induced flow field. In this way important criteria regarding the near-field stability of diffuser discharge will be deduced. Furthermore, in case of instabilities with resulting jet re-entrainment, predictions on diffuser performance will be developed.

This synthesis is done in Section 3.6 for the case of discharges with no net horizontal momentum (symmetric flow field) and in Section 3.7 for the more complex case of discharges with horizontal momentum.

3.5.1 Governing Non-dimensional Parameters

By dimensional analysis of the problem variables as defined in Fig. 3-2 and by inspection of the governing equations and their boundary conditions derived for each flow region the steady-state flow and temperature field is written as

$$\left(\frac{u}{U_o}, \frac{\Delta T}{\Delta T_o} \right) = f(F_s, \theta_o, H/B, L/H, f_o, f_i) \tag{3-210}$$

and

$$S = \frac{\Delta T_o}{\Delta T} \tag{3-211}$$

is the dilution at any point. This formulation assumes fully turbulent jet flow, hence independence of the jet Reynolds number of the slot

$$\mathbb{R}_j = \frac{U_o \, 2B}{\nu} \tag{3-212}$$

where ν = kinematic viscosity

and neglects heat loss to the atmosphere. Furthermore, the bottom shear stress coefficient in the flow away region is assumed to be in the turbulent flow range of the form

$$f_o = f(\mathbb{R}_2, \frac{k_s}{R_h}) \tag{3-213}$$

(White-Colebrook relation) in which

$$\mathbb{R}_2 = \frac{U_2 \, R_h}{\nu} = \text{lower layer Reynolds number}$$

R_h = hydraulic radius

k_s = absolute bottom roughness

and the interfacial shear stress coefficient is related by Eq. (3-197b)

$$f_i = A \, f_o \tag{3-214}$$

The ratio A can be assumed constant over a wide range of practical flow conditions, as is shown later. Through inspection of Eq. (3-188) it is found that f_o and L/H can be combined to a far field parameter

$$\Phi = f_o \, L/H \tag{3-215}$$

So that, finally the problem of the diffuser induced flow and temperature field (without ambient cross flow) is defined by these dimensionless parameters:

Near-field parameters: F_s = slot densimetric Froude number

θ_o = vertical angle of discharge

H/B = relative water depth

Far-field parameter: $\bar{\Phi}$

and Eq. (3-210) is reduced to:

$$\left(\frac{u}{U_o}, \frac{\Delta T}{\Delta T_o} \right) = f(F_s, \theta_o, H/B, \bar{\Phi}) \qquad (3\text{-}216)$$

The discussion of theoretical and experimental results is given for these parameters. The range of interest is

F_s = 10 to 1,000

θ_o = 90° (Section 3.6)

< 90° (Section 3.7)

H/B = 50 to 5,000

Φ = 0.1 to 1.0

which conforms to practical diffuser applications, as is shown in examples given in Chapter 5.

In the presentation of results, emphasis will be laid on the gross properties of diffuser discharges. In particular, the average non-dimensional surface temperature rise, or inversely the average surface dilution are chosen as the main descriptive parameters of the temperature field. The equivalent slot concept (F_s, H/B) is

used throughout in describing the multiport diffuser mechanics, based on the discussion in Chapter 2.

3.6 Theoretical Predictions: Diffusers With No Net Horizontal Momentum

Vertical discharge or discharge with nozzles pointing in alternating directions have no net horizontal momentum and thus will produce a flow field which is symmetrical to the diffuser axis.

3.6.1 The Near-Field Zone

The numerical integration of the buoyant jet equations (3-69) to (3-76) with initial conditions (3-78) is carried out for $\theta_o = 90°$ and various values of F_s. The integration yields jet properties as a function of vertical distance z/B. As an example the centerline dilution S_c along the jet path was shown in Fig. 3-6. The effect of the presence of the free surface is considered by solving the impingement equation (3-109). In the solution the energy loss coefficient k_L is taken as 0.2 throughout. The solution gives values for the thickness of the impingement layer h_i/H as shown in Fig. 3-18. The densimetric Froude number F_1 of the spreading layer after impingement is calculated from Eq. (3-126) and also included in Fig. 3-18. The graph indicates the asymptotic values for the plume in the high H/B, low F_s range, namely $h_i/H = 0.149$ and $F_1 = 2.63$ (Eqs. (3-120) and (3-129)). For the less buoyant range (large F_s) the value $h_i/H = 0.167 \simeq 1/6$ obtained from the solution of the momentum jet (Eq. (3-115)) is approached, although at low H/B there is a slight deviation to the fact that Eq. (3-115) assumes negligible slot width B compared to the depth H. For low H/B, high F_s the spreading layer

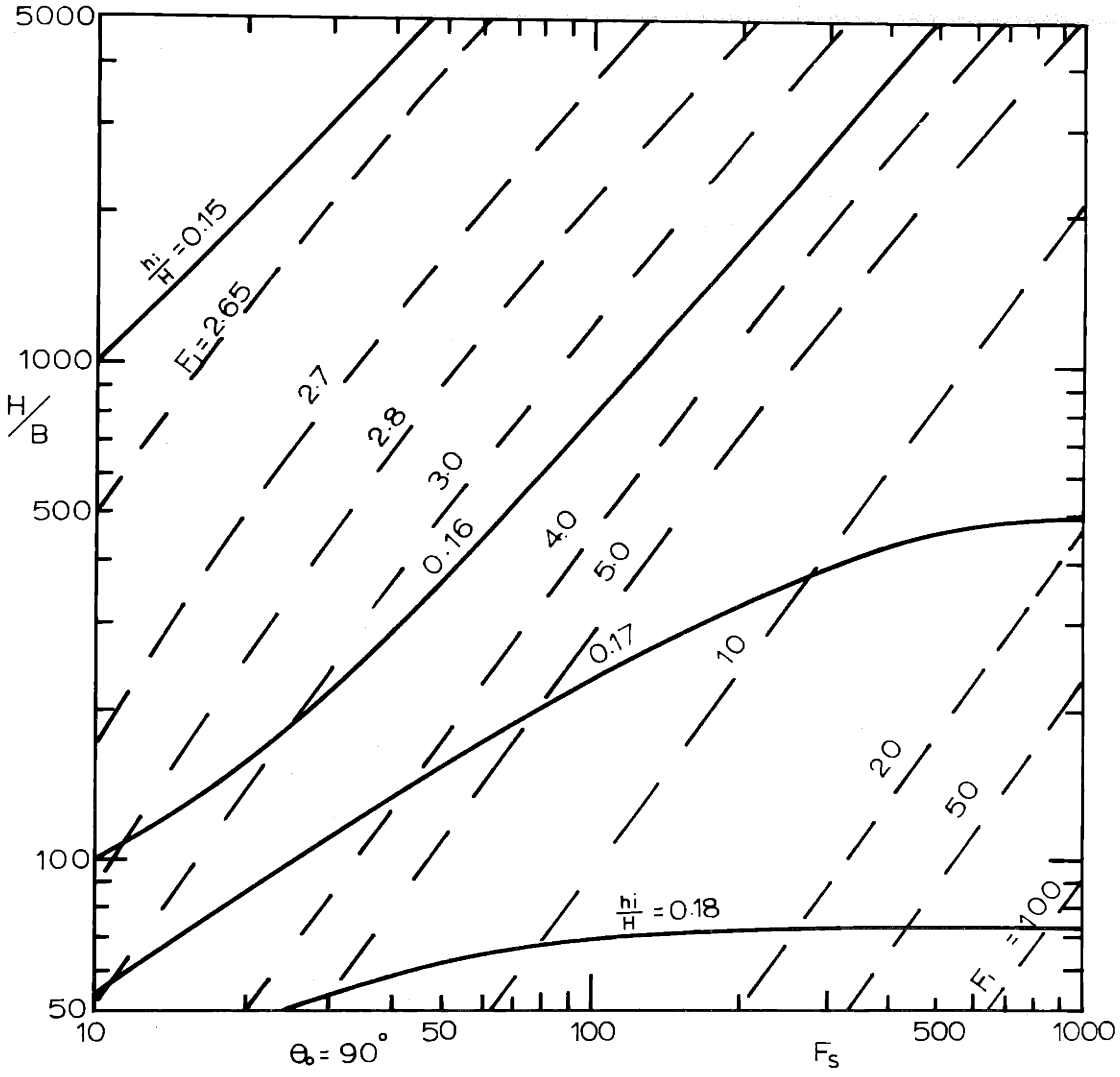

Fig. 3-18: **Thickness** h_i/H and Densimetric Froude Number F_1 of the Surface Impingement Layer, Vertical Discharge

Froude number F_1 becomes very large.

With given impingement layer thickness, the average surface dilution S_s is calculated. S_s is by virtue of the uniform mixing in the impingement process equal to the average jet dilution at the lower edge of the impingement region

$$S_s = \bar{S}(z = H - h_i) \tag{3-217}$$

Values of S_s are shown in Fig. 3-19.

With the given conditions prior to the internal hydraulic jump the jump equation (3-142) is evaluated giving solutions for the conjugate depth h_1'/H, as indicated in Fig. 3-19. For high H/B, low F_s the conjugate depth approaches one-half of the total depth, $h_1'/H \sim 0.5$. Proceeding toward the low H/B, high F_s range h_1'/H increases until $h_1'/H = 1 - h_1/H$, beyond which there is no positive solution to Eq. (3-142) possible (see Fig. 3-12b). This indicates the absence of a stable subcritical conjugate condition and re-entrainment into the jet region will occur, forming a local mixing zone. The transition is described by

$$F_H \approx 0.20 \tag{3-218}$$

where F_H is the average of F_{1_H} and F_{2_H} (Eq. (3-183)) and characterizes the dynamic characteristics of the counterflow system. In terms of discharge parameters F_s, H/B it can be deduced from the graph that

$$H/B = 1.84\, F_s^{4/3} \tag{3-219}$$

gives the criterion between stable and unstable near-field conditions. (See Fig. 3-20.) In consequence, dilution predictions S_s for the

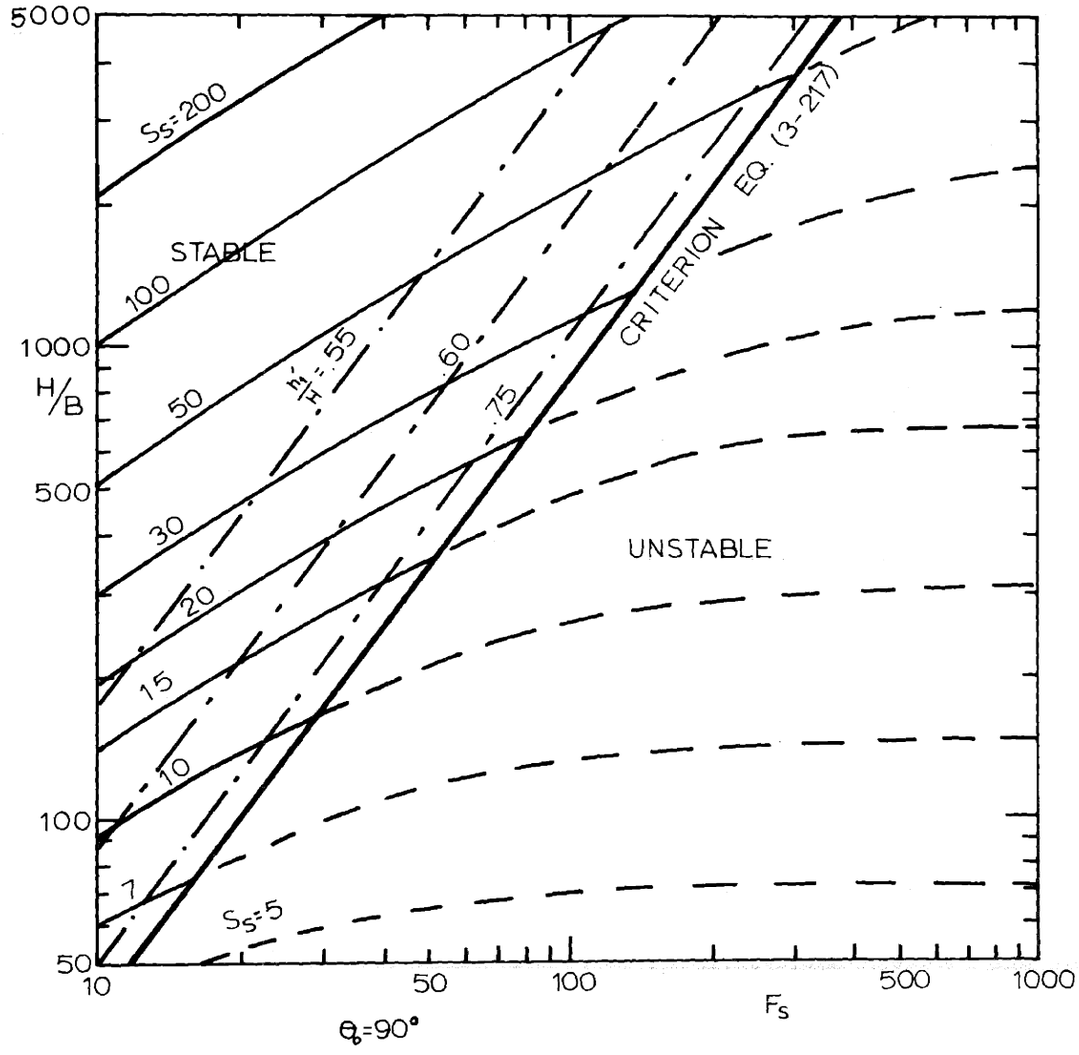

Fig. 3-19: Average Surface Dilution S_s Accounting for Thickness of Impingement Layer and Conjugate Depth h_1'/H for Internal Hydraulic Jump. Criterion Line Delineates Stable and Unstable Near-Field Zone

unstable parameter domain (drawn as dashed lines in Fig. 3-19) which are obtained as direct buoyant jet solutions, only accounting for the surface impingement, are in fact not applicable. Rather, dilutions in the unstable parameter domain are dependent on the dynamic conditions in the far field zone.

3.6.2 The Far-Field Zone

3.6.2.1 Interaction with near-field

The flow away from the near field zone forms a subcritical stratified counterflow region. The possibilities of interaction with the near-field zone are indicated in Fig. 3-20.

A) Stable near-field: In direct analogy to free surface hydraulic jumps, two conditions are possible depending on the backwater effects in the far-field which are determined by the control section (critical flow) of the channel end.

a) A normal internal jump is given when conjugate depth h_1' is larger than the depth h_{1_s} determined from the counterflow solution.

b) A submerged internal jump is given in the other case. Some re-entrainment of already mixed water into the jet region will occur until a condition is established in steady-state such that the increased buoyancy in the far-field will decrease the depth h_{1_s} until $h_1' = h_{1_s}$.

B) Unstable near-field: As no subcritical conjugate state exists in this case, local mixing and re-entrainment into the jet region takes place to a degree such that a critical section is established at the end of the local mixing zone as the limiting case of a subcritical flow

A) STABLE NEAR-FIELD

1. Normal Internal Jump

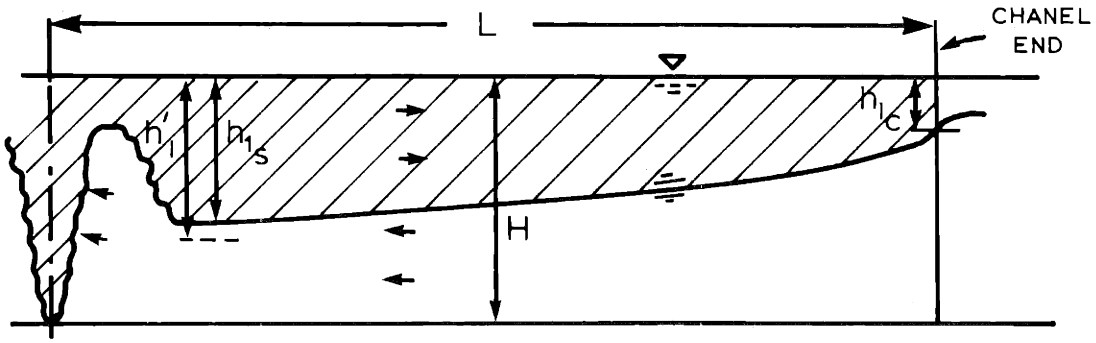

2. Submerged Internal Jump

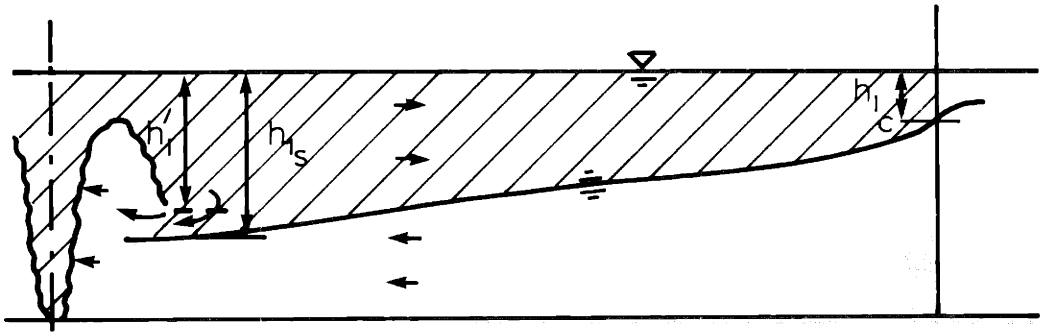

B) UNSTABLE NEAR-FIELD

Local Mixing and Reentrainment

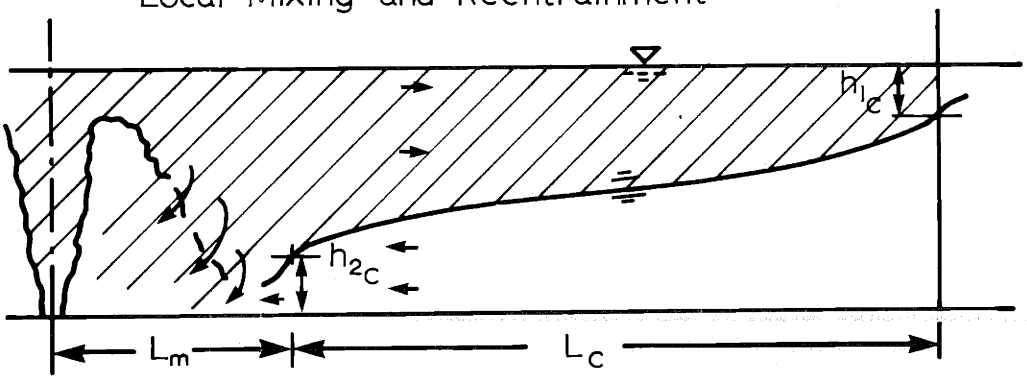

Fig. 3-20: Interaction of Near-Field and Far-Field Zones

(Vertical Diffuser Discharge)

condition. Stratified counterflow will then occur over the length, L_c, bounded by two critical sections. The length of the local mixing zone, L_m, is estimated as

$$L_m \approx 2.5\ H \tag{3-220}$$

from experiments made in this study which are in good agreement with Iamandi and Rouse's (1969) observations on circulation patterns induced by nonbuoyant jets in narrow channels. Consideration of L_m may be significant in the solution for short channels, for long channels, however, it may be neglected in comparison to L_c.

For the vertical diffuser discharge the effect of the far-field is considered by assuming an equal counterflow system. This is a good approximation for large dilutions, for which the entrainment flow is about equal to the flow-away of mixed water. The closed form solution for the position of the interface, Eq. (3-207), is applicable. The validity of Eq. (3-207) is restricted to subcritical flow, $F_H \leq 0.25$. For the case of stable near-field F_H is known from the solution of the near-field ($F_H \approx F_{1_H} = F_1\ h_1^3/H^3$) and the depth of the interface h_{1_s} at the distance L from the channel end is of interest. For the case of an unstable near-field the value of $F_H = F_{H_c}$ for which the length of the subcritical section, L_c, is equal to L (neglecting L_m) is of interest. The overall dilution S_s (outside the local mixing zone) is then determined from

$$F_{H_c} = \frac{q_1}{((\Delta\rho/\rho_a)\ g\ H^3)^{1/2}} = \frac{q_o\ S_s}{\left[(\Delta\rho_o/\rho_a)(1/S_s)\ g\ H^3\right]^{1/2}} \tag{3-221}$$

as

$$S_s = 4^{1/3} \left(\frac{F_{H_c}}{F_s} \right)^{2/3} \frac{H}{B} \qquad (3\text{-}222)$$

The far-field effect (friction and channel length) is given by the single parameter $\Phi = f_o\, L/H$ if $A = f_i/f_o$ is assumed constant.

3.6.2.2 Interfacial friction factor

While the boundary friction factor f_o can usually be estimated with good reliability as a function of Reynolds number and boundary roughness, there is a scarcity of data on the magnitude of the interfacial friction coefficient f_i in turbulent flows, in particular, in the high Reynolds number range. In addition, investigations indicate a certain dependence on the densimetric Froude numbers (F_1, F_2) of the layer flow (Lofquist (1960)). For density underflows, such as under a stagnant surface wedge, the ratio $A = f_i/f_o$ is about 0.43 (Harleman (1961)). For lock exchange flows, which resemble the equal counterflow situation, Abraham and Eysink (1971) gave f_i as drawn in Fig. 3-21. For large values of the lower layer Reynolds number a constant value of f_i is approached. For comparison the smooth wall friction relation for f_o is included in Fig. 3-21. In the Reynolds number range 5×10^2 to 10^5 $A = 0.4$ to 0.5 can be assumed. Based on this limited evidence A is taken as

$$A = \frac{f_i}{f_o} = 0.5 \qquad (3\text{-}223)$$

in all theoretical predictions given in this study.

3.6.2.3 Solution graphs - Surface dilution

Solution graphs giving the value of the surface dilution S_s (outside the local mixing region in case of an unstable

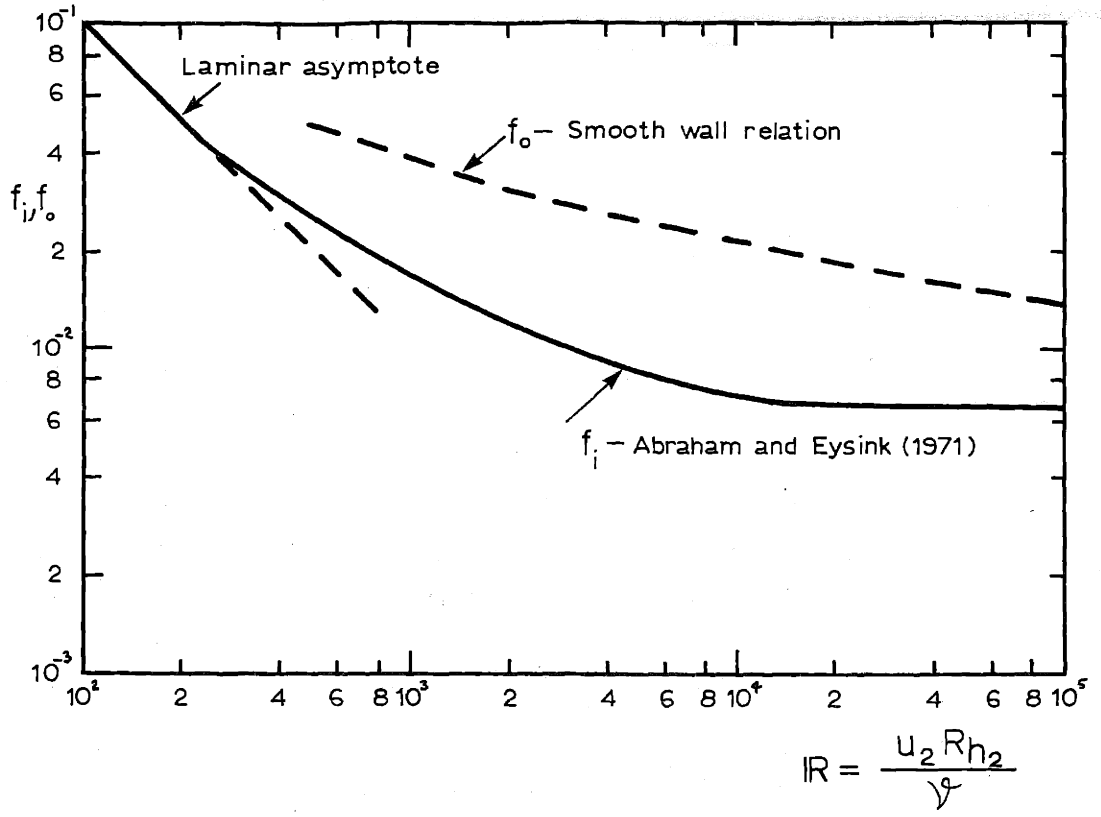

Fig. 3-21: Variation of interfacial stress coefficient f_i with Reynolds numbers (Abraham and Eysink (1971)).

near-field) as a function of F_s, H/B and $\Phi = f_o \frac{L}{H}$ are developed as follows:

a) For the stable near-field condition (Fig. 3-20 A-1) S_s is taken directly from the jet solution taking account of the impingement layer thickness. Thus the possibility of a submerged internal jump (Fig. 3-20 A-2) is not considered in the theoretical solutions, as this condition only becomes important for large values of Φ.

b) For the unstable near-field condition (Fig. 3-20B) the Froude number F_{H_c} of the equal counterflow system for which the length of the subcritical section is equal to the

channel length is calculated first. The value is F_{H_c} as a function of Φ (with A = 0.5) is plotted in Fig. 3-22. The dilutions S_s for any combination of F_s, H/B are then obtained from Eq. (3-222).

Examples of solution graphs within the practical range are given for weak far-field effects, $\Phi = 0.1$ in Fig. 3-23, and strong far-field effects, $\Phi = 1.0$ in Fig. 3-24. Comparison shows the decrease in dilutions for larger Φ. Furthermore, while for $\Phi = 0.1$ the lines for equal S_s for both near- and far-field approximately meet each other at the criterion line, there is a noticeable lack of matching for $\Phi = 1.0$. This indicates the submerged internal jump condition which is negligible for $\Phi = 0.1$ but which would provide for a smooth transition of equal dilution lines for $\Phi = 1.0$. This behavior can be seen by inspecting Fig. 3-22. As mentioned above the criterion line is characterized by $F_H \approx 0.20$ which is smaller than $F_{H_c}(\Phi = 0.1) \approx 0.22$ so that no back water effects leading to a submerged jump should be expected.

The important influence of near-field instabilities in combination with far-field effects is obvious when comparing the dilution predictions of Fig. 3-19 and Figs. 3-23 and 3-24.

Schematic illustration of the diffuser discharge, such as Fig. 3-20, showed a vertical diffuser discharge ($\theta_o = 90°$). However, the applicability of the two-dimensional slot representation with $\theta_o = 90°$ is pointed out also for diffusers with nozzles in alternating directions along the diffuser line. For the stable near-field case this can be inferred directly from the discussion of Liseth's (1970)

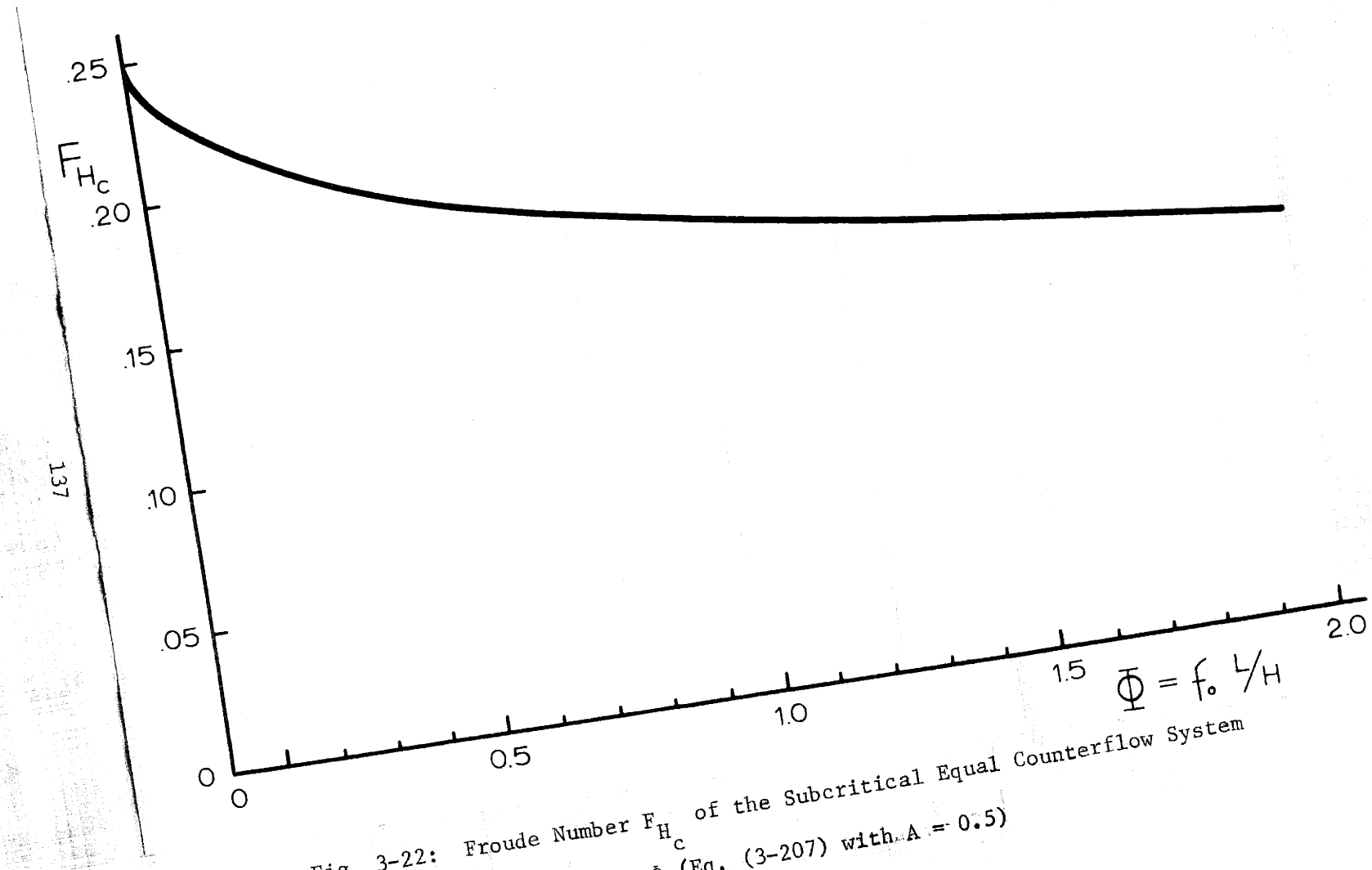

Fig. 3-22: Froude Number F_{H_c} of the Subcritical Equal Counterflow System as a Function Φ (Eq. (3-207) with A = 0.5)

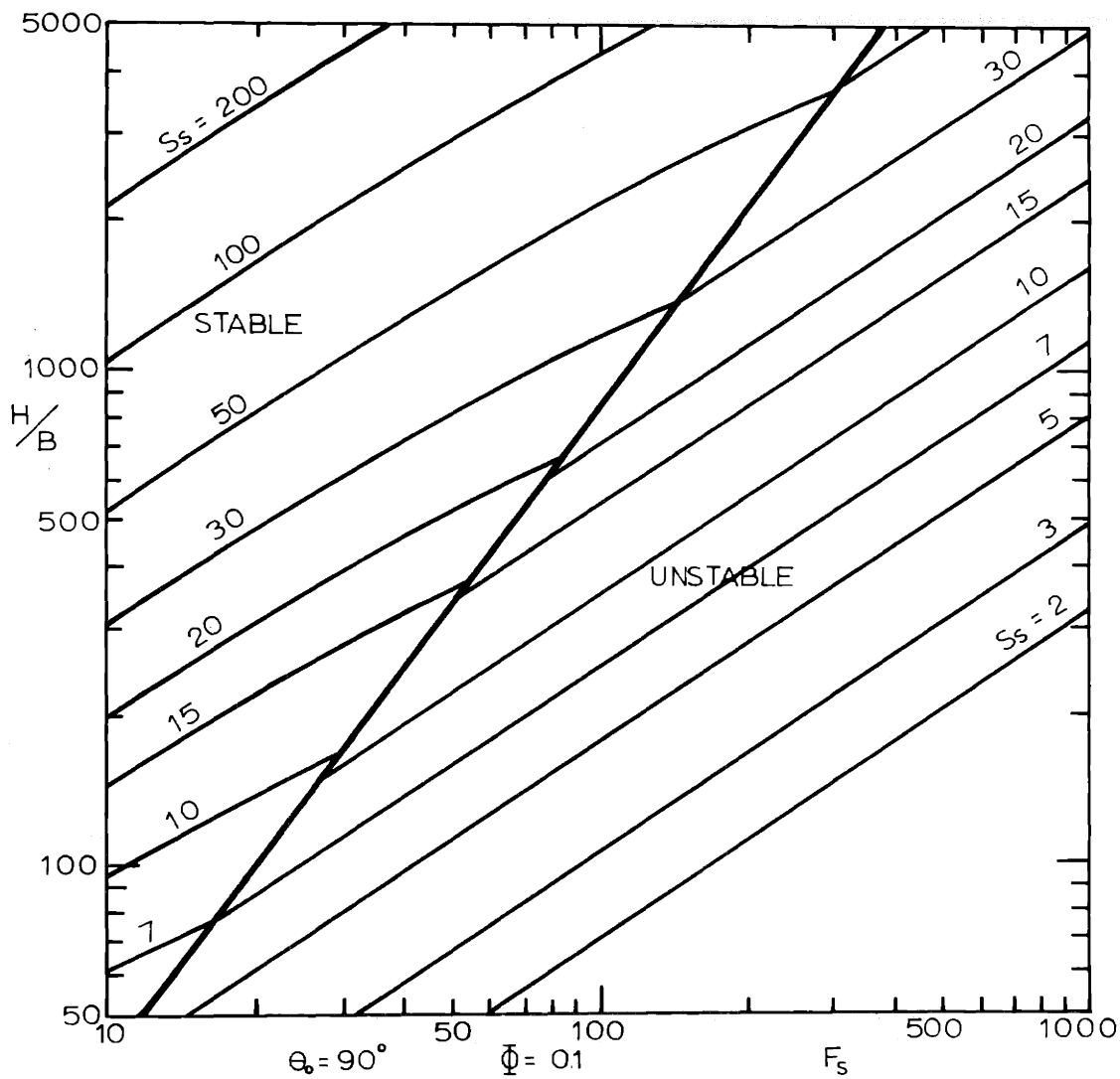

Fig. 3-23: Surface Dilution S_s as a Function of F_s, H/B.

Vertical Diffuser, Weak Far-Field Effects

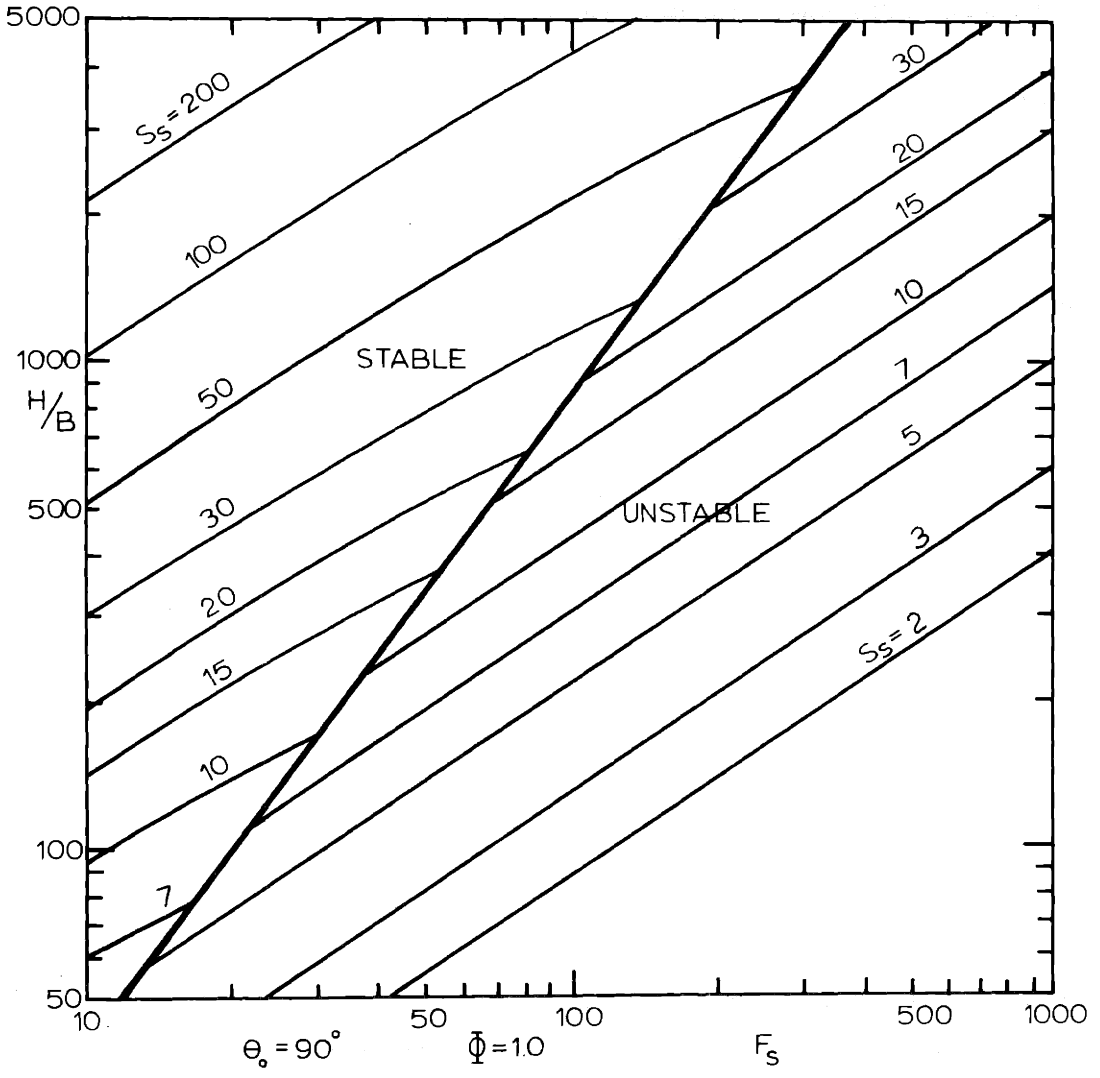

Fig. 3-24: Surface Dilutions S_s as a Function of F_s, H/b.

Vertical Diffuser, Strong Far-Field Effects

experimental result, as shown in Fig. 2-6. For the unstable near-field a local mixing zone is created which suppresses details of the jet discharge flow pattern (see Fig. 3-25). Dilution is determined

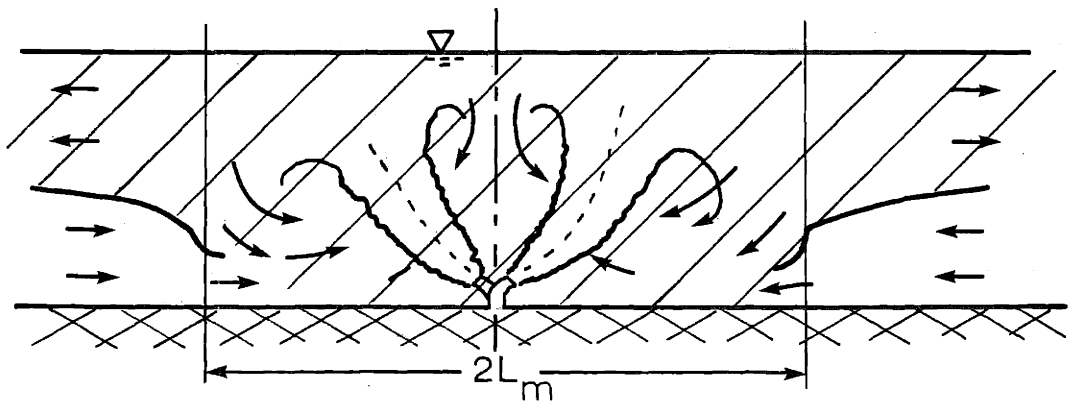

Fig. 3-25: Local behavior of diffuser discharge with alternating nozzles, unstable near-field.

merely by the interplay of far-field effects and buoyancy supply from the near-field zone, exactly as in the case of vertically discharging jets. The equivalent slot concept is thus applicable.

3.7 Theoretical Predictions: Diffusers with Net Horizontal Momentum

Diffusers with non-vertical nozzles pointing in the same direction (uni-directional discharge) can produce a variety of flow conditions which are somewhat more complicated to analyze than the previously discussed symmetric flow field generated by diffusers with no net horizontal momentum. Presentation of results is limited to $\theta_o = 45°$ and $\theta_o = 0°$ (horizontal discharge).

3.7.1 Near-Field Zone

The analysis of the buoyant jet region and the surface impingement is analogous to the previous section. A hydraulic jump occurs on both sides of the line of impingement, however, the jump at the right (section a in Fig. 3-8) becomes unstable earlier with increasing F_s or decreasing H/B. Furthermore, the stability is strongly dependent on the angle of discharge, θ_o. Figure 3-26 shows the criterion line delineating the stable and unstable near-field conditions for various θ_o. The average thickness of the impingement layer h_i/H within the stable range is again found to be about 1/6 for all θ_o. Outside the stable range h_i/H is rapidly increasing for increasing F_s and decreasing H/B. Yet the thickness in this range is not as important, as the near-field zone will be engulfed in a local mixing region due to the unstable jump condition.

3.7.2 Far-Field Zone

3.7.2.1 Possible flow conditions

The possible flow conditions in the far-field and the interaction with the near-field are indicated in Fig. 3-27.

A) Stable near-field

a) A normal internal jump and

b) a submerged internal jump are similar to the vertical discharge case.

B) Unstable near-field

Instabilities and jet re-entrainment lead to the formation of the local mixing zone. However, the conditions of the flow-away from

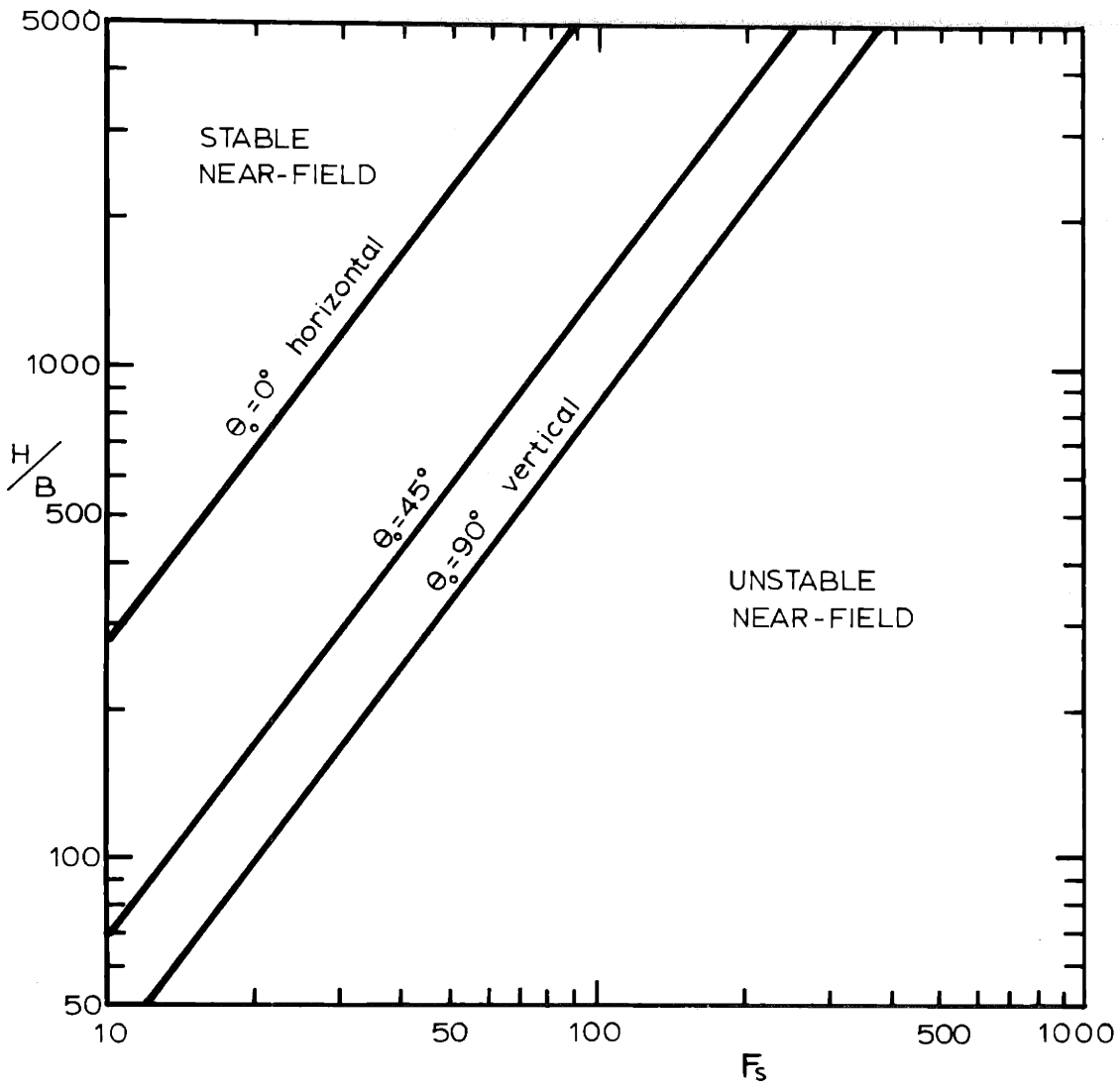

Fig. 3-26: Effect of Angle of Discharge θ_o on the Stability of the Near-Field Zone

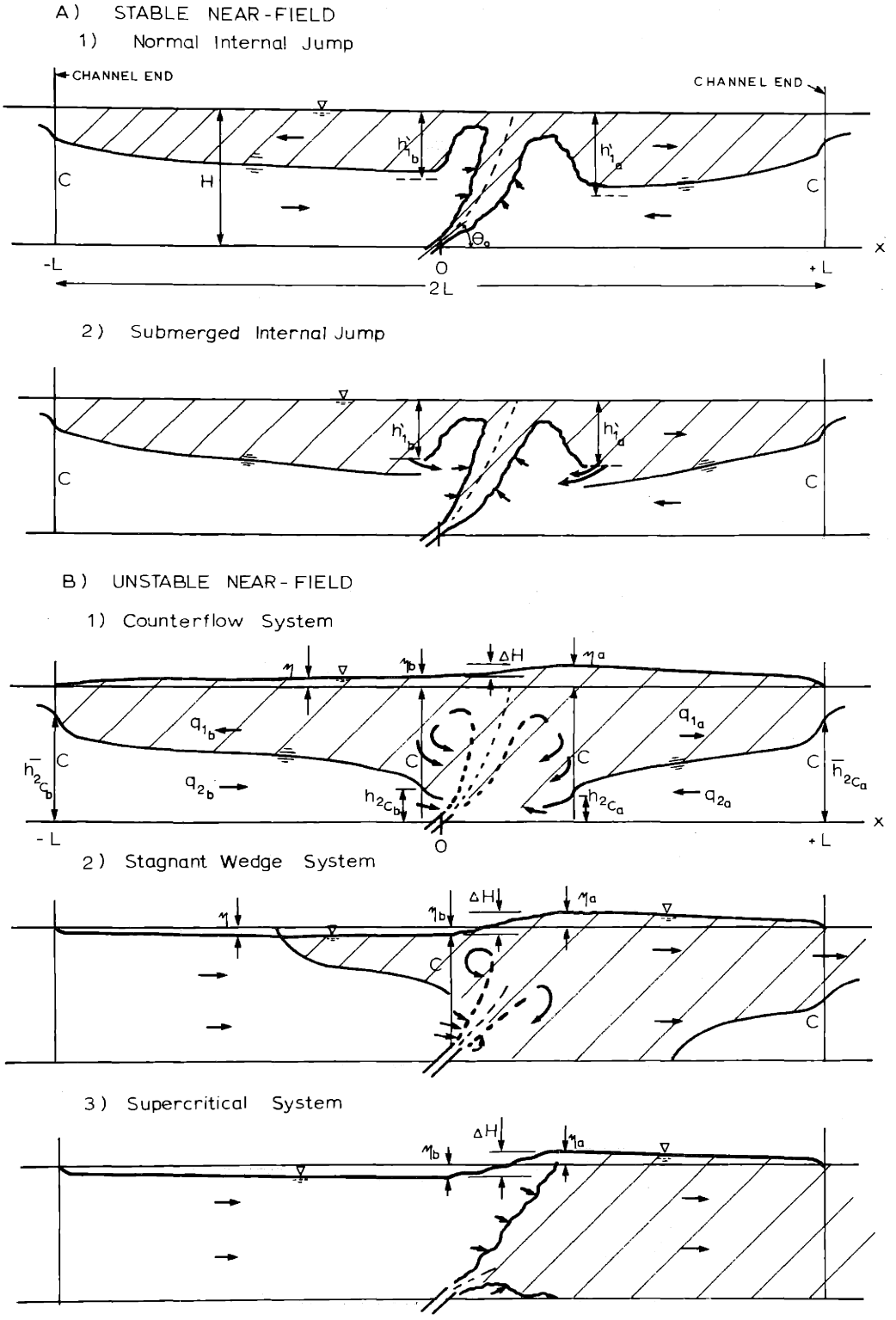

Fig. 3-27: Possible Flow Conditions for Discharges with Net Horizontal Momentum ("C" Denotes a Critical Section)

this mixing zone are affected by the strength of the horizontal jet momentum, which causes a net flow in one direction. Depending on the horizontal momentum 3 cases can be distinguished.

a) A Subcritical Counterflow System is given for weak horizontal momentum, somewhat similar to the vertical discharge case but with non-equal flows ($Q \neq -1$) in each layer. The existence criterion for this type of flow is (Eq. (3-190))

$$F_{2_H} < \frac{1}{(1 + \sqrt{|Q|})^2} \tag{3-224}$$

b) A Stagnant Wedge System is set up for larger horizontal momentum. Interfacial friction prevents motion of water against the direction of the jet discharge. Stagnant surface and bottom wedges are formed. For the upstream flow section the criterion is ($Q = 0$)

$$F_{2_H} < 1 \tag{3-225}$$

and similarly for the downstream section $F_{1_H} < 1$.

c) A Supercritical System results for still larger horizontal momentum, expelling the stagnant wedges. The densimetric Froude number of the flow is simply

$$F_H > 1 \tag{3-226}$$

This extreme flow system resulting in full vertical mixing is the case studied by Harleman et al. (1971) for horizontal discharge ($\cos \theta_o = 1$) and is described by Eq. (2-38) which for

the purpose of introducing the far-field parameter Φ and the angle θ_o rewritten as

$$S_s = \frac{1}{(1 + \Phi/2)^{1/2}} \left(2 \frac{H}{B} \cos \theta_o\right)^{1/2} \qquad (3\text{-}227)$$

For the analytical treatment of unstable near-field conditions it is necessary to consider the total head changes, η, due to friction in the far-field. η is indicated schematically in Fig. 3-27. The head change ΔH causes a pressure differential across the diffuser mixing zone which in steady state is balanced by the horizontal momentum of the diffuser. The equation for the head change η in stratified flow was developed earlier (Eq. 3-195) and solutions for the wedge cases were given in paragraph 3.4.4.4.

3.7.2.2 Solution Method

The counterflow system (Fig. 3-2 B1) is the most general form of the flow distribution in case of an unstable near-field. The flow system is made up of two counterflow regions bounded by critical sections. Its properties are described by the following 8 variables (subscripts a and b refer to conditions down- and upstream, respectively):

$$S_s, q_{1_a}, q_{1_b}, q_{2_a}, q_{2_b}, \eta_a, \eta_b, H$$

Given parameters are F_s, H/B, Φ and θ_o.

The variables are determined by the simultaneous solution of the following system of non-linear algebraic equations: (The equations are

all written in explicit, symbolic form to suggest the iterative solution method)

1) $S_s = q_{1_a} + q_{2_a}$

2) $q_{2_a} = q_{1_a}/Q_a\,(F_{1_{H_a}}, \Phi)$

where $Q_a(F_{1_{H_a}}, \Phi)$ denotes the explicit form of the interface Eq. (3-188) evaluated between 0 and L .

3) $q_{2_b} = (S_s - 1) - q_{2_a}$

4) $q_{1_a} = q_{2_a}\, Q_b\,(F_{2_{H_b}}, \Phi)$

where $Q_b(F_{2_{H_b}}, \Phi)$ is the explicit form of Eq. (3-188) evaluated between -L and 0 .

5) $$\frac{\Delta H/H}{\Delta\rho/\rho_a} = \left(F^2_{1_{H_b}} \frac{H}{H - h_{2_{c_b}}} + F_{2_{H_b}} \frac{H}{h_{2_{c_b}}} + S_s F_s^2 \frac{1}{(H/B)^2} \cos\theta_o \right.$$

$$\left. - F^2_{1_{H_a}} \frac{H}{H - h_{2_{c_a}}} - F^2_{2_{H_a}} \frac{H}{h_{2_{c_a}}} \right)$$

which is a horizontal momentum equation obtained by taking a control volume between the two critical sections bounding the local mixing zone. The critical depths $h_{2_{c_a}}$, $h_{2_{c_b}}$ are implicitly known from the solution of the interface equations

6) $$\frac{\eta_b/H}{\Delta\rho/\rho_a} = \frac{\eta/H}{\Delta\rho/\rho_a}(F_{2_{H_b}}, \Phi) + \frac{1}{2} F^2_{1_{H_b}} \frac{H^3}{h_{2_{c_b}}}$$

The first term is the head loss equation (3-195) evaluated between $-L$ and 0 and the second term accounts for the loss of the velocity head in the channel and due to dissipation outside the channel.

7) $$\frac{\eta_a/H}{\Delta\rho/\rho_a} = \frac{\Delta H/H}{\Delta\rho/\rho_a} - \frac{\eta_b/H}{\Delta\rho/\rho_a}$$

8) $$q_{1_a} = q_{2_a}\, Q_a \left(\frac{\eta_a/H}{\Delta\rho/\rho_a}\right)$$

where $Q_a\left(\frac{\eta_a/H}{\Delta\rho/\rho_a}\right)$ is the implicit form of an equation for the a-region similar to 6).

A Gauss-Seidel iteration method was used. In the given arrangement of equations 1) to 8), specification of initial values for S_s and Q_{1_a} is needed. Convergence to a stable value for S_s is fast, taking only 5 to 10 iterations depending on the initial guess.

In the above formulation the length of the mixing zone was neglected with respect to the channel length. Derivation of the horizontal momentum equation assumed hydrostatic conditions at the end of the mixing zone which is consistent with assumptions made for the stratified flow regions.

The stagnant wedge system (Fig. 3-27 B2) is described by a similar, but simpler system of equations.

3.7.2.3 Solution Graphs - Surface Dilution

Solution graphs giving surface dilutions S_s for both the stable and unstable near-field range are given for weak and strong far-

field effects for $\theta_o = 45°$ (Fig. 3-28, $\Phi = 0.1$ and Fig. 3-29, $\Phi = 1.0$) and for $\theta_o = 0°$ (Fig. 3-30, $\Phi = 0.1$ and Fig. 3-31, $\Phi = 1.0$). In all graphs three transition lines are included: 1) the criterion between stable and unstable near-field conditions, 2) the transition between the counterflow system and the stagnant wedge system is given when the wedge length is just equal to the channel length, and 3) the transition between the wedge system and supercritical flow, given when $F_H = 1$. Based on the solution in the supercritical case Eq. (3-227) this transition can be given as

$$H/B = F_s^{4/3} \frac{2 \cos \theta_o}{1 + \frac{\Phi}{2}} \qquad (3\text{-}228)$$

In the supercritical case the dilution S_s is independent of F_s and the flow is fully mixed vertically. The dilution is a minimum at the point of maximum wedge intrusion length. Similar to the vertical discharge case, the matching at the transition between stable and unstable near-field dilution predictions will be smoothed out through the submerged internal jump regime which is not considered in the prediction.

3.8 Summary

The mechanics of a submerged diffuser were analyzed in a two-dimensional "channel model". The channel model consists of a diffuser section bounded by channel walls of finite length and opening at both ends into a large reservoir. The rationale for the channel model is to simulate the predominantly two-dimensional flow which is postulated

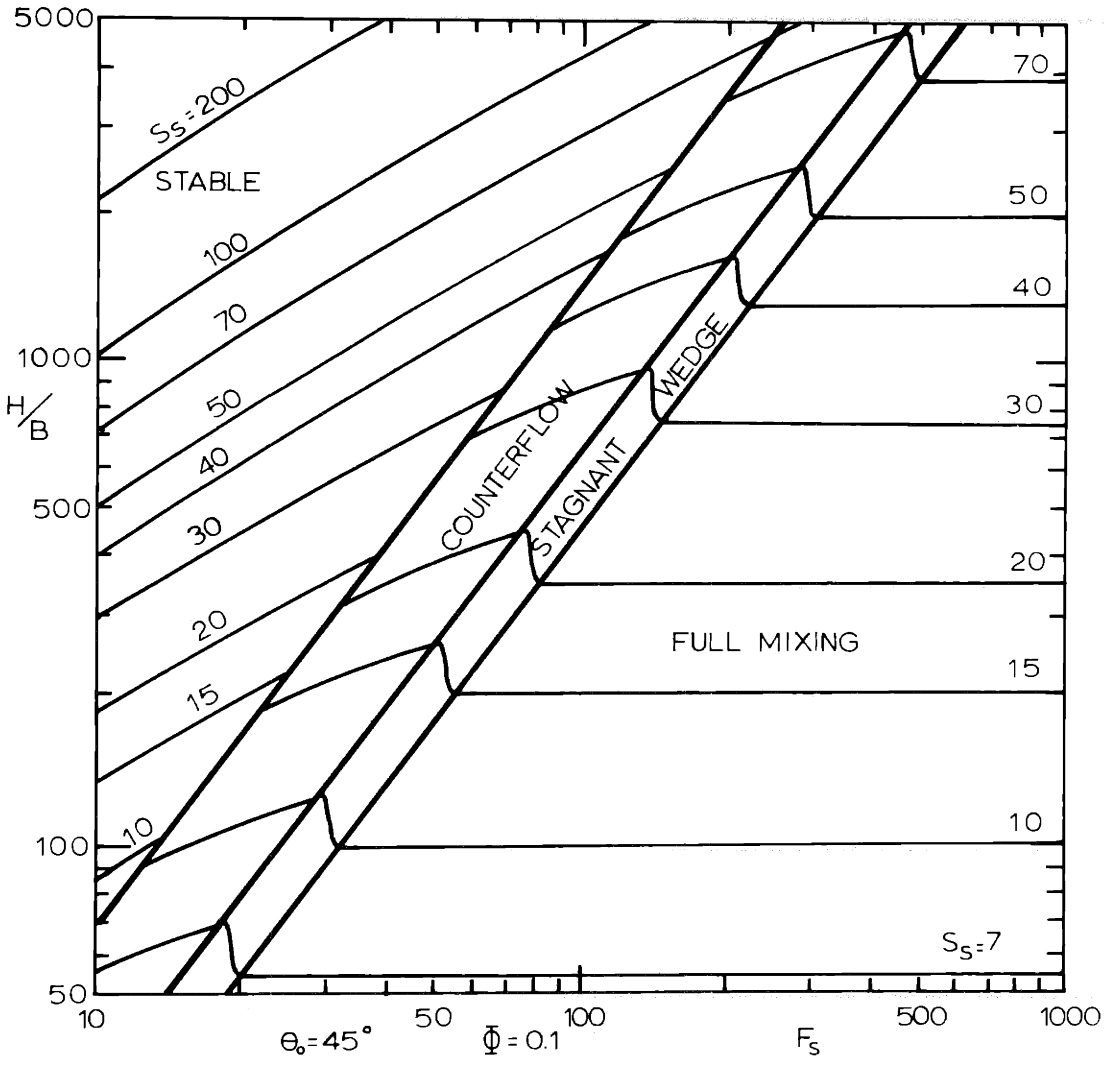

Fig. 3-28: Surface Dilution S_s as a Function of F_s, H/B. 45° Discharge, Weak Far-Field Effects

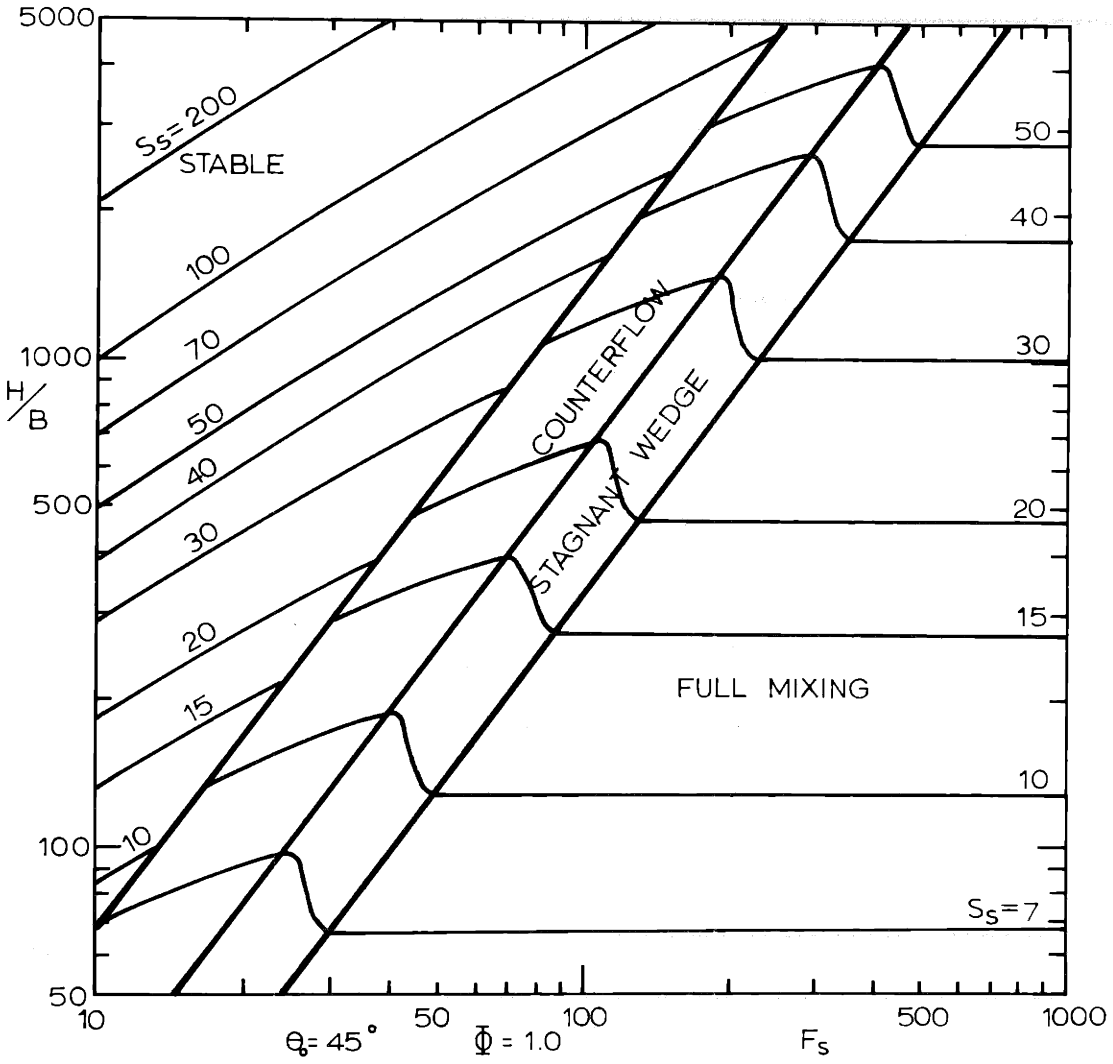

Fig. 3-29: Surface Dilution S_s as a Function of F_s, H/B.

45° Discharge, Strong Far-Field Effects

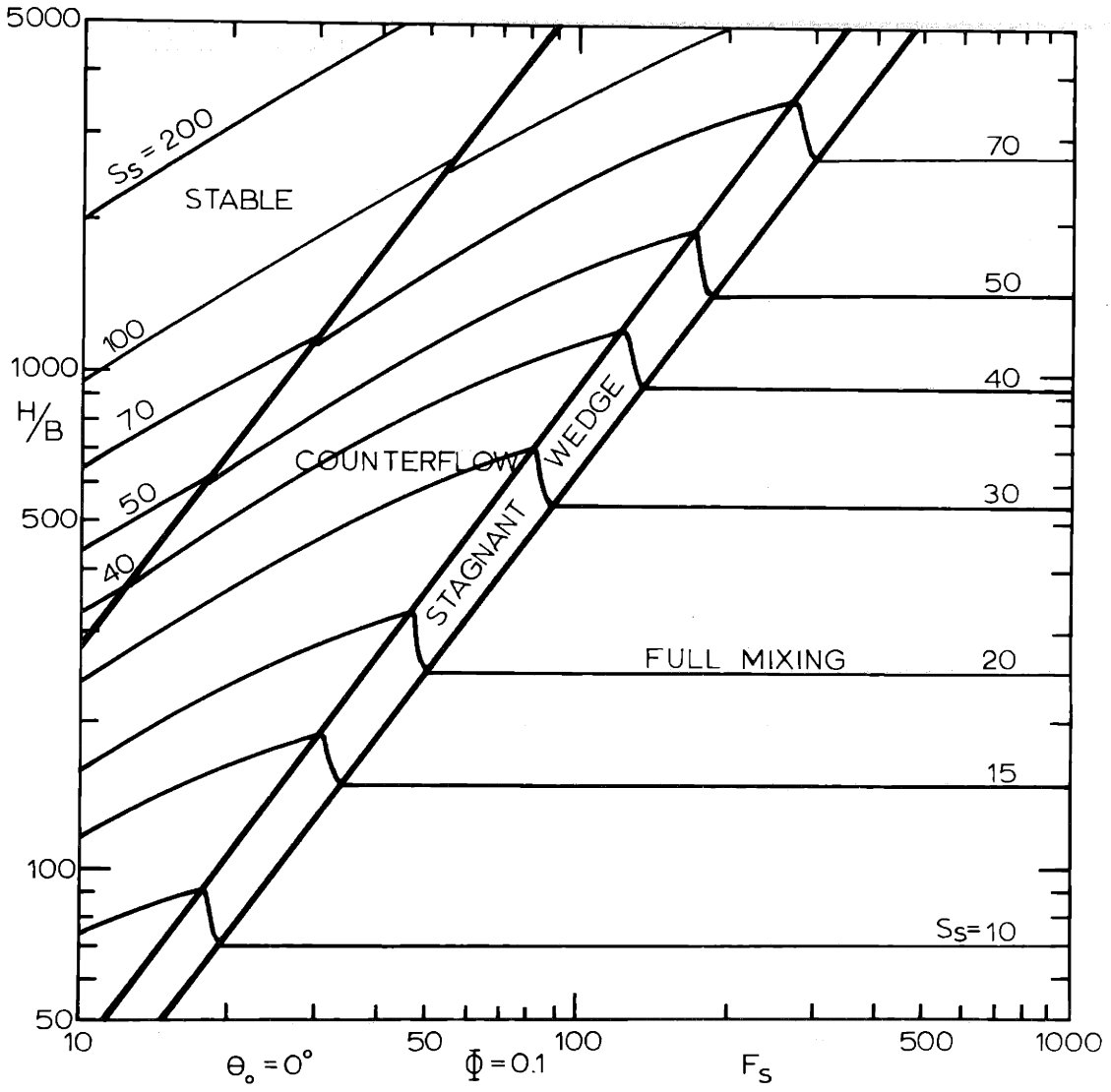

Fig. 3-30: Surface Dilution S_s as a Function of F_s, H/B.
Horizontal Discharge, Weak Far-Field Effects

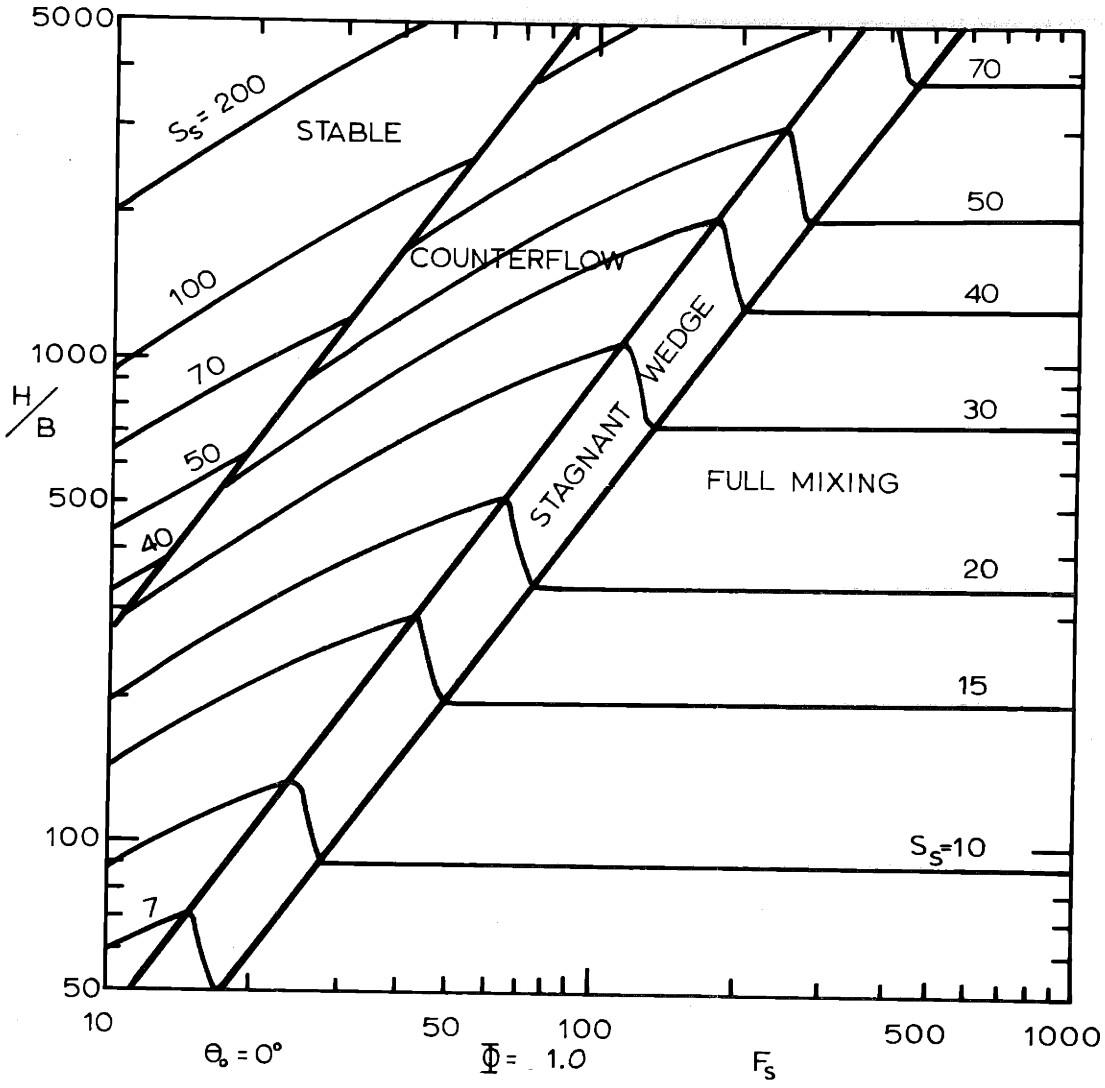

Fig. 3-31: Surface Dilution S_s as a Function of F_s, H/B.
Horizontal Discharge, Strong Far Field Effects

to exist in the center portion of a three-dimensional diffuser discharge. The multiport arrangement was represented by the equivalent slot concept, preserving the dynamic characteristics of the jet discharge.

In analyzing the two-dimensional flow field emphasis was laid on a detailed treatment of the four distinct flow regions which can be discerned in the general case. The objective was to obtain an overall description of the flow field by matching of the solutions for the individual regions. The four flow regions are: the buoyant jet region, the surface impingement region, the internal hydraulic jump region and the stratified counterflow region.

The buoyant jet region was analyzed using the entrainment concept proposed by Morton et al. (1956). A relationship for the entrainment coefficient (Eq. (3-48)), which depends on the local buoyant characteristics of the jet was deduced for jets with arbitrary discharge angle in a fashion similar to Fox's (1970) solution for the vertical jet. It was shown that all buoyant jets tend to an asymptotic case, the plume, which is characterized by a constant local densimetric Froude number, Eq. (3-57). The value of the entrainment coefficient (Eq. (3-48)) in this asymptotic case agrees well with Abraham's (1963) evaluation of Rouse et al.'s (1952) experimental data.

Important aspects of the analysis of the surface impingement region were the inclusion of an energy loss and a buoyancy term in the energy equation. It was found that the vertical flow distribution in the section after impingement is always distinguished by densimetrically supercritical flow conditions leading to a subsequent internal hydraulic jump.

The internal hydraulic jump region is described by a set of equations first derived by Yih and Guha (1955), which in general is dependent on the density ratio between the two layers and the free surface Froude numbers. As the problem of interest is characterized by small density differences and small free surface Froude numbers, an asymptotic solution for finite densimetric Froude numbers was derived giving a simple equation (3-142) for the conjugate jump condition.

The equations for a non-entraining stratified counterflow region with surface heat loss and interfacial mixing were developed. Scaling showed that for practical conditions of channel length scales the surface heat transfer processes can be neglected, so that the equations reduce to the classical Schijf and Schönfeld (1953) equations for stratified flow. The solution for the position of the interface, Eq. (3-188), is obtained assuming constant total depth as a first approximation, which again implies small density differences and free surface Froude numbers. With the given interface position, the change of the total head caused by frictional effects in the flow system was derived, Eq. (3-195). Analytical solutions for the interface and total head equations were given.

The diffuser problem is governed by four dimensionless parameters : F_s, H/B and θ_o are near-field parameters, $\Phi = f_o\, L/H$ is a far-field parameter.

Matching of the solutions for the flow regions yields the following important results: stability of the near-field zone is given only for a limited range of low F_s , high H/B . Furthermore, the range decreases for decreasing (more horizontal) θ_o (Fig. 3-25). It is only in this

limited range that the buoyant jet models in an unbounded receiving water (discussed in Chapter 2) are applicable to predict dilutions. It is found that in this range the thickness of the surface impingement layer which has to be accounted for in dilution predictions is about 1/6 of the water depth. The flow-away in the far-field has little effect on near-field dilution (except for large Φ leading to a submerged internal jump) and thus can be neglected for dilution predictions.

Outside the stable near-field range the diluted water is continuously re-entrained into the jet region forming a local mixing zone. This re-entrainment leads to a build-up of buoyancy of the near-field water until in steady state an equilibrium is reached which is essentially determined by the interplay of two factors: frictional effects in the far-field, represented by Φ , and the horizontal momentum input of the jet discharge, represented by θ_o .

For diffusers with no net horizontal momentum ($\theta_o = 90°$) the far-field flow is given by an equal counterflow system between two critical sections, one at the edge of the local mixing zone, one at the channel end.

For diffusers with net horizontal momentum ($\theta_o < 90°$) there are 3 possible far-field flow configurations: a counterflow system, a stagnant wedge system or supercritical flow. The supercritical flow case with resulting full vertical mixing downstream is the extreme case of surface and bottom interaction described by Harleman et al. (1971) and reviewed in Chapter 2. In the analysis of each of these conditions the horizontal momentum of the discharge is balanced by the depth change across the mixing zone resulting from far-field effects.

Composite surface dilution graphs describing both the near- and far-field range were presented.

The utility of the two-dimensional channel model in the study of the diffuser induced flow field is obvious:

(1) It provided necessary criteria giving the range of applicability for buoyant jet models to predict dilutions for diffuser discharge in finite depth.

(2) It gave insight into the vertical and longitudinal variations of the flow field.

(3) It demonstrated that it is necessary to describe the dynamics of the total flow field, and not merely the jet region, to give dilution predictions outside the stable near-field range.

However, as the underlying objective of this study is prediction of the three-dimensional diffuser flow field it will be necessary to provide some linkage between the far-field effects present in the two-dimensional channel model and the far-field effects present in the three-dimensional case. In particular, based on the requirement of equivalency of the far-field effects a relationship between the characteristic horizontal length scales, the two-dimensional channel length and the three-dimensional diffuser length, has to be developed. This linkage is provided in analytical fashion in Chapter 4 and comparisons with experimental results are given in Chapter 6.

IV. THREE-DIMENSIONAL ASPECTS OF THE DIFFUSER INDUCED FLOW FIELD

A multiport diffuser line of length, $2L_D$, placed in a large body of water of uniform depth, H, will generate a three-dimensional flow pattern. In the preceding chapter a two-dimensional channel model was formulated simulating the predominantly two-dimensional flow field which is postulated to exist in the center portion of the diffuser line (Fig. 3-1). Depending on discharge conditions it was found that a stable or unstable near-field condition persists. For the stable near-field, the diffuser-induced dilution is primarily governed by jet entrainment. However, for unstable near-field conditions, the dilution is influenced by far-field effects relating to the total resistance in the flow-away of mixed water from the near-field. As the objective of this study is dilution prediction in the general three-dimensional case, this chapter discusses the important three-dimensional aspects of the diffuser-induced flow field and their relation to the two-dimensional channel model:

i) A simplified model of the three-dimensional flow field is developed and the far-field effects are evaluated. Based on equivalency of far-field effects, the channel length of the corresponding two-dimensional model is related to the length of the three-dimensional diffuser. In this way predictions for the three-dimensional application may be given through the corresponding two-dimensional channel model.

ii) In addition to vertical circulations (such as in the stratified counterflow system), the diffuser is capable of producing circulations in the horizontal plane. The

existence of these circulations which ultimately lead to re-entrainment of mixed water is related to near-field instabilities. The control of these circulations through orientation of the diffuser nozzles in the horizontal plane is discussed.

4.1 Relating the Two-Dimensional Channel Model to the Three-Dimensional Flow Field

A quantitative relationship is given only for diffuser discharge with no net horizontal momentum and zero cross flow. Diffusers with net horizontal momentum are discussed qualitatively and experimental results are given.

4.1.1 Diffusers with No Net Horizontal Momentum

4.1.1.1 Equivalency Requirements

Figure 4-1 shows the vertical circulation and the horizontal flow pattern in the lower layer postulated for a diffuser with no net horizontal momentum. The horizontal flow pattern in the upper layer is similar with reversed directions. The three-dimensional situation and the two-dimensional channel model conceptualization are shown. In both cases the flow is set up by the entrainment demand and the buoyancy supply within the near-field zone. For comparison of the dilution characteristics of both systems it is required that the near-field parameters F_s, H/B are the same. Furthermore, the same friction coefficients f_o and $f_i = Af_o$ are given.

The objective of the comparison is to determine the channel length L so that the same dilution is obtained from the two-dimensional channel model as from the three-dimensional case. To obtain the same dilutions

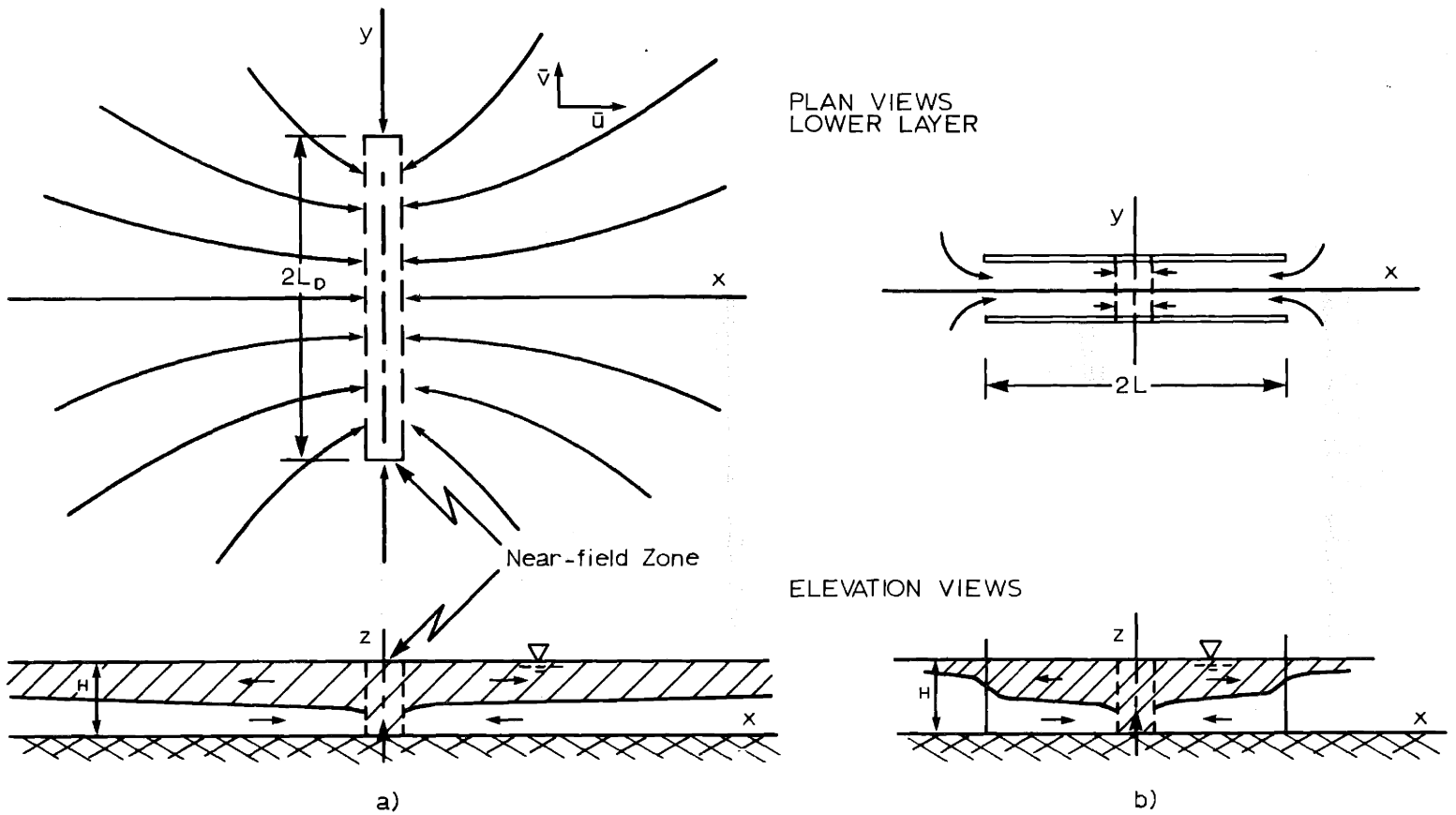

Fig. 4-1: Comparison of Flow Fields for a) Three-Dimensional Diffuser with Control and b) Two-Dimensional Channel Model Conceptualization

two requirements have to hold:

1) Kinematic Requirement

The dilution for the two-dimensional case is

$$S_{2-D} = \frac{|q|}{q_o/2} = \frac{|\bar{u}|H}{q_o/2} \tag{4-1}$$

where $|q| = q_1 = -q_2$ is the flow in each layer (large dilutions)

$\bar{u}$ = layer velocity u averaged over total depth H.

$\bar{u}$ is constant throughout the channel,

$$\bar{u} = \bar{u}_c \ . \tag{4-2}$$

The dilution for the three-dimensional case is

$$S_{3-D} = \frac{|q_{x_d}|}{q_o/2} = \frac{|\bar{u}_d|H}{q_o/2} \tag{4-3}$$

where q_{x_d} is the normal (x) component of the flow vector $\vec{q} = (q_x, q_y)$ evaluated at the diffuser $x \simeq 0$, $-L_D < y < L_D$

$\bar{u}_d$ is the normal component of the velocity vector averaged over the total depth $\vec{\bar{u}} = (\bar{u}, \bar{v})$ at the diffuser.

The magnitude of $\vec{\bar{u}}$ decreases away from the diffuser line.

The kinematic requirement for equivalent dilution follows

$$\bar{u}_c = \bar{u}_d \tag{4-4}$$

2) Dynamic Requirement

Discharge with stable near-field conditions is little affected by far-field effects and thus will behave similarly in both cases. Discharges with unstable near-field conditions depend strongly on the far-

field.

For the two-dimensional channel model dilution is uniquely controlled by the balance of far-field friction and buoyancy in the near-field region, expressed by the equal counterflow Equation (3-207) which is plotted in Figure 3-22 (A = 0.5). The functional relation is given as

$$\Phi = f_o \frac{L}{H} = f_1 (F_{H_c}) \tag{4-5}$$

where F_{H_c} is the densimetric Froude number of the counterflow system (Eq. 3-221). By virtue of the dilution relationship, Eq. (3-222), this equation is written as

$$f_o \frac{L}{H} = f_2(S_{2-D}) \tag{4-6}$$

and furthermore, multiplying both sides by $\bar{u}^2/8g$

$$h_{f_{2-D}} = \frac{f_o}{4} \frac{L}{H} \frac{\bar{u}_c^2}{2g} = f_3(S_{2-D}) \tag{4-7}$$

where $h_{f_{2-D}}$ is a head loss expression for the two-dimensional channel flow. By virtue of the constancy of $\bar{u}_c$, (Eq. (4-2)), $h_{f_{2-D}}$, is equivalent to the integration over the flow domain

$$h_{f_{2-D}} = \int_o^L \frac{f_o}{4H} \frac{\bar{u}_c^2}{2g} \, dx \tag{4-8}$$

The strongly two-dimensional character of the three-dimensional flow field in the vicinity of the diffuser centerportion is noted. Except for distances far from the diffuser line, the vertical counterflow

resembles that of the two-dimensional model. Therefore a functional relationship for the balance of far-field friction and buoyancy is hypothesized, similar to Eq. (4-7),

$$h_{f_{3-D}} = f_3 (S_{3-D}) \tag{4-9}$$

where $h_{f_{3-D}}$ is the integration over the flow path from the diffuser to infinity. In particular, by integration along the x-axis

$$h_{f_{3-D}} = \int_o^\infty \frac{f_o}{4H} \frac{\bar{u}^2(y=0)}{2g} dx \tag{4-10}$$

To evaluate the integral a description of the flow field $(\bar{u},\bar{v})$ is necessary.

The dynamic requirement for equivalent dilution ($S_{2-D} = S_{3-D}$) is the equality of far-field frictional effects

$$h_{f_{2-D}} = h_{f_{3-D}} \tag{4-11}$$

4.1.1.2 Model for the Three-Dimensional Flow Distribution

Evaluation of the three-dimensional far-field effects, Eq. (4-10), requires specification of the flow distribution. A simplified flow model is given describing the horizontal motion in each fluid layer. Density changes due to heat dissipation or interfacial mixing are neglected in view of the fact that the model application is primarily focused on the two-dimensional behavior in the diffuser vicinity; the heat loss scaling performed in paragraph 3.4.4.2 applies then as well.

The flow is gradually varying and two-dimensional in the horizontal plane. The equations of motion are written for the lower layer. The

flow velocities $\bar{u}$, $\bar{v}$ are averaged over the total depth, H.

$$\frac{\partial \bar{u}}{\partial x} + \frac{\partial \bar{v}}{\partial y} = 0 \tag{4-12}$$

$$\bar{u}\frac{\partial \bar{u}}{\partial x} + \bar{v}\frac{\partial \bar{u}}{\partial y} = -\frac{1}{\rho_a}\frac{\partial p}{\partial x} - \frac{\partial \bar{\tau}_{zx}}{\rho_a H} \tag{4-13}$$

$$\bar{u}\frac{\partial \bar{v}}{\partial x} + \bar{v}\frac{\partial \bar{v}}{\partial y} = -\frac{1}{\rho_a}\frac{\partial p}{\partial y} - \frac{\partial \bar{\tau}_{zy}}{\rho_a H} \tag{4-14}$$

where $\bar{\tau}_{zx}$, $\bar{\tau}_{zy}$ are total stress terms for both interfacial and bottom friction, written as

$$\bar{\tau}_{zx} = \frac{\bar{f}}{8}\rho_a \bar{u}|\bar{u}| \quad , \quad \bar{\tau}_{zy} = \frac{\bar{f}}{8}\rho_a \bar{v}|\bar{v}| \tag{4-15}$$

where $\bar{f}$ is the total friction coefficient. The relative importance of the terms in the momentum equations is determined by scaling:

$$\begin{aligned} (u^*, v^*) &= (\bar{u}, \bar{v})/\bar{u}_d \\ (x^*, y^*) &= (x, y)/L_D \\ p^* &= p/\rho_a \bar{u}_d^2 \end{aligned} \tag{4-16}$$

The diffuser length is chosen as the characteristic length scale of the problem as the local flow field in the diffuser vicinity is of interest. The x-momentum equation may be written in dimensionless form, substituting $\bar{\tau}_{xz}$ from Eq. (4-15) as

$$u^*\frac{\partial u^*}{\partial x^*} + v^*\frac{\partial u^*}{\partial y^*} = -\frac{\partial p^*}{\partial x^*} - \left[\frac{\bar{f}}{8}\frac{L_D}{H}\right] u^*|u^*| \tag{4-17}$$

Typical prototype values are chosen as in paragraph 3.4.4.2. L_D=1000 ft, H = 30 ft. and $\bar{f}$ is taken as 0.03. The bracketed term is evaluated as ~0.1 indicating that the flow field is governed by pressure and inertial forces. Thus neglecting the frictional term as a first approximation, the flow field can be determined assuming inviscid conditions (potential flow). With the calculated flow field the frictional term, $h_{f_{3-D}}$, can then be evaluated.

The potential flow formulation is

$$\nabla^2 \phi = 0 \tag{4-18}$$

with

$$\frac{\partial \phi}{\partial x} = \bar{u}, \quad \frac{\partial \phi}{\partial y} = \bar{v}$$

and the boundary condition at the diffuser line

$$\begin{aligned} \frac{\partial \phi}{\partial x} &= -\bar{u}_d \quad x \to +0 \\ & \qquad\qquad -L_D < y < L_D \\ &= +\bar{u}_d \quad x \to -0 \end{aligned} \tag{4-19}$$

The problem is solved in the complex plane (Figure 4-2). A complex potential W is defined as

$$W = \phi + i\,\psi \tag{4-20}$$

The complex potential due to a point sink at ζ is

$$W = -\frac{m_o}{2\pi} \log (z-\zeta) \tag{4-21}$$

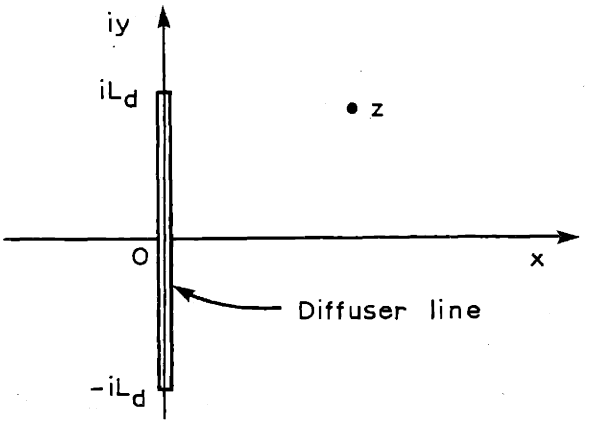

Fig. 4-2: Complex Solution Domain

Superposition of point sinks along the diffuser line leads to a line sink

$$W = \int_{-iL_D}^{iL_D} -\frac{m_o}{2\pi} \log (z-\zeta)\, d\zeta \tag{4-22}$$

and after integration

$$W = -\frac{m_o}{2\pi} \left\{ \log \frac{(z+iL_D)^{(z+iL_D)}}{(z-iL_D)^{(z-iL_D)}} - 2\, iL_D \right\} \tag{4-23}$$

The streamlines ψ are given by the imaginary part of W and are plotted in Figure 4-3 for half the flow field exhibiting the two-dimensional character in the centerportion. The complex velocities $\bar{u}$, $\bar{v}$ are obtained by differentiation

$$\frac{dW}{dz} = \bar{u} - i\bar{v} = \frac{m_o}{\pi} L_D \left[\tan^{-1} \frac{z}{L_D} - \frac{\pi}{2} \right] \tag{4-24}$$

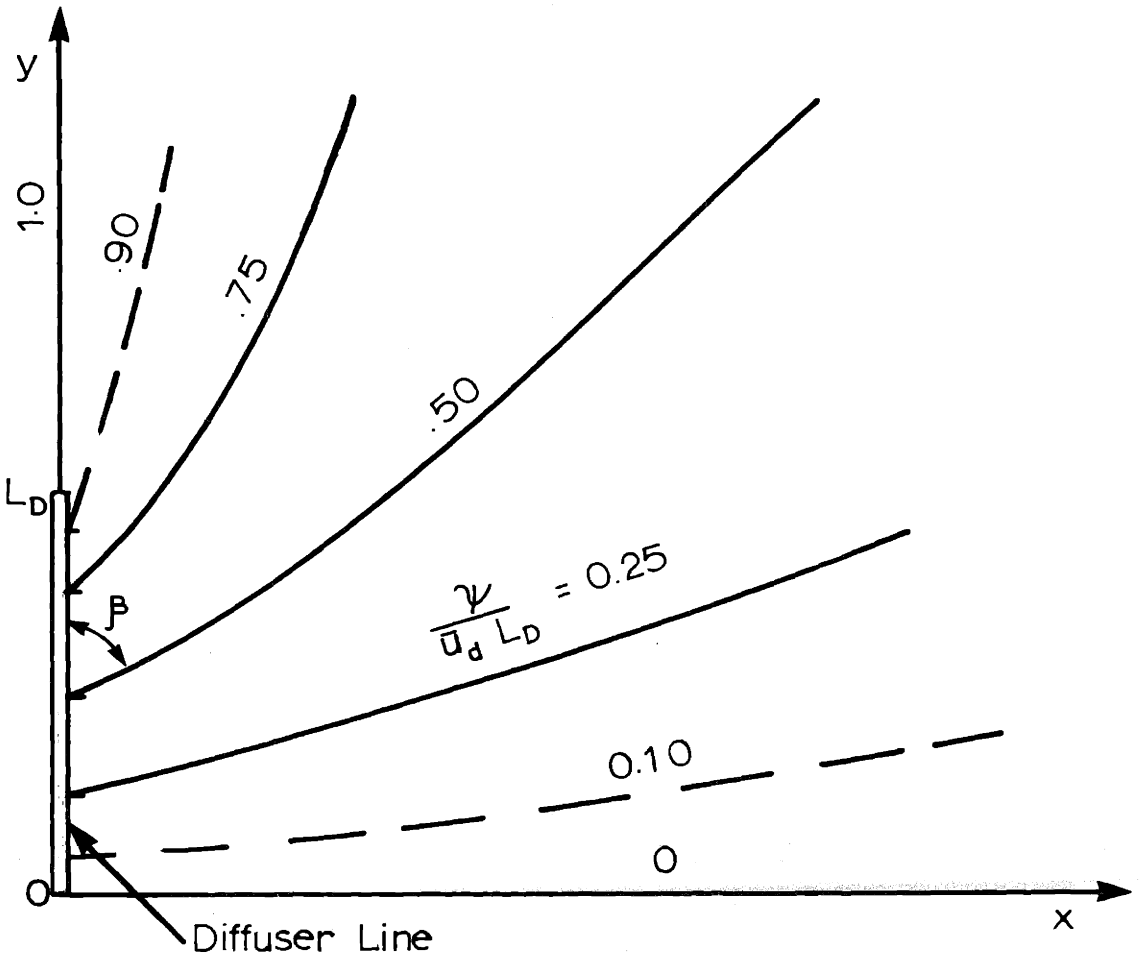

Fig. 4-3: Streamlines for One Quadrant of the Flow Field

The flow distribution at the diffuser line is given as

$$(\bar{u} - i\bar{v})_{\substack{x=0 \\ -iL_D<y<iL_D}} = \frac{m_o}{\pi} L_D \tan^{-1}\left[\frac{iy}{L_D} - \frac{\pi}{2}\right] \tag{4-25}$$

Using the boundary condition for the normal velocity $\bar{u}_d$ gives

$$m_o = \frac{2\bar{u}_d}{L_D} \tag{4-26}$$

The velocity along the x-axis is now given as

$$\left.\frac{dW}{dz}\right|_{y=0} = \bar{u} = \frac{2\bar{u}_d}{\pi}\left[\tan^{-1}\frac{x}{L_D} - \frac{\pi}{2}\right] \tag{4-27}$$

The head loss integral, Eq. (5-10), for the three-dimensional flow field can be evaluated as

$$h_{f_{3-D}} = \int_o^\infty \frac{f_o}{4H}\frac{1}{2g}\left[\frac{2\bar{u}_d}{\pi}\left(\tan^{-1}\frac{x}{L_D} - \frac{\pi}{2}\right)\right]^2 dx \tag{4-28}$$

or with $x = \xi L_D$

$$h_{f_{3-D}} = \frac{f_o}{4H}\frac{\bar{u}_d^2}{2g}\left(\frac{2}{\pi}\right)^2 L_D \int_o^\infty \left(\tan^{-1}\xi - \frac{\pi}{2}\right)^2 d\xi \tag{4-29}$$

The value of the definite integral in Eq. (4-29) is given by Gradshteyn and Ryshik (1965) as $\frac{\pi}{2}\log 2$ so that

$$h_{f_{3-D}} = \frac{f_o}{4H}\frac{\bar{u}_d^2}{2g}(0.884)\, L_D \tag{4-30}$$

The integral $\left(\frac{2}{\pi}\right)^2 \int_0^{\xi} (\tan^{-1}\xi - \frac{\pi}{2})^2 \, d\xi$ is computed numerically and plotted in Figure 4-4. The shape of the function indicates that the

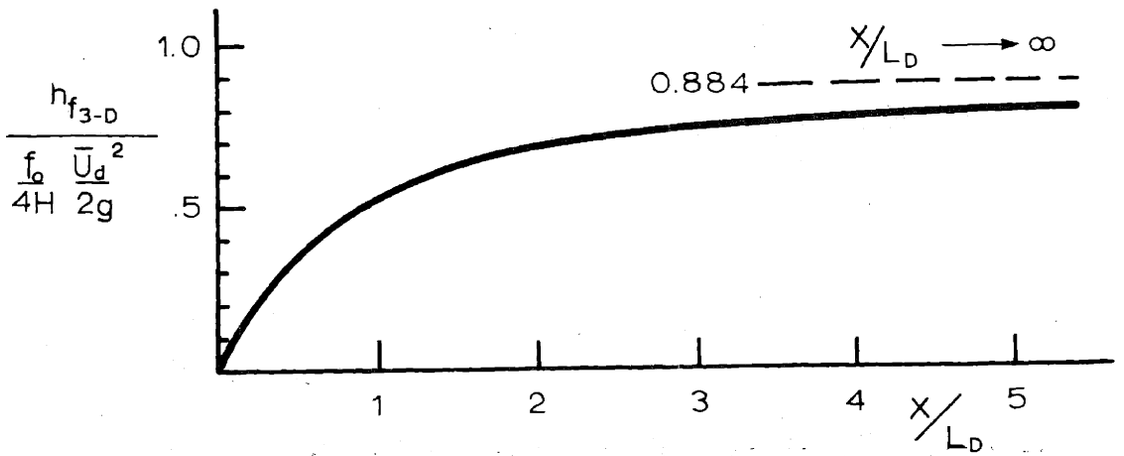

Fig. 4-4: Cumulative Head Loss, $h_{f_{3-D}}$, Along the Flow Path, x/L_D

major influence of the far-field effects is indeed restricted to the diffuser vicinity where the strongly two-dimensional flow character with reasonably high velocities persists. At 5 diffuser half-lengths the asymptotic value is approached to within 10%.

Invoking the kinematic and dynamic requirements for equivalency of diffuser-induced dilutions, by equating Equations (4-8) and (4-30) and substituting Eq. (4-4), it is found that

$$L = 0.884 \, L_D \tag{4-31}$$

gives the length of the corresponding two-dimensional channel model. For practical purposes Eq. (4-31) can be approximated as

$$L \approx L_D \tag{4-32}$$

For a diffuser with no net horizontal momentum, the channel length of the corresponding two-dimensional channel should be taken about equal to

the length of the three-dimensional diffuser.

4.1.2 Diffusers with Net Horizontal Momentum

Kinematic and dynamic requirements for equivalency of diffuser-induced dilutions can be derived in a manner similar to Equations (4-4) and (4-11). The evaluation of the three-dimensional head loss equation, $h_{f_{3-D}}$ (Eq. (4-10)), requires specification of the horizontal velocity distribution $(\bar{u},\bar{v})$. In developing a model for $(\bar{u},\bar{v})$ the horizontal momentum input of the diffuser ($\theta_o < 90°$) has to be included as a boundary condition. In the complex plane this can be accomplished by integrating a dipole distribution along the diffuser line. The resulting flow field will be that of two vortices centered at both diffuser ends. However, the total discharge over the diffuser line is found to be infinite for this simple model. This is nonrealistic in terms of the kinematic requirement. Therefore, a more intricate model must be developed to describe the three-dimensional flow field.

In this study it is assumed that the relation, $L \approx L_D$, developed for the diffuser with no net horizontal momentum is also approximately correct for the diffuser with net horizontal momentum. This assumption is appropriate for the case of a diffuser with a resulting counterflow system (Figure 3-27B1) which strongly resembles the equal counterflow system of the diffuser with no net horizontal momentum. The assumption is more hypothetical for discharges with full vertical mixing (Fig. 3-27B3) and essentially has to be substantiated by experimental evidence.

4.2 Diffuser Induced Horizontal Circulations

Diffuser discharges, even with no net horizontal momentum, are under certain conditions, capable of producing significant horizontal

circulations. These circulations are defined as currents which ultimately lead to recirculation of already mixed water into the diffuser line. Diffusers with stable near-field conditions do not produce such circulations, as a stable vertically stratified flow system is set up. The existence of horizontal circulations is intimately related to near-field instabilities. The generation mechanism for these circulations is discussed in a qualitative fashion. Control of the circulations can be achieved through specific orientation of the diffuser nozzles in the horizontal plane. Such control is desirable from practical considerations to prevent recirculation and maximize diffuser efficiency.

4.2.1. Diffuser with No Net Horizontal Momentum

4.2.1.1 Generating Mechanism

The velocity distribution at the diffuser line is given from the horizontal flow model for the lower layer by Eq. (4-25) with Eq. (4-26) substituted

$$(\bar{u} - i\bar{v})_{\substack{x=0 \\ -iL_D<y<iL_D}} = \frac{2\bar{u}_d}{\pi} \left[\frac{i}{2} \log \frac{1+y/L_D}{1-y/L_D} - \frac{\pi}{2} \right] \qquad (4\text{-}33)$$

The velocity is thus made up of a normal component, $\bar{u}_d$, accounting for the entrainment into the diffuser line and a tangential component, $\bar{v}_d$

$$\bar{v}_d = \frac{\bar{u}_d}{\pi} \log \frac{1+y/L_D}{1-y/L_D} \qquad (4\text{-}34)$$

The horizontal component is zero at the diffuser center and infinitely high at the diffuser ends. Such a sweeping motion from the diffuser end to its center is present as can be seen in Figure 4-3. The

existence of this current in the lower layer has been observed by Liseth (1970) and causes some inward bending of the jets issuing from the nozzles at the diffuser end. The motion is of no further concern for stable near-field conditions.

For unstable near-field conditions, however, the motion results in the generation of a strong horizontal eddying motion unless some control is invoked. The mechanism for this somewhat unexpected phenomenon (there is no net horizontal momentum!) is explained as follows, referring to Figure 4-5: Assume a flow particle is entrained into the vertical jet near the diffuser end. The particle is carried upward in the jet and deflected due to surface impingement. As the near-field zone is dynamically unstable the flow particle is carried again into the lower layer while being swept inward along the diffuser line. The particle gets re-entrained into the jets. The Lagrangian path of the particle is indicated. The total effect of the behavior is that all the repeatedly entrained diluted flow is transported towards the diffuser center from which it departs in the form of a vertically fully mixed strong current along the x-axis. By continuity the total approach flow along the y-axis is a similar strong current of ambient water. A horizontal circulation is generated which ultimately leads to recirculation and unsteady concentration build-up effects.

The close connection of the generating mechanism to the stability of the near-field zone is important. The vertically fully mixed flow-away at Section B-B (Fig. 4-5) does not agree with the vertically stratified flow in the diffuser center portion as indicated on Fig. 4-1. In fact, this postulated vertically stratified flow condition (which also

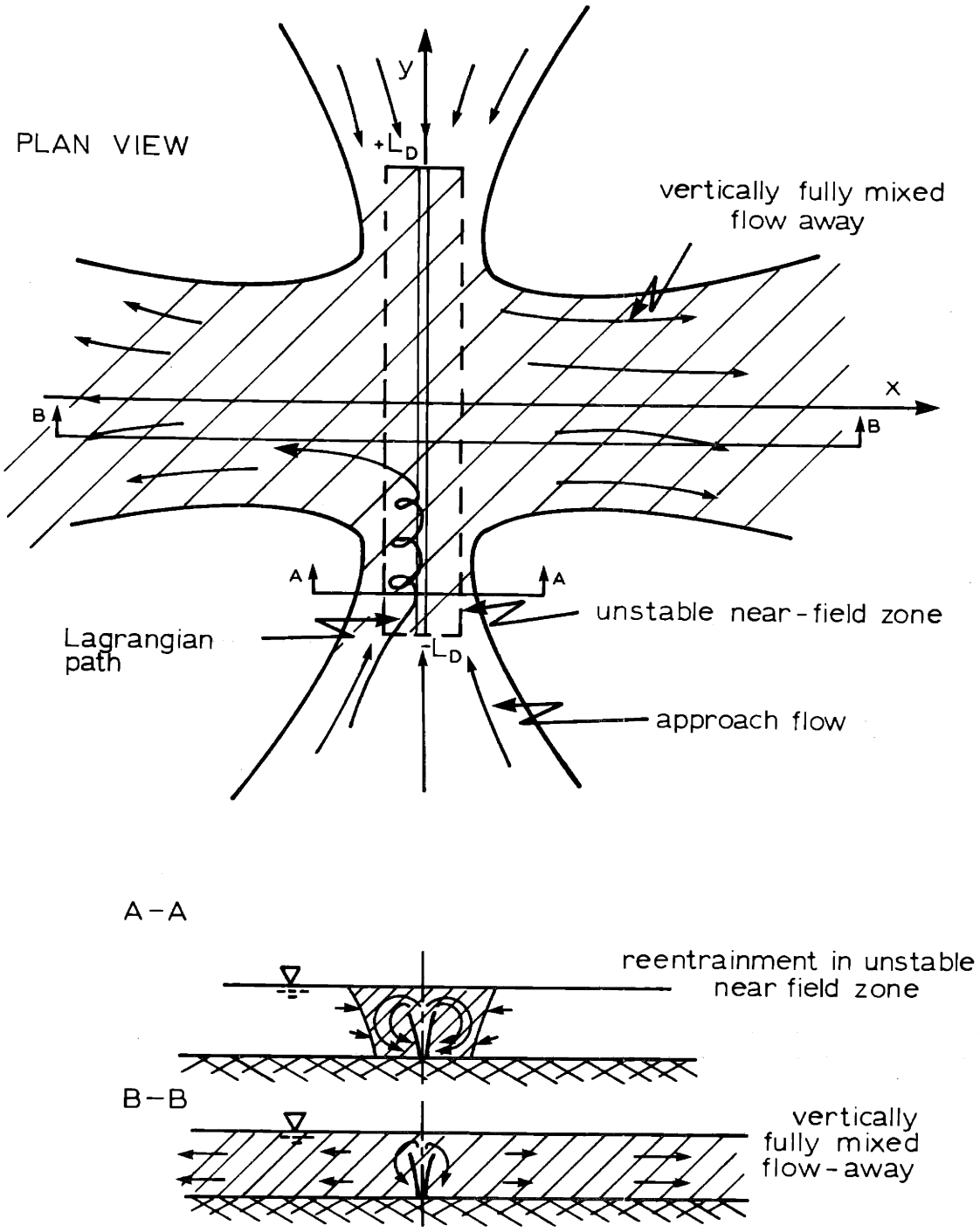

Fig. 4-5: Three-Dimensional Flow Field for Diffuser with Unstable Near-Field Zone (No Control)

forms the basis of the two-dimensional channel model conceptualization) requires control of the three-dimensional flow field. This control can be achieved through orientation of the diffuser nozzles in the horizontal plane and is desirable in view of the prevention of the repeated re-entrainment.

4.2.1.2 Control Methods

The objective of the control is the prevention of repeated entrainment within the unstable near-field zone (local mixing zone). This is achieved by opposing the inward current within the local mixing zone through orientation of the jet nozzles in the horizontal plane. The momentum of the inward flow is balanced by the momentum of the jet discharge. This stagnation of the inward flow within the local mixing zone, however, does not imply zero tangential flow at the edge of the local mixing zone. The flow outside the mixing zone will behave as predicted by the simple layer model and indicated in Figure 4-3. Control through nozzle orientation merely guarantees zero inward velocity within the local mixing zone and provides the proper starting conditions at the edge of the mixing zone for the establishment of a vertically stratified flow system outside.

The local angle $\beta(y)$ (see Fig. 4-3) under which the horizontal entrainment flow is entering the diffuser line is

$$\cot \beta(y) = \frac{\bar{v}_d}{\bar{u}_d} = \frac{1}{\pi} \log \frac{1+y/L_D}{1-y/L_D} \qquad (4\text{-}35)$$

To counteract this entrainment flow within the local mixing zone the individual nozzles of the alternating diffuser are directed against the

entrainment flow. The variation of the horizontal nozzle orientation along the diffuser line is then

$$\beta(y) = \cot^{-1} \left(\frac{1}{\pi} \log \frac{1+y/L_D}{1-y/L_D} \right) \qquad (4\text{-}36)$$

Local details of a diffuser section with alternating nozzles are shown in Figure 4-6. The vertical nozzle angle is θ_o. Efficient counteracting of the entrainment flow within the local mixing zone is only possible if the momentum flux of a nozzle discharge acting over the width

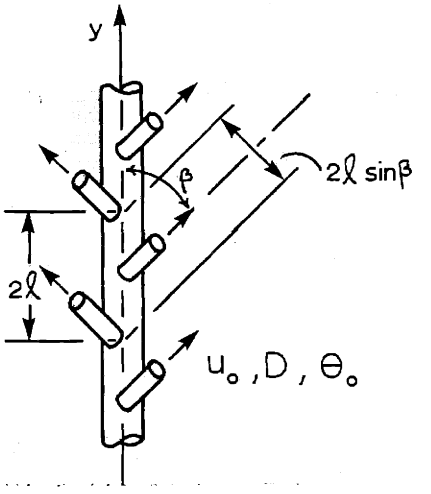

Fig. 4-6: Plan View of Diffuser Section; Alternating Nozzles with Vertical Angle θ_o

$2\ell\sin\beta$ is higher than the momentum of the entrainment flow. Obviously, no control is possible if $\theta_o = 90°$ (vertical discharge). There is a maximum angle $\theta_{o_{max}}$ up to which control is possible. The momentum flux of the entrainment flow over a diffuser length Δy is

$$\Delta\bar{m} = \rho_a \bar{u}_d H \left(\frac{\bar{u}_d}{\sin\beta} \right) \Delta y \qquad (4\text{-}37)$$

The momentum flux of the nozzle discharge is, over the diffuser length 2ℓ, (see Fig. 4-6)

$$m_n = \rho_o U_o \frac{D^2 \pi}{4} \frac{U_o}{\sin\beta} \cos \theta_o \tag{4-38}$$

and using the equivalent slot definition, Eq. (2-20) and also $\rho_a \tilde{} \rho_o$

$$m_n = \rho_a U_o^2 B \cos \theta_o \frac{1}{\sin\beta} \ell \tag{4-39}$$

The spacing ℓ is considered a differential length of the total diffuser, thus $\Delta y \sim \ell$ and $\Delta m \sim m_n$

$$\Delta m = \rho_a U_o^2 B \cos \theta_o \frac{1}{\sin\beta} \Delta y \tag{4-40}$$

To make a control possible

$$\frac{\Delta m}{\Delta \bar{m}} = \frac{U_o^2}{\bar{u}_d^2} \frac{B}{H} \cos \theta_o > 1 \tag{4-41}$$

With the definition (Eq. (4-3) and $q_o = U_o B$ one can write

$$\frac{4}{S_s^2} \frac{H}{B} \cos \theta_o > 1 \tag{4-42}$$

In the parameter range for the unstable near-field S_s is given by Eq. (3-222) which is substituted into Eq. (4-42) to give

$$\cos \theta_o > 4^{-1/3} \left(\frac{F_{H_c}}{F_s} \right)^{4/3} \frac{H}{B} \tag{4-43}$$

where F_{H_c} accounts for the far-field effects Φ by virtue of the interfacial equation (see Fig. 3-22). The maximum value of $\theta_o = \theta_{o_{max}}$ is estimated: Negligible far-field effects mean $F_{H_c} = 0.25$ and at the

criterion which describes the transition between the stable and unstable parameter range was established as

$$H/B = 1.84\ F_s^{4/3} \tag{3-219}$$

so that

$$\theta_{o_{max}} = \cos^{-1}\left[4^{-1/3}\ (1.84)\ (0.25)^{4/3}\right] \approx 79° \tag{4-44}$$

For larger F_s or smaller H/B, i.e. relatively stronger impact of the diffuser discharge on the receiving water, the angle $\theta_{o_{max}}$ is even larger. Similarly, for smaller F_{H_c}, i.e. larger resistance in the far-field, $\theta_{o_{max}}$ is larger. However, using Eq. (4-44) as the lower estimate, it can be stated in order to enable control of the three-dimensional flow field through horizontal orientation of the nozzles, $\beta(y)$ given by Eq. (4-36) the vertical angle of the discharge has to be less than ≈79°. It is immaterial how much less, since if $\theta_o < \theta_{max}$ the excess horizontal nozzle momentum is diffused in the local mixing zone, much like in the fashion indicated in Fig. 3-25. As mentioned above, the objective of the control is to counteract the tangential velocity, $\bar{v}_d$, within the local mixing zone. No horizontal motion can be induced by the nozzle discharge momentum outside the mixing zone, as can be shown by drawing a control volume around the diffuser area: The net horizontal momentum in any direction is zero! Thus it is emphasized, that the horizontal circulations which are set up by a diffuser with vertical and alternating nozzles are by no means a result of horizontal discharge momentum, but rather a complex interaction of vertical near-field

instabilities which are amplified by the entrainment flow sweeping along the diffuser line.

In summary, through control by local horizontal orientation, $\beta(y)$ in Eq. (4-36) of the nozzles of a multiport diffuser the development of horizontal circulations can be prevented. The control "consolidates" the local mixing zone. The flow outside the local mixing zone will then be characterized by the two-layered system which is in equilibrium between the buoyancy force of the near-field and the resistance in the far-field (Fig. 4-1). The two-dimensional channel model conceptualization is applicable. No control is required for diffusers with a stable near-field zone: The flow field outside the near-field will always be the stratified two-layered type.

Evaluation of the sensitivity of the form of the flow field for different orientations, $\beta(y)$, can only be made experimentally. In the experimental program various distributions, $\beta(y)$, were tested and changes in flow field behavior and resulting overall dilution are reported (Chapter 6).

4.2.2 Diffusers with Net Horizontal Momentum

4.2.2.1 Generating Mechanism

Diffusers with unidirectional nozzles produce horizontal circulations due to two factors: i) horizontal momentum of the discharge, and ii) instabilities in the near-field zone, similar to the discharge with no horizontal momentum. The relative strength of the two mechanisms is important.

As no analytical model for the description of the far-field has been developed, the following is hypothetical, partly in analogy to the

discharge with no horizontal momentum.

1) Diffusers with a stable near-field zone exhibit a two-layered system in the far-field. The horizontal orientation of the nozzles, $\beta(y)$, is not decisive.

2) Diffusers with an unstable near-field will produce circulations which are dependent on the nozzle orientation, $\beta(y)$. The discussion is given for parallel nozzles as shown in Fig. 4-7.

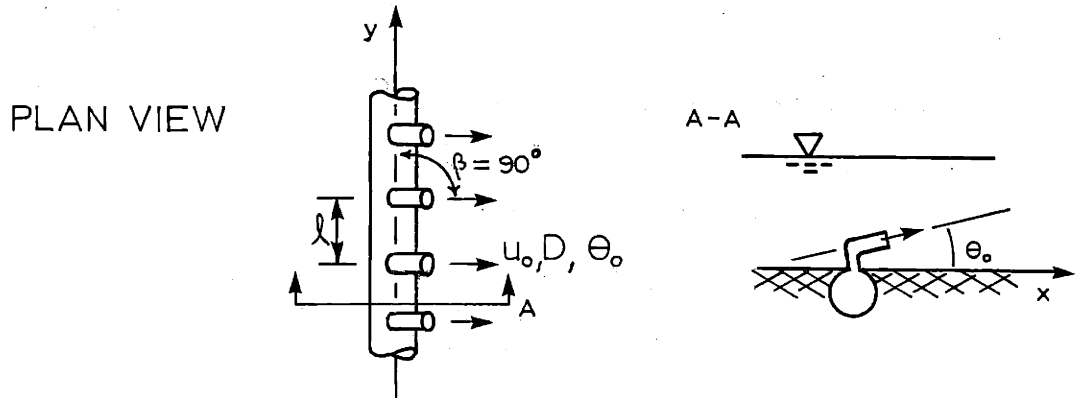

Fig. 4-7: Unidirectional Discharge with Parallel Nozzle Orientation ($\beta(y)$ = const = 90°)

a) For weak horizontal momentum (counterflow system) the set-up of horizontal circulations is primarily due to instabilities in the near-field zone in conjunction with an inward flow along the diffuser line. A flow field much like the one for the diffuser with no net horizontal momentum (Fig. 4-5) will result only somewhat modified by the momentum of the discharge so that the flow-away will be mainly along the +x-axis.

b) For strong horizontal momentum (supercritical system with full vertical mixing) the horizontal circulation is primarily caused by the momentum of the discharge. This is essentially the situation which has been described analytically by Adams (1971) as discussed in Chapter 2. Adams' model, when applied to zero crossflow conditions, Eq. (2-45), predicts a significant contraction ($c_c = 1/2$) of the flow field downstream of the diffuser line. This contraction is accompanied by a dilution decrease of 1/2 as compared to the corresponding two-dimensional channel model without far-field friction ($\Phi = 0$).

4.2.2.2 Control Methods

Control of the horizontal diffuser-induced circulations is aimed primarily at the prevention of the flow contraction downstream of the diffuser line. Such control is desirable as is shown by comparison of the dilution predictions from Adams' model and the two-dimensional channel model.

Prevention of the contraction is again achieved by counteracting the y-component of the entrainment flow as it enters the diffuser line through horizontal orientation of the diffuser nozzles. The variation of nozzle orientation, $\beta(y)$, cannot be computed analytically due to lack of a model for the three-dimensional flow field. In the experimental program unidirectional diffusers with parallel nozzles ($\beta = 90°$) and nozzles with $\beta(y)$ as given by Eq. 4-36 were studied. The assumption of this $\beta(y)$ may be well justified at least in the case of a stratified counterflow system in view of the flow-field similarities.

V. EXPERIMENTAL EQUIPMENT AND PROCEDURES

This chapter describes the laboratory equipment and procedures used in the experimental part of the investigation. Two different set-ups were used: (1) a flume set-up directed toward the study of the two-dimensional channel model, and (2) a basin set-up mainly directed toward the study of three-dimensional diffuser behavior, with few additional tests on the two-dimensional channel concept. In both set-ups the effect of cross-flow was investigated. The buoyancy of the discharge was introduced by using heated water.

The set-ups and procedures are described in detail below. However, first basic considerations reporting the experimental program are discussed. Experimental results are presented in Chapters 6 and 7, respectively.

5.1 Basic Considerations on Diffuser Experiments

5.1.1 Experimental Program

The objectives of the experimental program were:

a) to gain insight into the hydrodynamic properties of the diffuser-induced flow field and examine assumptions made in the theoretical development;

b) to measure the gross behavior of the diffuser-induced flow field and compare it with theoretical solutions (Chapter 6);

c) to determine the effect of ambient cross-flow on diffuser behavior and derive empirical relationships (Chapter 7).

The experimental program was planned to encompass a broad range of the governing dimensionless parameters for multipart diffuser dicharges. For the purely diffuser-induced behavior these parameters

are given in Eq. (3-215), namely, the densimetric Froude number of the (equivalent) slot diffuser, F_s, the vertical discharge angle, θ_o, the relative depth, H/B, and the far-field parameter, Φ . Two more parameters are introduced for the case of a diffuser in ambient cross-flow, namely,

$$V = \frac{u_a H}{U_o B} = \text{volume flux ratio}$$

and

γ = angle of diffuser axis with direction of cross-current, u_a .

The parameter range was intended to include practical prototype applications, the order of magnitude of which are outlined in the following examples with reference to the discussion in Chapter 1:

(1) Typical sewage diffuser with high dilution requirement: Liseth (1970) gave a survey of sewage multiport diffuser outfalls on the U.S. Pacific Coast. Selected average dimensions are shown in Table 5.1 and non-dimensional parameters for the equivalent slot diffuser are calculated.

(2) Typical thermal diffuser with lower dilution requirement: The discharge conditions from a 600 MW nuclear power plant with a diffuser in a shallow near-shore area are indicated in Table 5.1 for comparison (see, for example, Harleman et. al. (1971)). Equivalent slot parameters are calculated.

A bottom friction coefficient $f_o = 0.02$ was assumed in both cases, corresponding to an average Chezy C $\approx$ 110 $(ft)^{1/2}$/sec. In Chapter 4 the relation between channel length, L, and diffuser length, L_D, is derived as $L \approx L_D$, hence $\Phi \approx f_o L_D/H$. Comparison shows

Table 5.1: Comparison of Relevant Parameters for Typical Sewage and Thermal Diffuser Applications

Variables:	Sewage Diffuser	Thermal Diffuser
Water depth, H (ft)	200	20
Total discharge, Q_o (cfs)	400	1000
$\Delta\rho/\rho_a$	0.025	0.003
	(fresh - salt water)	($\Delta T_o \sim 20°F$)
Total Diffuser Length, $2L_D$ (ft)	3000	3000
Nozzle Diameter, D (ft)	0.5	1.0
Nozzle Spacing, ℓ (ft)	10	20
Discharge velocity, U_o (fps)	6.8	8.5
Ambient current velocity, u_o (fps)	0 to 0.1	0 to 0.5
Bottom friction coefficient, f_o	0.02	0.02
Equivalent slot width, B (ft)	0.02	0.04
Dimensionless parameters:		
F_s	70	140
H/B	10,000	500
θ_o	variable	variable
Φ	0.1	1.5
V	0 to 100	0 to 50
γ	variable	variable

some of the striking differences between these general diffuser types: The relative depth is considerably larger for the sewage diffuser, while its densimetric Froude number is somewhat smaller. The effect of the far field is more pronounced for the thermal diffuser.

5.1.2 Experimental Limitations

While laboratory experiments on submerged multiport diffusers have the distinct advantage of a localized observation area and a controllable environment, they have some limitations which have direct repercussions on the range of dimensionless parameters which can be studied. These limitations are related to the size of usually available laboratory facilities:

(1) Boundary effects: The theoretical treatment was directed toward the steady-state diffuser performance in a (infinitely) large body of water with uniform depth. If the diffuser is located in a basin of finite extent, it is clear that, depending on the size of the basin relative to the diffuser length, the flow induced by the diffuser will be influenced to a stronger or lesser degree through boundary effects. There is no influence in case of the two-dimensional channel model, in which critical sections at the channel ends define a clear steady-state boundary condition, the only requirement being that the reservoir outside the channel be somewhat larger than the channel itself. There is negligible influence in the case of a strong cross-flow.

There are cases which have some quasi-steady state condition, such as discharges with no net horizontal momentum and control, which create vertical stratification and an upper layer which far from the

diffuser (near to the basin boundaries) is only slowly increasing in depth and thus has little influence on the behavior in regions closer to the diffuser.

There may be considerable boundary influence for discharges with strong horizontal momentum: The steady-state condition requires experimental times long enough to overcome the inertia of the initially undisturbed receiving water. On the other hand, for longer times recirculation of the mixed water into the diffuser line will occur due to boundary effects. A real dilemma may result in certain instances.

Therefore, in general, minimization of boundary effects requires diffuser dimensions, L_D/H, which are small compared to the minimum size of the available basin L_{min}/H,

$$L_D/H \ll L_{min}/H \tag{5-1}$$

(2) Turbulence problems: In the analysis a fully turbulent jet region is assumed. This requires maintenance of a jet Reynolds number which is larger than some critical value, and poses a considerable constraint in studying the parameter range with low F_s and high H/B in view of the requirement (5-1). The change of the turbulent structure of a round non-buoyant jet with a Reynolds number defined as

$$IR_j = \frac{U_o D}{\nu} \tag{5-2}$$

was visually observed by Pearce (1968). Pearce found a fully turbulent jet structure with constant angle of spreading to be given for $IR_j > 3000$. For $IR_j < 500$ the jet effluent is laminar with only small instabilities. The transition region $500 < IR_j < 3000$ is

distinguished by an increasingly turbulent jet structure. Pearce did not investigate the entrainment efficiency of jets in this transition region, but presumably it will be lower and only approaching that of the fully turbulent jet, $\mathbb{R} > 3000$. Hence, for a jet Reynolds number $\mathbb{R}_j$ based on the hydraulic radius of the discharge opening, R_h , a criterion

$$\mathbb{R}_j = \frac{U\ 4\ R_h}{\nu} > 3000 \qquad (5\text{-}3)$$

should be met in experimental studies.

3) Measurement technique: The velocity and temperature fields are of interest. Yet the jet velocities decrease rapidly from the point of discharge and horizontal layer velocities are very low. There is as of now no practically feasible technique which allows velocity measurement of this order of magnitude. Only approximate visual or photographic observations can be made in certain instances. Thus the gross behavior of the diffuser discharge has to be primarily determined by measuring the temperature field.

5.2 The Flume Set-Up

Primary purpose of the flume set-up was the observation of the vertical structure of the temperature field produced by a heated water diffuser discharge. The multiport diffuser discharge was simulated as a continuous slot.

5.2.1 Equipment

Figures 5-1 and 5-2 show the experimental set-up. A 1 ft. wide channel test section of variable length 2L was installed in a metal flume 50' × 4.5' × 3'. The water volume outside the test

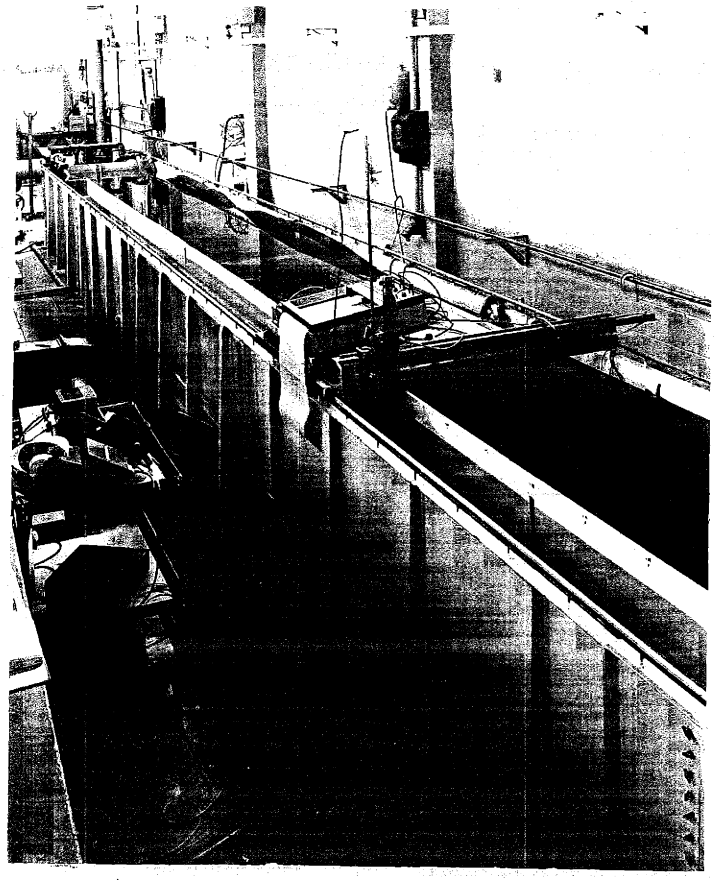

Fig. 5-1: Photograph of Flume Set-Up

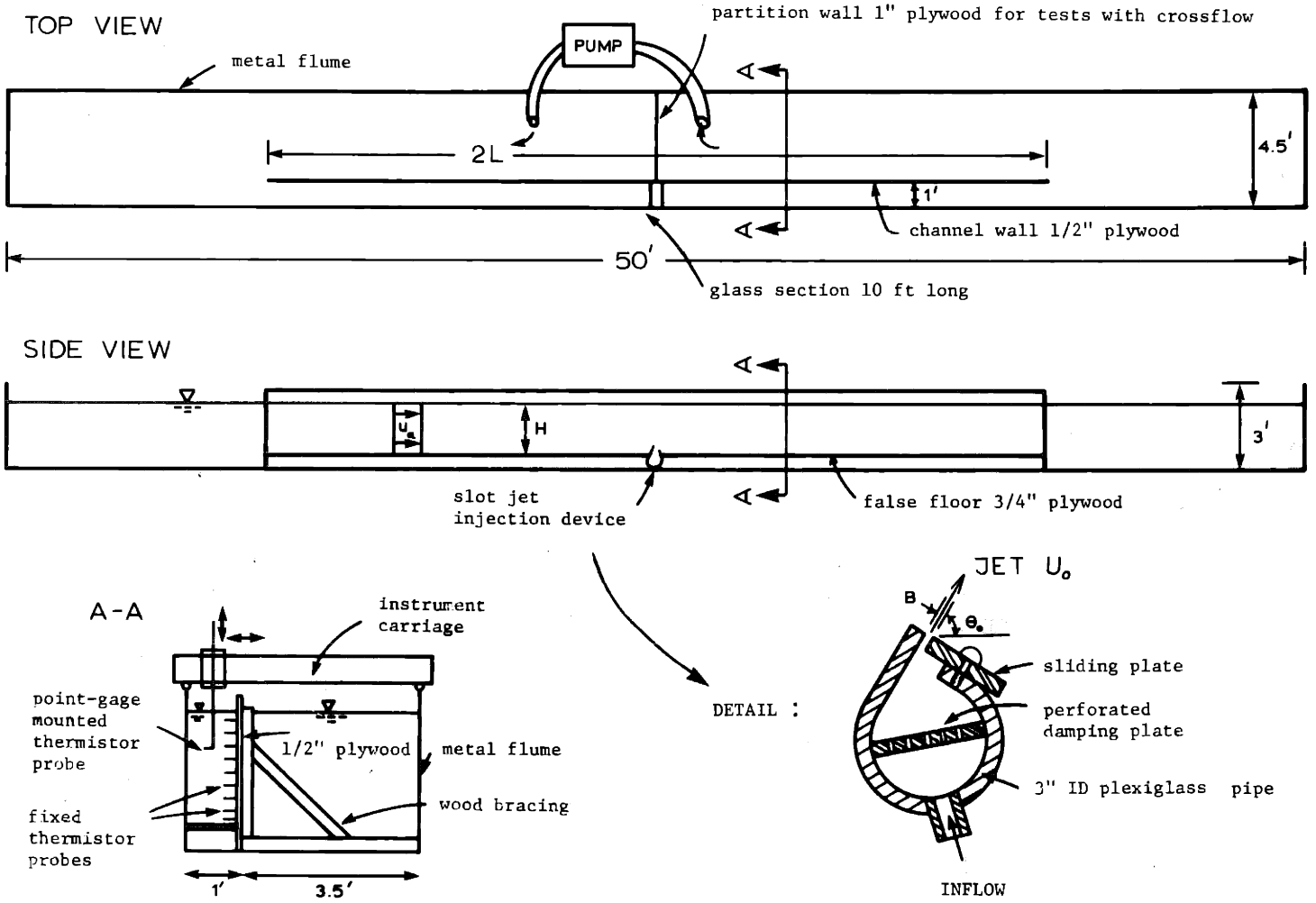

Fig. 5-2: Flume Set-Up

section formed a reservoir. The channel wall and false-floor were of marine plywood. The length of the channel could be varied by adding or removing 8 ft. long plywood panels. The flume has a 10 ft. long glass wall section allowing observation of the flow from the side.

The slot jet injection device had a 1 ft. long, 3" ID plexiglass pipe as its basic component and was equipped with an adjustable sliding plate for changing the slot width B. A perforated damping plate provided for uniform jet exit velocities. The injection device was mounted on U-shaped supports in an opening of the false channel floor and could be rotated to give the desired discharge angle θ_o . A few tests were made using a single round nozzle placed in the channel center as the jet source. The nozzles used were commercially avaiable copper fittings with various diameters and angles. Heated discharge water was supplied from a steam heat exchanger capable of delivering up to 60 gallons per minute of water at a constant temperature up to 150°F. An amount equal to the jet discharge could be withdrawn from the reservoir in the back of the channel to guarantee constant water depth.

For tests with cross-flow a plywood partition wall was inserted in the reservoir behind the channel and a five HP centrifugal pump was used to generate cross-flow in the channel by pumping across the partition. All flows are monitored by Brooks rotameter flowmeters.

Temperature measurements were taken in two components: (1) Fixed probe system: 50 Yellow Springs Instruments No. 401 thermistor probes were mounted in fixed positions in the set-up. Thirty-six (36) probes were mounted through the channel walls forming 4 vertical

transects of 9 probes each (see Fig. 5-2) and the remainder were installed in the reservoir and in in- and outflow lines. The probes were connected to a Digitec (United Systems) scanning and printing unit. The temperature in degrees Fahrenheit was printed on paper tape at a rate of 1.5 seconds per probe. The probes have an accuracy of $\pm$ 0.25°F and were individually calibrated. The time constant is 7 sec. which filters out turbulent fluctuations.

(2) Moveable probe: A Fenwal GA51SM2 thermistor probe was installed on a point gage which is driven by a small DC motor capable of vertically traversing 1.5 feet per minute. The vertical position of the probe was recorded via a potentiometer circuit on the vertical axis of a Valtec x-y plotter. The thermistor was connected to a wheatstone bridge circuit to the horizontal axis of the x-y plotter. As the moveable probe made a vertical traverse a direct plot of depth versus the millivolt output of the thermistor circuit resulted. The thermistor had a small time constant of 0.07 sec, important in view of the traversing speed. The probe was calibrated against the reading of a mercury thermometer. The point gage itself was mounted on an instrument carriage running on the rails of the metal flume and could be moved into any position.

The glass wall section of the flume allowed visual observation of the flow field through dye (FDC-Blue) injected into the jet discharge. Limited velocity measurements could be made through the time-lapse photographic recordings of dye traces formed by falling dye crystals.

5.2.2 Experimental Procedure

Before the start of an experiment an initial temperature scan was made to check the uniformity of temperature throughout the flume. In case of a run with ambient cross-flow the desired cross-flow velocity was established in the channel. At run start the heated water discharge was turned on and the withdrawal flow was started. Dye was injected into the initial discharge flow and the advance of the dye front was observed. The flow has an initial unsteady phase, until the dye front reached the channel end at which time the steady state phase began. The steady state phase itself is limited in time due to the restricted area of the reservoir outside the channel section. A build-up of the thickness of the less dense layer results in the reservoir and whenever the thickness becomes larger than the critical depth at the channel end unsteady back water effects will be felt in the channel itself. Depending on the discharge conditions the initial unsteady portion varied between 5 to 10 minutes and the steady state phase between 15 to 30 minutes. Temperature measurements taken during the steady state phase show an essentially constant behavior of the flow field.

5.2.3 Experimental Runs

The run parameters for each run are given in Chapters 6 and 7 together with experimental results. Three series of tests were performed in the flume:

Series FN - no net horizontal momentum (Section 6.1)

Series FH - net horizontal momentum (Section 6.2)

Series FC - with ambient cross-flow (Chapter 7)

5.2.4 Data Reduction

Data for temperature and flow rates as measured for each experiment were reduced as follows. The ambient temperature, T_a, is defined as the initial flume temperature before heated water is injected. Temperature rises, ΔT, above ambient are calculated by subtracting T_a from the measured temperature, T, at any point. This applies to data both from fixed probes and from the moveable probe (x-y recordings). All temperature rises are normalized by ΔT_o, the discharge temperature differential. The normalized temperature distributions are plotted in a plot of the x-z plane. All distances are normalized by the water depth, H. Examples of these plots are shown in Chapter 6.

For comparison with the theoretical solution the surface dilution S_s outside the local mixing zone (about 2.5 H away from the discharge) is given as the reciprocal of the non-dimensional temperature rise. Values of the far-field parameter Φ are calculated: f_o is obtained from the White-Colebrook relation as a function of Reynolds number of the lower layer and the channel roughness k_s, taken as 0.002 ft for plane-wood flumes. While in the theoretical development the friction at the channel walls was not considered, it has to be included in comparison of experimental data, in particular for the narrow deep channel tested. For the lower layer a correction c_2 is obtained as

$$c_2 = 1 + \frac{\tau_{w_2}}{\tau_b - \tau_i} \frac{2\, h_2}{W} \qquad (5\text{-}4)$$

in which W = channel width

τ_w = wall friction for the lower layer

Assuming the well friction factor equal to f_o and taking $h_2 \approx H/2$ as an average

$$c_2 = 1 + \frac{f_o}{f_o + 4f_i} \frac{H}{W} \qquad (5\text{-}5)$$

and the bottom friction factor corrected for wall friction, f_o^*, is

$$f_o^* = c_2 f_o \qquad (5\text{-}6)$$

so that

$$\Phi = f_o^* L/H$$

5.3 The Basin Set-Up

The main objective of the basin set-up was the determination of the general three-dimensional structure of the temperature and current field produced by a multiport diffuser. However, as the vertical structure had been studied extensively in the flume set-up, major emphasis was put on variations in the horizontal plane.

5.3.1 Equipment

The basin set-up is shown in Figs. 5-3 and 5-4. The basin dimensions were 38 × 22 × 1.5 ft. To provide space for the underground diffuser pipe the basin was laid out with 6 in high concrete blocks which were grounded on top for leveling. A 6 ft long, 0.5 ft wide plexiglas flume with an inside mirror inclined under 45° was installed in one basin wall to allow flow observation in the diffuser vicinity.

Two diffuser arrangements were chosen. The majority of the experiments, including all with zero cross-flow, were done with the diffuser pipe as shown on Fig. 5-4 (Basin Set-Up A). Thus, the basin wall

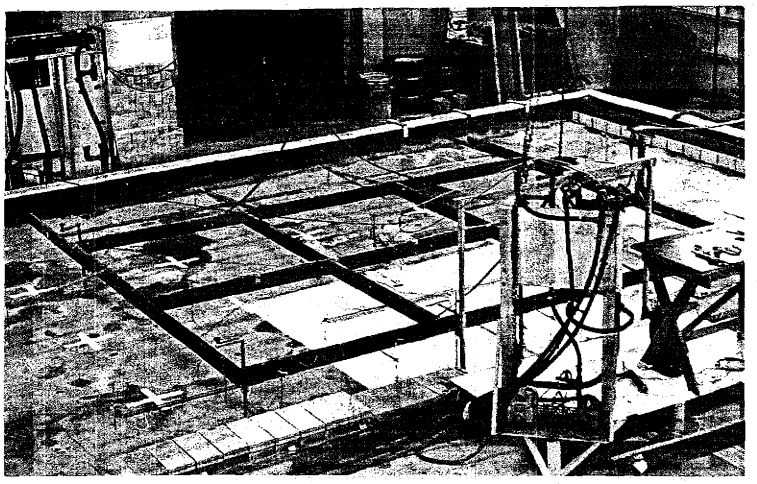

a) Overall View with Probe Frame

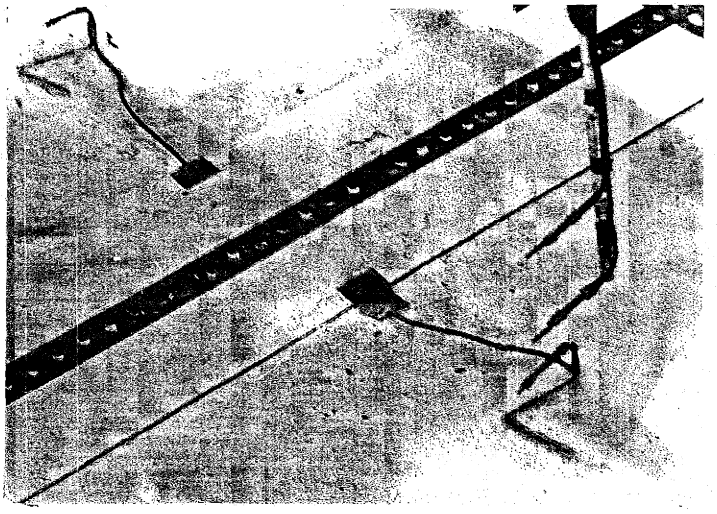

b) Diffuser Close-Up (Vertical Nozzles) with Thermistor Probes

Fig. 5-3: Photographs of Basin Set-Up

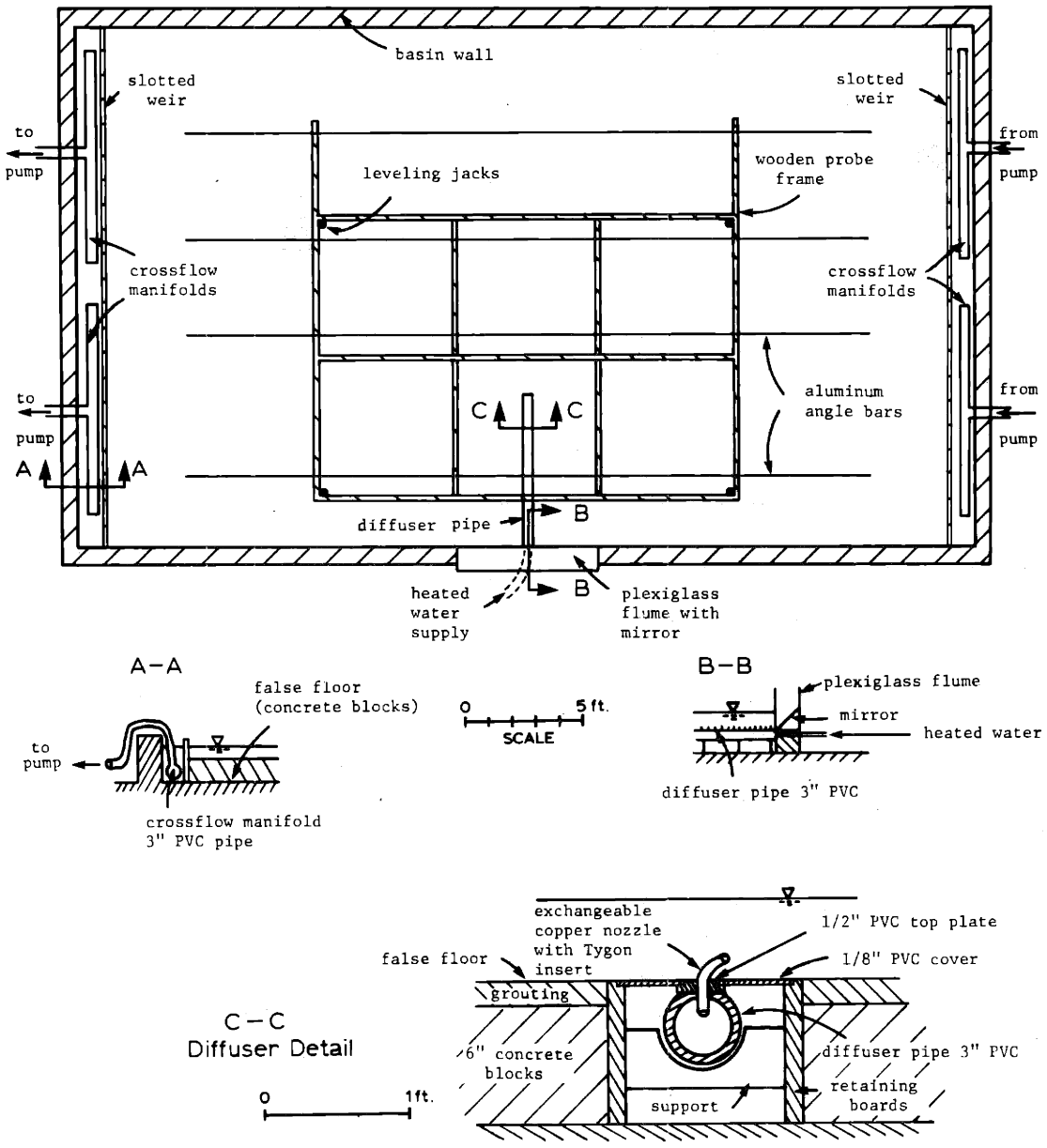

Fig. 5-4: Basin Set-Up

essentially formed a symmetry line for the diffuser flow field and the effective basin size was doubled. Additional tests were made with the diffuser pipe in the middle of the basin and parallel to the longitudinal extent of the basin (Basin Set-Up B). A detail of the diffuser pipe is shown in Fig. 5-4. The diffuser was made up of 6.4 ft long PVC pipe with 3 in. I.D. This large pipe size was chosen to guarantee negligible velocities in the pipe and thus uniform discharge from all diffuser nozzles. A segment of the pipe wall was removed and a 1/2 in PVC plate was attached. 80 holes were drilled in the PVC plate at a spacing of 0.08 ft. The diffuser nozzles were assembled as copper fittings (1/8 in nominal) with variable angle into which Tygon plastic tubing with variable inside diameter was inserted. These nozzles fitted snug into the holes in the PVC plate and could be rotated in any direction. Holes could be plugged up as required to provide nozzle spacings larger than 0.08 ft. The height of the nozzles above the floor varied between 1 and 3 nozzle diameters. To compare the two-dimensional channel model concept a few experiments were made with Basin Set-Up A by installing a 12 ft. long ($L \approx L_D$) false wall parallel to the diffuser symmetry line as shown in Fig. 5-5a. The channel thus formed was 2.3 ft wide and all diffuser nozzles outside the channel were plugged.

The heated water flow was obtained from a heat exchanger as in the flume set-up. Cross-flow in the basin was generated using two 200 gpm, 5 HP pumps. The flow was withdrawn and discharged through cross-flow manifold pipes. This feature in conjunction with the slotted weir (1/2 in slots at 1 ft centers) gave good uniformity of the cross-flows in particular when additional resistance in front of the weirs

by the installation of horse-hair mats was provided. All flows were monitored with Brooks flow meters.

Somewhat different temperature measurement instrumentation was used in the basin set-up: (1) Fixed probe system: 60 Yellow Springs Instruments No. 701 linear thermistor probes were mounted within the basin. The probes have an accuracy of 0.25°F, a time constant of 9 sec and were individually calibrated. The probe arrangement in the basin is shown in Figs. 5-5a and 5-5b for the two diffuser pipe layouts. The probe mounting can be seen in Fig. 5-3 . Thirty-seven (37) probes were mounted on probe holders which were attached to the wooden probe frame. The probe frame could be leveled with jacks so that the probes were accurately positioned at 1/4 in below the water surface (30 probes) and 3 in below the water surface (7 probes). Sixteen (16) probes were mounted 1 in above the basin floor. The remainder of the probes (7) were used to measure temperatures of the heated water and of the cross-flow water. The heated discharge temperature was measured with 3 probes inside the diffuser pipe. The probes were automatically scanned by a Digitec scanner-printer system connected to a HP computer for on-line data acquisition. A complete scan took about 1.5 minutes. (2) Moveable probes: Four moveable probe units were built and could be positioned at desired locations within the basin. The basic components were the same as described in the flume set-up. The point gages were mounted on stands. A switching mechanism allowed sequential control of the 4 probes and recording on a Houston Instruments x-y plotter. A complete record of all 4 probes took about 2 minutes.

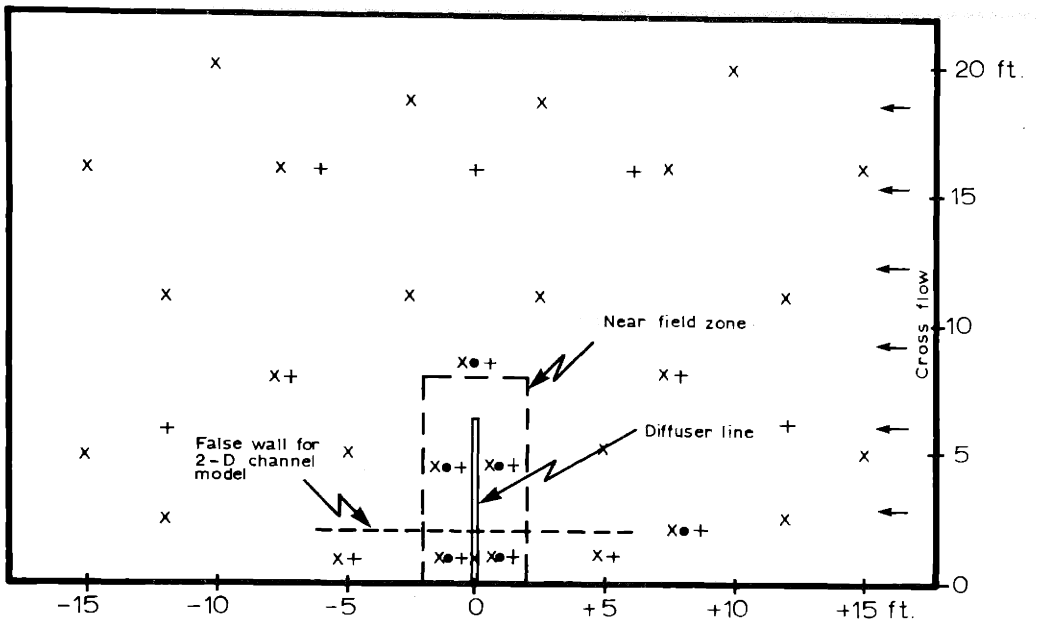

a) Fixed probe arrangement, Basin Set-Up A

x Probes 1/4 in. below surface
• Probes 3 in. below surface
+ Probes 1 in. above bottom

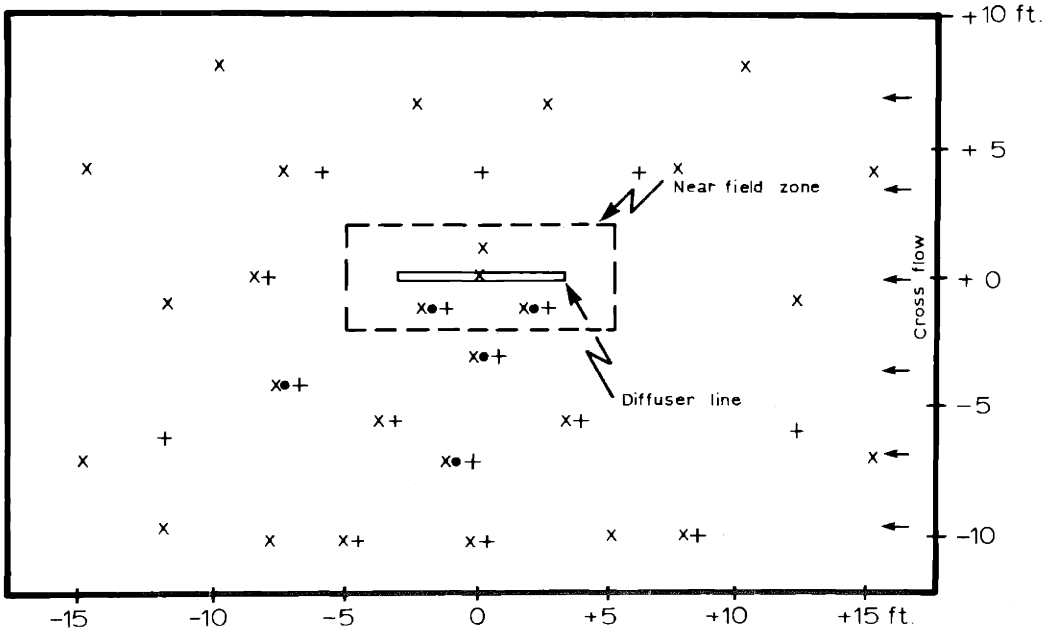

b) Fixed probe arrangement, Basin Set-Up B

Fig. 5-5: Arrangement of Temperature Measurement System

5.3.2 Experimental Procedure

An initial temperature scan served to check uniformity and to define the ambient basin temperature. For runs with cross-flow the desired cross-flow velocity was established. Before the start the diffuser pipe was "primed", i.e., heated water was discharged into an end of the diffuser pipe while at the other end an equal amount was withdrawn. This procedure (about 1 to 2 minutes duration) established the desired discharge temperature in the pipe.

At the run start the withdrawal flow from the diffuser pipe was stopped and the heated water discharged through the nozzles. An amount equal to the diffuser flow was withdrawn from the basin side channels to keep the water level constant during the run. Dye was injected to observe the circulation pattern. Automatic temperature scans were taken at 5 minute intervals throughout the run. The moveable probes were operated in similar intervals.

The steady state or quasi-steady state portion was limited to a varying degree for each experiment and depended strongly on diffuser characteristics. The main factor was the net horizontal momentum of the diffuser discharge. In general, establishment of a steady state circulation pattern in the basin required about 5 to 10 minutes. For runs with no net horizontal momentum this was followed by an essentially steady portion of 10 to 30 minutes, i.e. dilutions in the diffuser vicinity were not changing. For runs with net horizontal momentum the steady state portion with respect to dilutions in the diffuser vicinity was in some instances strongly limited, that is, recirculation of mixed water resulted in an unsteady dilution decrease.

5.3.3 Experimental Runs

The run parameters are given in Chapters 6 and 7, together with experimental results. Three series of experiments were performed in the basin:

Series BN - No net horizontal momentum (Section 6.1)

Series BH - Net horizontal momentum (Section 6.2)

Series BC - With ambient cross-flow (Chapter 7)

5.3.4 Data Reduction

The principle of the data reduction is the same as for the flume experiments. Normalized surface temperature rises are plotted in the form of isotherms in Chapters 6 and 7 for selected experiments. In addition the non-dimensional vertical temperature rise profiles given at four points in the basin are indicated.

For the purpose of comparing with the theoretical surface dilution S_s and area, 4 ft wide, describing the near field zone, is defined around the diffuser line as indicated in Fig. 5-5. The extent of this area is comparable to Eq. (3-220) describing the length of the local mixing zone. The experimental dilution is then defined as the inverse of the maximum non-dimensional surface temperature observed at the edge of this near-field zone.

The bottom friction factor for the basin is calculated by the White-Colebrook relation with an absolute roughness $k_s = 0.03$ ft for grouted concrete surfaces. Φ is calculated as $\Phi \approx f_o L_D/H$. For the channel tests a correction factor, Eq. (5-5), was applied.

5.4 Experiments by Other Investigators

Basic experimental investigation of submerged multiport diffusers, in particular, three-dimensional phenomena, are scarce. Most diffuser studies reported in the literature are applied model studies of specific design problems and thus have peculiar features of topography and current distribution. Few investigations address the general problem of a diffuser in water of uniform depth with or without an ambient current, as considered in this study.

The two-dimensional experiments by Liseth (1970) on diffusers in deep water (stable near-field) were discussed in Chapter 2. Liseth only reports dilutions in the buoyant jet region and does not consider the effect of the free surface.

Two-dimensional channel model experiments were reported by Harleman et al. (1971). The bulk of that experiment was performed in a 21 ft long, 4.5 ft wide channel placed in a larger basin. The nozzle discharge was undirectional with a zero or near zero vertical angle. Most of their runs were made in the parameter range with full vertical mixing (supercritical flow) and only a few runs resulted in a stagnant wedge system. In Chapter 6 their results are compared with the present theory.

Two-dimensional experiments were also made by Larsen and Hecker (1972). However, in their experiments the nozzles were installed at a considerable height above the bottom (in some cases at half depth) which has limited practical significance. Their results cannot be compared to the present theory.

Three-dimensional diffuser tests were also performed by Harleman et al. (1971) and are summarized by Adams (1972). All these tests were made in a basin 46 × 28 × 1.5 ft and had ambient cross-flow. In Chapter 7 their results are compared with the cross-flow experiments of this study.

VI. DIFFUSERS WITHOUT AMBIENT CROSSFLOW: COMPARISON OF THEORY AND EXPERIMENTS

6.1 Diffusers with No Net Horizontal Momentum

6.1.1 Two-Dimensional Flume Experiments

The two-dimensional flume experiments with vertical discharge angle, Series FN, are summarized in Table 6.1. The relevant physical variables and non-dimensional parameters are given. Most of the experiments used a continuous slot discharge, a few experiments were done with a single nozzle. The jet Reynolds number did not, in all cases, satisfy the requirement, Equation (5-3). Although visual inspection showed that the jet structure was always clearly turbulent, nevertheless it is possible that the turbulent entrainment capacity of the jet is weaker than predicted by the theoretical analysis assuming a fully turbulent jet. In the experimental range the bottom friction factor, f_o, is both dependent on channel Reynolds number and relative roughness. The channel Reynolds number, Equation (3-212), can be estimated using the theoretical prediction of dilution as a good approximation.

The vertical structure of the flow field in the two-dimensional channel model can be inferred from temperature measurements and visual observation. Figure 6-1 gives a comparison between the typical flow fields for (a) a stable and (b) an unstable near-field zone. The theoretical location of the interface, Equation (3-207), shows good agreement with the observed temperature profile. The internal hydraulic jump region is clearly visible in Figure 6-1a,

Table 6.1: Flume Diffuser Experiments, Series FN

	Physical Variables						Secondary Parameters					Governing Parameters				Observed	Predicted
	H (ft)	B (10^{-3} ft)	U_o (ft/sec)	L (ft)	T_a (^oF)	ΔT_o (^oF)	IR_j	L/H	f_o	c_2	f_o^*	F_s	H/B	θ_o (dgr)	Φ	S_s	S_s
FN-1	2.00	10.4	0.64	20	67.5	15.3	1,610	10	0.039	1.7	0.066	25	192	90	0.7	11.8	12.2
2	2.00	10.4	0.43	20	66.4	29.0	1,070	10	0.039	1.7	0.066	13	192	90	0.7	17.0	17.0
3	2.00	10.4	4.27	20	64.7	16.3	10,700	10	0.032	1.7	0.054	160	192	90	0.5	4.5	3.5
4	2.00	3.3	1.72	20	67.4	24.1	1,370	10	0.038	1.7	0.065	87	600	90	0.6	15.0	16.5
5	2.00	3.3	0.88	20	68.0	10.9	700	10	0.042	1.7	0.071	71	600	90	0.7	15.5	19.0
6	2.00	3.3	1.51	20	68.2	29.5	1,200	10	0.035	1.7	0.060	67	600	90	0.6	14.7	19.2
7	2.00	3.3	4.71	20	66.1	17.5	3,750	10	0.036	1.7	0.061	291	600	90	0.6	6.7	7.3
8	1.33	3.3	2.69	20	67.3	22.0	2,140	15	0.041	1.4	0.058	144	400	90	0.9	7.3	7.0
9	1.00	5.2	1.86	20	66.9	17.9	2,330	20	0.047	1.3	0.061	91	192	90	1.2	5.1	4.9
10	1.00	5.2	5.34	20	67.6	16.9	6,700	20	0.042	1.3	0.055	270	192	90	1.1	2.7	3.2
11	2.17	5.2	0.64	20	65.4	24.8	810	9	0.040	1.7	0.068	31	416	90	0.6	17.7	21.0
12	2.00	10.4	2.13	20	65.8	16.1	5,350	10	0.036	1.3	0.047	80	192	90	0.5	5.5	5.6
13	1.25	20.8	1.07	20	67.5	21.0	5,360	16	0.037	1.4	0.052	23	60	90	0.8	4.6	4.4
14	2.17	1.7	1.31	20	69.0	14.4	540	9	0.041	1.7	0.070	128	1300	90	0.6	20.6	28.0
15	2.17	1.7	3.92	20	69.0	23.0	1,610	9	0.037	1.7	0.063	293	1300	90	0.6	17.7	16.4
16	2.17	1.7	1.30	20	69.4	28.4	540	9	0.040	1.7	0.068	85	1300	90	0.6	25.6	36.0
17	2.00	10.4	1.86	12	67.5	15.5	4,760	6	0.035	1.7	0.060	70	192	90	0.4	6.7	6.2
18	2.00	3.3	4.71	12	68.2	15.1	3,750	6	0.036	1.7	0.061	312	600	90	0.4	7.5	7.0
19	1.25	20.8	1.07	12	68.2	21.4	5,360	10	0.037	1.4	0.052	23	60	90	0.5	4.1	4.0
20n	2.00	3.4n	2.61	20	73.0	22.2	2,140	10	0.037	1.7	0.063	131	585	90	0.6	11.1	12.1
21n	2.00	3.4n	1.63	20	73.2	28.3	1,340	10	0.038	1.7	0.065	71	585	90	0.6	13.0	18.0
22n	2.17	1.7n	3.92	20	71.2	23.7	1,610	9	0.037	1.7	0.063	231	1240	90	0.6	15.0	18.2
23n	1.33	3.4n	2.61	20	67.5	21.8	2,140	15	0.041	1.4	0.058	140	390	90	0.9	7.2	7.0
FN-24n	2.17	5.8n	0.57	20	67.5	24.6	810	9	0.041	1.7	0.070	22	377	90	0.6	12.3	23.0

Note: "n" denotes experiments with a single nozzle, equivalent slot width (spacing 1.0 ft)

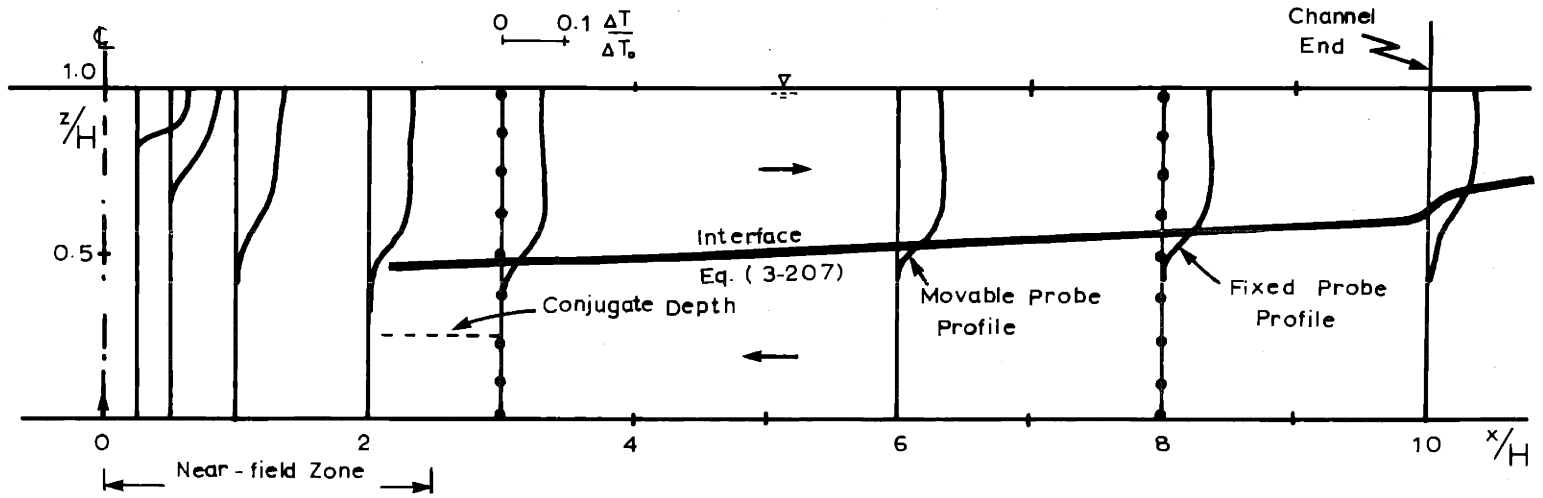

a) Run FN-6, F_s = 67, H/B = 600, θ_o = 90°, Φ = 0.6, Stable Near-Field

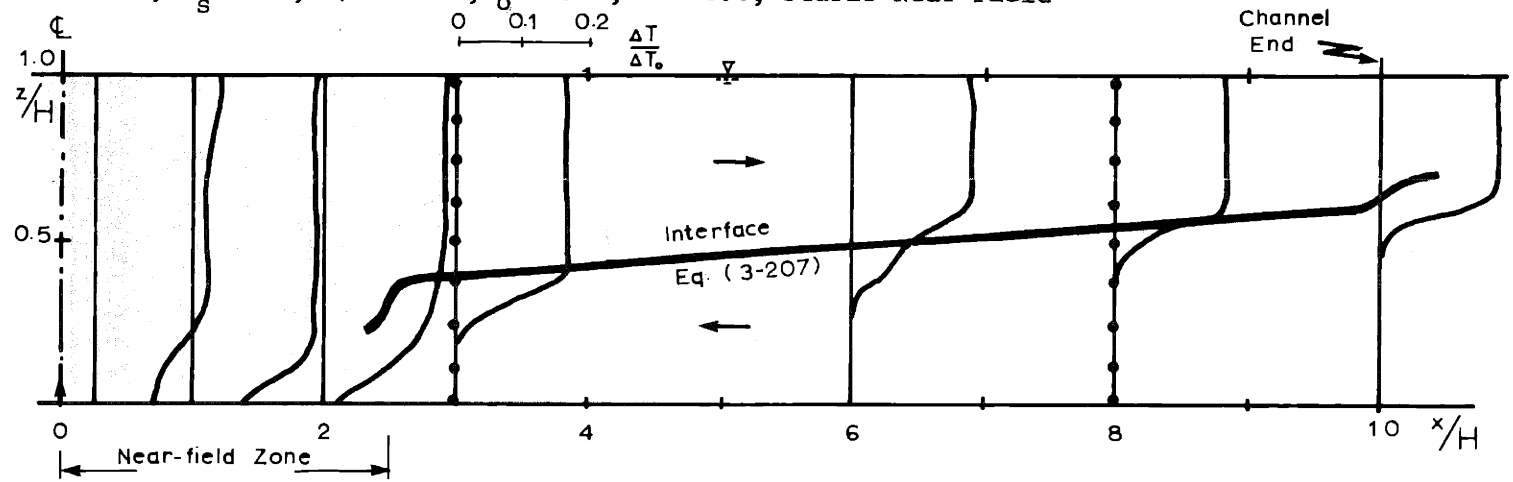

b) Run FN-12, F_s = 80, H/B = 192, θ_o = 90°, Φ = 0.5, Unstable Near-Field

Fig. 6-1: Steady-State Vertical Flow Structure: Observed Temperature Profiles Vs. Interface Eq. (3-207)

as is the local mixing zone with a critical section (rapid change in the location of the interface) in Figure 6-1b.

Table 6-1 also provides the comparison between observed surface dilution, $S_s = \frac{\Delta T_o}{\Delta T}$ (where ΔT is the surface temperature rise at the edge of the near field zone as shown in Figure 6-1), and the theoretical dilution as developed in Chapter 3. This comparison is also given in Figures 6-6 ($\Phi \approx 0.5$) and 6-7 ($\Phi \simeq 1.0$) along with the results from the three-dimensional basin tests. (Filled or unfilled symbols indicate an unstable or stable near-field, respectively, as determined by visual observation and by temperature profiles). In general, there is excellent agreement between theory and experiments, both with regard to the criterion between stable and unstable domain and with regard to the dilutions. The observed dilutions are somewhat lower than predicted for some experiments in the stable domain, which is attributed to low Reynolds numbers of the jet discharge. The results for the single nozzle tests agree well with the slot tests for the unstable domain, but are somewhat lower in the stable domain indicating incomplete lateral merging for a spacing, ℓ, equal to half the depth, H.

6.1.2 Three-Dimensional Basin Experiments

Table 6.2 is the summary of the basin experiments of multiport diffusers with no net horizontal momentum, Series BN. Most of the runs were three-dimensional, a few were done on the two-dimensional channel model by introducing a false wall parallel to the x-axis. Again in some tests the nozzle Reynolds number is lower than the given requirement.

Table 6.2: Basin Diffuser Experiments, Series BN

	Physical Variables							Secondary Parameters			Governing Parameters						Observed	Predicted
	H (ft)	D (10^{-3} ft)	ℓ (ft)	U_o (ft/sec)	L_D (ft)	T_a (^oF)	ΔT_o (^oF)	IR_j	ℓ/H	L_D/H	f_o	F_s	H/B	θ_o (dgr)	Φ	β (v)	S_s	S_s
BN-1	0.67	10.4	0.08	2.42	6.4	58.8	27.0	2,870	0.12	10	0.09	158	628	90	0.9	NOR	5.9	N.A.
2	0.67	10.4	0.08	2.42	6.4	64.0	25.3	3,000	0.12	10	0.09	160	628	45-A	0.9	LIN	10.0	N.A.
3	0.67	10.4	0.08	2.42	6.4	65.3	26.4	3,090	0.12	10	0.09	157	628	45-A	0.9	SIN	11.8	N.A.
4	0.67	10.4	0.08	2.42	6.4	67.9	27.3	3,210	0.12	10	0.09	154	628	45-A	0.9	N-S	10.0	N.A.
5	0.67	10.4	0.08	2.42	6.4	65.6	27.4	3,120	0.12	10	0.09	154	628	45-A	0.9	LOG	9.5	10.6
6	0.67	10.4	0.08	3.60	6.4	67.2	26.6	4,700	0.12	10	0.08	231	628	45-A	0.9	LOG	8.3	8.0
7	0.67	10.4	0.16	4.84	6.4	68.5	24.6	6,260	0.24	10	0.09	458	1256	45-A	0.9	LOG	13.2	10.4
8	0.43	10.4	0.08	1.21	6.4	63.2	24.9	1,480	0.19	15	0.08	81	402	45-A	1.2	LOG	9.1	10.5
9	0.67	15.6	0.16	2.15	6.4	63.7	26.0	4,010	0.24	10	0.09	131	558	45-A	0.9	LOG	10.0	10.4
10	0.67	21.3	0.32	2.31	6.4	64.8	24.7	5,810	0.48	10	0.11	150	600	45-A	1.1	LOG	10.5	10.5
11	0.67	10.4	0.16	1.50	6.4	64.2	23.0	1,820	0.24	10	0.10	148	1256	90	1.0	NOR	17.3	22.0
12	0.92	10.4	0.16	1.50	6.4	64.0	23.0	1,810	0.17	7	0.08	148	1727	90	0.6	NOR	27.0	37.0
13	0.67	10.4	0.08	2.42	6.4	64.7	26.1	3,040	0.12	10	0.09	158	628	0-A	0.9	LOG	10.4	10.5
14	0.67	10.4	0.16	4.84	6.4	65.2	25.3	6,070	0.24	10	0.09	454	1256	0-A	0.9	LOG	10.5	10.4
15	0.67	15.6	0.16	2.15	6.4	65.9	25.9	4,110	0.24	10	0.09	133	558	0-A	0.9	LOG	10.0	10.4
16	0.67	15.6	0.16	0.87	6.4	66.6	22.5	1,610	0.24	10	0.10	58	558	0-A	1.0	LOG	15.1	19.5
17c	0.67	10.4	0.08	2.42	6.0c	63.9	29.3	3,130	0.12	9c	0.09	149	628	90	0.8	-	8.6	10.4
18c	0.66	15.6	0.16	2.15	6.0c	64.4	22.7	3,890	0.24	9c	0.09	142	552	45-A	0.8	-	9.1	10.4
19c	0.67	10.4	0.08	2.42	6.0c	64.7	27.1	3,080	0.12	9c	0.09	155	628	45-A	0.8	-	9.4	10.5
20c	0.67	10.4	0.16	2.43	6.0c	63.4	26.4	3,020	0.24	9c	0.09	223	1256	45-A	0.8	-	12.2	16.7
21c	0.67	10.4	0.16	1.50	6.0c	63.4	26.5	1,860	0.24	9c	0.09	137	1256	45-A	0.8	-	15.0	22.5
22c	0.67	15.6	0.16	2.15	6.0c	64.3	28.3	4,140	0.24	9c	0.09	127	558	0-A	0.8	-	9.2	10.4
BN-23c	0.67	10.4	0.16	4.84	6.0c	63.4	28.4	6,150	0.24	9c	0.09	429	1256	0-A	0.8	-	9.3	10.7

Note: "c" denotes channel experiments, with the channel length, L, given under L_D

"A" denotes alternating nozzles

The first five experiments served to establish the use of the horizontal nozzle orientation as a control of the horizontal circulations induced by a diffuser discharge with an unstable near-field. In Chapter 4 the theoretical solution for the horizontal nozzle orientation, $\beta(y)$, along the diffuser line has been derived, Equation (4-36), based on the model of the three-dimensional strafified flow field. To check the validity of this equation and also the sensitivity due to deviations in the nozzle orientation the following $\beta(y)$ were checked:

1) Normal distribution (NOR): All nozzles are normal to the diffuser axis or vertically upward, thus providing no discharge momentum in the y-direction (along the axis of the diffuser).

$$\beta(y) = 90^{o} = \text{const.} \qquad (6\text{-}1)$$

2) Linear distribution (LIN):

$$\beta(y) = 90^{o}\ (1 - \frac{y}{L_D}) \qquad (6\text{-}2)$$

3) Sinusoidal distribution (SIN):

$$\beta(y) = \cos^{-1}(\frac{y}{L_D}) \qquad (6\text{-}3)$$

4) Normal-sinusoidal distribution (N-S)

$$\beta(y) = \begin{cases} 90^{o} & 0 < y < L_D/2 \\ \cos^{-1}(2\,\frac{y}{L_D} - 1) & L_D/2 < y < L_D \end{cases} \qquad (6\text{-}4)$$

The distribution given by Equation (4-36) is called for simplicity the:

5) "Logarithmic"distribution (LOG):

$$\beta(y) = \cot^{-1}\ (\frac{1}{\pi}\log\frac{1 + y/L_D}{1 - y/L_D}) \qquad (4\text{-}36)$$

The different $\beta(y)$ are plotted in Figure 6-2. Runs BN-1 to 5 have closely similar discharge conditions. The resulting temperature fields for runs 1, 2 and 5 are shown in Figures 6-3a,b and 6-4a. Vertical temperature profiles at four points are given and surface current directions and magnitudes are indicated qualitatively. For the normal distribution (NOR), Figure 6-3a, without any diffuser momentum opposing the inward flow along the diffuser line, a strong, vertically fully mixed flow-away along the x-axis results. The situation is reversed for the linear distribution (LIN), Figure 6-3b; too much nozzle orientation in the y direction results in a dominant flow-away along the y-axis (diffuser line) which is again rather well mixed. For the "logarithmic distribution" (LOG), Figure 6-4a, however, the flow field is approximately uniform in all directions and the vertical temperature profiles indicate the stratified counterflow system at all points in the diffuser vicinity. In general, it is found (see Figure 6-2) that nozzle orientations providing less discharge momentum in the y-direction than indicated by Equation (4-36) tend to a flow-away along the x-axis and vice versa. The flow condition near to the LOG distribution is not very sensitive. The theoretical dilution, assuming control, is 10.6 for these cases. It is seen that the NOR distribution has a strongly reduced dilution, while for the other nozzle distributions, the observed and theoretical dilutions are in good agreement. It should be noted, however, that all distributions, except the LOG distribution, set up horizontal circulations which ultimately lead to recirculation

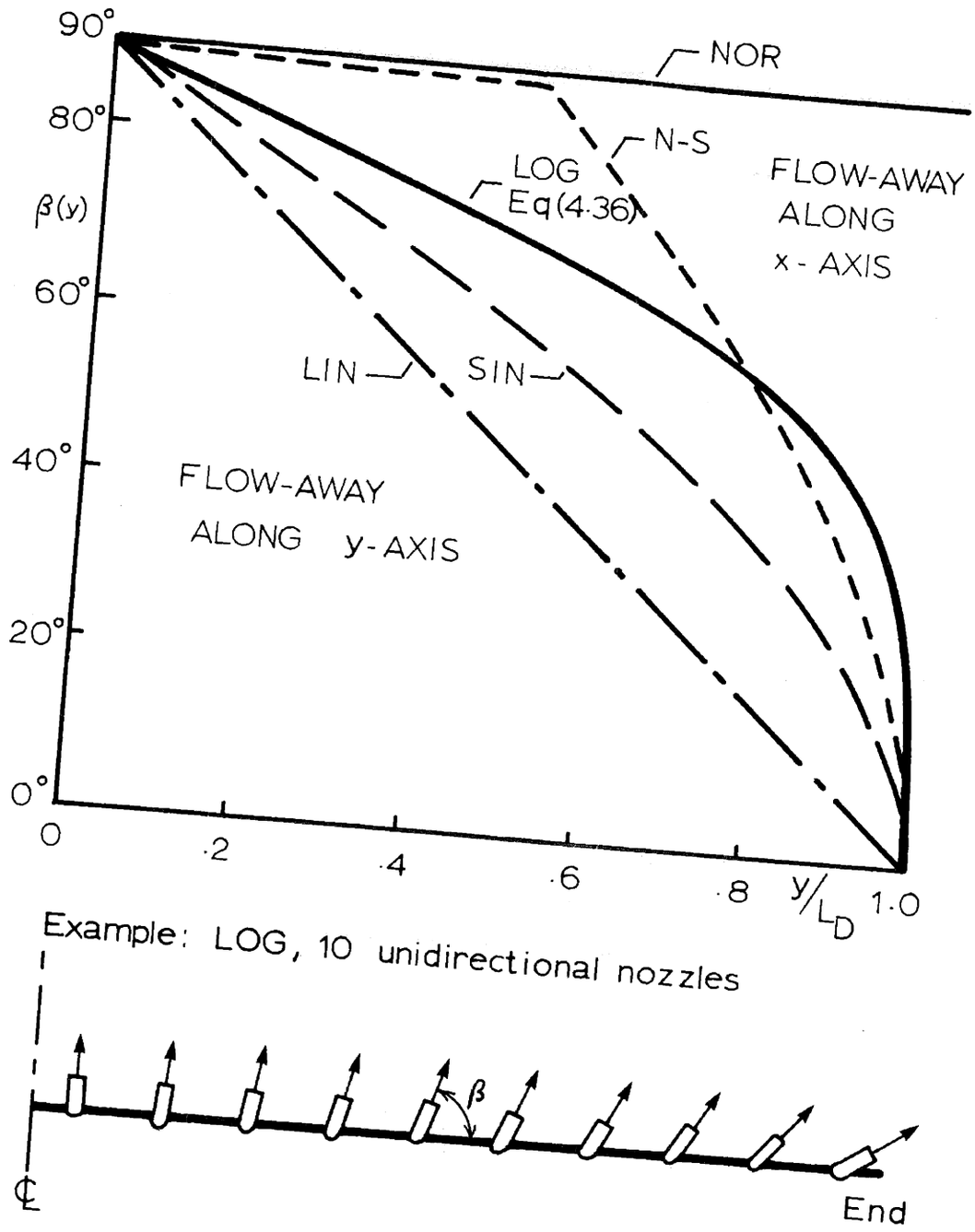

Fig. 6-2: Nozzle Orientation, β(y), Along the Diffuser Line

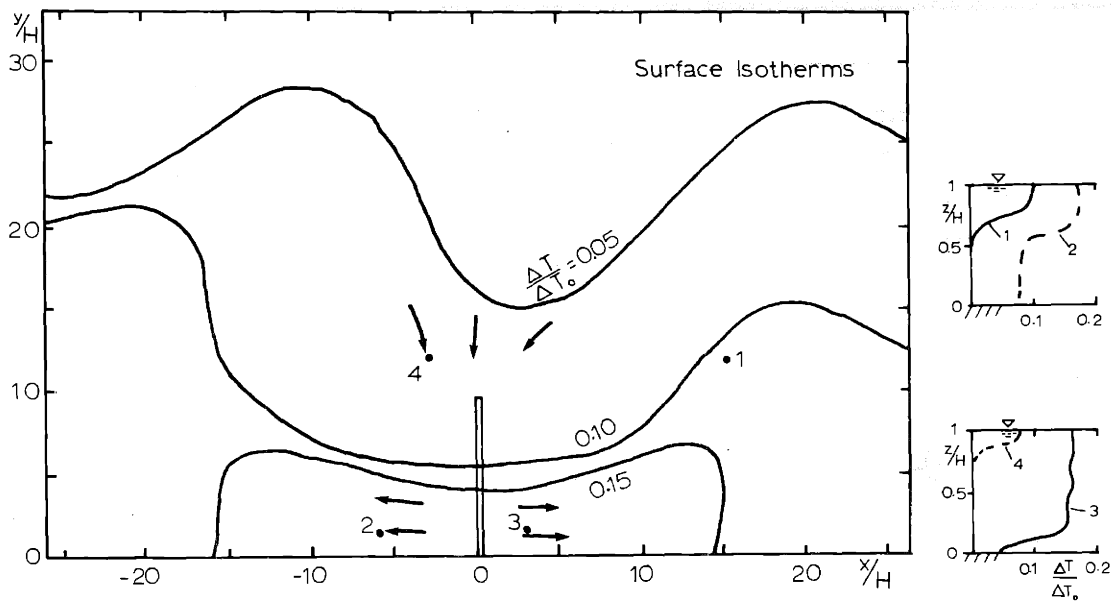

a) Run BN-1, F_s = 158, H/B = 628, θ_o = 90°, Φ = 0.9, $\beta(y)$ = NOR

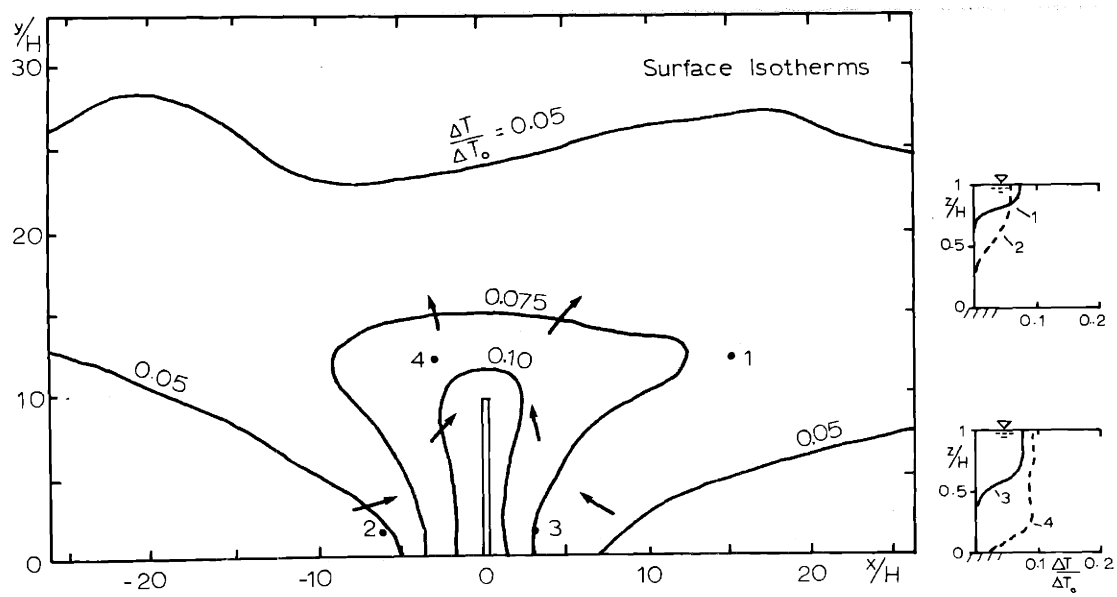

b) Run BN-2, F_s = 160, H/B = 628, θ_o = 45°-A, Φ = 0.9, $\beta(y)$ = LIN

Fig. 6-3: Observed Temperature and Flow Field, Series BN

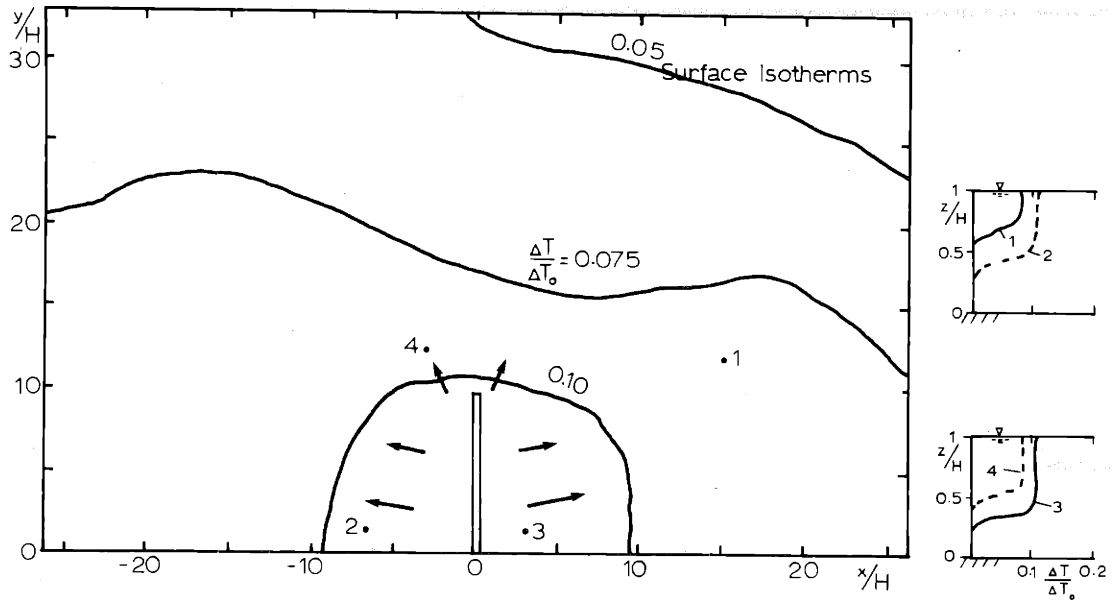

a) Run BN-5, F_s = 154, H/B = 628, θ_o = 45°-A, Φ = 0.9, $\beta(y)$ = LOG

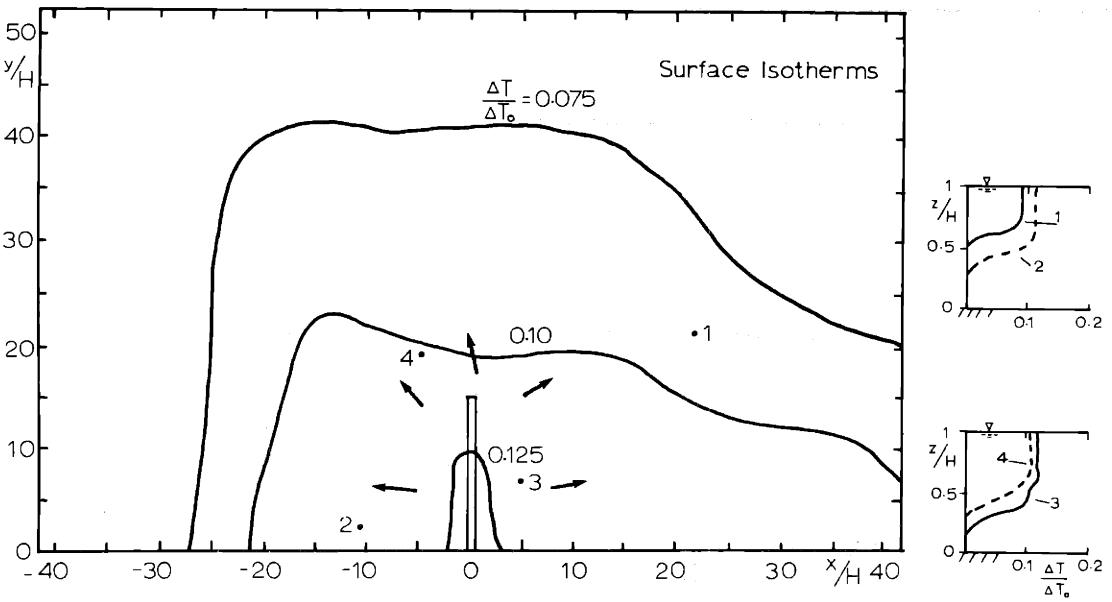

b) Run BN-8, F_s = 81, H/B = 402, θ_o = 45°-A, Φ = 1.2, $\beta(y)$ = LOG

Fig. 6-4: Observed Temperature and Flow Field, Series BN

into the diffuser line. The dilutions given do not account for this effect. In this respect the LOG distribution is the only one which creates a stably stratified flow system in the far-field which is not prone to recirculation.

Two more examples of the temperature field produced by a discharge with LOG distribution are given in Figure 6-4b ($\theta_o = 45^o$, more shallow water) and Figure 6-5a ($\theta_o = 0^o$). These experiments have a relatively higher value for the y-momentum of the discharge as compared to Figure 6-4a. The resulting flow field, however, is similar, giving support to the discussion in Chapter 4, that it is not the absolute value of the discharge y-momentum that is important, but rather its distribution as long as the vertical angle is below $\theta_{o_{max}}$, Equation (4-43)

A diffuser with a stable near-field (thus requiring no control $\beta(y)$ = NOR) is shown in Figure 6-5b. The flow field can be compared to Figure 6-3a. With a stable near-field the flow-away is uniform in all directions. The experiment in Figure 6-5b is near the edge of the stable zone (see Figure 6-6) and may be somewhat affected by instabilities explaining the weaker flow-away in the y-direction.

Observed and theoretical surface dilutions are compared in Table 6.2 and Figures 6-6 ($\Phi \approx 0.5$) and 6-7 ($\Phi \approx 1.0$). Good agreement is found for both three-dimensional and two-dimensional basin experiments. Due to experimental limitations (jet turbulence) the experiments were mainly restricted to the unstable near-field domain. Various experiments with similar F_s, H/B but different vertical angle θ_o and spacing ℓ/H, were made to assess

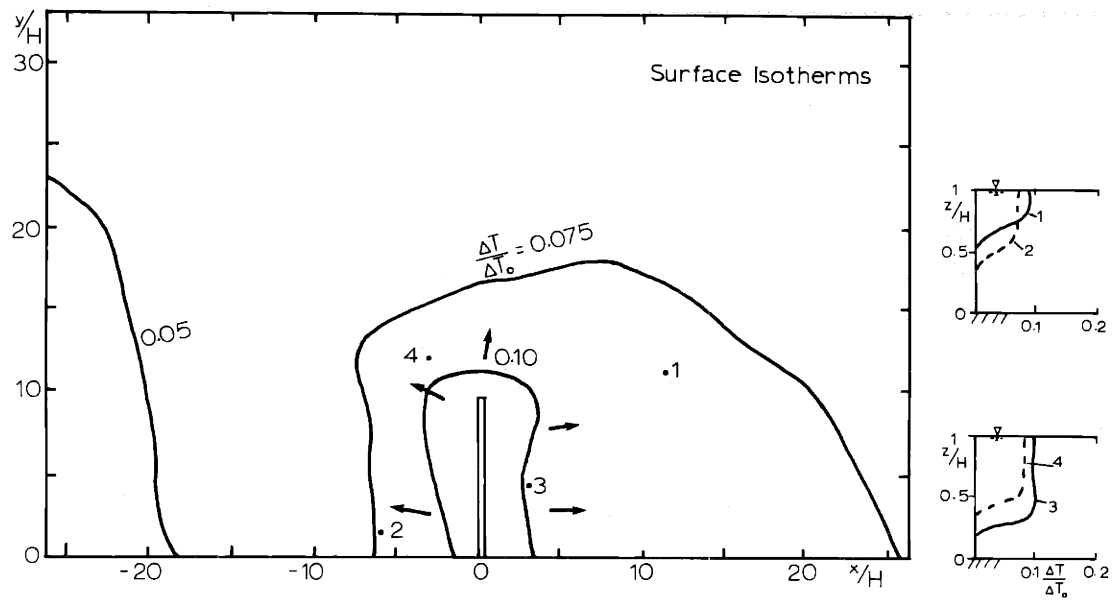

a) Run BN-13, F_s = 158, H/B = 628, θ_o = 0°-A, Φ = 0.9, $\beta(y)$ = LOG

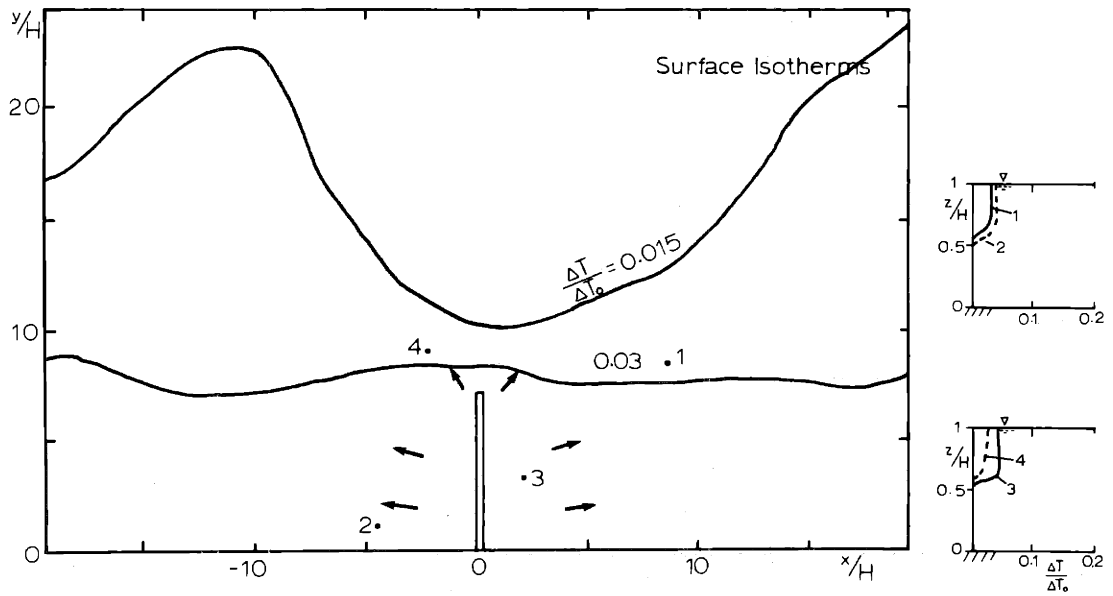

b) Run BN-12, F_s = 148, H/B = 1727, θ_o = 90°, Φ = 0.6, $\beta(y)$ = NOR, Stable

Fig. 6-5: Observed Temperature and Velocity Field, Series BN

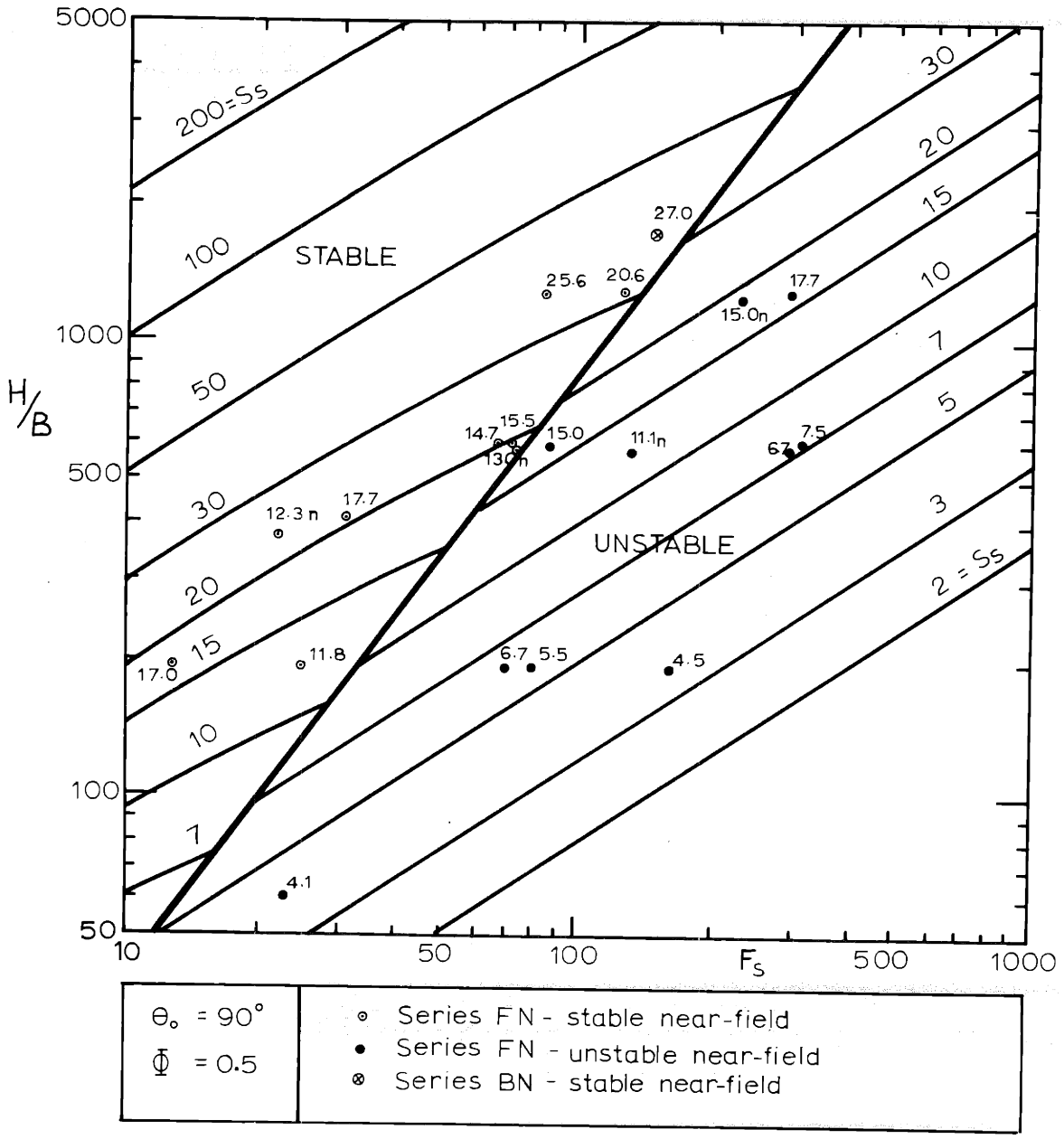

Fig. 6-6: Predicted Vs. Observed Dilutions, S_s

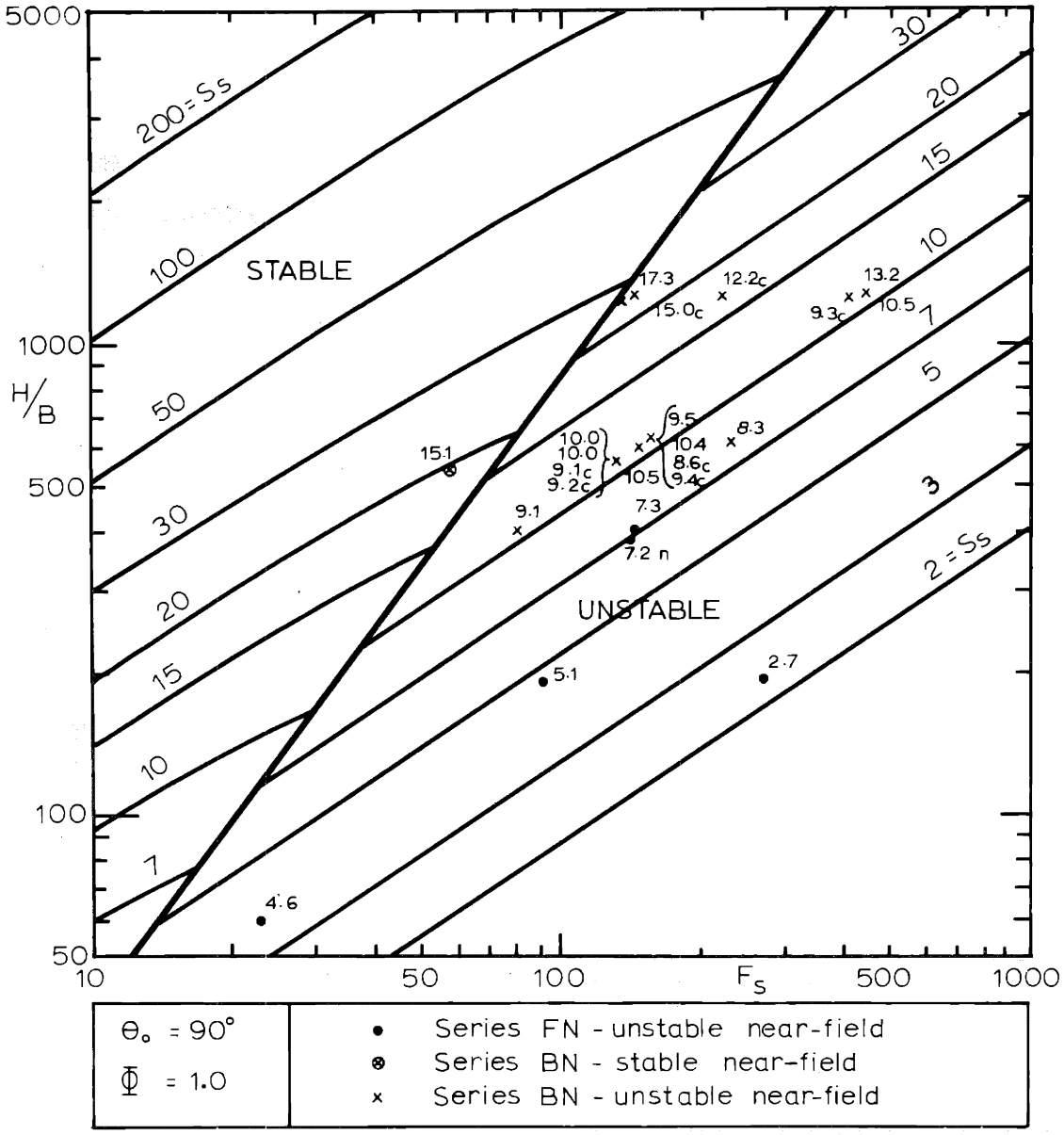

Fig. 6-7; Predicted Vs. Observed Dilutions, S_s

the equivalent slot concept for diffusers with alternating nozzles. As can be seen the dilutions are, indeed, independent of vertical angle and spacing, so that the equivalent slot representation is valid.

6.2 Diffusers with Net Horizontal Momentum

6.2.1 Two-Dimensional Flume Experiments

Run parameters for the flume experiments with unidirectional discharge, Series FH, are given in Table 6.3. The runs were limited to the low F_s, high H/B range for the following reasons:

(i) The fully mixed range (high F_s, low H/B, $\theta_o = 0$) has been extensively investigated in the channel experiments by Harleman et al. (1971). Their experimental results were analysed using $k_s = 0.002$ ft (planed-wood flume) and are compared in Figures 6-12 ($\Phi \approx 0.5$) and 6-13 ($\Phi \approx 1$) to theoretical predictions.

(ii) Preliminary experiments of the flume set-up in the fully mixed range established two shortcomings: (a) The "reservoir" outside the channel test section was not large enough, thus velocities and incurred head losses were not negligible; (b) For strong jet discharges the slot jet became attached to the channel bottom resulting in significant momentum dissipation. It may be concluded that while the equivalent slot concept can always be used in mathematical terms to represent a multiport diffuser it is not a desirable experimental schematization under all conditions. In particular, it does not allow penetration of ambient entrainment water coming from the upstream direction

Table 6.3: Flume Diffuser Experiments, Series FH

	Physical Variables						Secondary Parameters					Governing Parameters				Observed	Predicted
	H (ft)	B (10^{-3} ft)	U_o (ft/sec)	L (ft)	T_a (^oF)	ΔT_o (^oF)	IR_j	L/H	f_o	c_2	f_o^*	F_s	H/B	θ_o (dgr)	Φ	S_s	S_s
FH-1	2.00	3.3	1.68	20	71.4	31.3	1,340	10	0.036	1.7	0.061	64	600	45	0.6	17.5	23.0
2	2.00	10.4	0.64	20	65.7	16.9	1,610	10	0.038	1.7	0.065	23	192	45	0.7	10.1	13.2
3n	2.00	3.4n	1.63	20	69.1	29.9	1,340	10	0.037	1.7	0.063	71	585	45	0.6	13.6	20.5
4	2.17	1.7	1.31	20	66.6	14.9	540	9	0.038	1.7	0.065	129	1300	0	0.6	29.5	37.0
5	2.00	3.3	1.68	20	67.0	29.0	1,340	10	0.037	1.7	0.063	86	600	0	0.6	16.1	26.0
6	2.00	10.4	0.64	20	70.2	13.6	1,610	10	0.037	1.7	0.063	20	192	0	0.6	13.6	15.0
FH-7n	2.00	3.4n	1.64	20	68.9	29.1	1,340	10	0.037	1.7	0.063	72	585	0	0.6	19.5	25.0

Note: "n" denotes single nozzle experiments, spacing 1.0 ft.

and thus leads to a low pressure zone and jet attachment downstream of the discharge.

Observed dilutions in the experimental range (stratified counterflow conditions) are somewhat lower than predicted, probably a consequence of the low Reynolds number of the discharge. There is good correspondence between slot and individual nozzle experiments.

All, but three, of the channel experiments by Harleman et al. (1971) resulted in a fully mixed regime. In general, their results agree well with the theoretical predictions. The three experiments resulting in a stagnant wedge regime exhibit somewhat lower dilutions than predicted (Figure 6-13)

6.2.2 Three-Dimensional Basin Experiments

The diffuser experiments with undirectional discharge in the basin, Series BH, are summarized in Table 6.4. Runs 1 to 9 were made with a 45^{o} vertical angle, the rest with horizontal discharge (0^{o}). A few experiments were made on the two-dimensional channel concept focusing on the "deep water" regime (high H/B, low F_s). The bulk of the experiments was concentrated on the three-dimensional behaviour: Runs 1 to 6 (with 45^{o}) and runs 10 to 15 (with 0^{o}) were all in the deep water range, while runs 16 to 24 (with 0^{o}) were in the "shallow water" range (low H/B, high F_s) resulting in full vertical mixing.

The question of the horizontal nozzle orientation, $\beta(y)$, for diffuser control was addressed by investigating the normal distribution (NOR) and the "logarithmic" distribution (LOG) in pairs

Table 6.4: Basin Diffuser Experiments, Series BH

	Physical Variables							Secondary Parameters			Governing Parameters						Predicted		
																	Observed	This study	Adams (1972)
	H (ft)	D (10^{-3} ft)	ℓ (ft)	U_o (ft/sec)	L_D (ft)	T_a (^oF)	ΔT_o (^oF)	IR_j	ℓ/H	L_D/H	f_o	F_s	H/B	θ_o (dgr)	Φ	$\beta(y)$	S_s	S_s	S_s
BH-1	0.92	18.7	0.16	0.58	6.4	58.2	24.1	1,190	0.18	7	0.090	31	534	45	0.6	LOG	17.9	28.0	N.A.
2	0.92	15.6	0.16	0.83	6.4	57.5	24.8	1,430	0.18	7	0.085	53	768	45	0.6	LOG	18.5	30.0	N.A.
3	0.65	15.6	0.16	2.15	6.4	61.5	25.6	3,900	0.24	10	0.090	137	546	45	0.9	LOG	13.3	21.0	N.A.
4	0.65	15.6	0.16	1.08	6.4	61.5	23.9	1,910	0.24	10	0.095	69	546	45	1.0	LOG	11.8	18.5	N.A.
5	0.67	15.6	0.32	1.66	6.4	62.6	22.4	2,950	0.48	10	0.095	156	1116	45	1.0	LOG	18.2	27.0	N.A.
6	0.67	15.6	0.32	1.66	6.4	62.9	22.4	2,950	0.48	10	0.095	156	1116	45	1.0	NOR	16.7	N.A.	N.A.
7c	0.92	21.3	0.32	0.89	6.0c	63.5	24.6	2,230	0.35	7c	0.090	59	824	45	0.6	-	21.8	30.0	N.A.
8c	0.92	21.3	0.16	0.45	6.0c	63.5	24.6	1,110	0.18	7c	0.090	21	412	45	0.6	-	18.9	28.0	N.A.
9c	0.92	15.6	0.16	0.83	6.0c	63.6	21.8	1,480	0.18	7c	0.090	56	768	45	0.6	-	18.2	28.0	N.A.
10	0.67	15.6	0.16	1.08	6.4	60.7	25.4	1,930	0.24	10	0.095	67	558	0	1.0	LOG	14.3	20.5	N.A.
11	0.67	15.6	0.16	1.08	6.4	59.5	26.4	1,930	0.24	10	0.100	66	558	0	1.0	NOR	13.2	N.A.	N.A.
12	0.92	21.3	0.32	0.89	6.4	59.5	24.0	2,120	0.35	7	0.090	59	824	0	0.6	LOG	20.0	32.0	N.A.
13	0.92	21.3	0.32	0.89	6.4	59.9	23.8	2,120	0.35	7	0.090	60	824	0	0.6	NOR	16.1	N.A.	N.A.
14	0.67	15.6	0.32	1.66	6.4	61.6	23.5	2,950	0.48	10	0.090	152	1116	0	0.9	LOG	21.3	34.5	N.A.
15	0.92	18.7	0.16	0.58	6.4	58.8	23.7	1,190	0.18	7	0.090	31	534	0	0.6	LOG	19.6	27.2	N.A.
16	0.67	15.6	0.16	2.15	6.4	60.7	27.2	3,930	0.24	10	0.100	130	558	0	1.0	LOG	18.2	25.6	N.A.
17	0.67	15.6	0.16	2.15	6.4	59.5	28.2	3,930	0.24	10	0.085	128	558	0	0.9	NOR	13.5	N.A.	16.7
18	0.49	21.3	0.32	1.56	6.4	59.8	27.2	3,850	0.64	13	0.100	97	436	0	1.3	LOG	18.2	22.5	N.A.
19	0.49	21.3	0.32	1.56	6.4	60.6	26.6	3,850	0.64	13	0.100	99	440	0	1.3	NOR	16.7	N.A.	14.7
20	0.50	15.6	0.32	2.91	6.4	61.9	25.1	5,250	0.64	13	0.090	258	837	0	1.2	LOG	19.2	31.8	N.A.
21	0.50	15.6	0.32	2.91	6.4	62.2	25.9	5,320	0.64	13	0.090	254	837	0	1.2	NOR	17.2	N.A.	20.5
22	0.50	10.4	0.08	2.42	6.4	62.5	26.5	2,980	0.16	13	0.085	157	471	0	1.1	LOG	13.9	23.6	N.A.
23	0.50	10.4	0.08	2.42	6.4	62.8	26.1	2,980	0.16	13	0.085	158	471	0	1.1	NOR	14.3	N.A.	15.3
24	0.50	21.3	0.32	2.31	6.4	60.3	25.0	4,420	0.64	13	0.085	150	449	0	1.1	NOR	16.7	23.4	15.0
25c	0.92	15.6	0.16	0.83	6.0c	63.1	22.5	1,480	0.18	7c	0.080	55	768	0	0.6	-	18.2	28.7	N.A.
26c	0.92	21.3	0.32	0.89	6.0c	63.2	23.6	2,190	0.35	7c	0.080	60	824	0	0.6	-	19.6	29.5	N.A.
BH-27c	0.92	21.3	0.16	0.45	6.0c	63.3	22.6	1,090	0.18	7c	0.085	22	412	0	0.6	-	18.2	26.0	N.A.

Note: "c" denotes channel experiments, with the channel length, L, given under L_D

with equal H/B, F_s, θ_o (Runs 5 and 6, 10 and 11, 16 and 17, 18 and 19, 20 and 21, 22 and 23).

The results of the investigation with respect to the observed flow field confirmed (a) the criteria for the occurrence of a stratified or fully mixed flow-away, established in Chapter 3, and (b) the effect of diffuser control, $\beta(y)$. However, observed dilutions, S_s, were in general lower than predicted by this study, in certain cases up to 40% lower. This is attributable to experimental limitations as discussed below.

Diffuser flow fields in "deep water" for a LOG distribution (Run 5) and for a NOR distribution (Run 6) are shown in Figure 6-8. The diffuser with control (LOG) tends to establish a stronger lateral spreading of the discharge with a distinctly stratified condition, which is predicted from Figure 6-11. On the other hand, the diffuser without control (NOR) has a concentrated fully mixed flow-away along the x-axis. Both diffusers show some surface eddying at the diffuser end.

In the "shallow water" range the comparison is given in Figure 6-9 (Run 18, LOG, and Run 19, NOR). Both diffusers show full vertical mixing as predicted. Again the diffuser without control tends to establish the concentrated flow-away with a contraction, as predicted by the theory of Adams (1972). At the edge of the flow-away zone density effects lead to stratification and lateral spreading, to a stronger degree so for the LOG distribution. This phenomenon makes the observation of the contraction

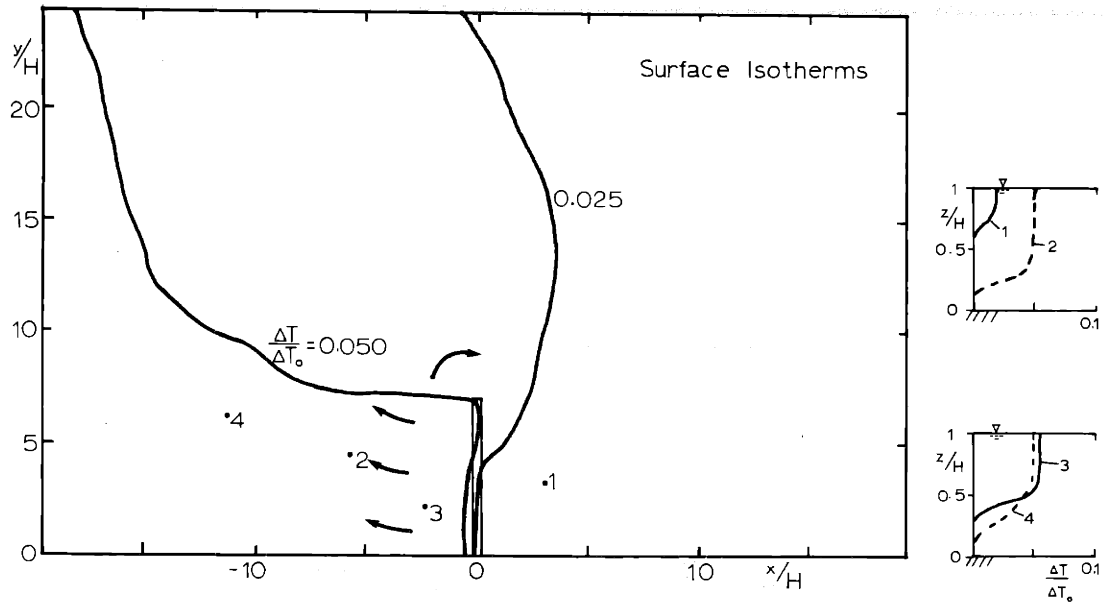

a) Run BH-5, F_s = 156, H/B = 1116, θ_o = 45°, Φ = 1.0, $\beta(y)$ = LOG

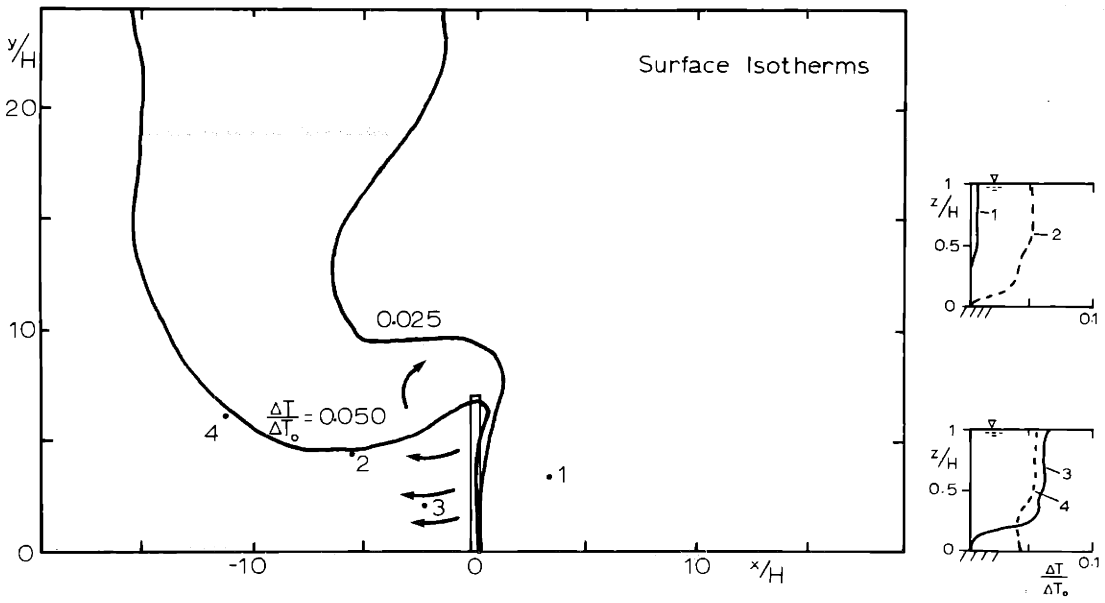

b) Run BH-6, F_s = 156, H/B = 1116, θ_o = 45°, Φ = 1.0, $\beta(y)$ = NOR

Fig. 6-8: Observed Temperature and Velocity Field, Series BH

(Nozzles Directed to the Left)

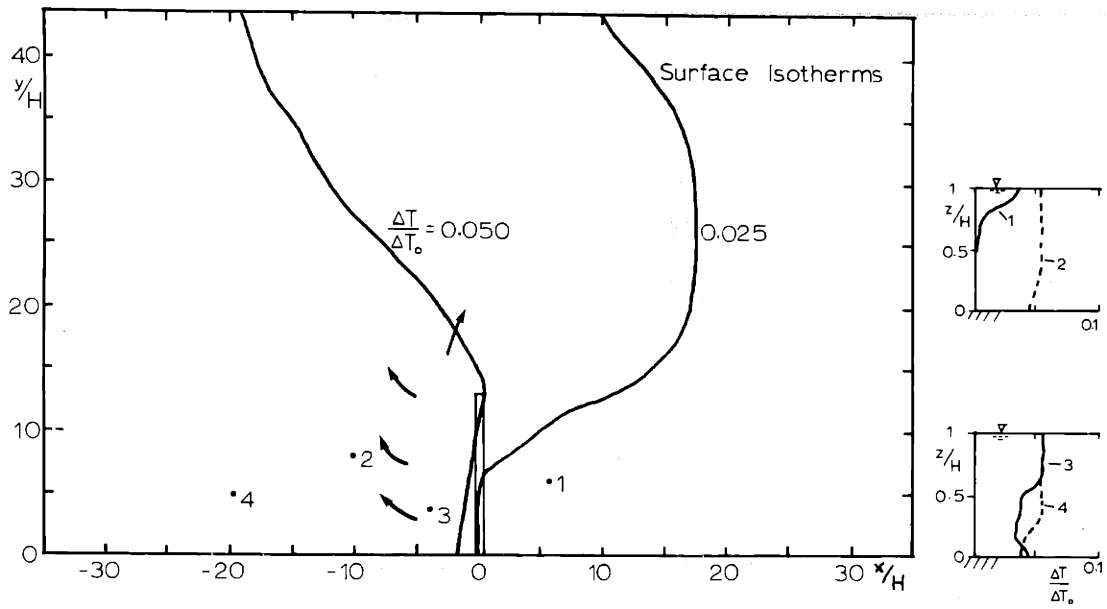

a) Run BH-18, F_s = 97, H/B = 436, θ_o = 0°, Φ = 1.3, $\beta(y)$ = LOG

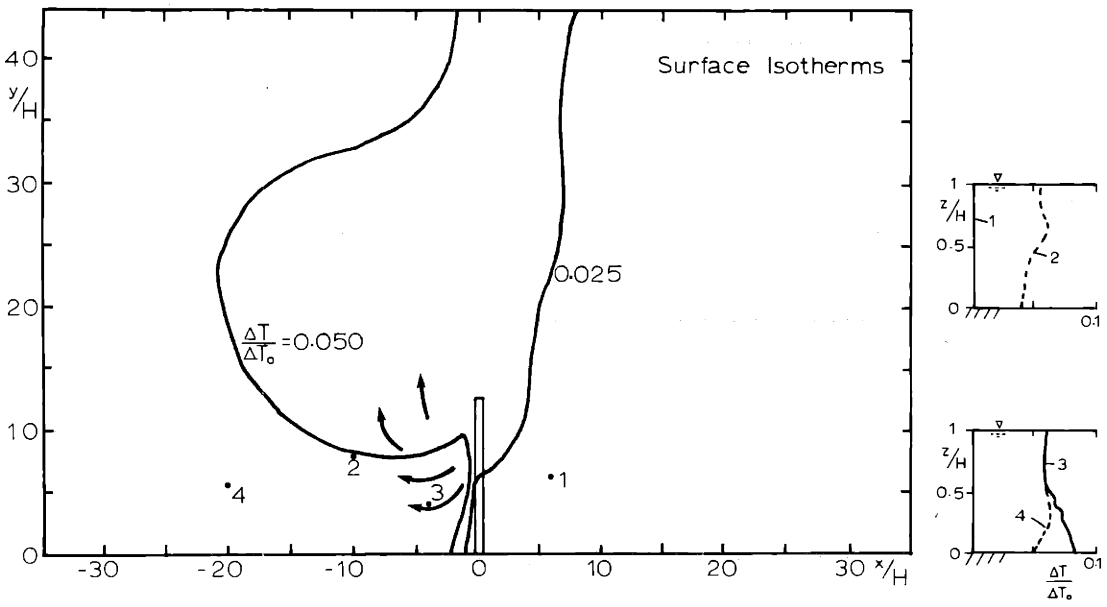

b) Run BH-19, F_s = 99, H/B = 440, θ_o = 0°, Φ = 1.3, $\beta(y)$ = NOR

Fig. 6-9: Observed Temperature and Velocity Field, Series BH

(Nozzles Directed to the Left)

of the flow field somewhat inaccurate, but as an approximate measure, obtained from dye observations, a contraction of 0.7 is typical for diffusers in the shallow water range (as compared to 0.5 from Adams' theory, neglecting friction in the flow-away).

In Table 6.4 observed dilutions, S_s, are compared with the predictions of this study (applicable only to diffusers with control, having no contraction) and the predictions by Adams (applicable only (a) to diffusers without control, with contraction, and (b) in the shallow water range with full vertical mixing). As mentioned, the observed dilutions in the basin experiments are in general lower that predicted by this study, in certain cases up to 40% lower (see Figures 6-10 to 6-13). It is argued that this lack of agreement solely reflects the experimental limitations of a relatively small basin as discussed in Chapter 4:

(i) In the "deep water" range the jet turbulence is too low, as in the case of the experiments on diffusers with no net horizontal momentum.

(ii) In the "shallow water" range the relative strength of the horizontal circulations as influenced by the basin boundaries leads to a dilemma: (a) To obtain steady-state conditions the experiment has to last long enough, while (b) with increasing time an increasing recirculation into the diffuser line takes place.

All measured dilutions, S_s, given in Table 6.4 do not contain

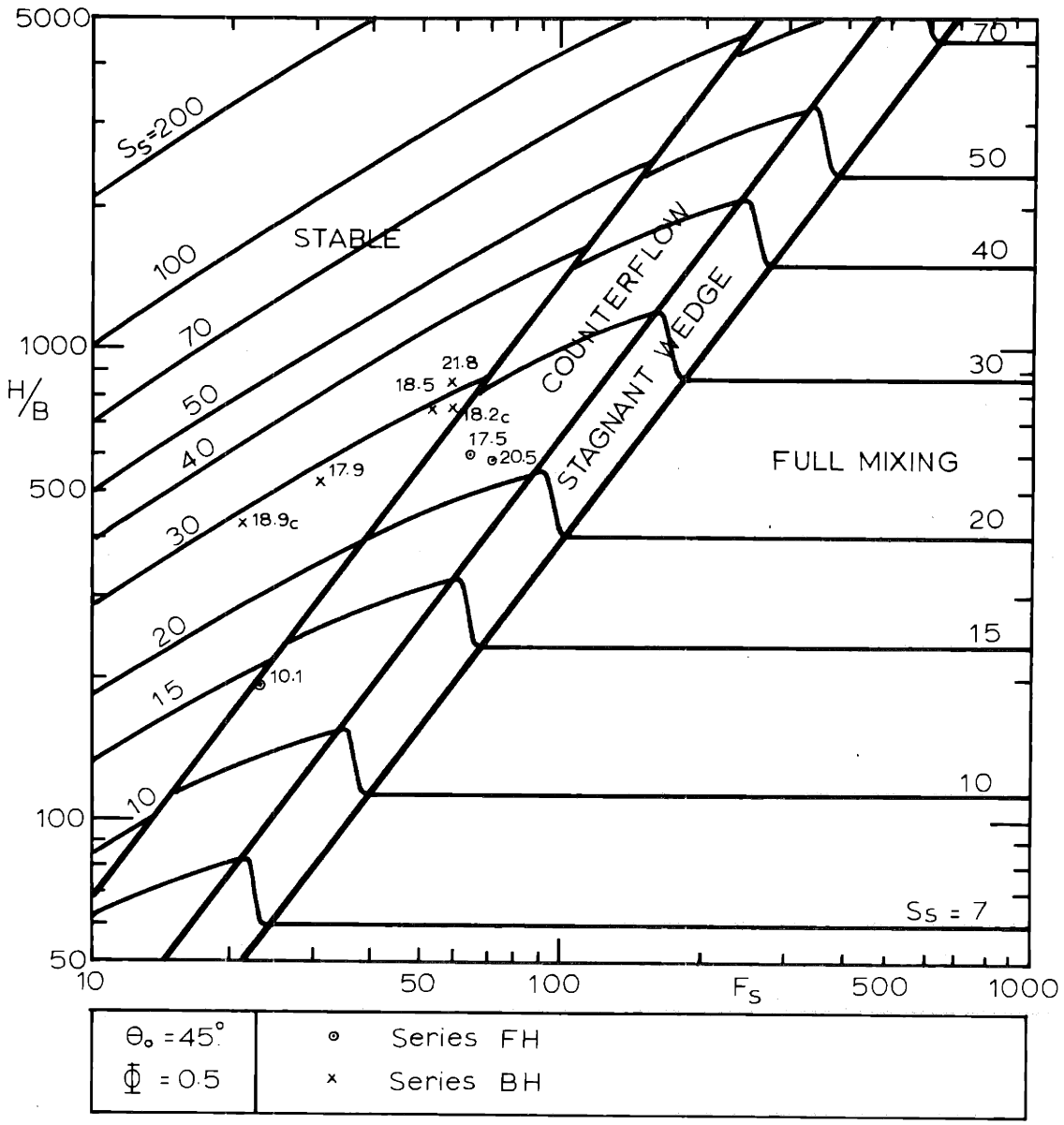

Fig. 6-10: Predicted Vs. Observed Dilutions, S_s

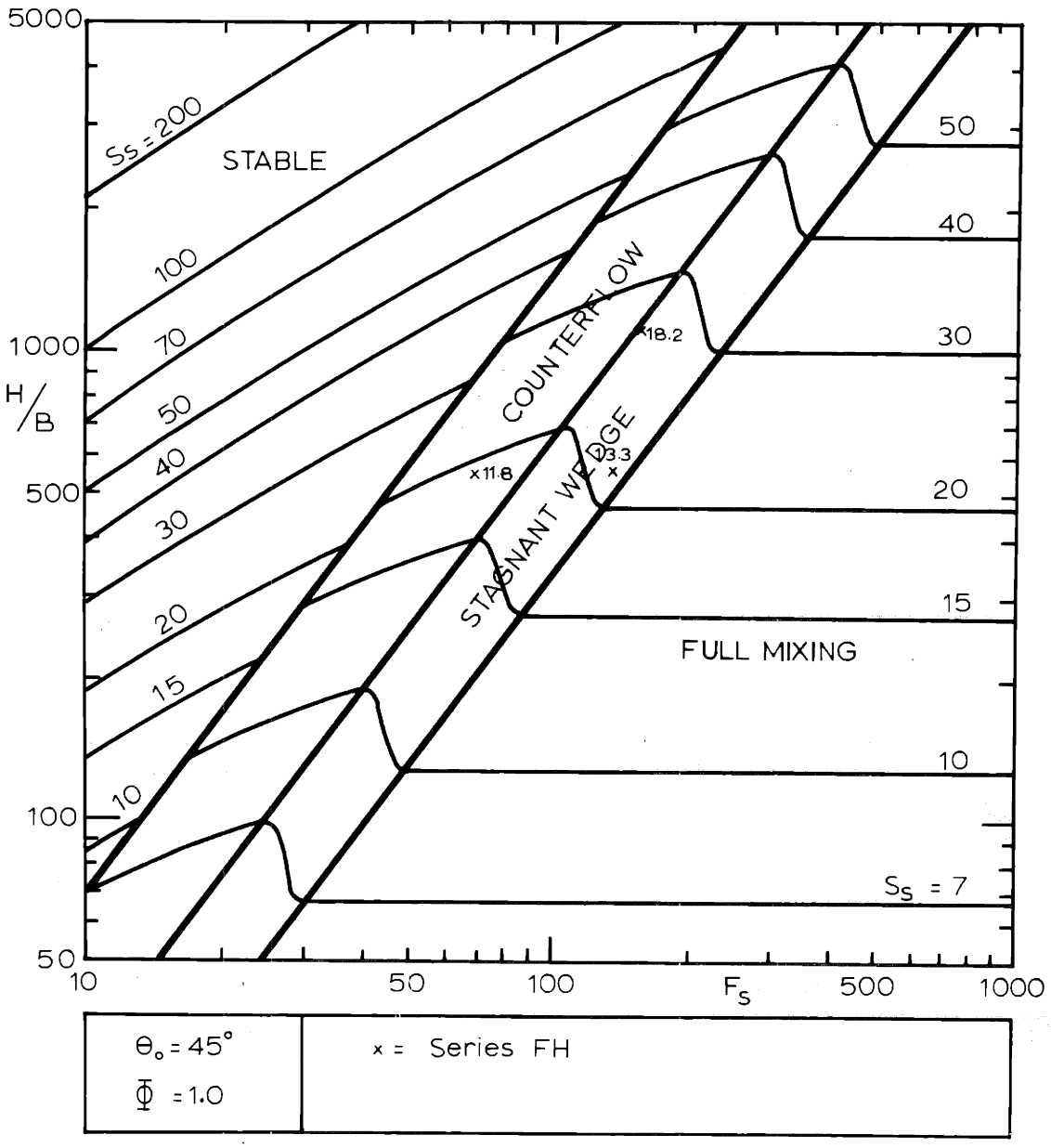

Fig. 6-11; Predicted Vs. Observed Dilutions, S_s

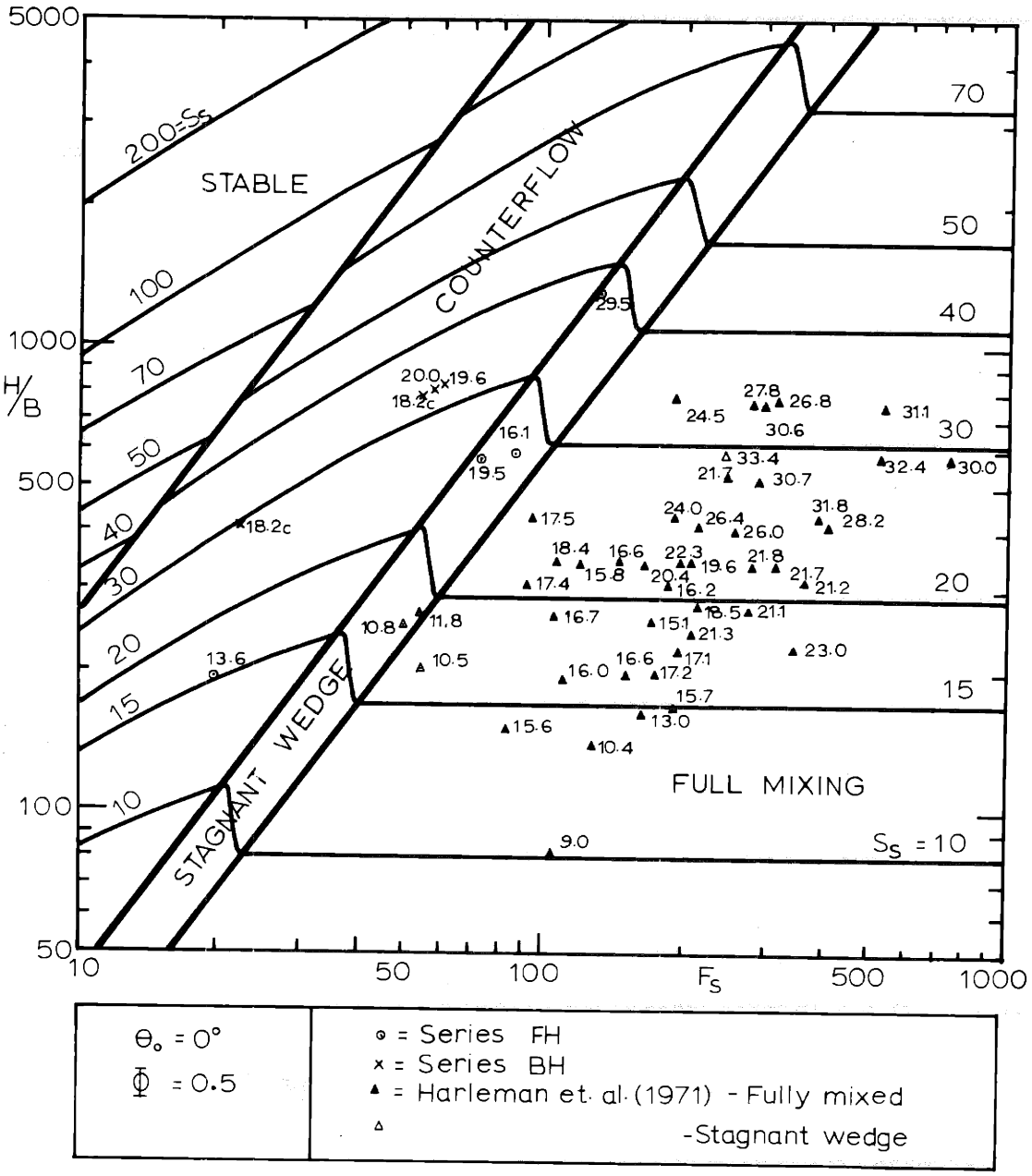

Fig. 6-12: Predicted Vs. Observed Dilutions, S_s

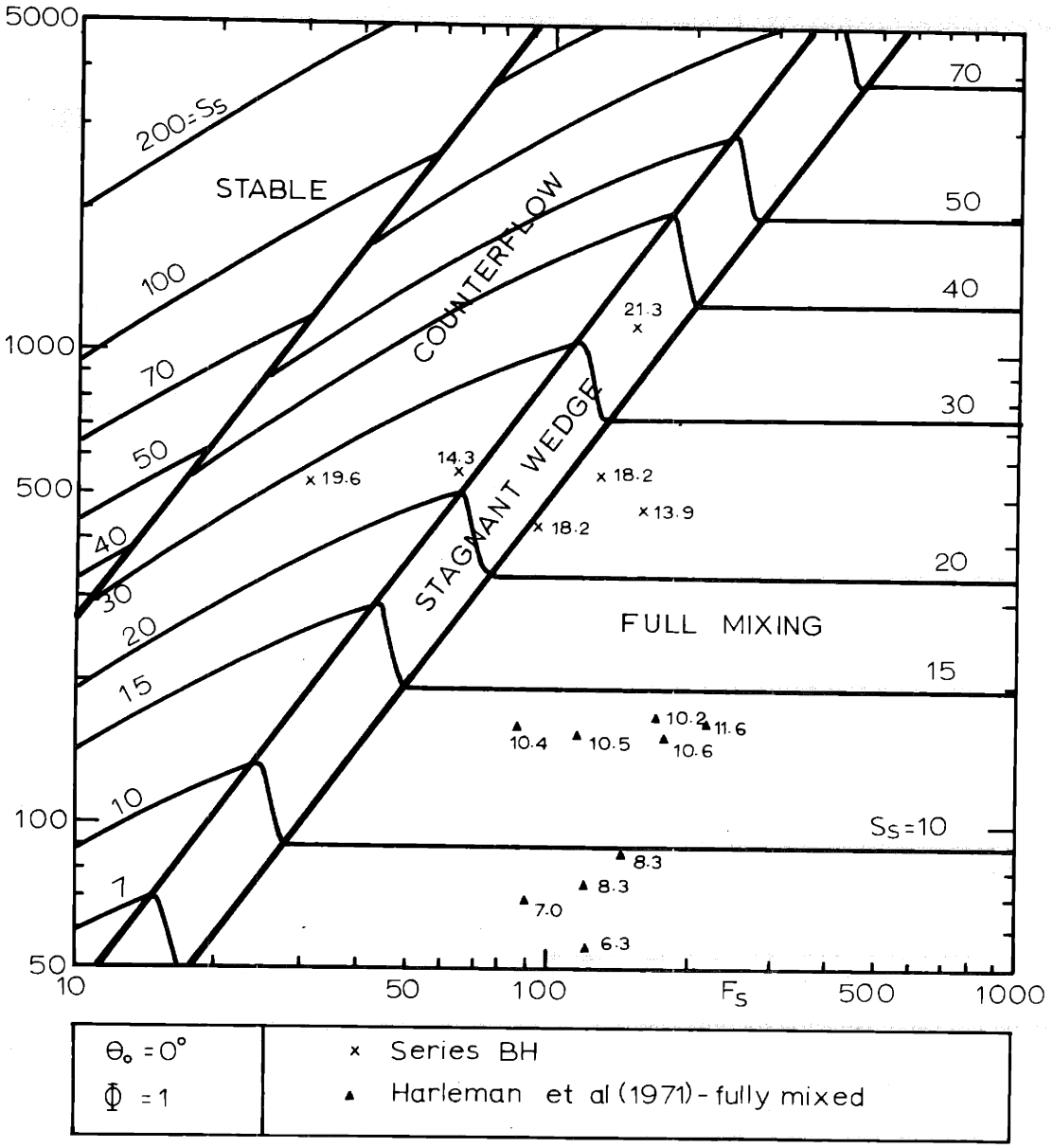

Fig. 6-13: Predicted Vs. Observed Dilutions, S_s

any effect of recirculation, i.e., care was taken to make a measurement as late as possible while not having recirculation. Figures 6-8 and 6-9 are characteristic plots of this situation. On the other hand, the establishment of an approaching "steady-state" could not be insured in this fashion.

In this context it is emphasized that all diffusers with significant horizontal momentum, even in a truly unbounded situation (absence of basin walls) will exhibit some recirculation, as can be shown by the Rankine-theorem of the potential flow analogy (vortex flow). It is, however, the degree and the time scale of the recirculation which is strongly affected by the basin boundaries. Another factor which probably has some effect on the low values of the observed dilutions is jet attachement for the horizontal diffuser discharge ($\theta_o = 0^o$) leading to dissipation of horizontal momentum. Observation through the mirror flume showed a pronounced attachement of the individual round jets before merging and of the slot jet after merging.

The observed dilutions (see Table 6.4) for "shallow water" diffusers without control agree well with Adams' prediction, but have to be taken with reservation in the light of the above discussion as these experiments are similarly influenced by unsteady effects and boundary effects. Furthermore, comparison shows that, in general, for the case of net horizontal momentum diffusers with control perform only slightly better ($\sim$ 10% higher dilution) than diffusers without control. The difference lies mainly in the

strength of the horizontal current generated.

The effect of spacing, ℓ/H, was studied in certain test combinations (keeping F_s and H/B about equal), for example (23,24). (7c,9c) and (25c,26c). No influence of nozzle spacing on the diffuser performance is evident.

6.3 Conclusions: Diffusers without Ambient Crossflow

The theoretical analysis of two-dimensional characteristics (Chapter 3) and three-dimensional aspects (Chapter 4) of diffusers without ambient crossflow in combination with the experimental program (this chapter) enables the following conclusions to be drawn:

1) Equivalent slot concept

Any multiport diffuser can, for analytical purposes, be represented by an equivalent slot diffuser. This includes diffusers with alternating nozzles as has been shown by the analysis of Liseth's experiments of deep water diffusers (Chapter 2) and by the results of this study for shallow water diffusers with an unstable near-field. Utilizing the equivalent slot concept introduces a convenient tool for comparing diffuser studies and prototype applications: the variables D and ℓ are replaced by the single variable B. A diffuser is characterized by F_s, H/B and θ_o, where $\theta_o = 90^o$ for diffusers with alternating nozzles.

2) Two-dimensional diffuser characteristics

A stable near-field zone, with a dominant buoyant jet region, exists only for a limited range of F_s and H/B. The range is

dependent on θ_o. Outside this range the diffuser performance is governed by the frictional characteristics of the flow-away in the far-field, governed by $\Phi = f_o L/H$. Different vertical flow structures will result as a function of θ_o and Φ.

3) Three-dimensional diffuser aspects

The flow distribution in the horizontal plane is intimately related to near-field instabilities along the diffuser line and to the strength of the horizontal momentum input of the diffuser discharge. Horizontal circulations will be generated by this interaction, except for the case of a stable near-field ("deep water" diffusers) where a vertically stratified two-layered system is built up.

4) Control of horizontal circulations

Horizontal circulations can be controlled through horizontal orientation, $\beta(y)$, of the individual nozzles along the diffuser. For diffusers with no net horizontal momentum, $\beta(y)$ given by Equation (4-43) ("logarithmic" distribution - LOG), insures a stably stratified counter-flow system in the far-field. For diffusers with net horizontal momentum, the LOG distribution prevents contraction of the flow downstream of the diffuser and promotes vertical stratification.

5) Dilution predictions

Theoretical dilutions obtained from the two-dimensional "channel model" can be applied to the three-dimensional diffuser with control by means of the requirement of equivalency of far-field

effects, Equations (4-4) and (4-11). In mathematical terms, equivalent far-field effects require $L \approx L_D$, i.e., the length of the two-dimensional "channel model" is about equal to the diffuser length. Experimentally, diffuser studies in a two-dimensional channel model require a sufficiently large reservoir outside the channel and account has to be taken for the increased friction due to the sidewalls of the channel.

The implications of these findings on practical diffuser design and on the operation of hydraulic scale models of diffusers are discussed in Chapter 8.

The interaction of the diffuser-induced flows and temperature field with an ambient current system is treated in the subsequent chapter.

FUSERS IN AMBIENT CROSSFLOW: EXPERIMENTAL RESULTS

c Considerations

the preceding chapters the flow and temperature induced by the
a multiport diffuser in an otherwise stagnant unstratified
ater of uniform depth was analyzed. It was found that the
performance is basically determined by four dimensionless para-
amely the equivalent slot Froude number, F_s, the relative depth,
vertical angle of discharge, θ_o, and the far-field effect,
H. In addition, for control of horizontal circulations the
1 nozzle orientation, $\beta(y)$, is important.

complexity of the problem is appreciably increased if the
on of the diffuser discharge with an ambient current system is
d, as shown in Figure 7-1. Two more dimensionless parameters

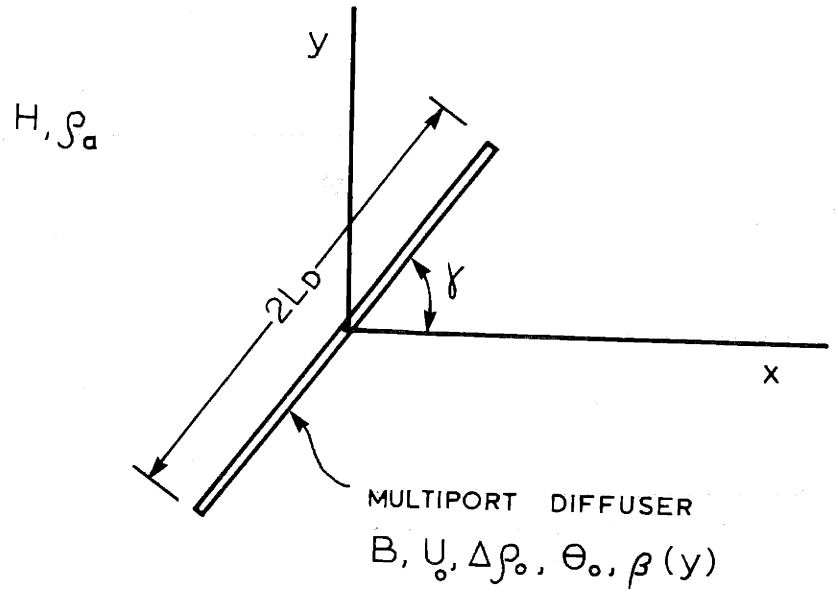

. 7-1: Multiport Diffuser in Ambient Crossflow

can be introduced,

$$V = \frac{u_a H}{U_o B} = \frac{\text{unit width discharge of cross flow}}{\text{unit width dishcarge of diffuser}} = \text{volume flux ratio}$$

γ = angle of diffuser axis with direction of crossflow

in which u_a = undisturbed crossflow velocity upstream. Thus in general, the diffuser flow field in ambient crossflow is depending on 7 dimensionless parameters.

The effects of crossflow may be classified into two groups:

1) Effect on the Near-Field Zone: The crossflow causes a deflection of the buoyant jet trajectors as discussed in Paragraph 2.1.7. Depending on V and γ, such effects as bending into adjacent jets, jet attachment to the bottom and instabilities of the surface layer can ensue. In the case of an unstable near-field zone a current sweeping along the diffuser line (γ = 0) can cause repeated re-entrainment, somewhat similar to diffuser induced circulations without control by nozzle orientation.

2) Effect on the Far-Field Zone: The diffuser induced currents, driven by buoyancy and by the discharge momentum, are modified through the ambient current system. Spreading of the diffuser flow against the current is inhibited to a stronger or lesser degree.

7.2 Method of Analysis

The diffuser in a uniform ambient cross-current was investigated experimentally. No complete theory describing the full range of the

governing parameters has been developed. However, for the purpose of qualitative discussion and quantitative data presentation, extreme cases of diffuser behavior (regimes) can be isolated and described by mathematical models. The advantage of doing so is that the number of significant parameters is considerably reduced in these regimes. To isolate the regimes, the treatment is restricted to diffusers with an unstable near-field zone (shallow water type). Diffusers with a stable near-field zone are in general little affected by the crossflow except for the deflection of the buoyant jets. The crossflow will merely translate the stable surface layer without causing re-entrainment.

For diffusers with an unstable near-field zone in a crossflow three regimes can be isolated: A) buoyancy induced counterflow, B) momentum induced currents, and C) crossflow mixing. The two first regimes have been discussed in the theoretical analysis of Chapter 3 and are summarized here:

A) Buoyancy Induced Counterflow: For weak crossflow and little horizontal diffuser momentum, the flow field will approach that of the diffuser with no net horizontal momentum. The theoretical near-field dilution is then

$$S_s = 4^{1/3} \left(\frac{F_{H_c}(\Phi)}{F_s} \right)^{2/3} \frac{H}{B} \qquad (3\text{-}222)$$

in which F_{H_c} is the densimetric Froude number of the counterflow system dependent on the frictional effects in the far-field, Φ (counterflow Equation (3-207) and Fig. 3-23).

Defining the "diffuser load", F_T,

$$F_T = \frac{F_s}{\left(\frac{H}{B}\right)^{3/2}} = \frac{q_o}{\left(\frac{\Delta\rho_o}{\rho_a} gH^3\right)^{1/2}} \qquad (7\text{-}1)$$

Equation (3-222) is written as

$$S_s = 4^{1/3} \left(\frac{F_{H_c}(\Phi)}{F_T}\right)^{2/3} \qquad (7\text{-}2)$$

The "diffuser load" is a significant parameter for diffusers with an unstable near-field zone (shallow water) and is a densimetric Froude number describing the impact (discharge, $q_o = U_o B$, and buoyancy, $\Delta\rho_o/\rho_a$) of the discharge on the total depth. Its implications on diffuser design are further discussed in Chapter 8.

B) Momentum Induced Currents: For weak crossflow and strong horizontal diffuser momentum, horizontal currents with full vertical mixing will be set up. The behavior of these currents is dependent on the diffuser control through horizontal nozzle orientation, $\beta(y)$:

i) For the LOG distribution ($\beta(y)$ from Eq. (4-36)), with a predominantly two-dimensional flow pattern in the diffuser vicinity, the two-dimensional channel model concept can be used:

$$S_s = \frac{1}{(1+\Phi/2)^{1/2}} \left(2 \frac{H}{B} \cos \theta_o\right)^{1/2} \qquad (3\text{-}227)$$

ii) For the NOR distribution ($\beta(y) = 90°$, no control), with

typical contraction of the flow field downstream of the discharge, Adams' model can be used neglecting frictional far-field effects. Equation (2-45) is modified, including the effect of vertical angle θ_o, to

$$S_s = \frac{1}{2} \left(2 \frac{H}{B} \cos \theta_o\right)^{1/2} \tag{7-3}$$

C) Cross-Flow Mixing: For strong crossflow and weak effects of buoyancy and horizontal diffuser momentum the dilution is equal to the ratio of the crossflow sweeping over the diffuser to the diffuser discharge.

$$S_s = V \sin \gamma \tag{7-4}$$

Essentially, regimes B and C, both with full vertical mixing, can be combined by simple superposition:

i) For the LOG distribution: In the two-dimensional channel model derivation (Section 2.2.1 with Figure 2-7) the total head loss (Eq. (2-35)) is in presence of an ambient current, taken to be related to the excess velocity head, $(u_m^2 - u_a^2 \sin^2\gamma)/2g$. The dilution prediction follows in similarity to Eq. (3-227)

$$S_s = V^* = \left(V^2 \sin^2\gamma + \frac{2\ H/B \cos \theta_o}{1 + \Phi/2}\right)^{1/2} \tag{7-5}$$

The expressions in the bracket show the relative contributions of dilution by the cross-flow and by diffuser induced momentum.

ii) For the NOR distribution: The effect of cross-flow is included in Adams' Eq. (2-44) written as

$$S_s = V^* = \frac{1}{2} V \sin\gamma + \frac{1}{2} \left(V^2 \sin^2\gamma + 2 \frac{H}{B} \cos \theta_o\right)^{1/2} \qquad (7\text{-}6)$$

In the general case of a mixed regime, dilutions can be assumed to be somewhat dependent on these limiting cases. As a consequence it follows that the 7 parameter problem may be reasonably approximated by the 4 parameters: F_T, Φ, V^*, $\beta(y)$ (Note: $\beta(y)$ determines whether V^* is taken from Eq. (7-5) or (7-6)). These parameters are used in the data presentation.

In the experimental program the diffuser arrangement was limited to two values of γ:

a) $\gamma = 0°$: Parallel Diffuser, i.e. the diffuser axis is parallel to the cross-flow direction, and

b) $\gamma = 90°$: Perpendicular Diffuser, i.e. the diffuser axis is perpendicular to the crossflow direction. Two-dimensional channel model studies on the perpendicular diffuser performed in the flume set-up are described first (Section 7.3). Both perpendicular and parallel diffusers were tested in the basin set-ups A and B, and are discussed in Section 7.4.

7.3 Flume Experiments: Perpendicular Diffuser

Table 7.1 summarizes the run characteristics for the diffuser experiments with ambient crossflow in the flume set-up, Series FC. The

Table 7.1: Flume Diffuser Experiments with Crossflow, Series FC

	Physical Variables						Secondary Parameters				Governing Parameters					
	H (ft)	u_a (ft/sec)	B (10^{-3}ft)	U_o (ft/sec)	T_a (^oF)	ΔT_o (^oF)	IR_j	L/H	f_o^*	F_s	H/B	θ_o (dgr)	Φ	V	F_T (10^{-3})	Observed S_s
FC-1	2.00	0.100	3.3	2.69	69.9	21.9	2,140	10	0.066	141	600	90	0.7	22.5	9.5	21.7
2	2.00	0.044	3.3	2.69	70.3	22.5	2,140	10	0.073	122	600	90	0.7	10.0	8.2	14.1
3	2.00	0.022	3.3	2.69	71.0	22.0	2,140	10	0.080	122	600	90	0.8	5.0	8.2	9.6
4	2.00	0.011	3.3	2.69	71.8	21.7	2,140	10	0.076	139	600	90	0.8	2.5	9.4	12.8
5	2.00	0.049	3.3	1.68	72.3	31.5	1,340	10	0.080	69	600	90	0.8	16.0	4.6	16.7
6	2.00	0.067	3.3	1.68	72.9	30.8	1,340	10	0.066	70	600	90	0.7	24.0	4.7	31.3
7	2.00	0.100	3.3	4.71	67.5	15.1	3,750	10	0.066	314	600	90	0.7	12.9	21.0	11.6
8	2.00	0.033	3.3	4.71	68.5	15.5	3,750	10	0.076	306	600	90	0.8	4.3	20.7	7.4
9	2.00	0.067	3.3	0.88	69.5	9.0	700	10	0.082	77	600	90	0.8	45.8	5.2	30.3
10	1.33	0.100	3.3	2.69	69.8	23.6	2,140	15	0.053	135	400	90	0.8	15.0	16.7	14.7
11	2.17	0.049	1.7	3.92	68.6	23.1	1,610	9	0.078	292	1300	90	0.7	13.3	6.4	15.4
12	2.17	0.020	1.7	3.92	69.4	22.0	1,610	9	0.082	298	1300	90	0.7	6.7	6.6	13.7
13	2.17	0.061	5.2	0.55	67.1	24.1	700	9	0.085	27	416	90	0.8	46.2	3.2	27.8
14	1.00	0.133	5.2	5.34	68.7	15.9	6,700	20	0.044	276	192	90	0.9	4.8	104.0	5.8
15	1.00	0.067	5.2	5.34	68.7	15.7	6,700	20	0.051	278	192	90	1.0	2.4	104.4	3.8
16	1.00	0.278	5.2	1.87	70.3	16.8	2,350	20	0.059	78	192	90	1.2	5.7	29.2	7.0
17	2.00	0.033	10.4	0.64	66.9	15.4	1,610	10	0.085	24	192	90	0.9	10.0	9.0	11.0
18	1.25	0.153	20.8	1.07	67.8	20.4	5,350	16	0.048	24	60	90	0.8	8.6	51.5	8.5
19	1.25	0.062	20.8	1.07	67.8	20.6	5,350	16	0.056	24	60	90	0.9	3.5	51.5	5.1
20	2.00	0.967	3.3	2.69	75.2	22.3	2,140	10	0.065	133	600	0	0.7	21.8	8.9	20.4
21	2.00	0.044	3.3	2.69	75.2	21.9	2,140	10	0.075	134	600	0	0.8	10.0	9.0	13.7
22	2.00	0.078	3.3	1.68	73.6	30.8	1,340	10	0.072	70	600	0	0.7	28.0	4.7	25.6
23	1.33	0.033	3.3	2.69	69.3	22.0	2,140	15	0.064	141	400	0	1.0	5.0	17.5	8.5
24	2.17	0.041	1.7	3.92	68.8	21.1	1,610	9	0.078	309	1300	0	0.7	13.3	6.8	15.2
25	2.00	0.100	3.3	2.69	66.5	24.1	2,140	10	0.065	139	600	180	0.7	22.5	9.3	21.3
26	2.00	0.044	3.3	1.68	67.5	20.5	1,340	10	0.080	73	600	180	0.8	16.0	4.9	17.0
FC-27	1.33	0.033	3.3	2.69	68.3	24.6	2,140	15	0.066	133	400	180	1.0	5.0	16.5	7.6

Note: 1) Channel length, L = 20 ft.

2) $\theta_o = 180^o$ indicates horizontal discharge against the current

crossflow was generated by pumping across a partition wall in the reservoir behind the channel as was shown in Figure 5-1. In all tests the discharge was from a continuous slot. The discharge angle, θ_o, was primarily 90° with additional tests with 0° (discharge in the current direction) and 180° (against the current). Resultant surface dilutions, S_s, are included on Table 7.1. Typical flow distributions are shown in Figure 7-2.

The data are analyzed considering the specific feature of the flume set-up: A current having a unit width discharge $u_a H$ is <u>forced</u> through the channel. The horizontal diffuser momentum (θ_o = 0° or 180°) cannot alter this discharge; the effect of the horizontal momentum is merely to build up a high and a low pressure region in the channel. The consequence of this forced current is the independence of the diffuser performance (outside some local zone) on the horizontal momentum (thus θ_o = 90° as with no net horizontal momentum).

The two limiting regimes for this discharge situation are the counterflow system (F_T, Φ) and the crossflow mixing (V, as sin γ = 1).

These limiting regimes are shown in Fig. 7-3. As most runs had $\Phi \gtrsim 1$, F_{H_c} is taken as 0.165 (Fig. 3-24). The limiting value for low crossflow is assumed at V = 1. A criterion of applicability of the fully mixed regime is given by considering that below a crossflow Froude number F_H = 1 stagnant wedges will form. Thus

$$F_H = \frac{u_a}{\left(\frac{\Delta\rho_o}{\rho} \frac{1}{S_s} gH\right)^{1/2}} = 1 \qquad (7\text{-}7)$$

and using S_s = V and the appropriate definitions the criterion is

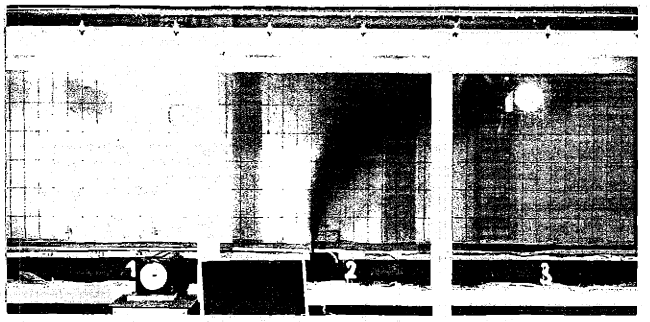

a) Run FC-8, Deflected Jet, Counterflow System

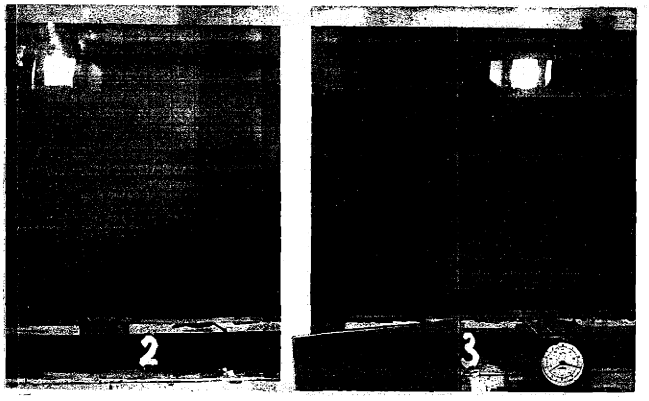

b) Run FC-6, Incipient Upstream Wedge, Full Mixing

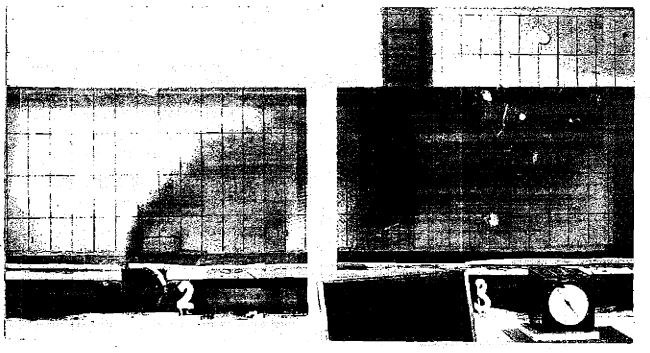

c) Run FC-10, No Upstream Wedge, Full Mixing

Fig. 7-2: Typical Flow Regimes for Diffusers with Forced Ambient Crossflow

$$\frac{1}{F_T} = V^{3/2} \tag{7-8}$$

The stagnant wedge system, still characterized by $S_s = V$, is bounded when the surface wedge length, L_{ss}, is equal to the channel length, L. With $\Phi = 1$ the Froude number F_H for this situation is, from Eq. (3-197), $F_H = 0.45$ so that

$$\frac{0.45}{F_T} = V^{3/2} \tag{7-9}$$

Equations (7-8) and (7-9) are shown as criteria lines in Figure 7-3. The iso-dilution lines in the counterflow domain are drawn somewhat tentatively connecting the limiting values.

The agreement with the experimental data is satisfactory both with respect to observed dilutions and observed flow regimes (see Fig. 7-2). No dependence on θ_o can be detected.

Also shown on Figure 7-3 are qualitative results obtained by Cederwall (1971). The comparison is somewhat limited, as the Φ of Cederwall's experiments is not defined since he used a channel set-up with no clearly defined upstream condition (control section), and thus no steady state condition. Cederwall classified the flow regimes which were observed visually. No dilutions were measured. These observations agree well with the proposed criteria.

The above considerations lead to the following conclusions: The interaction of a three-dimensional diffuser with an ambient crossflow system cannot be studied in a two-dimensional model with forced crossflow. In the three-dimensional case the flow over the diffuser line is

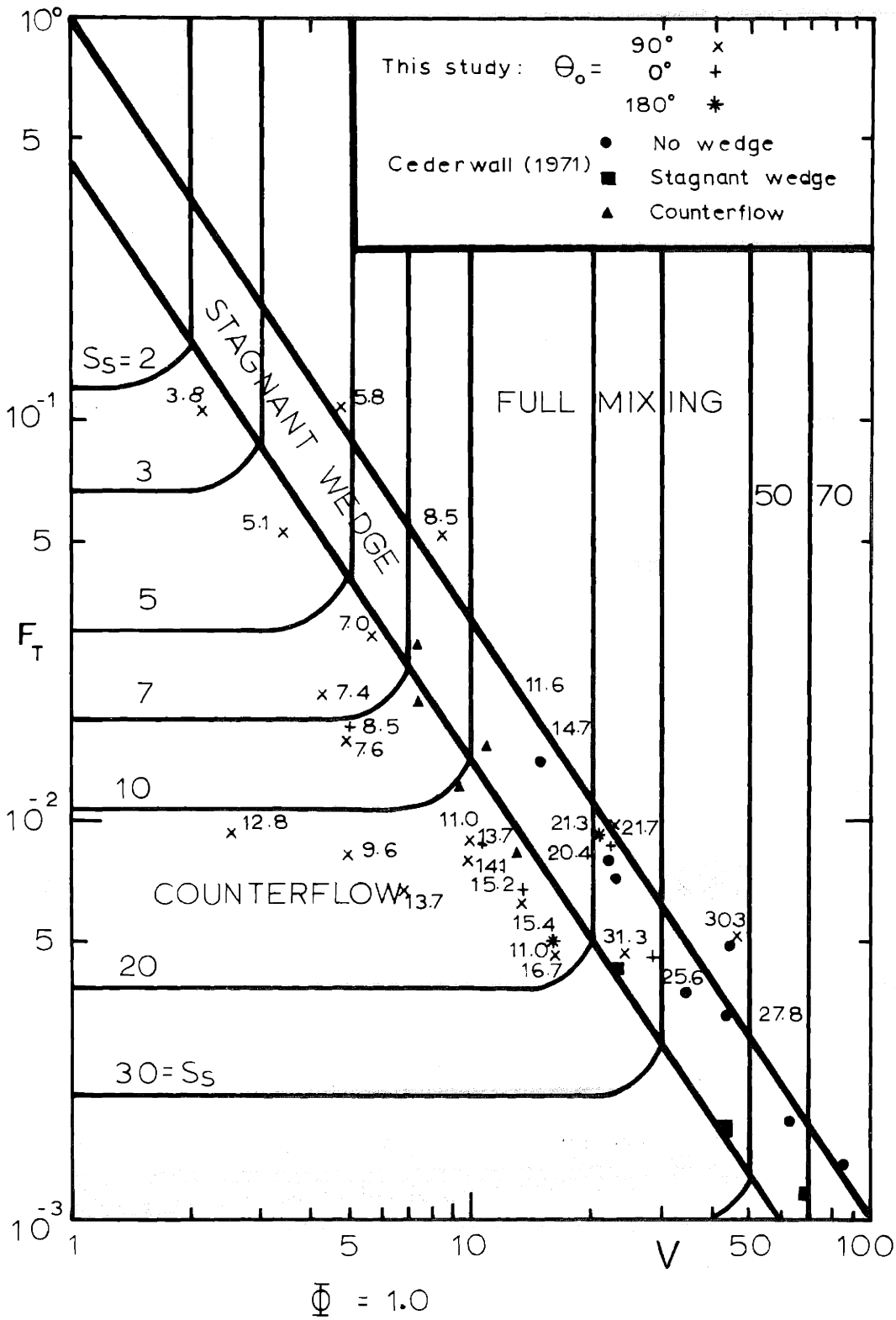

Fig. 7-3: Flume Experiments with Forced Crossflow

dependent on both ambient crossflow and horizontal diffuser momentum. Thus the results of the flume experiments are only applicable to the situation which they simulate, namely forced crossflow between lateral boundaries. Practical applications may be diffusers in a river or in any geometry with dominant lateral confinement.

The interaction of diffusers with crossflow in a laterally unconfined situation (Fig. 7-1) should be studied in a three-dimensional experiment, such as described in the following section.

7.4 Three-Dimensional Basin Experiments

For convenience the discussion is first given for diffusers with no net horizontal momentum (alternating nozzles) and then for diffusers with net horizontal momentum (unidirectional nozzles).

7.4.1 Diffusers with No Net Horizontal Momentum

The run parameters of the basin experiments with crossflow, Series BC, with alternating nozzles are given in Table 7.2a. Runs 1 to 10 were made with a perpendicular ($\gamma = 90°$) diffuser, Runs 11 to 20 with a parallel ($\gamma = 0°$) diffuser. Most runs were made with $\theta_o = 45°$, some with 0° (horizontal discharge). In all runs the LOG distribution for the horizontal nozzle orientation, $\beta(y)$, was used based on the results of the no crossflow tests (Series BN).

Typical flow and temperature fields for perpendicular and parallel diffusers are shown in Figure 7-4 for a moderately strong cross-current ($V \approx 13$) which does not result in full mixing (see Fig. 7-5). The diffuser load, F_T, (i.e. buoyancy flux and discharge per unit length) was the same for both the perpendicular (Fig. 7-4a) and the parallel (Fig. 7-4b) diffuser. Because of the line of symmetry used in the

Table 7.2a: Basin Experiments with Crossflow, Series BC, a) Discharge with No Net Horizontal Momentum

	Physical Variables						Secondary Parameters			Governing Parameters									
	H (ft)	u_a (ft/sec)	U_o (ft/sec)	L_D (ft)	T_a (^oF)	ΔT_o (^oF)	R_j	ℓ/H	f_o	F_s	H/B	θ_o (dgr)	Φ	$\beta(y)$	V	γ (dgr)	F_T (10^{-3})	V*	Observed S_s
BC-1	0.67	0.024	2.15	6.4	63.2	27.6	4,050	0.24	0.043	128	558	45-A	0.4	LOG	6.2	90	10.0	6.2	10.9
2	0.67	0.012	2.15	6.4	63.2	27.6	4,050	0.24	0.050	128	558	45-A	0.5	LOG	3.1	90	10.0	3.1	9.5
3	0.67	0.027	1.08	6.4	64.5	24.3	1,980	0.24	0.043	69	558	45-A	0.4	LOG	14.0	90	5.2	14.0	16.2
4	0.67	0.012	1.08	6.4	64.5	24.4	1,980	0.24	0.050	69	558	45-A	0.5	LOG	6.2	90	5.2	6.2	13.9
5	0.67	0.024	1.08	3.2	65.4	22.4	1,960	0.24	0.043	72	558	45-A	0.3	LOG	12.4	90	5.4	12.4	16.7
6	0.67	0.012	1.08	3.2	65.4	22.4	1,960	0.24	0.050	72	558	45-A	0.3	LOG	6.2	90	5.4	6.2	16.1
7	0.50	0.024	1.08	6.4	67.5	25.9	2,090	0.32	0.045	66	418	45-A	0.5	LOG	9.3	90	7.8	9.3	12.0
8	0.50	0.012	1.08	6.4	67.5	25.8	2,090	0.32	0.053	66	418	45-A	0.6	LOG	4.7	90	7.8	4.7	11.2
9	0.67	0.024	1.45	6.4	65.6	25.9	2,760	0.24	0.043	90	558	0-A	0.4	LOG	9.2	90	6.8	9.2	13.0
10	0.67	0.009	1.45	6.4	65.6	26.0	2,770	0.24	0.053	90	558	0-A	0.5	LOG	3.4	90	6.8	3.4	13.7
11	0.67	0.024	2.15	3.2	54.8	26.5	3,650	0.24	0.043	132	558	45-A	0.2	LOG	6.2	0	10.0	0	9.0
12	0.67	0.012	2.15	3.2	54.8	26.5	3,660	0.24	0.050	131	558	45-A	0.3	LOG	3.1	0	10.0	0	7.7
13	0.67	0.024	1.08	3.2	58.2	26.3	1,890	0.24	0.043	66	558	45-A	0.2	LOG	12.4	0	5.0	0	13.2
14	0.67	0.012	1.08	3.2	58.2	26.3	1,890	0.24	0.050	66	558	45-A	0.3	LOG	6.2	0	5.0	0	12.0
15	0.67	0.024	1.08	3.2	56.4	23.7	1,810	0.24	0.043	70	558	0-A	0.2	LOG	12.4	0	5.2	0	13.0
16	0.67	0.009	1.08	3.2	56.4	23.9	1,810	0.24	0.053	70	558	0-A	0.3	LOG	4.7	0	5.2	0	10.6
17	0.50	0.032	1.08	3.2	61.7	23.0	1,900	0.32	0.043	71	418	45-A	0.3	LOG	12.4	0	8.3	0	11.2
18	0.50	0.012	1.08	3.2	61.7	23.0	1,900	0.32	0.056	71	418	45-A	0.4	LOG	4.7	0	8.3	0	10.2
19	0.67	0.024	1.45	3.2	55.1	22.6	2,380	0.24	0.043	96	558	0-A	0.2	LOG	9.2	0	7.3	0	11.2
BC-20	0.67	0.009	1.45	3.2	55.1	22.7	2,380	0.24	0.053	96	558	0-A	0.3	LOG	3.4	0	7.3	0	9.9

Note: 1) All runs with D = 0.0156 ft and ℓ = 0.16 ft.

2) "A" denotes alternating nozzles

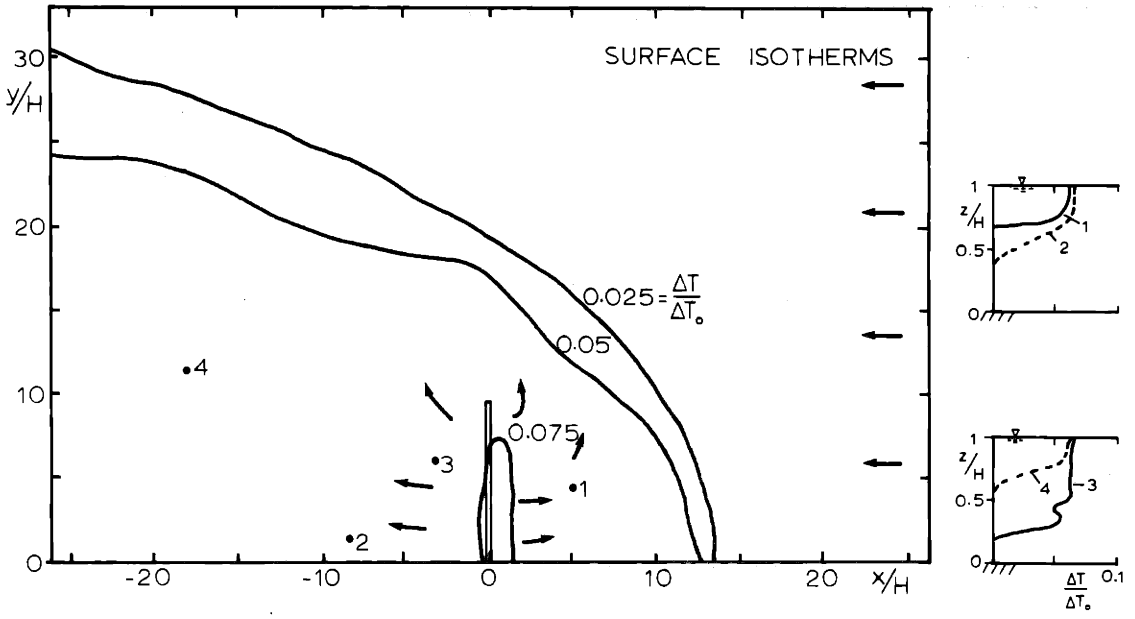

a) Run BC-3, F_s = 69, H/B = 558, θ_o = 45°-A, Φ = 0.4, $\beta(y)$ = LOG, V = 14.0, γ = 90°

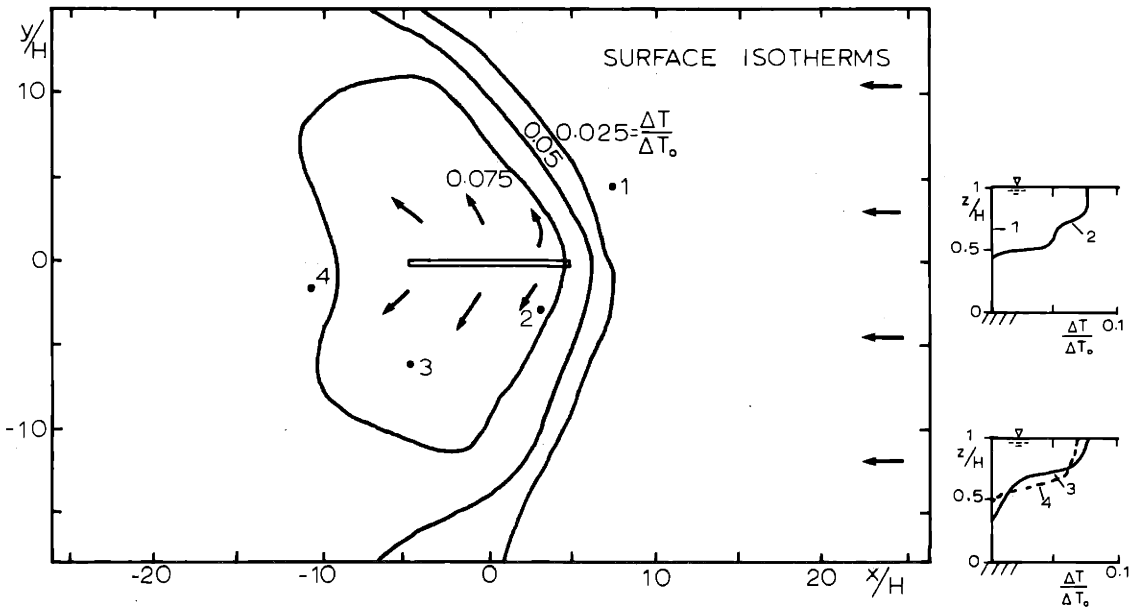

b) Run BC-B, F_s = 66, H/B = 558, θ_o = 45°-A, Φ = 0.2, $\beta(y)$ = LOG V = 12.4, γ = 0°

Fig. 7-4: Observed Temperature and Velocity Field, Series BC, Alternating Nozzles

experimental set-up, the total length of the perpendicular diffuser was twice the length of the parallel diffuser. This difference is expressed by the value of the far-field parameter Φ as shown in the figure captions. In both cases the flow field is well stratified and upstream wedges are present.

In Figure 7-5a the experimental dilutions for the perpendicular diffuser taken at the edge of the near-field zone are compared with the predictions for the limiting regimes. Figure 7-5a was developed in the same manner as Figure 7-3, but with $\Phi = 0.5$ ($F_{H_c} = 0.187$) corresponding to most runs. (No experiments were made in the fully mixed regime due to limitations in the crossflow generation system.)

Figure 7-5a also shows for the general case $V^* = V \sin \gamma$ the criteria for the different regimes, with hypothetical iso-dilution lines in the counterflow region. Only the results of the perpendicular diffuser experiments ($\gamma = 90°$) are shown in Figure 7-5a, with very good agreement. For the parallel diffuser, $V^* = 0$. This would mean that the dilution is dependent only on the characteristics of the buoyant counterflow regime. This is not considered appropriate and indicates that due to the "lumping" of the parameters, such as in Equations 4-6 and 4-7, some of the dependency of the original 7 parameter problem is lost. It can be expected that for the parallel diffuser, the current sweeping along the diffuser line (see Figure 7-4b) will cause repeated re-entrainment and some decreased dilutions, especially for a strong current. A comparison between the dilutions obtained with the parallel diffuser versus those of the perpendicular one is given in Figure 7-5b (see also Table 7-2a) as a function of V (i.e. the potential dilution).

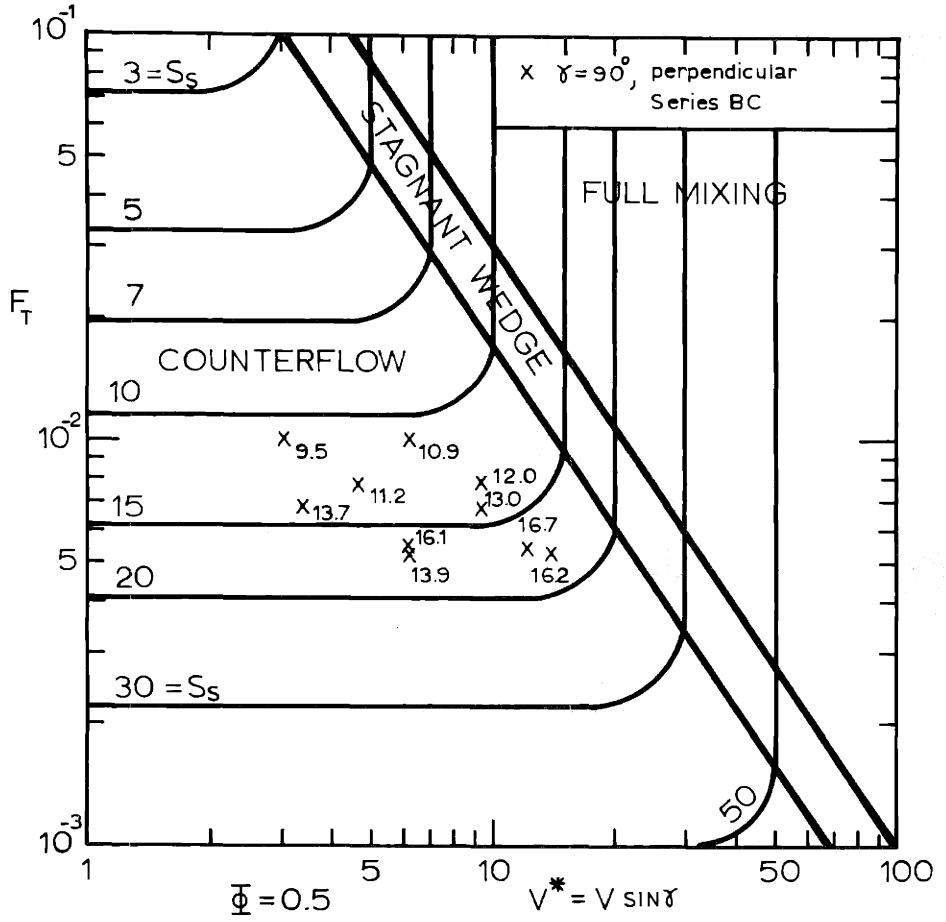

a) Dilutions of Perpendicular Diffuser

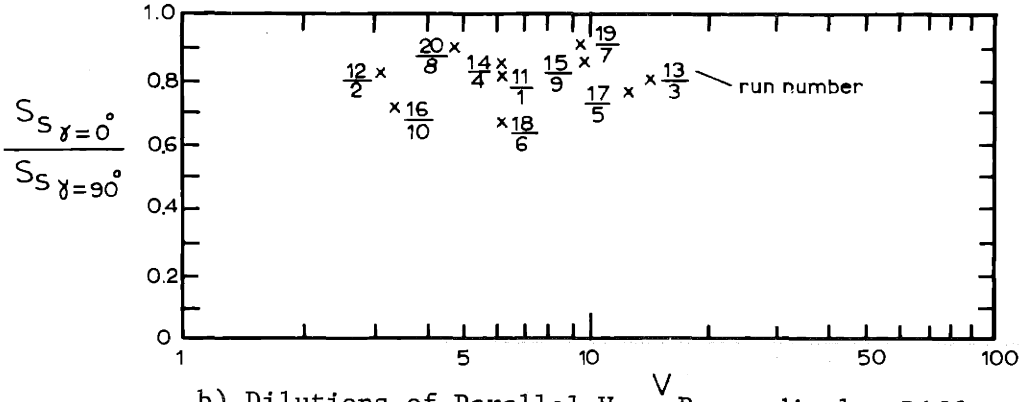

b) Dilutions of Parallel Vs. Perpendicular Diffuser

Fig. 7-5: Three-Dimensional Diffusers in Crossflow, (Series BC) No Net Horizontal Momentum, LOG Distribution

In general, the parallel diffuser has about a 20% lower dilution capacity than the corresponding perpendicular one which as has been noted is twice as long in the present experimental set-up (resulting in a difference of Φ).

7.4.2 Diffusers with Net Horizontal Momentum

Table 7.2b summarizes the three-dimensional diffuser experiments in crossflow, Series BC, with unidirectional nozzles. Runs 21 to 34 relate to the perpendicular, Runs 35 to 48 to the parallel diffuser. In addition to the diffuser arrangement, γ, emphasis was put on the control of the horizontal circulations through nozzle orientation $\beta(y)$: LOG and NOR distributions were tested. The vertical angle θ_o was varied between 45° and 0°.

The tests on diffusers with net horizontal momentum in the presence of an ambient current exhibit some of the experimental difficulties and limitations as was discussed in Section 6.2.2 for the no crossflow tests (Series BH), namely unsteady effects and boundary effects. Again, in taking temperature measurements care was taken not to include recirculation effects due to basin boundaries.

Characteristic flow fields for corresponding parallel and perpendicular diffusers with net horizontal momentum are shown in Figures 7-6, 7-7 and 7-8. Figure 7-6 (LOG) should be compared with the alternating nozzle case (Figure 7-4) as the experiments have similar parameters. The full mixing downstream of the discharge for the perpendicular diffuser is characteristic and predicted from theoretical considerations (see Figure 7-9). The full mixing for the parallel diffuser is less pronounced indicating penetration and travel of ambient crossflow water

Table 7.2b: Basin Diffuser Experiments with Crossflow, Series BC

Basin Diffuser Tab) Discharge with Net Horizontal Momentum

	Physical Variables						Secondary Parameters			Governing Parameters									
	H (ft)	u_a (ft/sec)	U_o (ft/sec)	L_D (ft)	T_a (°F)	ΔT_o (°F)	R_j	ℓ/H	f_o	F_s	H/B	θ_o (dgr)	Φ	$\beta(y)$	V	γ (dgr)	F_T (10^{-3})	V*	Observed S_s
BC-21	0.67	0.024	2.12	6.4	64.8	26.3	4,060	0.24	0.043	132	558	45	0.4	LOG	6.2	90	10.0	25.9a	15.4
22	0.67	0.012	2.12	6.4	64.8	26.2	4,060	0.24	0.050	132	558	45	0.5	LOG	3.1	90	10.0	25.3a	13.8
23	0.67	0.024	1.08	6.4	65.4	23.5	1,990	0.24	0.043	70	558	45	0.4	LOG	14.4	90	5.3	25.6a	16.4
24	0.67	0.009	1.08	6.4	65.4	23.5	1,990	0.24	0.053	80	558	45	0.5	LOG	4.7	90	5.3	29.0a	14.3
25	0.67	0.024	1.08	6.4	66.2	24.3	2,020	0.24	0.043	69	558	0	0.4	LOG	12.4	90	5.3	32.4a	17.6
26	0.67	0.009	1.08	6.4	66.2	24.2	2,020	0.24	0.053	69	558	0	0.5	LOG	4.7	90	5.3	30.2a	15.4
27	0.67	0.024	1.08	6.4	66.5	23.8	2,929	0.24	0.043	69	558	0	0.4	NOR	12.4	90	5.3	24.0b	13.4
28	0.67	0.009	1.08	6.4	66.5	23.9	2,929	0.24	0.053	69	558	0	0.5	NOR	4.7	90	5.3	19.2b	12.5
29	0.50	0.024	1.45	6.4	67.3	27.6	2,880	0.32	0.045	87	419	0	0.4	LOG	6.7	90	10.3	26.6a	18.2
30	0.50	0.012	1.45	6.4	67.3	26.6	2,840	0.32	0.053	88	419	0	0.6	LOG	3.5	90	10.3	26.1a	15.4
31	0.50	0.024	1.45	3.2	67.4	25.0	2,800	0.32	0.045	91	419	0	0.3	LOG	6.9	90	10.7	26.8a	19.2
32	0.50	0.012	1.45	3.2	67.4	25.2	2,800	0.32	0.053	91	419	0	0.3	LOG	3.5	90	10.6	26.1a	16.7
33	0.50	0.024	1.45	6.4	67.7	26.9	2,870	0.32	0.045	88	419	0	0.5	NOR	6.9	90	10.3	18.3b	13.3
34	0.50	0.012	1.45	6.4	67.7	26.9	2,870	0.32	0.053	88	419	0	0.6	NOR	3.5	90	10.2	16.3b	12.2
35	0.67	0.024	2.15	3.2	60.5	26.0	3,870	0.24	0.043	133	558	45	0.2	LOG	6.2	0	10.0	25.1a	13.0
36	0.67	0.012	2.15	3.2	60.5	25.9	3,870	0.24	0.050	133	558	45	0.3	LOG	3.1	0	10.0	25.1a	11.1
37	0.67	0.024	1.08	3.2	61.2	23.2	1,890	0.24	0.043	70	558	45	0.2	LOG	12.4	0	5.3	25.1a	12.5
38	0.67	0.012	1.08	3.2	61.2	23.6	1,900	0.24	0.050	70	558	45	0.3	LOG	6.2	0	5.3	25.1a	12.5
39	0.67	0.024	1.08	3.2	61.6	23.1	1,900	0.24	0.043	70	558	45	0.2	NOR	12.4	0	5.3	14.0b	12.0
40	0.67	0.012	1.08	3.2	61.6	23.3	1,900	0.24	0.050	70	558	45	0.3	NOR	6.2	0	5.3	14.0b	11.8
41	0.67	0.024	1.08	3.2	58.8	21.4	1,810	0.24	0.043	73	558	0	0.2	LOG	12.4	0	5.5	29.9a	12.7
42	0.67	0.009	1.08	3.2	58.8	21.0	1,810	0.24	0.053	73	558	0	0.3	LOG	4.7	0	5.5	29.9a	10.6
43	0.67	0.024	1.08	3.2	59.7	26.1	1,920	0.24	0.043	66	558	0	0.2	NOR	12.4	0	5.0	16.7b	12.5
44	0.67	0.009	1.08	3.2	59.7	26.1	1,920	0.24	0.053	66	558	0	0.3	NOR	4.7	0	5.0	16.7b	12.0
45	0.50	0.024	1.45	3.2	61.0	25.7	2,620	0.32	0.045	90	419	0	0.2	LOG	6.7	0	10.5	25.9a	12.0
46	0.50	0.012	1.45	3.2	61.0	25.7	2,630	0.32	0.053	90	419	0	0.3	LOG	3.5	0	10.5	25.9a	10.8
47	0.50	0.024	1.45	3.2	60.2	26.8	2,630	0.32	0.045	88	419	0	0.2	NOR	6.7	0	10.3	14.5b	9.5
BC-48	0.50	0.012	1.45	3.2	60.2	26.8	2,630	0.32	0.053	88	419	0	0.3	NOR	3.5	0	10.3	14.5b	10.2

Note: 1) All runs with D = 0.0156 ft and ℓ = 0.16 ft.
2) In column V*: "a" calculated from Equation (7-6), "b" calculated from Equation (7-7)

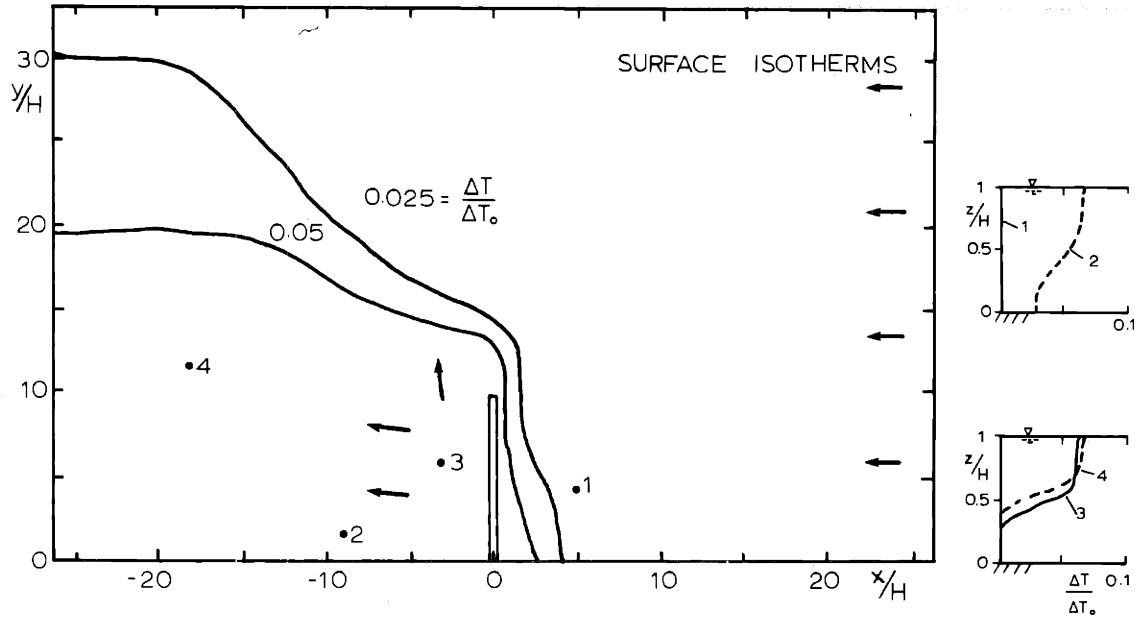

a) Run BC = 23, F_s = 70, H/B = 558, θ_o = 45°, Φ = 0.4, $\beta(y)$ = LOG, V = 6.2, γ = 90° (Nozzles Directed to the Left)

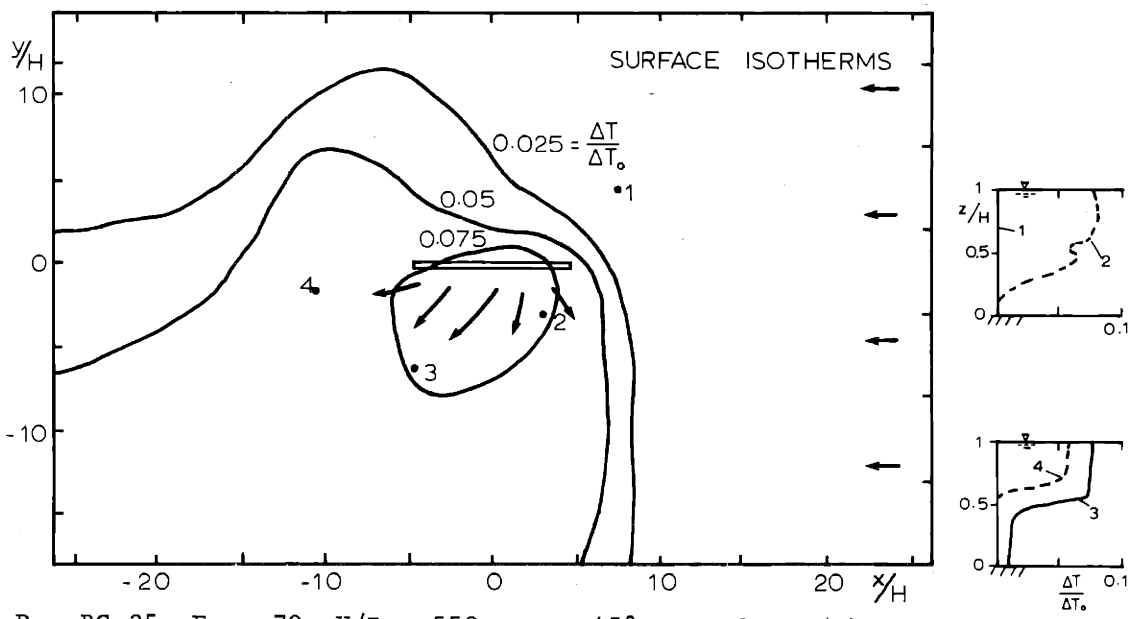

b) Run BC-35, F_s = 70, H/B = 558, θ_o = 45°, Φ = 0.2, $\beta(y)$ = LOG, V = 6.2, γ = 0° (Nozzles Directed Downward)

Fig. 7-6: Observed Temperature and Velocity Field with Crossflow, Series BC, Unidirectional Nozzles

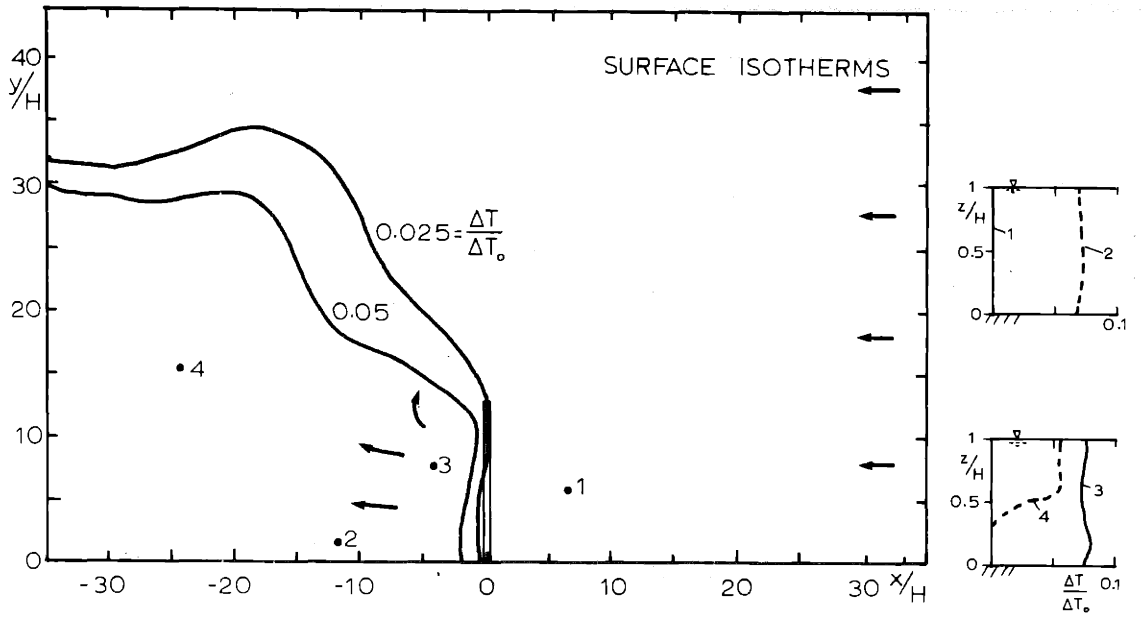

a) Run BC-29, F_s = 87, H/B = 419, θ_o = 0°, Φ = 0.4, $\beta(y)$ = LOG, V = 6.7, γ = 90° (Nozzles Directed to the Left)

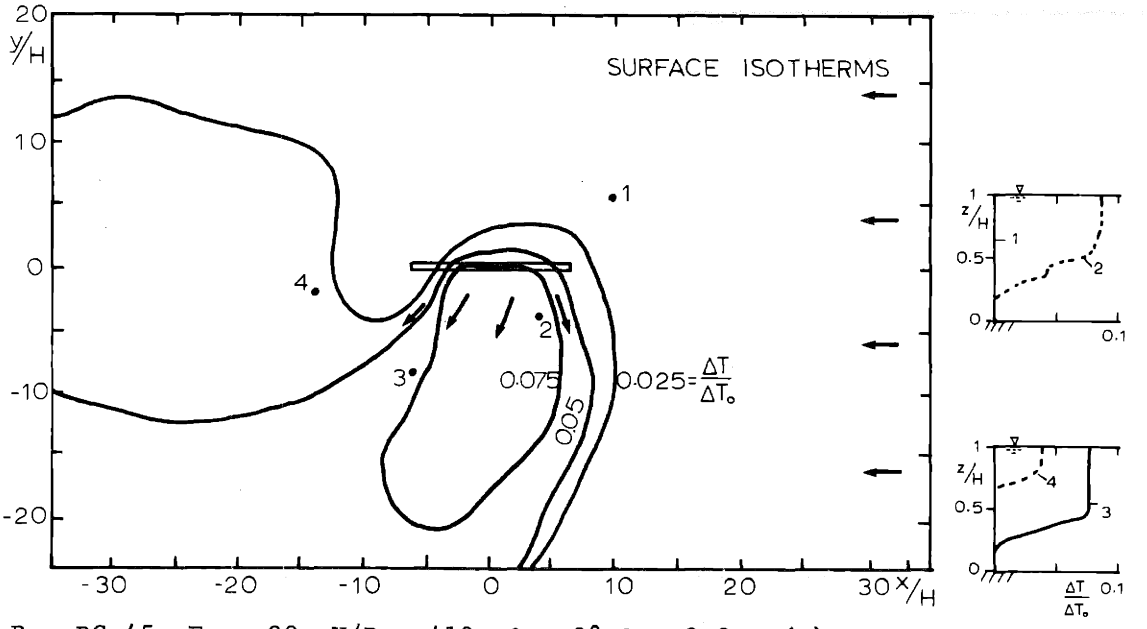

b) Run BC-45, F_s = 90, H/B - 419, θ = 0°, Φ = 0.2, $\beta(y)$ = LOG V = 6.7, γ = 0° (Nozzles Directed Downward)

Fig. 7-7: Observed Temperature and Velocity Field, Series BC, Unidirectional Nozzles

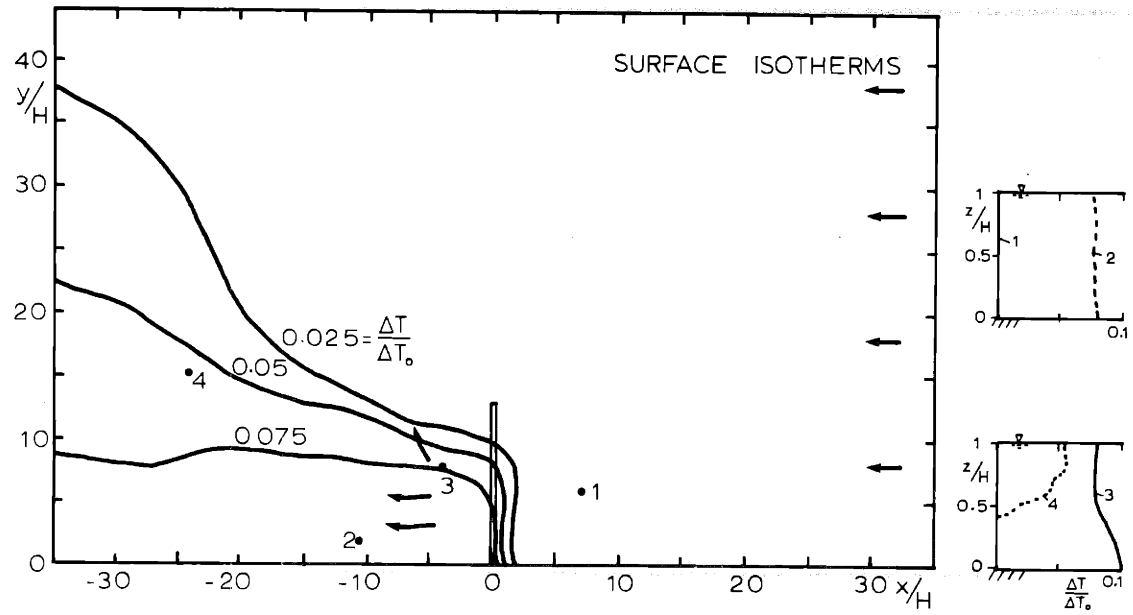

a) Run BC-33, F_s = 88, H/B = 419, θ_o = 0°, Φ = 0.5, $\beta(y)$ = NOR, V = 6.9, γ = 90° (Nozzles Directed to the Left)

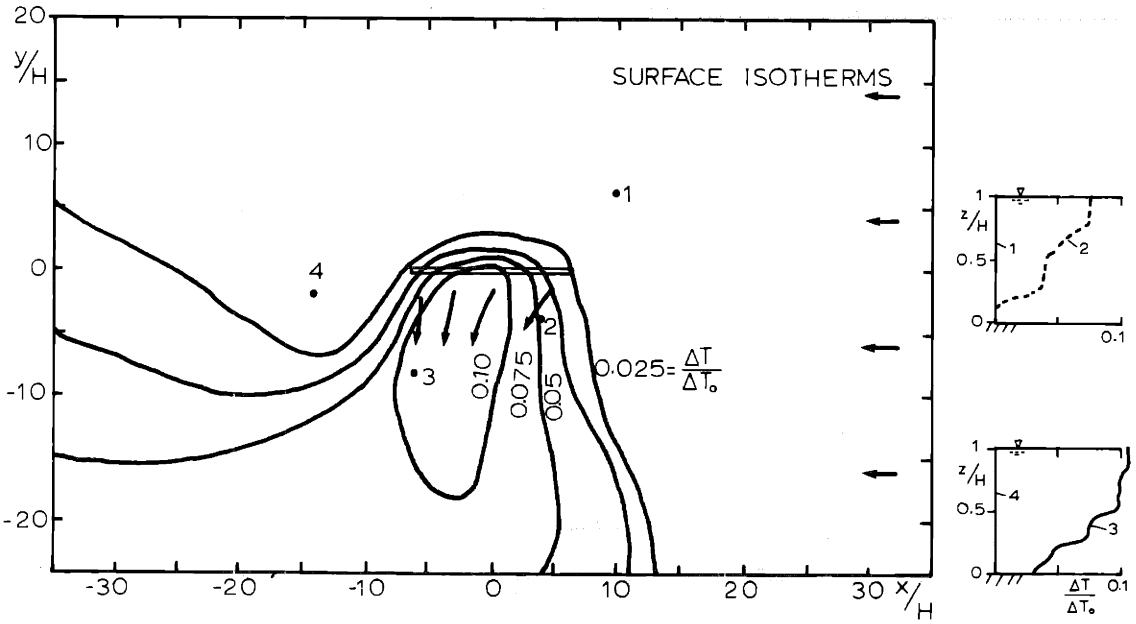

b) Run BC = 47, F_s = 88, H/B = 419, θ_o = 0°, Φ = 0.2, $\beta(y)$ = NOR V = 6.7, γ = 0° (Nozzles Directed Downward)

Fig. 7-8: Observed Temperature and Velocity Field, Series BC, Unidirectional Nozzles

underneath the surface layer. This phenomenon may be somewhat accentuated by boundary effects.

Figure 7-7 in comparison with Figure 7-6 shows the effect of decreased ambient depth, H, and increased diffuser momentum (θ_o = 0° vs. 45°). Both figures show LOG distributions. The increased strength of the diffuser induced currents is apparent; boundary effects are enhanced.

The effect of LOG versus NOR distribution is shown by comparing Figures 7-8 (NOR) and 7-7 (LOG). The further increased strength of the circulation and the tendency to contract downstream of the diffuser line can be seen. Observed dilutions are compared with predicted limiting regimes and criteria. Figure 7-9 applies to the LOG distributions with a predominantly two-dimensional flow field: The combined mixing effect, V*, of crossflow and horizontal diffuser momentum is given by Equation 7-5. The range of applicability of the fully mixed and stagnant wedge domains is given by arguments, Equations (7-7) and (7-9), only substituting $S_s = V^*$ (F_H = 0.52 for Φ = 0.5). The run parameters are strongly concentrated in Figure 7-9, indicating the dominance of the horizontal momentum induced mixing over the limited experimental range. Dilutions are considerably (30 to 50%) lower than predicted both for parallel and perpendicular diffusers, which is consistent with the observation for the basin experiments with zero crossflow (Series BH) and may be attributed to experimental limitations.

Figure 7-10 applies to the NOR distribution with a contracted flow field: Adams' Eq. (7-6) is used and criteria lines are developed in similar fashion as for Figure 7-9. There is no predictive model for $V^* \to 0$, i.e. in the counterflow range. In the fully mixed range observed

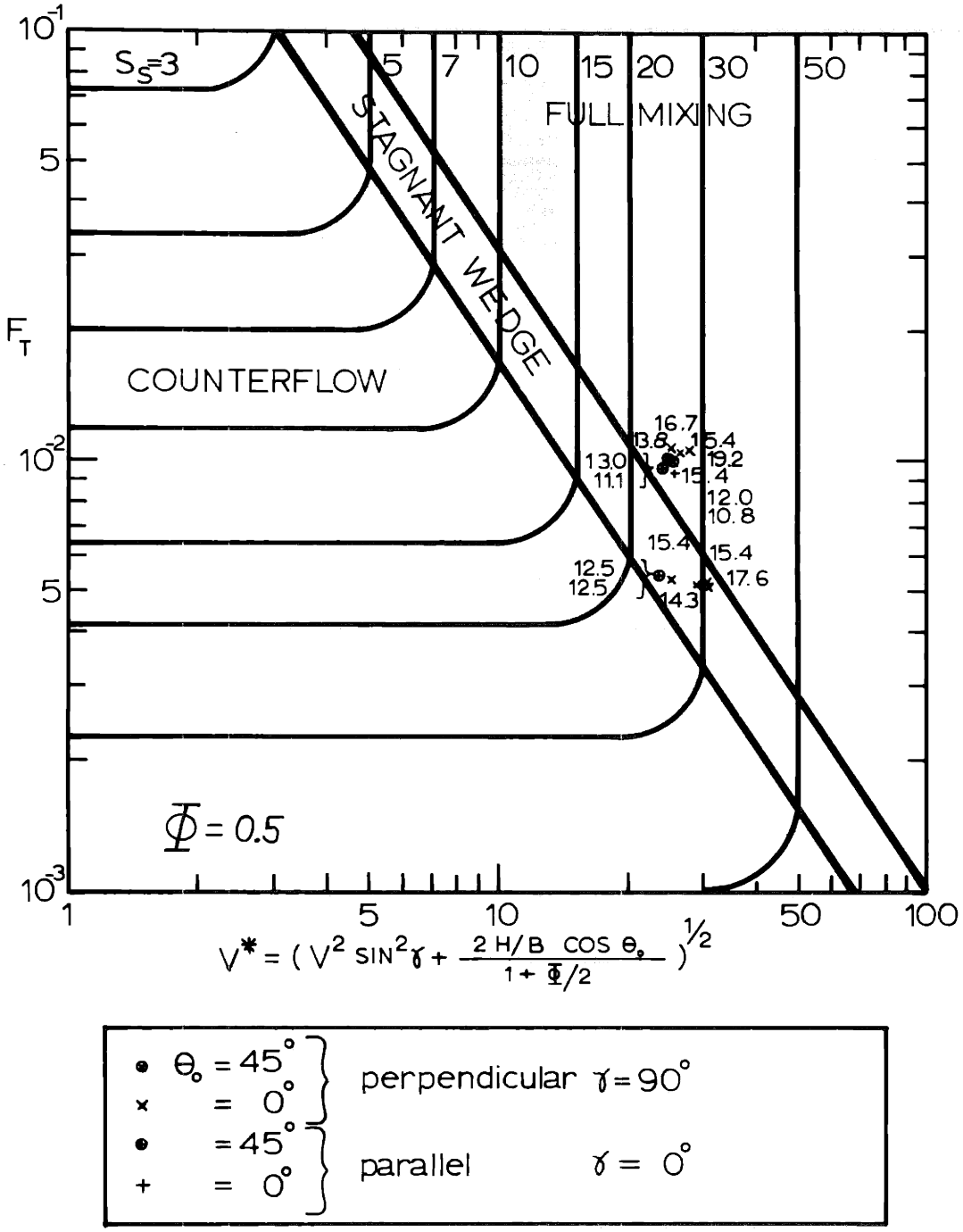

Fig. 7-9: Diffusers in Crossflow, Net Horizontal Momentum, with Control (LOG Distribution)

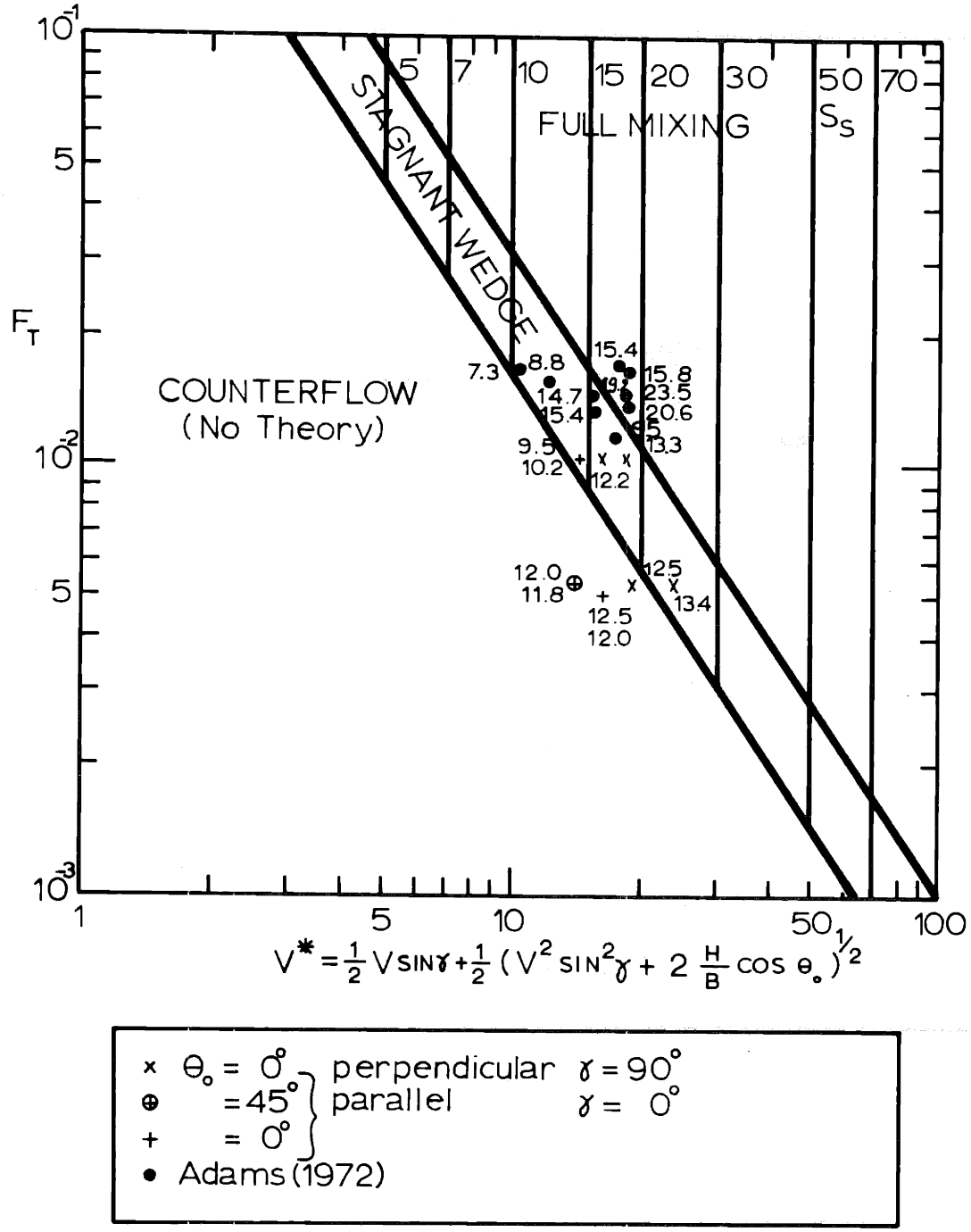

Fig. 7-10: Diffusers in Crossflow, Net Horizontal Momentum, no Control (NOR Distribution)

dilutions agree reasonably well (about 20% lower) with the predicted values. Also included are the data by Adams (1972) for perpendicular diffusers showing better agreement, although it is pointed out that Adams' dilution data are averaged values taken a considerable distance downstream from the diffuser as opposed to this study where dilution is defined as the maximum temperature at the edge of the near-field zone.

A comparison of relative diffuser performanced is given in Fig. 7-11 for experiments with similar diffuser parameters but varying γ and $\beta(y)$. Figure 7-11a compares corresponding parallel and perpendicular diffusers, showing about 20% reduced dilution capacity for the first. Similarly about 20% reduced performance is seen for the NOR distribution (no control) compared to the LOG distribution (control). This is consistent with observation of the zero crossflow tests (Series BH).

7.5 Conclusions: Diffusers with Ambient Crossflow

Results of the experimental investigation analyzed within the framework of the limiting flow regimes enable the following conclusions to be drawn on the effect of an ambient crossflow on diffuser performance:

1) Diffuser Arrangement

In the presence of ambient currents the single most critical parameters of diffuser behavior is the arrangement, γ, of the diffuser with respect to the current direction. Depending on the arrangement, the effect of crossflow may increase or decrease observed dilutions with reference to the situation of zero crossflow:

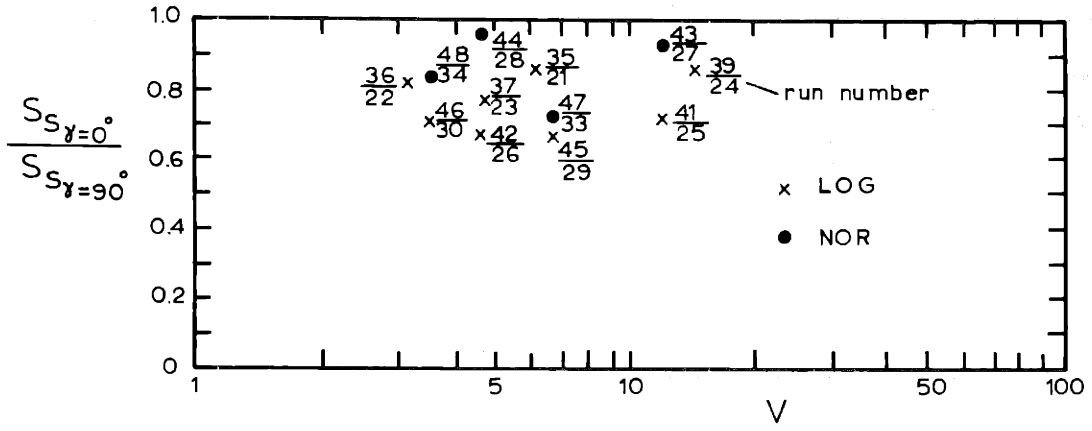

a) Parallel Diffuser Vs. Perpendicular Diffuser

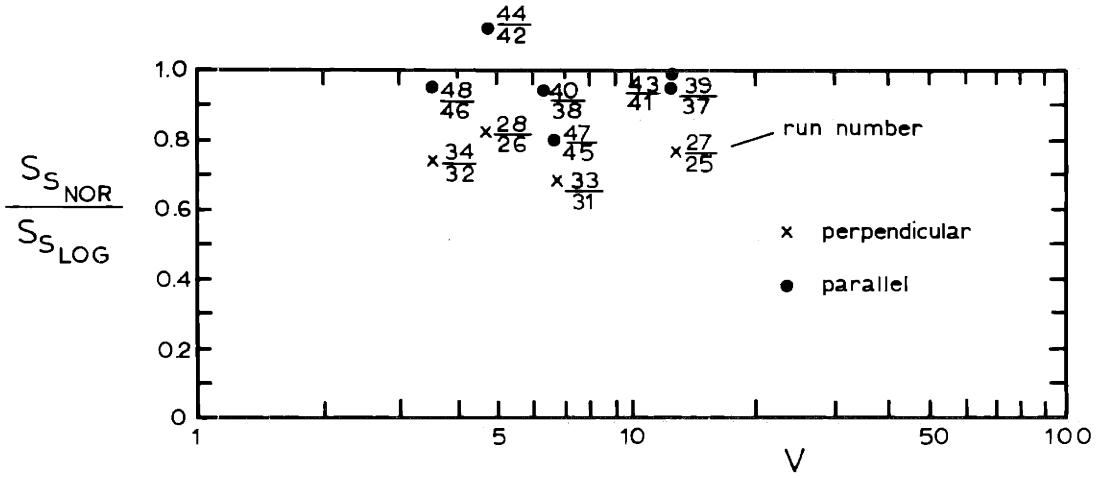

b) NOR Distribution Vs. LOG Distribution

Fig. 7-11: Comparison of Relative Diffuser Performance in Crossflow (Series BC) with Unidirectional Discharge

a) Perpendicular Diffuser: The presence of a crossflow increases the dilution observed downstream of the diffuser in the case of alternating nozzles and in in the case of nozzles discharging in the direction of the current. The case of nozzles discharging against the current was not studied in this investigation, however, other studies (Harleman et. al. (1971)) indicate qualitatively a marked decrease in dilution due to stagnation effects and unsteady recirculation.

b) Parallel Diffuser: The effect of cross currents causes in all conditions (alternating or unidirectional discharge) a decrease in dilutions as compared to the zero crossflow situation. This fact is due to (i) the current sweeping along the diffuser line causing repeated re-entrainment and (ii) for the case of unidirectional discharge with full vertical mixing, an effective blocking of the oncoming ambient flow is given causing eddying and unsteady recirculation of the mixed water at the downstream diffuser end.

2) Diffuser Control

Control of the induced horizontal circulations through horizontal nozzle orientation, $\beta(y)$, is equally important as in the zero crossflow case.

3) Two-Dimensional Experiments

The interplay between the diffuser induced and the ambient flow field for the three-dimensional diffuser cannot be simulated

in a two-dimensional channel model with forced ambient crossflow. The application of such experiments is limited to laterally strongly confined situations.

VIII. APPLICATION OF RESULTS TO DESIGN AND HYDRAULIC SCALE MODELING OF SUBMERGED MULTIPORT DIFFUSERS

The theoretical and experimental analysis treated the mechanics of a submerged multiport diffuser for buoyant discharges into an unstratified, large body of water of constant depth with a uniform current system running at an arbitrary angle to the diffuser axis. The results of this study, presented in the form of solution graphs, can be used for diffuser design for the configuration considered and - with proper schematization - for the preliminary design estimate for a variety of other, more complicated discharge configurations. For complicated discharge conditions hydraulic scale models have to be used to evaluate diffuser performance. In this case the theory developed in this study enables the formulation of modeling requirements for the operation of scale models.

The design of diffuser structures is an integral part of a waste management system and thus is governed by a host of factors relating to economical, engineering and environmental objectives. A complete diffuser design is carried out in three broad steps, each with implications on the above objectives:

(i) Site Selection is the choice of a general area for the location of the diffuser outfall.

(ii) Diffuser Design for Dilution Requirement involves the hydrodynamic design of the discharge structure within the selected site with the purpose of reducing the concentration of the effluent material so as to conform to environmental criteria.

(iii) Internal Hydraulic Design of the Diffuser Pipe is the computation of the manifold problem with the goal of achieving reasonably uniform nozzle exit velocities along the diffuser line.

This study was primarily addressed to design step (ii). However, certain considerations regarding step (i) can be discussed in the context of this study. The internal hydraulic design, step (iii), has been treated elsewhere (see Rawn et al. (1960)) and computer programs have been developed. An important result of Rawn et al.'s work is summarized here, as it directly relates to step (ii): In order to insure reasonable uniformity of the discharge velocities from the diffuser nozzles it is necessary that the cross-sectional area of the diffuser pipe (feeder line) be larger than the total area of the nozzles. (In other words, no uniformity is possible if the flow has to be decelerated before leaving the pipe.) The design considerations presented herein are primarily directed at "thermal" diffusers for discharge of heated condenser water from steam-electric power plants. A typical example for a thermal diffuser in comparison with a typical sewage diffuser has been given in Table 5.1. Sewage diffusers with a high dilution requirement (more than 100) are generally limited to deep water and thus do not exhibit the intricacies introduced by a constraining water depth, namely an unstable near-field zone with local re-entrainment and the generation of horizontal circulations.

8.1 Site Characteristics

Selection of a site for the location of a thermal diffuser outfall involves a variety of considerations, such as distance from the

shore line, available offshore area, prevention of recirculation into the power plant intake, requirements for providing a zone of passage etc... Rather than discussing these aspects which have to be evaluated individually in each case, a description of possible site characteristics is given here:

(i) Site topography. The vertical extent and the lateral confinement of the receiving water are important. The water body can be laterally unconfined (diffuser located far away from shore, or offshore power plant), laterally semi-confined (diffuser located close to shoreline) or laterally confined (diffuser in rivers, canals or other constraining geometries). A particularly strong boundary effect may occur for diffusers located in embayments or regions which are somehow separated from the main body of water and do not have a strong throughflow.

The vertical extent of the diffuser site can be uniformly shallow (such as on a coastal shelf or in rivers) or have variable sloping offshore depths.

(ii) Current System. The ambient current at the diffuser site may be weak and unpronounced (in intermediate size lakes and reservoirs primarily dependent on unsteady wind action). Significant current action may occur in river applications and in coastal or large lake sites with strong tidal or inertial currents. The current system may be predominantly in one direction (river, lake, or ocean longshore currents) or may be oscillating (tidal currents). For diffuser sites in estuaries or tidal bays the ambient flow may pass repeatedly (during several tidal cycles) over the site.

(iii) Ambient Density Stratification. Occurrence of temperature stratification during summer months is typical for lakes and reservoirs in the moderate climate zone. Similarly, temperature stratification has also been observed in shallow coastal zones although limited to periods of moderate wave action. Salinity stratification is typical in estuarine sites.

(iv) Ambient Turbulence. The ambient turbulent intensity has implications on the stability of both ambient and diffuser-induced stratification. Increased turbulence, as through significant wave action, may lead to erosion and breakdown of density stratification.

(v) Wind Stress. In addition to creating convective currents and ambient turbulence, the wind acting on the water surface exerts a stress on the diffuser induced flow field and may influence the flow-away, or lead to recirculation at the intake.

8.2 Diffuser Design for Dilution Requirement

Once the general site for the diffuser location has been selected, the diffuser structure is designed with the primary purpose of achieving a certain mixing of the discharged heated water with the ambient water (nearfield dilution requirement). In addition, the diffuser should meet other environmental and economical objectives.

8.2.1 Glossary of design parameters

The following nomenclature is suggested for use in design of submerged multiport diffusers:

Equivalent Slot Diffuser: Any multiport diffuser with nozzle diameter, D, and spacing, ℓ, can in physical terms be described by its equivalent slot diffuser. This concept retains the relative dynamic

characteristics of the diffuser discharge and <u>should</u> be used for mathematical analysis, classification of diffusers, comparison of different diffusers and design. The slot width, B, of the equivalent slot diffuser is

$$B = \frac{D^2 \pi}{4\ell} \tag{2-20}$$

Important design parameters are then the slot densimetric Froude number

$$F_s = \frac{U_o}{\left(\frac{\Delta\rho_o}{\rho_a} g B\right)^{1/2}}$$

and the relative water depth, H/B .

<u>Diffuser Load</u>: F_T , is a densimetric Froude number

$$F_T = \frac{F_s}{\left(\frac{H}{B}\right)^{3/2}} = \frac{q_o}{\left(\frac{\Delta\rho_o}{\rho_a} g H^3\right)^{1/2}} \tag{7-1}$$

where q_o = diffuser discharge per unit length which describes the impact (discharge and buoyancy effects) of the discharge on the <u>total depth</u>.

<u>Vertical Angle of Discharge, θ_o</u> : Varying between horizontal ($\theta_o = 0°$) and vertical ($\theta_o = 90°$).

<u>Direction of Discharge</u>: The nozzles may all be directed to one side of the diffuser axis (<u>unidirectional</u> discharge with net horizontal diffuser momentum) or may point into both directions (<u>alternating</u> discharge with no net horizontal diffuser momentum). A limiting case of

alternating discharge is the vertical discharge. In terms of the equivalent slot concept all alternating discharges can be represented by $\theta_o = 90°$.

Control through Horizontal Nozzle Orientation, $\beta(y)$: The horizontal circulations produced by a diffuser discharge (with unstable near-field) can be controlled through individual horizontal orientation of the diffuser nozzles along the diffuser line of half length, L_D (see Fig. 6-2). Particularly important distributions for $\beta(y)$ are the "LOG" distribution

$$\beta(y) = \cot^{-1}\left(\frac{1}{\pi}\log\frac{1 + y/L_D}{1 - y/L_D}\right) \qquad (4\text{-}36)$$

which in the case of alternating nozzles results in a three-dimensional stratified counterflow situation and the "NOR" distribution

$$\beta(y) = 90°$$

in which all nozzles are oriented normal to the diffuser axis typically resulting in a contracted flow-away from the diffuser.

Arrangement of the Diffuser Axis with Respect to the Ambient Current Direction, γ : Referring to Fig. 7-1, limiting values of γ are the parallel diffuser ($\gamma = 0°$) and the perpendicular diffuser ($\gamma = 90°$).

8.2.2 Design objectives

Typical thermal diffusers with a low dilution requirement and located in shallow water can have a significant dynamic impact on the receiving water. Vertical instabilities arise in the near-field related to which is the generation of horizontal circulations induced in the receiving water as discussed in Chapter 4. In addition horizontal circulations are caused by the net discharge momentum (unidirectional

nozzles). Nonetheless, through effective diffuser design this dynamic impact can be controlled to such a degree as to achieve given design objectives.

General objectives relate to environmental and engineering requirements. Most important for design is the conformity with legal temperature standards: diffuser-induced temperatures shall not exceed prescribed limits during certain time periods and outside a given area ("mixing zone"). Typically these limits apply to surface temperatures. In addition, environmental goals may include the desirability of vertical stratification to minimize thermal impact on the bottom substrate, and the specification of a passageway in laterally bounded sites, to avoid a "thermal blockage" for aquatic organisms.. Also it might be required to keep the heated discharge away from the shoreline. Engineering requirements are concerned with the control of the diffuser flow field for proper location of the cooling water intake and to prevent recirculation into the intake.

Obviously, from the design point of view these general objectives can always be met (assuming the site geometry is not constraining), for example, by building a "long diffuser" far away from the shoreline. At this point economic requirements enter the discussion: the diffuser should be designed to meet the above general objectives at a minimum cost. Thus, based on the understanding of the mechanics of the diffuser action obtained in this study the following specific objectives can be formulated:

a) The diffuser induced temperature rises should be uniform along the whole diffuser line, or else the diffuser capacity is not

fully utilized. This relates to (i) the flow distribution ("diffuser load") in case of a variable depth, H, and (ii) to the maximum nozzle spacing (prevention of isolated "hot" spots).

b) No currents, either induced by the diffuser action itself or given by the ambient crossflow, should sweep along the diffuser axis resulting in repeated entrainment. The questions of diffuser control through horizontal nozzle orientation, $\beta(y)$, and the arrangement with respect to the crossflow, γ , are important.

c) In order that diffuser designs perform well under a variety of ambient conditions, such as tidal or wind-driven currents with varying direction and magnitude, it is desirable to achieve a stratified flow field. The degree of recirculation into the diffuser line under adverse flow conditions is minimized for such diffusers.

8.2.3 Design procedure

By virtue of the number of important variables involved, diffuser design has to be an iterative procedure evaluating a set of alternatives (also different sites). Whenever the discharge geometry can be schematized as to resemble the geometry considered in this basic study, a diffuser design or preliminary design estimate (e.g. for further testing in a hydraulic scale model) can be developed. The logical steps and decisions which have to be made in the design procedure are illustrated in two specific examples: a) Design of a diffuser in a reversing tidal current system (this includes the limiting case of zero

crossflow), and b) Design of a diffuser in a uniform (approximately) steady crossflow (such as a lake or ocean longshore current).

The following is given in the design problem:

1) Site characteristics (depth, geometry, currents).

2) Environmental and engineering requirements (allowable maximum temperature rise, area of "mixing zone").

3) Plant characteristics, namely:

Q_o = total condenser water flow rate

T_o = temperature of condenser water. For simplicity, the ambient water temperature, T_a, is assumed homogeneous, so that

$\Delta T_o = T_o - T_a$ = discharge temperature rise.

The effect of a stratified receiving water is evaluated as the last design step.

8.2.3.1 Example: Diffuser in a reversing tidal current system

Figure 8-1 shows the hypothetical situation with a sloping

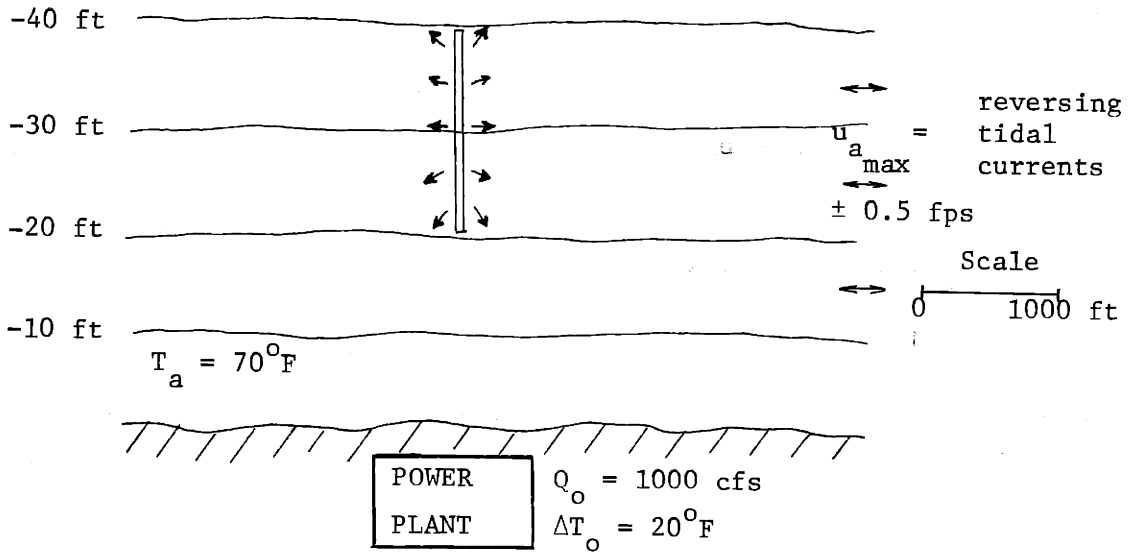

Fig. 8-1: Diffuser Design in Tidal Current System

offshore topography and tidal currents running parallel to the shoreline. The ambient temperature is $T_a = 70°F$, the plant flow is 1,000 cfs with a temperature rise $\Delta T_o = 20°F$ (the corresponding $\Delta\rho_o/\rho_a = 0.03$). The bottom coefficient, f_o, in the offshore area is estimated as ~ 0.015 (average value for sandy bottom). The governing temperature standard is $\Delta T_{max} = 2°F$, thus giving a minimum near-field dilution requirement $S_{s_{min}} = \Delta T_o/\Delta T_{max} = 10$.

The following design steps are considered:

A) Choice of Arrangement and Direction of Discharge (Alternating vs. Unidirectional Nozzles):

A diffuser arrangement perpendicular to the prevailing tidal current direction is chosen, since this results as a general rule in higher dilutions as compared to the corresponding parallel diffuser (this is true for both alternating nozzles, see Fig. 7-5b, and for unidirectional nozzles, see Fig. 7-11a). (Note: A possible exception to this rule may be a parallel diffuser located on a shallow shelf discharging unidirectionally into an offshore deep water region with strong advective currents, preventing recirculation).

A diffuser discharge with alternating nozzles ($\theta_o = 90°$) is chosen. A diffuser with unidirectional nozzles would perform well only during one half of the tidal cycle (when the current direction is the same as the nozzle direction). During the other half of the tidal cycle when the nozzles point against the current, stagnation effects occur, resulting in unsteady temperature increase and strongly reduced performance (as an example for this phenomenon, see Harleman et al. (1971).

B) Control through Horizontal Nozzle Orientation $\beta(y)$: For alternating diffusers (no net horizontal momentum) control through horizontal nozzle orientation according to the "LOG" distribution (Eq. (4-36), see also Fig. 6-2) should always be used. This distribution insures a stratified flow field in the far-field (outside the unstable near-field zone) which is desirable from the standpoint of preventing recirculation with unsteady temperature rises. If the LOG distribution is not used (e.g. NOR distribution), currents will sweep along the diffuser axis resulting in repeated re-entrainment and strongly reduced performance (see Fig. 4-5 and Fig. 6-3a as compared to Fig. 6-4a).

Application of the three-dimensional LOG distribution, which produces a predominantly two-dimensional flow field in the diffuser centerposition, allows usage of the near-field dilution graphs for design (e.g. Figs. 3-23, 3-24 or 6-6).

C) Initial Design: The offshore topography is sloping. An initial design can be made using an average depth. (The design is refined subsequently). Assume the diffuser is centered around the 30 ft depth contour, hence H_{ave} = 30 ft is taken as the design depth.

The ambient currents are unsteady and reversing. The initial design is made for the worst condition, namely slack tide (zero current). The performance under current conditions is improved (Chapter 7) and can be estimated later.

In order to use a dilution graph for alternating discharge it is necessary to obtain a value for the far-field parameter, $\Phi = f_o L_D/H_{ave}$, where L_D is the half-length of the diffuser. If it is assumed that

the total diffuser length is $2L_D \approx 2000$ ft , $\Phi = 0.5$ (this will have to be adjusted if the computed $2L_D$ is more than 10 to 20% different from the original assumption). Thus graph, Fig. 6-6, is applicable (if Φ is different from the values plotted in this study, graphs can be constructed following the procedure of Paragraph 3.6.2.3).

Figure 6-6 shows that the dilution requirement ($S_s = 10$) can be met for different combinations of F_s and H/B and that the dilution requirement can be met with either a stable or unstable near-field regime. In terms of three-dimensional diffuser characteristics, the parameters F_s , H/B can be expressed as ($Q_o = U_o\ B\ (2L_D)$)

$$F_s = \frac{U_o^{3/2}\ (2L_D)^{1/2}}{\left(\frac{\Delta\rho_o}{\rho_a}\ g\ Q_o\right)^{1/2}} \qquad (8\text{-}1)$$

$$\frac{H}{B} = \frac{H_{ave}\ U_o (2L_D)}{Q_o} \qquad (8\text{-}2)$$

Q_o , $\Delta\rho_o/\rho_a$ and H_{ave} (assumed location) are fixed at this point. Only U_o and $(2L_D)$ can be varied.

In selecting an initial combination of F_s , H/B on the graph, it is desirable to be as close as possible to the stable near-field region because diffusers with a stable near-field are less prone to the onset of undesirable horizontal circulations. (They do not require control through horizontal nozzle orientation.) An initial combination is taken at the criterion line between the stable and unstable near-field (i.e., $F_s = 32$, $H/B = 200$). With these values the two unknowns

in Eqs. (8-1) and (8-2) are evaluated

$$2L_D = \frac{\left(\frac{H}{B}\right)^{3/2} Q_o}{F_s \left(\frac{\Delta\rho_o}{\rho_a} g\right)^{1/2} H^{3/2}} \qquad (8\text{-}3)$$

$$U_o = F_s \left[\frac{\frac{\Delta\rho_o}{\rho_a} g H}{\frac{H}{B}} \right]^{1/2} \qquad (8\text{-}4)$$

as $2L_D = 1{,}700$ ft and $U_o = 3.7$ fps .

At this point economic considerations of internal diffuser hydraulics enter the analysis. Low jet discharge velocities require a large diameter diffuser pipe in order to have uniformity of discharge along the diffuser. This results in excessively high costs and the possibility of sedimentation in the pipe. In practical problems, jet exit velocities vary between 10 to 15 fps, with the upper limit given by considerations of pump size and pumping costs. Increasing U_o also increases H/B as seen from Eq. (8-2). Thus in order to increase the jet exit velocity it is necessary to move to the right along the $S_s = 10$ line in Fig. 6-6 (i.e. move further into the unstable region). It should be noted that typical thermal diffuser designs are almost always located in the unstable parameter range, purely for economic reasons (keeping $2L_D$ short, and U_o reasonably high).

In moving upward along the line $S_s = 10$, the required diffuser length, $2L_D = 1{,}700$ ft does not change. This is a consequence of the slope of the lines and can also be inferred from Eq. (3-222) or Eq. (7-2), which state that the near-field dilution S_s is dependent

only on the diffuser load F_T

$$F_T = \frac{F_s}{\left(\frac{H}{B}\right)^{3/2}} = \frac{Q_o}{\left(\frac{\Delta\rho_o}{\rho_a} g H_{ave}^3\right)^{1/2} (2L_D)} \qquad (8\text{-}5)$$

Thus, $2L_D$ = 1,700 ft, is the required diffuser length, regardless of which combination of F_s , H/B is chosen. The choice is dependent on the design jet velocity and on the objective to be close as possible to the stable range. (These two requirements are in opposition). If U_o = 10 fps is chosen, then from Eq. (8-2) H/B = 51.0 and from Fig. 6-6 F_s = 150. The value of $\Phi = f_o L_D/H_{ave}$ is calculated again, Φ = 0.43, which is close enough to the initial assumption (0.5), so that no iteration is necessary.

If the dilution requirement were higher, $S_s > 10$, only two measures could be taken: increasing the diffuser length, $2L_D$, or moving the diffuser further offshore, increasing the depth, H .

D) Design Refinement: The initial design with an average depth, H_{ave} = 30 ft, yielded a length $2L_D$ = 1700 ft ; the average discharge per unit length is q_o = 0.59 cfs/ft. Referring to Fig. 8-1 the diffuser is centered around the 30 ft depth contour and roughly extends between the 20 ft and 40 ft contours. Obviously, the diffuser discharge per unit length, q_o ,should be varied with the objective of achieving a uniform temperature field along the diffuser. By virtue of Eq. (7-2) the requirement of constant S_s in case of variable depth is tantamount to the requirement of a constant diffuser load, F_T ,

$$F_T = \text{const.} = \frac{q_o}{\left(\frac{\Delta\rho_o}{\rho_o} g H^3\right)^{1/2}} \qquad (8\text{-}6)$$

If H is a variable, then q_o should change as

$$q_o \sim H^{3/2} \qquad (8\text{-}7)$$

Thus, in the example, the discharge at the offshore end (twice as deep) should be increased by a factor of $2^{3/2} = 2.8$ compared to the discharge at the near-shore end.

E) Details of Multiport Diffuser

It remains to choose the secondary variables of the multiport diffuser ℓ, D and θ_o (vertical angle). The nozzle spacing, ℓ, should be chosen so that there is good local uniformity of temperature rise along the diffuser line. Based on jet spreading laws, complete jet interference before surface impingement requires $\ell/H \lesssim 0.5$. This might be somewhat restrictive as additional interaction takes place laterally even after impingement. Based on experimental observations $\ell \lesssim H$ is recommended in order to prevent isolated "hot spots" and jet "boil areas". The nozzle diameter D, is then $D = \sqrt{\frac{B4\ell}{\pi}}$, where $B = Q_o/(U_o 2L_D)$.

The vertical angle of the jets should be large enough to prevent bottom attachement and resultant bottom scour. A minimum angle of $\theta_o \gtrsim 20^o$ is suggested for both alternating and unidirectional discharges. For the same reasons the height, h_s, of the nozzles above bottom should be $h_s \gtrsim 3D$. For the control ($\beta(y)$ given by the LOG distribution) the maximum vertical nozzle angle $\theta_o < 79^o$, Equation (4-44). No

vertical discharge should be used for unstable near-field conditions.

F) Effect of Cross Currents

The initial design was carried out for the slack (worst) condition. For perpendicular diffusers with alternating nozzles the effect of cross flow is always beneficial on dilution performance. Assuming the tidal current varies between $u_a = \pm 0.5$ fps, the performance at non-slack conditions may be checked by using a crossflow graph, Figure 7-5 ($\Phi = 0.5$). The effect of crossflow is introduced by $V^* = V\sin\gamma$ ($\gamma = 90^o$, perpendicular diffuser and $V = u_o H_{ave}/q_o$). The diffuser load, F_T, is from Equation (8-5) with the appropriate values, $F_T = 0.012$. The value of V is changing with the current magnitude, for $u_{a_{max}} = 0.5$ fps, $V = (0.5)(30)/(0.50) = 25.4$ and the corresponding dilution is $S_s = 25.4$. Under this condition the diffuser is operating in the fully mixed regime. For an average current $u_a = 0.25$ fps, and $V = 12.7$, the dilution $S_s = 12.0$ and the diffuser is operating at the edge of the stagnant wedge regime. For $u_a < 0.25$ fps there is a stratified counterflow upstream of the discharge and the dilutions approach those for the slack tide condition.

Graphs of near-field dilutions (not accounting for any possible heat return due to tidal motion) as a function of tidal time can be constructed.

G) Effect of Ambient Stratification

In this example the ambient water has been assumed to be unstratified. The effect of ambient stratification may be evaluated as follows: If a step change in ambient density (temperature) occurs

at half depth and provides an effective "ceiling" to the flow field, then the design depth would be reduced to H/2. As a consequence, the dilution would decrease by a factor or 2 (Equation (8-3)) and the temperature rise of the mixed water would be doubled. Unless the ambient stratification is very pronounced (of the order of about half the discharge temperature rise), the diffuser discharge will break up the natural stratification and "substitute" an artificial stratification. The ambient temperature can then be defined as the average vertical temperature, $T_{a_{ave}}$, and

$$\Delta T_o = T_o - T_{a_{ave}}$$

is taken as the design variable and all induced temperature rises are similarly referred to $T_{a_{ave}}$.

8.2.3.2 Example: Diffuser in Steady Uniform Crossflow

The site characteristics are shown in Figure 8-2

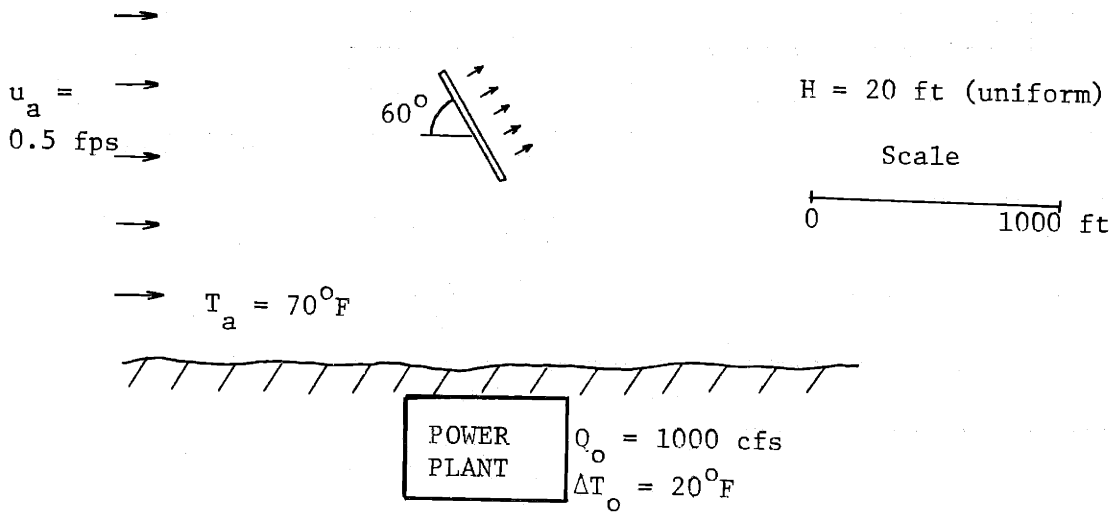

Fig. 8-2: Diffuser Design in Steady Uniform Crossflow

The offshore topography is uniformly shallow, H = 20 ft, the current magnitude is 0.5 fps and does not have strong unsteady fluctuations. The same plant characteristics and the same dilution requirement (10) as in the previous example are assumed.

A) Choice of Arrangement and Direction of Nozzle Discharge

An arrangement $\gamma = 60^{o}$ and a unidirectional discharge is chosen. The objective is to intercept substantial amount of crossflow (hence avoiding $\gamma \sim 0^{o}$) while also providing some momentum into the offshore direction to "push" the temperature field into deeper offshore areas. The vertical nozzle angle is chosen as $\theta_{o} = 20^{o}$, to provide maximum horizontal momentum while preventing bottom scour.

B) Horizontal Nozzle Orientation, $\beta(y)$

All unidirectional diffusers which provide enough horizontal momentum to result in full mixing (criteria lines in Figures 3-28 to 3-31 and 6-10 to 6-13) are subject to recirculation. The degree of recirculation depends primarily on an ambient advective mechanism (such as the present current system), which carries the temperature field away from the diffuser line, and on the nozzle orientation, $\beta(y)$. In general, the LOG distribution while providing somewhat higher near-field dilutions is somewhat more liable to recirculation. The NOR distribution ($\beta(y) = 90^{o}$) results in a contracted flow field and is less liable to recirculation. A NOR distribution is chosen.

C) Initial Design

For a unidirectional diffuser with NOR distribution, full vertical mixing and under the influence of a crossflow, Figure 7-10

(Adams' model) is applicable. Figure 7-10 also includes criteria of applicability for the theoretical prediction. In the fully mixed regime the dilution, S_s, is equal to V*

$$V^* = \frac{1}{2} V\sin\gamma + \frac{1}{2} (V^2\sin^2\gamma + 2 \frac{H}{B} \cos \theta_o)^{1/2} \qquad (7\text{-}6)$$

that is, the combined effect of cross flow and diffuser momentum, and the dilution is independent of the diffuser load, F_T. This would indicate the desirability of making F_T as large as possible to reduce the diffuser length, $2L_D$ (see Equation (8-5)). By doing so, however, the strength of the momentum-induced current will increase and the potential for recirculation at the diffuser will also increase. Usually, the constraint on diffuser length is given by the range of possible jet exit velocities (see considerations in the first example). A jet exit velocity U_o = 10 fps is chosen. With V* = S_s, Equation (7-6) can be modified to give the required diffuser length

$$2L_D = S_s^2 \frac{Q_o}{H} \left[\frac{1}{S_s u_a \sin\gamma + \frac{1}{2} U_o \cos \theta_o}\right] \qquad (8\text{-}8)$$

Using the above values, Equation(8-8) gives $2L_D$ = 550 ft. It remains to check a) whether this design is in the fully mixed range and b) whether it is liable to recirculation effects.

a) The diffuser load, F_T, Equation (8-5) is calculated as F_T = 0.06, which from Figure 7-10 indicates that it is well inside the fully mixed range. No upstream wedge will occur.

b) The crossflow mixing ratio is $V\sin\gamma = u_a H\sin\gamma / q_o$ = 4.9. The remaining contribution to the total dilution (S_s = 10) is 5.1 from momentum-induced currents. As a rule of thumb

it is hypothesized that the degree of recirculation is negligible only if the contribution from the crossflow mixing is at least ∿ 50% of the total dilution. In other cases, the strength of the ambient advective mechanism will not be sufficient to prevent circulation

Thus in case of unsteady currents (lower velocities) the diffuser performance may be drastically decreased. The overall performance depends on the duration of the low current velocities: Such effects have to be determined from a hydraulic scale model.

E) Details of Multiport Diffuser

Diffuser details are determined as in the previous example.

8.3 The Use of Hydraulic Scale Models

Certain sites having complex topographic features and non-uniform or unsteady ambient currents may present difficulties in schematization and application of the theoretical predictions developed in this study. Nevertheless, it will usually be possible to use the design charts to arrive at an initial design which can be tested and modified by means of a hydraulic scale model. Additional features that can be included in a model study are the possibility of re-circulation at the condenser water inlet and the unsteady build-up of heat due to recirculation at the diffuser. The latter is particularly important in the case of diffusers with significant horizontal momentum input.

Typical problems associated with the operation of diffuser scale models are those which were discussed for the present basic experimental

studies (Section 6.1.2), namely, boundary effects and turbulence requirements. Both problems relate to the limited size of available testing facilities.

In this section modeling requirements for diffuser scale models are discussed, in particular the use of distorted scale models is investigated, and methods of model boundary control, to minimize boundary effects, are explored.

8.3.1 Modeling Requirements

The diffuser flow field involves several different regions. Modeling laws require the equality of geometric and dynamic non-dimensional parameters for model (subscript m) and prototype (subscript p). In general, in any modeling problem, all parameters cannot be kept equal, and a choice relating to the relative importance of certain parameters has to be made.

The objective of scale models is the determination of the three-dimensional temperature (dilutions) and velocity field.

a) The near-field surface dilution, S_s, (outside the local mixing zone in case of an unstable near-field) in a general crossflow situation (Chapter 7) is a function of the dimensionless variables.

$$S_s = f(F_s, \frac{H}{B}, \theta_o, \Phi, \beta(y), V, \gamma) \qquad (8\text{-}9)$$

b) In addition, dilutions within the buoyant jet region are dependent on the distance

$$s/B \qquad (3\text{-}81)$$

and the jet Reynolds number

$$\mathrm{IR}_j = \frac{U_o 4R_h}{\nu} \gtrsim 3{,}000 \qquad (5\text{-}3)$$

to insure fully turbulent jet behaviour.

c) The three-dimensional temperature field outside of the immediate near-field zone is dependent on the ratio of the diffuser half length to depth

$$\frac{L_D}{H} \qquad (8\text{-}10)$$

d) At larger distances away from the near-field, the temperature distribution is affected by surface heat loss. The governing parameter for this region is (from Equation 3-168)

$$\frac{\kappa}{\rho_a c_p H} \frac{L_D}{U_o} \qquad (8\text{-}11)$$

taking L_D as the characteristic horizontal length and U_o as the velocity scale.

It is pointed out again that local diffuser details, ℓ/H, h_s/H, do not influence the diffuser performance as long as reasonable jet interference is obtained ($\ell/H < 1$). The nozzle orientation, $\beta(y)$, however, is important.

The ratio of the governing parameters for model and prototype is investigated for both undistorted and distorted models. For this purpose the following ratios are defined:

L_r = horizontal length ratio

z_r = vertical length ratio

u_r = velocity ratio

$(\frac{\Delta\rho_o}{\rho_a} g)_r$ = reduced gravity ratio

The distortion is given by $\frac{z_r}{L_r}$. For an undistorted model $z_r = L_r$. All models have to be densimetric Froude models as a minimum requirement. Thus

$$F_{sr} = 1 \quad \text{or} \quad u_r = [(\frac{\Delta\rho_o}{\rho_a} g)_r \, z_r]^{1/2} \tag{8-12}$$

Heated discharge models are usually operated with $(\frac{\Delta\rho_o}{\rho_a} g)_r \approx 1$, i.e., same temperature differentials as in the prototype, due to measurement and control problems, so that $u_r \approx z_r^{1/2}$ typically as in a free surface Froude model.

The bottom friction factors, f_o, in the far-field parameter, $\Phi = f_o \, L_D/H$ in Equation (8-9), is different for model and prototype. The parameter f_o depends on the relative roughness of the bottom k_s/R_h. Prototype values are $f_{o_p} \sim 0.01$ to 0.02 independent of the Reynolds number, while model values are strongly scale (Reynolds number) dependent and may vary between $f_{o_m} \sim 0.03$ to 0.08. Furthermore, Equation (8-9) assumes $f_i = Af_o$ where $A \sim 0.4$ to 0.5 (see Paragraph 3.6.2.2) over a wide range of Reynolds numbers.

Typical values for the surface heat exchange coefficient, κ, are for the prototype $\kappa_p = 150$ to 200 BTU/ft^2, day, ^oF and for the model $\kappa_m = 100$ to 150 BTU/ft^2, day, ^oF reflecting the different heat flux phenomena involved.

8.3.2 Undistorted Models ($z_r = L_r$)

For undistorted diffuser models, the ratio of all governing parameters (a) to d) above) is unity except for

$$\Phi_r = \frac{f_{o_m}}{f_{o_p}} = f_{o_r} \tag{8-13}$$

and

$$\left(\frac{\kappa}{\rho_a \tilde{} p H} \frac{L_D}{U_o}\right)_r = \frac{\kappa_r}{L_r^{1/2}} \tag{8-14}$$

The effect of Equations (8-13) and (8-14) is strongly scale dependent. For diffuser models it is desirable to reproduce as large an area as possible (to minimize boundary effects). The minimum scale ratio, L_r, however, is given by the discharge turbulence requirement, Equation (5-3), for usual conditions L_r equals 1/100 to 1/120. The small scale ratio has implications on the values of f_{o_m} (and hence Φ_r) and $K_r/L_r^{1/2}$. Typical values are

$$\Phi_r \sim 2 \text{ to } 5 \tag{8-15}$$

$$\frac{\kappa_r}{L_r^{1/2}} \sim 4 \text{ to } 15 \tag{8-16}$$

with κ_r between 0.5 and 0.75.

The effect of the exaggerated far-field effects, Equation (8-10), on near-field dilution, S_s, can be estimated for an alternating diffuser from Equation (7-2): Assume $\Phi_p = 0.5$ and $\Phi_m = 2.0$ (i.e., $\Phi_r = 4$) the dilution ratio $S_{s_r} \approx 0.83$ (using Figure 3-23). For larger Φ_p the error in prediction is decreased. In general, an undistorted model gives a somewhat conservative prediction of the near field dilution

(in the extreme about 20% lower).

The effect of the increased heat loss to the atmosphere, Equation (8-16), becomes important only at distances from the diffuser; it has a negligible influence on near-field dilutions (see paragraph 3.4.4.2). As undistorted diffuser models replicate a limited far-field range, this effect is not important.

Undistorted diffuser models reproduce correctly the geometric properties of the diffuser flow field, such as extent of the temperature field, local mixing zone, interaction with an ambient current, but are somewhat conservative in dilution prediction. The conservativeness can be estimated in any case. Their major disadvantage is the limited far-field range which can be simulated.

8.3.3 Distorted Models ($z_r > L_r$)

It is required to reproduce the same near-field characteristics relating to the stability criterion and to the horizontal momentum input, so that in Equation (8-9)

$$\left(\frac{H}{B}\right)_r = 1 \quad \text{and} \quad \theta_{o_r} = 1 \tag{8-17}$$

This is tantamount to saying that the detailed diffuser geometry should be locally undistorted (not $\theta_{o_r} = z_r/L_r$!), that is, the diffuser should be modelled with the vertical scale ratio, $z_r = B_r$. Then

$$\Phi_r = f_{o_r} \frac{L_r}{z_r} \tag{8-18}$$

and in particular if the distortion ratio is chosen such that $z_r/L_r = f_{o_r}$, $\Phi_r = 1$, the same far-field effects.

However, the relative diffuser half length, (8-10), is affected by distortion

$$\left(\frac{L_D}{H}\right)_r = \frac{L_r}{z_r} \tag{8-19}$$

instead of 1, and the extent of the near-field zone, governed by jet dynamics, (3-81), is exaggerated since $\left(\frac{s}{B}\right)_r = 1$, instead of L_r/z_r. The heat loss ratio is

$$\left(\frac{\kappa}{\rho_a c_p H} \frac{L_D}{U_o}\right)_r = \frac{\kappa_r L_r}{z_r^{3/2}} \tag{8-20}$$

which can be equal to unity only if $z_r^{3/2}/L_r = 1$.

As in the undistorted model, the vertical scale ratio z_r has a minimum of 1/100 to 1/120 for jet turbulence requirements.

The distortion factor may be chosen primarily in consideration of Equation (8-13), thus $z_r/L_r = f_{o_r}$. This will also insure a more realistic far-field heat loss, Equation (8-20), which may be important in distorted models replicating larger areas.

However, the geometric effects, Equations (8-19) and $\left(\frac{s}{B}\right)_r = 1$, may be critical in certain cases: Distorted models do not represent the correct three-dimensional temperature field induced by a diffuser. The extent of the near-field zone is exaggerated by z_r/L_r, as shown above, which can have repercussions when designing for a "mixing zone" defined in legal standards. In addition, the relative "shortening" of the diffuser half length, L_D/H, has two effects: (i) Whenever currents are sweeping along the diffuser axis (parallel diffuser, or diffuser with alternating nozzles and no control) the

degree of repeated entrainment is strongly dependent on L_D/H.

(ii) For unidirectional discharge with a vertically fully mixed flow-away, lateral density currents act at the end of the flow away zone (lateral wedge intrusion). This effect is exaggerated due to the relative shortening of the diffuser and results in easier stratification and less tendency to recirculate. In these cases predictions from distorted models are non-conservative.

To counterbalance these effects, a distortion ratio z_r/L_r less than f_{o_r} may be chosen: The near-field dilution prediction, S_s, is then somewhat conservative, yet the far-field effects are modeled in a more reliable manner.

It is concluded, that distorted models while being less conservative in the prediction of the near-field dilution, do not represent the true three-dimensional flow field: The extent of the mixing zone is exaggerated (sometimes grossly conservative) and for certain diffuser schemes, the interaction with currents is decreased (non-conservative). Yet in a variety of situations, such as an alternating, perpendicular diffuser, a distortion can always be used and may even be desirable (accounting for the exaggeration of a local mixing zone). The major advantage of distorted models is the large horizontal area which can be reproduced.

The choice of nozzle details, ℓ, h_s, is unimportant in the hydraulic scale model, and need not agree with the prototype values, provided, however, that the equivalent slot concept is maintained and that $\ell/H \lesssim 1$, preventing non-uniformity of temperatures in the near-field.

8.3.4 Boundary Control

The objective of boundary control methods is the minimization of model boundary effects. These boundary effects are particularly difficult in studying diffuser induced circulations. It is essentially desired to simulate a condition as if the boundary would not be present, that is mixed or ambient water is withdrawn or supplied at the boundary without accelerating or decelerating the currents. However, these control methods require the a priori knowledge of the correct withdrawal and supply rate, and are thus rather subjective. An iterative method observing the behaviour of the current system could be suggested, but is again difficult to evaluate. In general, emphasis should be put on diffuser designs which do not input considerable horizontal momentum and thus do not require extensive boundary control.

IX SUMMARY AND CONCLUSIONS

9.1 Background

A submerged multiport diffuser is an effective device for disposal of water containing heat or other degradable wastes into a natural body of water. A high degree of dilution can be obtained and the environmental impact of concentrated waste can be constrained to a small area.

The submerged multiport diffuser is essentially a pipeline laid on the bottom of the receiving water. The waste water is discharged in the form of round turbulent jets through ports or nozzles which are spaced along the pipeline. The resulting distribution of concentration of the discharged waste materials within the receiving water depends on a variety of physical processes.

This investigation is concerned with the development of predictive methods for buoyant discharges from submerged multiport diffusers. The following physical situation is considered: A multiport diffuser with given length, nozzle spacing and vertical angle of nozzles is located on the bottom of a large body of water of uniform depth. The ambient water is unstratified and may be stagnant or have a uniform current which runs at an arbitrary angle to the axis of the diffuser.

The general case of a diffuser in arbitrary depth of water and arbitrary buoyancy is treated. However, emphasis is put on the diffuser in shallow receiving water with low buoyancy, the type used for discharge of condenser cooling water from thermal power plants.

The development of predictive methods is important in view of:

-- Economical design of the diffuser structure.

-- Design to meet specific water quality requirements.

-- Evaluation of the impact in regions away from the diffuser, such as the possibility of recirculation into the cooling water intake of thermal power plants.

-- Design and operation of hydraulic scale models.

9.2 Previous Predictive Techniques

Previous predictive models for submerged diffuser discharge have been developed for two limiting cases of diffuser discharge: discharge in unconfined deep water in the form of rising buoyant jets (jet models), and discharge into shallow water with extreme boundary interaction resulting in a uniformly mixed current.

These models are not applicable for submerged diffusers in water of intermediate depth and no criteria of applicability have been established.

9.3 Summary

An analytical and experimental investigation of the diffuser problem is conducted. In the analysis the equivalent slot diffuser concept was used throughout as the salient representation of a multiport diffuser with laterally interfering or merging jets.

9.3.1 Diffusers without Ambient Crossflows

a) Two-Dimensional Channel Model

A multiport diffuser will produce a general three-dimensional flow field. Yet the predominantly two-dimensional flow which is

postulated to exist in the center portion of the three-dimensional diffuser can be analysed as a two-dimensional "channel model". The "channel model" consists of a diffuser section bounded by channel walls of finite length and opening at both ends into a large reservoir. Within the channel the diffuser flow field consists of four distinct flow regions: a buoyant jet region, a surface impingement region, an internal hydraulic jump region and a stratified counterflow region. The objective of the analysis is to obtain an overall description of the flow field by matching of the solutions for the individual regions.

The buoyant jet region is analyzed using the entrainment concept proposed by Morton et al. (1956). A relationship for the entrainment coefficient (Equation (3-48)), which depends on the local buoyant characteristics of the jet is deduced for jets with arbitrary discharge angle in a fashion similar to Fox's (1970) solution for the vertical jet. It is shown that all buoyant jets tend to an asymptotic case, the plume, which is characterized by a constant local densimetric Froude number, Equation (3-57). The value of the entrainment coefficient (Equation (3-48)) in this asymptotic case agrees well with Abraham's (1963) evaluation of Rouse et al.'s (1952) experimental data.

Tha analysis of the surface impingement region shows that the vertical flow distribution in the section after impingement is always distinguished by densimetrically supercritical flow conditions leading to a subsequent internal hydraulic jump.

The internal hydraulic jump region is described by a set of equations first derived by Yih and Guha (1955), which in general is dependent on the density ratio between the two layers and the free surface Froude numbers. An asymptotic solution for finite densimetric Froude numbers but small density differences and small free surface Froude numbers is derived giving a single equation (3-142) for the conjugate jump condition.

The equations for a non-entraining stratified counterflow region with surface heat loss and interfacial mixing are developed. Scaling shows that for practical diffuser problems the surface heat transfer processes can be neglected, so that the equations reduce to the classical Schijf and Schönfeld (1953) equations for stratified flow. The solution for the position of the interface, Equation (3-188), is obtained assuming constant total depth as a first approximation. With the given interface position, the change of the total head caused by frictional effects in the flow system is derived, Equation (3-195). Analytical solutions for the interface and total head equations are given.

The two-dimensional diffuser problem is governed by four dimensionless parameters: F_s, H/B and θ_o are near-field parameters, $\Phi = f_o L/H$ is a far-field parameter.

Matching of the solutions for the flow regions yields the following important results: stability of the near-field zone is given only for a limited range of low F_s, high H/B. Furthermore, the range decreases for decreasing (more horizontal) θ_o (Figure 3-2).

It is only in this limited range that simple buoyant jet models assuming an unbounded receiving water are applicable to predict dilutions. It is found that in this range the thickness of the surface impingement layer which has to be accounted for in dilution predictions is about 1/6 of the water depth. The flow-away in the far-field has little effect on near-field dilution and thus can be neglected for dilution predictions.

Outside the stable near-field range the diluted water is continuously re-entrained into the jet region forming a local mixing zone. This re-entrainment leads to a build-up of buoyancy of the near-field water until in steady state an equilibrium is reached which is essentially determined by the interplay of two factors: frictional effects in the far-field, represented by Φ, and the horizontal momentum input of the jet discharge, represented by θ_o.

For diffusers with no net horizontal momentum ($\theta_o = 90^o$) the far-field flow is given by an equal counterflow system between two critical sections, one at the edge of the local mixing zone, one at the channel end (Figure 3-20).

For diffusers with net horizontal momentum ($\theta_o < 90^o$) there are 3 possible far-field flow configurations: a counterflow system, a stagnant wedge system or supercritical flow (Figure 3-27). The supercritical flow case with resulting full vertical mixing downstream is the extreme case of surface and bottom interaction. In the analysis of each of these conditions the horizontal momentum of the discharge is balanced by the depth change across the mixing zone resulting from

far-field effects.

Composite surface dilution graphs describing both the near- and far-field range are presented.

b) Three-Dimensional Diffuser Behaviour

A model of the three-dimensional flow field for diffusers with no net horizontal momentum is developed. Scaling shows that in the diffuser vicinity the flow is given by a balance of inertial effects and pressure, hence a potential flow solution is possible. The model describes a three-dimensional stratified counterflow system and is used in two ways:

(i) Based on equivalency of far-field effects, the channel length, L, of the corresponding two-dimensional model is related to the length of the three-dimensional diffuser, L_D. In this way predictions for the three-dimensional application may be given through the corresponding two-dimensional channel model. It is found that

$$L = 0.884\ L_D \approx L_D \qquad (4\text{-}31)$$

provides a similar near-field dilution.

(ii) In addition to vertical circulations, a three-dimensional diffuser is capable of producing circulations in the horizontal plane. (Figure 4-5).

The existence of these circulations which ultimately lead to re-entrainment of mixed water is related to the near-field instabilities. Control (prevention) of these circulations is desirable and can be achieved through horizontal orientation of the diffuser nozzles

along the diffuser axis. In particular, the nozzle orientation (LOG distribution)

$$\beta(y) = \cot^{-1}\left(\frac{1}{\pi} \log \frac{1 + y/L_D}{1 - y/L_D}\right) \qquad (4\text{-}36)$$

insures a stably stratified counterflow regime outside the unstable near-field zone.

The maximum vertical angle θ_o which can be utilized to control the horizontal circulation is found to be $\sim 79^o$ (Equation (4-44)). No control is needed for diffusers with a stable near-field zone.

No three-dimensional flow model has been developed for the case of diffuser discharge with net horizontal momentum. It is hypothesized that $L \simeq L_D$ also provides equivalency of far-field effects for this case.

c) Experiments

Experiments were performed in two set-ups, investigating both a two-dimensional slot diffuser and a three-dimensional diffuser. Diffuser induced temperature rises are measured and compared with theoretical predictions.

9.3.2 Diffusers with Ambient Crossflows

The diffuser in a uniform ambient cross-current is investigated experimentally. No complete theory describing the full range of the governing parameters is developed. However, for the purpose of qualitative discussions and quantitative data presentation, extreme cases of diffuser behavior (regimes) can be isolated and described analytically. The advantage is that the number of significant

parameters is considerably reduced in these regimes. To isolate the regimes, the treatment is restricted to diffusers with an unstable near-field zone. Diffusers with a stable near-field zone are in general little affected by the crossflow except for the deflection of the buoyant jets. The crossflow will merely translate the stable surface layer without causing re-entrainment.

For diffusers with an unstable near-field zone in a crossflow three regimes are important: buoyancy induced counterflow, momentum induced currents, and crossflow mixing. Dilution graphs with criteria delineating the flow regimes are presented. The diffuser performance is found to be dependent on the arrangement of the diffuser axis with respect to the crossflow direction. A perpendicular diffuser generally yields better performance than a parallel diffuser.

9.4 Conclusions

The agreement between theoretical predictions of near-field dilutions and experimental results is satisfactory for diffusers with no horizontal momentum. Diffusers with horizontal momentum exhibit unsteady circulation patterns which are strongly affected by the boundaries of the experimental facilities. The agreement between predicted and observed dilutions is fair.

The following general conclusions are made:

1) Any multiport diffuser can, for analytical purposes, be represented by an equivalent slot diffuser. This includes diffusers with alternating nozzles. Thus details of the near-field geometry, such as nozzle spacings and height

above the bottom, have only a secondary influence on the diffuser behaviour. The equivalent slot concept introduces a convenient tool for comparing diffuser studies and prototype applications.

2) The mechanics of multiport diffusers are substantially different for diffusers in deep water with high buoyancy of the discharge (typical sewage diffusers) and for diffusers in shallow water with low buoyancy (typical thermal diffusers, Table 5.1). Sewage diffusers exhibit a stable near-field which is a) not prone to vertical instabilities and re-entrainment, and b) not liable to generate horizontal circulations. On the contrary, typical thermal diffusers have an unstable near-field with considerable re-entrainment and are in the absence of control through nozzle orientation liable to generate horizontal circulations leading to unsteady temperature increases.

3) A successful diffuser design should meet the following objectives:

   i) The induced temperature field should be uniform along the diffuser line, thus in case of variable depth the discharge per unit diffuser length should be varied according to Equation (8- 7), i.e., providing a constant diffuser load, and the nozzle spacing should be less than the water depth.

ii) The diffuser should be arranged perpendicularly to the prevailing cross-current (if possible) and the diffuser induced flow field should be controlled through horizontal nozzle orientation along the diffuser axis (LOG distribution). Both these features prevent currents from sweeping along the diffuser line which result in repeated re-entrainment and thus in decreased performance.

iii) For a diffuser to perform in a consistent and satisfactory manner under a variety of ambient conditions (e.g. reversing tidal currents) it is desirable to achieve a stratified flow in the far-field, thus minimizing the degree of recirculation into the near-field. Diffusers with alternating nozzles achieve such a stratified flow field.

4) With proper schematization of the site geometry the theoretical predictions of this study can be used to provide a diffuser design or preliminary design estimate for the screening of alternative discharge schemes and/or for further investigation in a hydraulic scale model.

5) Undistorted diffuser scale models correctly reproduce the areal extent of the temperature field and the current interaction, but are always somewhat conservative in predicting near-field dilution. The degree of conservativeness can be estimated. Distorted scale models, with proper distortion, give a less conservative prediction of near-field dilution and can also simulate the heat loss in the far-field.

However, the extent of the near-field zone (important for conforming to legal temperature standards) is exaggerated and the distortion of the ratio of diffuser length to water depth can have non-conservative effects on the performance prediction.

9.5 Recommendations for Future Research

The theoretical approach should be adapted to include the interaction with an ambient crossflow. In addition, the effect of wind stress on the free surface could be incorporated to determine the translation of the temperature field.

For diffusers with net horizontal momentum the need is for the development of a simple circulation model which provides a) the linkage to the two-dimensional channel model and b) information on the degree of potential circulation. Also the behaviour of "short" diffusers (only a few multiples of the water depth long) which do not have a clearly two-dimensional center portion should be investigated.

The total performance of a diffuser outfall in the water environment is closely linked to the interaction between near-field and far-field effects. To this end the development of a horizontally two-dimensional, vertically two-layered mathematical model, incorporating effects of far-field boundaries, advection, heat loss and turbulence, and coupling to the near-field properties as developed in this work, should be investigated.

Some careful experimental work should be directed to the buoyant

jet region to validate entrainment relationships and to study the effect of jet interaction. In addition, there is immediate need for large scale experiments on diffuser behaviour, which are well in the turbulent domain and reasonably free of boundary effects.

LIST OF REFERENCES

Abraham, G., "Jet Diffusion in Stagnant Ambient Fluid", Delft Hyd. Lab., Publ. No. 29 (1963).

Abraham, G. and Eysink, W. D., "Magnitude of Interfacial Shear in Exchange Flow", J. of Hydraulic Research, I.A.H.R., Vol. 9, No. 2 (1971).

Abramovich, G. N., "The Theory of Turbulent Jets", The M.I.T. Press, M.I.T. Cambridge, Massachusetts (1963).

Adams, E. E., "Submerged Multiport Diffusers in Shallow Water with Current", M.I.T., S.M. Thesis (Civil Engineering), June (1972).

Albertson, M. L., Dai, Y. B., Jensen, R. A., and Rouse, H., "Diffusion of Submerged Jets", Trans. ASCE, 115 (1950).

Bata, G. L., "Recirculation of Cooling Water in Rivers and Canals", Jour. of Hyd. Div., ASCE, Vol. 83, No. HY3, June (1957).

Cederwall, K., "Buoyant Slot Jets Into Stagnant or Flowing Environments", W. M. Keck Laboratory for Water Resources and Hydraulics, Report No. KH-R-25, California Institute of Technology, April (1971).

Cola, R., "Diffusion of a Vertical Plane Jet in a Water Basin of Limited Height", (In Italian), L'Energia Elletrica, Vol. XLIII, (1966).

Ditmars, J. D., "Computer Program for Round Buoyant Jets Into Stratified Ambient Environments", W. M. Keck Laboratory of Hydraulics and Water Resources, Tech. Memo 69-1, California Institute of Technology, March (1969).

Edinger, J. E. and Geyer, J. C., "Heat Exchange in the Environment", Research Project RP-49, Department of Sanitary Engineering and Water Resources, The Johns Hopkins University, Baltimore, Maryland, June (1965).

Ellison, T. H. and Turner, J. S., "Turbulent Entrainment in Stratified Flows", J. Fluid Mech., Vol. 6, Pt. 3, October (1959).

Fan, Loh-Nien, "Turbulent Buoyant Jets into Stratified or Flowing Ambient Fluids", W. M. Keck Laboratory of Hydraulics and Water Resources, California Institute of Technology, Report No. KH-R-15, June (1967).

Fan, L.-N. and Brooks, N. H., Discussion of "Horizontal Jets in Stagnant Fluid of Other Density", by Abraham G., Proc. ASCE, J. of Hyd. Div., HY2, March (1966).

Fan, L.-N. and Brooks, N. H., "Numerical Solution of Turbulent Buoyant Jet Problems", W. M. Keck Laboratory, California Institute of Technology, Report No. KH-R-18, January (1969).

Fox, D. G., "Forced Plume in a Stratified Fluid", J. of Geophys. Res., Vol. 75, No. 33, November (1970).

Gradshteyn, I. S. and Ryzhik, I. M., "Tables of Integrals, Series and Products", 4th Ed., Translated from Russian by Scripta Technica, Academic Press, New York (1965).

Harleman, D. R. F., "Stratified Flow", in Handbook of Fluid Dynamics, V. L. Streeter, Ed., McGraw Hill Book Company, Inc., (1961).

Harleman, D. R. F., Jirka, G. and Stolzenbach, K. D., "A Study of Submerged Multiport Diffusers for Condenser Water Discharge with Application to the Shoreham Nuclear Power Station", M.I.T. Parsons Laboratory for Water Resources and Hydrodynamics Technical Report No. 139, June (1971).

Harleman, D. R. F., Jirka, G., Adams, E. E. and Watanabe, M., "Investigation of a Submerged, Slotted Pipe Diffuser for Condenser Water Discharge from the Canal Plant, Cape Cod Canal", M.I.T. Parsons Laboratory for Water Resources and Hydrodynamics Technical Report No. 141, October (1971a).

Hirst, E., "Buoyant Jets Discharged to Quiescent Stratified Ambients", J. of Geophys. Res., Vol. 76, No. 30, October (1971).

Iamandi, C. and Rouse, H., "Jet-Induced Circulation and Diffusion", Proc. ASCE, J. of Hydr. Div., HY2, March (1969).

Ito, H., "Pressure Losses in Smooth Pipe Bends", Trans. ASME, Series D: J. of Basic Eng., 82, 1 (1960).

Koh, R. C. Y., and Fan, L.-N., "Mathematical Models for the Prediction of Temperature Distributions Resulting from the Discharge of Heated Water in Large Bodies of Water", EPA Water Pollution Control Research Series 16130 DWO, October (1970).

Larsen, J., and Hecker, A. M., "Design of Submerged Diffusers and Jet Interaction", ASCE Nat. Water Resources Engineering Meeting, Atlanta, Georgia, Preprint 1614, January (1972).

Lee, S. L. and Emmons, H. W., "A Study of Natural Convection Above a Line Fire", J. of Fluid Mech., 11 (1961).

Liseth, P., "Mixing of Merging Buoyant Jets from a Manifold in Stagnant Receiving Water of Uniform Density", Hydraulic Engineering Laboratory, University of California, Berkeley, Rep. No. HEL 23-1, November (1970).

Lofquist, J., "Flow and Stress Near an Interface Between Stratified Liquids", The Physics of Fluids, Vol. 3, No. 2, March-April (1960).

Mih, W. C. and Hoopes, J. A., "Mean and Turbulent Velocities for a Plane Jet", Proc. ASCE, J. of Hydr. Div., HY7 (1972).

Morton, B. R., "Forced Plumes", J. of Fluid Mech., 5 (1959).

Morton, B. R., Taylor, G. I. and Turner, J. S., "Turbulent Gravitational Convection from Maintained and Instantaneous Sources", Proc. Roy. Soc. London, A234 (1956).

Murota, A. and Muraoka, K., "Turbulent Diffusion of a Vertically Upward Jet", Proc. 12th Congress, IAHR, Ft. Collins, Colorado (1967).

Pearce, A. F., "Critical Reynolds Number for Fully-Developed Turbulence in Circular Submerged Water Jets", National Mechanical Engineering Research Institute, Council for Scientific and Industrial Research, CSIR Report MEG 475, Pretoria, South Africa, August (1966).

Prandtl, L., "The Essentials of Fluid Dynamics", Blackie and Sons, London (1949).

Rawn, A. M., Bowerman, F. R. and Brooks, N. H., "Diffusers for Disposal of Sewage in Sea Water", Trans. ASCE, Vol. 126, Part III (1961).

Reichardt, H., "Gesetzmässigkeiten der Freien Turbulenz", V.D.I., Forschungsheft, 13 (1942).

Rigter, B. P., "Density Induced Return Currents in Outlet Channels", Proc. ASCE, J. of Hydr. Div., HY2, February (1970).

Rouse, H., Yih, C. S. and Humphreys, H. W., "Gravitational Convection from a Boundary Source", Tellus, 4 (1952).

Schijf, J. B. and Schönfeld, J. C., "Theoretical Considerations on the Motion of Salt and Fresh Water", Proc. Minnesota Int. Hydraulics Convention, IAHR and Hydr. Div., ASCE, September (1953).

Schlichting, H., "Boundary Layer Theory", McGraw Hill, New York, New York (1960).

Shirazi, M. A. and Davis, L. R., "Workbook on Thermal Plume Prediction, Volume 1: Submerged Discharges", EPA Water Pollution Control Research Series 16130 FHH, August (1972).

Yih, C. S., "Dynamics of Nonhomogeneous Fluids", The MacMillan Co. (1965).

Yih, C. S. and Guha, C. R., "Hydraulic Jump in a Fluid System of Two Layers", Tellus VII (1955).

LIST OF FIGURES

LIST OF TABLES

GLOSSARY OF SYMBOLS

Subscripts	
1,2	upper, lower layers in stratified flow
a,b	vertical sections a,b
c	critical section in stratified flow
o	discharge variables
s,i,b	surface, interface, bottom boundary conditions

Superscripts	
*	dimensionless variables

A	ratio of interfacial to bottom shear stress coefficients
B	equivalent slot width
b	nominal jet width
b_i	nominal jet width at impingement
c	concentration
c_c	centerline concentration
c_c	contraction coefficient
c_p	specific heat
c_2	correction factor for channel wall effects
D	nozzle diameter
F	layer densimetric Froude number
F_H	densimetric Froude number based on total depth
F_{H_C}	critical F_H for counterflow system
F_L	local jet densimetric Froude number
$\hat{F}_L$	constant plume densimetric Froude number
F_n	nozzle densimetric Froude number

F_s	slot densimetric Froude number
F_T	diffuser load
F^*	free surface Froude number
f_i	interfacial stress coefficient
f_o	bottom stress coefficient
f_o^*	bottom stress coefficient including channel wall effects
g	gravitational acceleration
H	water depth
H_1, H_2	normalized layer depths
h	layer depth in stratified flow
h_f	head loss in layer motion
h_i	thickness of jet impingement layer
h_L	head loss in surface impingement
h_s	height of nozzles above bottom
I	integral Equation (3-45)
K_z	vertical eddy diffusion coefficient for mass, heat
k	frictional head loss coefficient
k_L	head loss coefficient for impingement
k_s	absolute wall roughness
L	length of two-dimensional channel model
L_c	length of subcritical stratified flow section
L_D	diffuser half length
L_m	length of local mixing zone
L_s	length of wedge intrusion
ℓ	nozzle spacing
m_o	sink or source strength

n	transverse coordinate
p	pressure
p'	pressure fluctuation
p_n	hydrostatic pressure
p_r	reduced pressure
Q	flow ratio in stratified flow
Q_o	total diffuser flow (plant discharge)
q	volume flux per unit width
q_H	heat flux
q_o	discharge per unit diffuser length
$\mathbb{R}$	Reynolds number
$\mathbb{R}_j$	jet Reynolds number
R_h	hydraulic radius
r	radial coordinate
S	dilution
S_c	jet centerline dilution
$\bar{S}$	average jet dilution
S_s	surface dilution
s	axial coordinate
T	temperature
T'	temperature fluctuation
T_a	ambient temperature
T_c	jet centerline temperature
T_e	equilibrium temperature
T_o	discharge temperature
T_s	surface temperature

U_o	jet discharge velocity
u,v,w	velocities in Cartesian coordinate system
$\bar{u},\bar{v}$	layer velocities averaged over total depth
$\tilde{u},\tilde{v}$	jet velocities in local coordinates
u_a	ambient cross flow velocity
$\bar{u}_c$	averaged layer velocity in channel
$\tilde{u}_c$	jet centerline velocity
$\bar{u}_d,\bar{v}_d$	averaged layer velocities at diffuser
$\tilde{u}_i$	jet velocity at impingement
V	volume flux ratio
V^*	combined mixing by crossflow and diffuser momentum Equation (7-5) or (7-6)
v_e	jet entrainment velocity
W	complex potential
X	normalized horizontal distance
x,y,z	Cartesian coordinates
α	buoyant jet entrainment coefficient
$\hat{\alpha}$	constant plume entrainment coefficient
α_1	non-buoyant jet entrainment coefficient
β	coefficient of thermal expansion
$\beta(y)$	horizontal nozzle orientation with diffuser axis
γ	arrangement of diffuser axis with crossflow
ΔH	head change in free surface flow
ΔT	temperature rise above ambient
ΔT_c	jet centerline temperature rise
ΔT_o	discharge temperature rise

$\Delta\rho$	density deficiency
$\Delta\rho_c$	centerline density deficiency
$\Delta\rho_i$	density deficiency at impingement section
$\Delta\rho_o$	discharge density deficiency
ε_z	vertical eddy diffusion coefficient for momentum
ζ	complex position variable
η	water surface disturbance
θ	local jet angle
θ_i	angle of jet surface impingement
θ_o	jet discharge angle
κ	surface heat exchange coefficient
λ	jet spreading ratio between mass and momentum
$\hat{\lambda}$	plume spreading ratio between mass and momentum
ν	kinematic viscosity
ρ	density
ρ_a	ambient density
ρ_c	jet centerline density
ρ_o	discharge density
τ	shear stress
Φ	far-field parameters
ϕ	velocity potential
ψ	stream function

BIOGRAPHICAL NOTE

Gerhard Jirka was born in Kasten, Austria, on September 14, 1944. He received his primary and secondary education in Steyr and Linz, Austria. From 1962 to 1963 he served in the Austrian army. He attended the Hochschule für Bodenkultur in Vienna from October 1963 to May 1969, studying in the Department of Civil Engineering and Water Resources (Kulturtechnik und Wasserwirtschaft). He finished his studies with honours receiving the degree of Diplom-Ingenieur in May 1969. In September 1969 he received a Fulbright Travel Grant and a research assistantship at the Massachusetts Institute of Technology enabling him to continue his studies toward the degree of Master of Science (January 1971) and the doctorate.

His publications include:

"Location of Thermal Power Plants under Environmental Considerations", Co-author with D. H. Marks, Technical Report, M.I.T., Urban Systems Laboratory, (1971)

"Environmental Screening Model for the Location of Power Generating Facilities", Co-author with D. H. Marks, Paper FA 2.6, 39th National Meeting, Operations Research Society of America, Dallas, Texas, (1971)

"A Study of Submerged Multiport Diffusers for Condenser Water Discharge with Application to the Shoreham Nuclear Power Station", Co-author with D. R. F. Harleman and K. D. Stolzenbach, M.I.T., Parsons Laboratory for Water Resources and Hydrodynamics, Technical Report No. 139, (1971)

"Investigation of a Submerged, Slotted Pipe Diffuser for Condenser Water Discharge from the Canal Plant, Cape Cod Canal", Co-author with D. R. F. Harleman, E. E. Adams and M. Watanabe, M.I.T. Parsons Laboratory for Water Resources and Hydrodynamics, Technical Report No. 141, (1971)